Design of Functionalized Covalent-Organic Framework Materials for Utilization of Carbon Dioxide

Doctoral Thesis

by **Gulshan Singh**(2019CYZ0017)



DEPARTMENT OF CHEMISTRY INDIAN INSTITUTE OF TECHNOLOGY ROPAR

October, 2024

Design of Functionalized Covalent-Organic Framework Materials for Utilization of Carbon Dioxide

A Thesis Submitted
In Partial Fulfillment of the Requirements
for the Degree of

DOCTOR OF PHILOSOPHY

by

Gulshan Singh

(2019CYZ0017)



DEPARTMENT OF CHEMISTRY INDIAN INSTITUTE OF TECHNOLOGY ROPAR

October, 2024

Gulshan Singh: Design of Functionalized Covalent-Organic Framework Materials for Utilization of Carbon Dioxide

Copyright © 2024, Indian Institute of Technology Ropar

All Rights Reserved

DEDICATED TO MY PARENTS **Declaration of Originality**

I hereby declare that the work which is being presented in the thesis entitled **Design of**

Functionalized Covalent-Organic Framework Materials for Utilization of Carbon

Dioxide has been solely authored by me. It presents the result of my own independent

investigation/research conducted during the time period from July 2019 to October 2024 under

the supervision of Professor C. M. Nagaraja, IIT Ropar. To the best of my knowledge, it is an

original work, both in terms of research content and narrative, and has not been submitted or

accepted elsewhere, in part or in full, for the award of any degree, diploma, fellowship,

associateship, or similar title of any university or institution. Further, due credit has been

attributed to the relevant state-of-the-art and collaborations with appropriate citations and

acknowledgments, in line with established ethical norms and practices. I also declare that any

idea/data/fact/source stated in my thesis has not been fabricated/ falsified/ misrepresented. All

the principles of academic honesty and integrity have been followed. I fully understand that if

the thesis is found to be unoriginal, fabricated, or plagiarized, the Institute reserves the right to

withdraw the thesis from its archive and revoke the associated Degree conferred. Additionally,

the Institute also reserves the right to appraise all concerned sections of society of the matter for

their information and necessary action If accepted, I hereby consent for my thesis to be

available online in the Institute's Open Access repository, inter-library loan, and the title &

abstract to be made available to outside organizations.

Signature

Name: Gulshan Singh

Entry Number: 2019CYZ0017

Program: PhD

Department: Chemistry

Indian Institute of Technology Ropar

Rupnagar, Punjab 140001

Date: 23/10/2024

ν

Acknowledgments

I would like to take this opportunity to acknowledge some very special people who have been a vital part of my journey so far.

First and foremost, I would like to express my deepest gratitude to my Ph.D. supervisor, **Dr. C. M. Nagaraja**, for his constant support, help, and motivation throughout my Ph.D. studies. My Ph.D. journey would not have been possible without his guidance and trust in me. When I joined, I knew very little about porous materials, but he trusted me and introduced me to the field of porous materials, CO₂ capture, and conversion. His expertise and dedication have significantly impacted my progress as a scientist.

I would also like to thank my Ph.D. chairperson, **Dr. T. J. Dhilip Kumar**, and my doctoral committee (DC) members, **Dr. Narinder Singh**, **Dr. Indranil Chatterjee** from the Chemistry Department of IIT Ropar, and **Dr. Navin Gopinathan** from the Chemical Engineering Department of IIT Ropar, for their valuable time and for evaluating my progress reports during this tenure. Their insightful discussions, suggestions, and motivations helped me to stay on track with my Ph.D. and have significantly improved my research work. Additionally, I would like to thank the director of IIT Ropar, **Prof. Rajeev Ahuja**, for providing excellent research facilities and infrastructure, including labs for our research work, and for providing funding for national and international conferences.

I am incredibly grateful to my brothers, **Gulab**, **Sanjeeb**, and **Anchal**, who encouraged me to pursue higher studies and have supported me in reaching this point of completing my Ph.D. I will never forget their sacrifices and I am eternally grateful for having brothers like them.

My heartfelt gratitude also extends to all my excellent labmates (Dr. Bharat, Dr. Sandeep, Dr. Rekha, Dr. Nayuesh, Dr. Suman, Dr. Rajesh, Dr. Bharti, Dr. Anbu, Dr. Kamal, Shambu, Akanksha, Amit, Piyush, Bhawna, Vaibhav, Ram, Paltu, Shubham, Tarun, Sakshi, Srijan, Sahil, Mehak, Beekesh, Aniket, Rajesh Sahoo, Bharat, Dr. Pooja), who developed an excellent research environment in the lab. All of them were extremely supportive and helpful, and together we formed a lovely family at IIT Ropar. I will cherish these memories and friendships for the rest of my life.

I am immensely thankful to my school and college teachers (Mr. Dilip, Dr. Kulwinder, Mrs. Jyoti, Dr. Rashmi, Mrs. Priyanka, Mrs. Charanjeet, and Mrs. Kiran) who encouraged me in the chemistry subject. I am also grateful to my batchmates Priyank, Vishal, Ganesh, Man,

Akansha, Rakesh, Arijit, Saurav, Sandeep, Ritika, Anoop, Shain, Sweta, and Vatan for their moral support during the challenging phases of my research.

Additionally, I would like to thank Ganga, Dr. Gaje, Dr. Navpreet, Dr. Debarshi, Nidhi, Ketan, Humanshu, Dr. Nahida, Dr. Moumita, Deepa, Yashika, Arjun, Atul, Aarjoo, Himanshi Shivi, and Kamalpreet for their help and support. My gratitude also goes to the staff members of the Chemistry Department, Mrs. Poonam, Mrs. Samita, Mrs. Hanspreet, Mr. Sushil, Mr. Nagendra, Mr. Manish, and Mr. Gurwinder for their constant support throughout my Ph.D.

Lastly, I would like to thank my parents, **Mr. Balbir Singh** and **Mrs. Rama Rani** for their dedication, and inspiration, and for being the backbone of my Ph.D. journey. This achievement would not have been possible without their sacrifices. I dedicate this thesis to my parents as a small recognition of their unconditional support.

My special thanks to almighty God who encouraged me to choose this path and gave me the strength to accomplish this Ph.D. degree.

Gulshan Singh

Certificate

This is to certify that the thesis entitled **Design of Functionalized Covalent-Organic Framework Materials for Utilization of Carbon Dioxide**, submitted by **Gulshan Singh**(2019CYZ0017) for the award of the degree of **Doctor of Philosophy** of Indian Institute of Technology Ropar, is a record of bonafide research work carried out under my (our) guidance and supervision. To the best of my knowledge and belief, the work presented in this thesis is original and has not been submitted, either in part or full, for the award of any other degree, diploma, fellowship, associateship or similar title of any university or institution.

In my opinion, the thesis has reached the standard fulfilling the requirements of the regulations relating to the Degree.

Signature of the Supervisor(s)

Dr. C. M. Nagaraja
Department of Chemistry
Indian Institute of Technology Ropar

Carlagas

Rupnagar, Punjab 140001

Date: 23/10/2024

Lay Summary

The combustion of oil, coal, and natural gas produces significant amounts of greenhouse gases in the atmosphere, including carbon dioxide (CO2), methane, nitrous oxide, and fluorinated gases. As a result, atmospheric CO₂ concentration is increasing rapidly, and it has exceeded 425 ppm currently. This rising CO₂ concentration has resulted in several environmental issues, including extreme weather, rising sea levels, and increasing global temperature. Carbon capture and sequestration (CCS) has been used to reduce the growing concentration of carbon dioxide. However, carbon capture and utilization (CCU) is a promising value-added alternative that uses CO₂ as a C1 source to produce a variety of valueadded chemicals and fuels. Also, it provides dual benefits of mitigating rising CO₂ concentration and producing various value-added chemicals. Among the several catalytic transformations of carbon dioxide to value-added chemicals and fuels, the cycloaddition of epoxide with CO₂ to produce cyclic carbonates (CCs) has received significant attention owing to 100% atom efficiency of the reaction and broad spectrum of industrial applications of CCs. Besides, synthesis of α -alkylidene cyclic carbonates (α -aCCs) by combining propargylic alcohols with CO₂ has received significant attention due to their potential applications as commodity chemicals for polycarbonates and polyurethanes synthesis. Furthermore, the onepot synthesis of styrene carbonates from readily available styrene and CO2 has received substantial attention from researchers due to the promising applications of styrene carbonates as precursors for synthesizing styrene carbamates, vicinal diols and polymers. Notably, the one-step synthesis of styrene carbonates (SCs) from styrene and CO2 presents an environmentally friendly alternative to the two-step approach that needs styrene oxides (epoxides).

In addition, utilization of CO₂ for production of bioactive molecules is of potential significance. Thus, carboxylation of terminal alkynes with CO₂ to produce alkynyl carboxylic acids, a value-added chemical, is potentially noteworthy. The extensive use of alkynyl carboxylic acids in preparing anticancer medicines such as coumarin makes this conversion an excellent way to transfer carbon dioxide into value-added products. Furthermore, converting CO₂ to bioactive oxazolidinones, an important building blocks of antibiotics, by carboxylative cyclization with propargylic amines is highly beneficial. However, most of the catalytic systems reported for carbon dioxide fixation require either high temperature and/or high pressure of carbon dioxide to synthesize these valuable compounds. Consequently, developing an active catalyst capable of converting CO₂ to high-value chemicals at ambient conditions is extremely desirable. Towards this direction, we intend to synthesize framework-

based materials composed of high CO₂ philic basic and acidic (Lewis/Brønsted) sites suitable for selective capture and conversion of carbon dioxide under mild conditions.

Furthermore, the catalyst employed should exhibit high stability and recyclability for several cycles of reuse. In this direction, covalent organic frameworks (COFs) formed by covalent linking of organic precursors composed of light (B, C, N, O, F, and S) elements have gained much interest due to their modular nature facilitating rational design with tailored properties. COFs feature unique properties of high surface area/porosity and good thermal/chemical stability, rendering them promising candidate materials for selective capture and conversion of CO₂ to value-added chemicals. The primary objectives of this thesis were to design functionalized covalent organic frameworks (COFs) and their utilization as recyclable catalysts to transform CO₂ into value-added chemicals/fuels under environmentally benign reaction conditions. Consequently, several functionalized COFs were synthesized, and their application for selective capture and functionalization of CO₂ into commodity chemicals was investigated. The thesis has been organized into five chapters, as summarized below.

Chapter 1: This chapter comprehensively introduces the topic, the importance of carbon capture and utilization (CCU), and various methods employed for chemical fixation of CO₂ into high-value compounds. Also, the potential application of COF-based porous materials for effective CCU is discussed.

Chapter 2: This chapter presents application of a polar functionalized covalent organic framework, COF-SO₃H, for metal/solvent-free CO₂ fixation to cyclic carbonates (CCs) under mild conditions. Here, COF-SO₃H demonstrated high CO₂ adsorption, with a heat of adsorption (Qst) value of 42.1 kJ/mol and good catalytic performance for cycloaddition of epoxides with CO₂ to produce value-added cyclic carbonates under atmospheric pressure conditions. Furthermore, the role of -SO₃H group in improving the catalytic fixation of CO₂ was further established using an analogous COF (COF-H), which lacks a polar sulfonic acid group. Indeed, COF-SO₃H showed effective catalytic activity for CO₂ chemical fixation to cyclic carbonates at ambient CO₂ pressure.

Chapter 3: In this chapter synthesis of bipyridine-functionalized covalent triazine framework (CTF) and its utilization for stable anchoring of non-noble, alkynophilic Cu(I) active site is reported. The Cu(I)@bipy-CTF was employed as a recyclable catalyst to generate value-added α-alkylidene cyclic carbonates (α-aCCs) by coupling propargylic alcohol with dilute CO₂ (13% CO₂) at ambient conditions. The presence of both CO₂-philic nitrogen and alkynophilic Cu(I) sites decorated in the 1D channels of bipy-CTF rendered excellent catalytic activity for CO₂ utilization under atmospheric pressure conditions.

Furthermore, Cu(I)@bipy-CTF showed excellent recyclability and structural stability, even after numerous cycles of reuse.

Chapter 4: This chapter describes the use of Fe(III)-centered porphyrin-based covalent organic framework (Fe(III)@P-COF) for one-pot green synthesis of styrene carbonates (SCs) from easily available styrene and CO₂ under ambient conditions. Furthermore, the catalytic activity was enhanced for the one-pot conversion of different alkenes (aliphatic and aromatic) to their corresponding cyclic carbonates. This one-step cyclic carbonate synthesis is a environmentally friendly alternative to traditional two-step procedure employing epoxides. Thus, this study constitutes a greener approach for synthesizing styrene carbonates from easily available styrenes under atmospheric pressure conditions.

Chapter 5: This chapter presents rational design of a highly porous bipyridine functionalized pyrene-based covalent organic framework (Pybpy-COF) and its application for stable anchoring of Ag NPs at the bipy sites exposed in 1D channels of the framework. Due to the presence of alkynophillic Ag and CO₂ philic basic sites in the framework, Ag@Pybpy-COF demonstrated substantial catalytic activity for carboxylation of terminal alkynes to alkynyl carboxylic acids via C-H bond functionalization under atmospheric pressure conditions. Besides, carboxylative cyclization of propargylic amines with CO₂ to obtain oxazolidinones has also been achieved using Ag@Pybpy-COF under ambient conditions. Further, theoretical calculations unveiled insight mechanistic aspects of carboxylation of terminal alkynes/propargylic amines with CO₂ to produce alkynyl carboxylic acids/oxazolidinones. Thus, this study demonstrates effective utilization of CO₂ in synthesizing two useful compounds under mild conditions.

Abstract

The rising carbon dioxide (CO₂) concentrations in the atmosphere contribute to various environmental issues, including extreme weather, climate change, and global warming. As a result, it is essential to control growing CO₂ levels by utilizing it as a C1 feedstock for generating value-added chemicals and fuels. However, the functionalization of CO₂ under ambient conditions is challenging due to its high kinetic inertness and thermodynamic stability. Consequently, it is extremely desirable to synthesize effective catalysts capable of selectively capturing CO2 and converting it into commodity chemicals. However, to accomplish efficient chemical fixation of CO₂, most catalysts require high temperatures and pressure conditions. On the other hand, green and sustainable chemistry practices prefer recyclable catalysts capable of transforming CO₂ into value-added chemicals under ecofriendly mild conditions. In this context, covalent organic frameworks (COFs), a new family of porous organic polymers, have sparked widespread interest among researchers due to their modular nature facilitating the introduction of CO₂-philic and catalytic sites. Motivated by the potential uses of COFs in the chemical fixation of CO₂ to value-added chemicals, we sought to develop various functionalized frameworks suitable for environmentally friendly chemical fixation of CO₂ into high-value compounds. The thesis work has been organized into five chapters. Chapter 1 presents importance of carbon capture utilization (CCU) and various strategies for converting CO₂ into high-value chemicals or fuels. The advantages of COFbased materials in CO₂ capture and utilization are also discussed. Thus, motivated by CO₂ conversion to value-added chemicals to mitigate rising CO₂ concentrations, we intend to develop functionalized COFs for effective CCU. In this context, Chapter 2 involves the rational construction of a polar functionalized COF with Brønsted acidic (-SO₃H) sites decorated in the 1D channels and its investigation for metal/solvent-free cycloaddition of epoxide with CO₂ to generate cyclic carbonates (CCs) under mild conditions. Further, the role of Brønsted acidic sites on the catalytic conversion of CO₂ has been ascertained by utilizing a COF-H, which lacks acidic sites.

In **Chapter 3**, synthesis of a highly CO₂-phillic and thermally stable covalent triazine framework (bipy-CTF) and its functionalization to anchor non-noble metal Cu(I) for fixation of CO₂ from dilute gas into value-added α-alkylidine cyclic carbonate (α-aCC) under mild conditions has been studied. Furthermore, considering the potential benefits of porphyrin-based linkers in selective CO₂ capture and conversion, in **Chapter 4**, we developed Fe(III)-embedded porphyrin-based COF (P-COF) and its catalytic performance for one-pot synthesis of styrene carbonates (SCs) from readily available styrene and CO₂ under ambient conditions.

In **Chapter 5**, the application of silver nanoparticles (Ag NPs) anchored pyrene-based COF for carboxylation of terminal alkynes with CO₂ to produce value-added alkynyl carboxylic acids via C-H bond functionalization and carboxylative cyclization of propargylic amines to generate bio-active oxazolidinones under atmospheric conditions is presented. Overall, the thesis work involves the rational synthesis and functionalization of porous covalent organic framework materials with CO₂-philic and catalytic sites ideal for environmentally friendly chemical fixation of carbon dioxide, a greenhouse gas, into various value-added chemicals.

List of Publications from Thesis

- **Singh, G.;** Nagaraja, C. M. Highly efficient metal/solvent-free chemical fixation of CO₂ at atmospheric pressure conditions using functionalized porous covalent organic frameworks. *J. CO₂ Util.* **2021**, *53*, 101716.
- **Singh, G.;** Nagaraja, C. M. Rational design of Cu(I)-anchored porous covalent triazine framework (CTF) for simultaneous capture and conversion of CO₂ at ambient conditions. *J. CO₂ Util.* **2022**, *63*, 102132.
- **Singh, G.**; Prakash, K.; Nagaraja, C. M. Fe(III)-Anchored Porphyrin-Based Nanoporous Covalent Organic Frameworks for Green Synthesis of Cyclic Carbonates from Olefins and CO₂ under Atmospheric Pressure Conditions. *Inorg. Chem.* **2023**, *62*, 13058-13068.
- **Singh, G.;** Duhan, N.; Kumar, T. J. D.; Nagaraja, C. M. Pyrene-Based Nanoporous Covalent Organic Framework for Carxylation of C-H Bonds with CO₂ and Value-Added 2-Oxazolidinones Synthesis under Ambient Conditions. *ACS Appl. Mater. Interfaces* **2024**, *16*, 5857-5868.



Table of Contents

Declaration	V
Acknowledgment	vii
Certificate	ix
Lay Summary	xi
Abstract	XV
List of Publications	xvii
List of Figures	xxiii
List of Schemes	xxvii
List of Tables	xxix
Notations and Abbreviations	xxxi
Chapter 1: Introduction	1
1.1 Carbon dioxide (CO ₂), a greenhouse gas	3
1.2 Carbon capture and utilization	4
1.3 Framework-based materials	6
1.3.1. Metal-Organic Frameworks (MOFs)	6
1.3.2. Covalent-Organic Frameworks (COFs)	6
1.3.2.1. History of COFs	7
1.4. Applications of COFs	9
1.5. COFs for CO ₂ capture and utilization	10
1.5.1. COFs for CO ₂ capture	10
1.5.2. COFs for CO ₂ utilization	13
1.5.2.1. Modification in the backbone of COFs	14
1.5.2.2. Functionalization of COFs	15
1.5.2.3. Incorporation of catalytic active metal sites into COFs	16
1.5.3. Utilization of CO_2 via C - X ($X = O$, N , and C) bond formation	17
1.5.3.1. Utilization of CO ₂ via C-O bond formation	18
1.5.3.2. Utilization of CO ₂ via C-N bond formation	21
1.5.3.3. Utilization of CO ₂ via C-C bond formation	23
1.6. Summary	24
1.7. References	24
Chapter 2: Highly Efficient Metal/Solvent-free Chemical Fixation of CO ₂	39
at Atmospheric Pressure Conditions Using Functionalized Porous	

Covalent Organic Frameworks	
2.1. Introduction	41
2.2. Experimental section	42
2.2.1. Materials	42
2.2.2. Physical measurements	42
2.2.3. Synthesis	43
2.2.3.1. Synthesis of COF-SO ₃ H	43
2.2.3.2. Synthesis of COF-H	43
2.2.4. Metal-free cycloaddition of CO ₂ with epoxides	43
2.2.5. Structure simulation and modeling of COF-SO ₃ H and COF-H	44
2.2.6. Gas adsorption measurements	46
2.3. Results and discussion	46
2.3.1. Synthesis and structural description	46
2.3.3. Gas adsorption studies	48
2.3.4. Metal-free utilization of CO ₂	50
2.3.5. Recyclability and catalyst leaching test	54
2.3.6. Plausible mechanism	55
2.4. Conclusion	55
2.5. References	56
Chapter 3: Rational Design of Cu(I)-anchored Porous Covalent Triazine	67
Framework (CTF) for Simultaneous Capture and Conversion of CO ₂ at	
Ambient Conditions	
3.1. Introduction	69
3.2. Experimental section	70
3.2.1. Materials	70
3.2.2. Physical measurements	70
3.2.3. Synthesis	70
3.2.3.1. Synthesis of bipy-CTF	70
3.2.3.2. Synthesis of Cu(I)@bipy-CTF	71
3.2.4. Catalytic cycloaddition reaction of CO ₂ with propargylic alcohol	71
3.2.5. Adsorption measurements	71
3.3. Results and discussion	72
3.3.1. Synthesis and Characterizations	72
3.3.2. Gas sorption analysis	74

3.3.3. Coupling of CO ₂ with propargylic alcohol at atmospheric conditions	76
3.3.4. Coupling of propargylic alcohols with dilute CO ₂ (13%)	79
3.3.5. Recyclability and catalyst leaching test	82
3.3.6. Plausible mechanism	82
3.4. Conclusion	83
3.5. References	84
Chapter 4: Fe(III)-Anchored Porphyrin-Based Nanoporous Covalent	91
Organic Frameworks for Green Synthesis of Cyclic Carbonates from	
Olefins and CO ₂ under Atmospheric Pressure Conditions	
4.1. Introduction	93
4.2. Experimental Section	94
4.2.1. Materials	94
4.2.2. Physical measurements	95
4.2.3. Synthesis	95
4.2.3.1. Synthesis of porphyrin COF (P-COF)	95
4.2.3.2. Synthesis of Fe(III)@P-COF	95
4.2.3.3. Synthesis of Fe(II)/Zn(II)@P-COF	96
4.2.4. Catalytic epoxidation of styrene	96
4.2.5. One-pot oxidative carboxylation of styrene	96
4.2.6. Structure simulation and modeling of P-COF	96
4.2.7. Gas adsorption measurements	97
4.3. Results and discussion	98
4.3.1 Synthesis and structural description	98
4.3.2. Gas adsorption analysis	102
4.3.3. Catalytic epoxidation of styrenes	102
4.3.4. One-pot cyclic carboxylation of olefins	105
4.3.5. Catalyst recycling and leaching test	108
4.3.6. Plausible mechanism	109
4.4. Conclusion	110
4.5. References	111
Chapter 5: Pyrene-Based Nanoporous Covalent Organic Framework for	121
Carboxylation of C-H Bonds with CO ₂ and Value-Added	
2-Oxazolidinones Synthesis under Ambient Conditions	
5.1. Introduction	123

5.2. Experimental section	124
5.2.1. Materials	124
5.2.2. Physical measurements	125
5.2.3. Synthesis Procedures	125
5.2.3.1. Synthesis of Pybpy-COF	125
5.2.3.2. Synthesis of Ag@Pybpy-COF	125
5.2.4. Catalytic carboxylation of terminal alkynes	126
5.2.5. Synthesis of propargylic amines	126
5.2.6. Carboxylative cyclization of propargylic amines	127
5.2.7. Structure simulation and modeling of Pybpy-COF.	127
5.3. Results and discussion	128
5.3.1. Gas adsorption analysis	132
5.3.2. Carboxylation of terminal alkynes with CO ₂ catalyzed by	133
Ag@Pybpy- COF	
5.3.3. Carboxylative cyclization of propargylic amines with CO ₂ catalyzed	138
by Ag@Pybpy-COF	
5.3.4. Mechanistic investigation for carboxylation of terminal alkynes with CO ₂	141
5.3.5. Mechanistic investigation for carboxylation of propargylic amines with	142
CO_2	
5.3.6. Catalyst recycling and leaching test	144
5.4. Conclusion	145
5.5. References	145
6. Annexure	153

List of Figures

S. No.	Figure caption	Page No.
1.	(a) Global greenhouse gas emissions. (b) Global greenhouse gas	3
	emission by different economic sectors.	
2.	Schematic representation of CO ₂ utilization as a C1 source in	5
	constructing various value-added chemicals. Reproduced with	
	permission from reference 38.	
3.	Construction of 1D chain, 2D sheet, and 3D framework of COFs	7
	connected through different linkers.	
4.	Development of COFs with different linkages.	9
5.	A schematic representation of the various applications of COFs.	10
6.	A schematic representation of CO ₂ utilization catalyzed by COF	14
	catalysts.	
7.	Representation of various strategies to incorporate catalytic active	15
	sites into a COF structure. Reproduced with permission from	
	reference number 57.	
8.	Utilization of CO ₂ through C-X bond formation.	
9.	The unit cell of COF-SO ₃ H in different display style representation,	45
	(A) Line, (B) stick, (C) ball and stick, and (D) stacked 2D layers of	
	COF-SO₃H.	
10.	The unit cell of COF-H in different display style representation, (A)	45
	Line, (B) stick, (C) ball and stick, and (D) stacked 2D layers of COF-	
	H.	
11.	¹³ C CP-MASS solid-state NMR spectrum of COF-SO ₃ H (a) and	48
	COF-H (b). Comparison of theoretical and experimental PXRD	
	patterns of COF-SO ₃ H, (c) and COF-H (d). SEM images of COF-	
	SO ₃ H (e) and COF-H (f).	
12.	N ₂ adsorption isotherms for COF-SO ₃ H and COF-H carried out at 77	50
	K (a). The CO ₂ adsorption-desorption isotherms of COF-SO ₃ H (b)	
	and COF-H (c). Selective CO ₂ adsorption isotherms of COF-SO ₃ H	
	(d).	
13.	The catalytic optimization by varying reaction temperature, (a) and	51
	time (b). Conditions: Epoxide (20 mmol), COF-SO ₃ H (0.01 mmol),	

	TBAB (2.5 mol %), and 1 bar CO ₂ .	
14.	(a) Recyclability test and (b) leaching test of COF-SO ₃ H.	54
15.	(a) FT-IR plots of dicyanobipyridine (black), bipy-CTF (red), and	73
	Cu(I)@bipy-CTF (blue). (b) ¹³ C CP-MAS solid-state NMR spectrum	
	of bipy-CTF. The SEM images of bipy-CTF (c) and Cu(I)@bipy-	
	CTF (d).	
916.	XPS spectra (a) N 1s spectrum of bipy-CTF, (b) N 1s spectrum of	74
	Cu(I)@bipy-CTF, (c) Cu 2p spectrum of Cu(I)@bipy-CTF, and (d)	
	Thermogravimetric analysis (TGA) plots for bipy-CTF (red) and	
	Cu(I)@bipy-CTF (blue).	
17.	N ₂ sorption isotherm for bipy-CTF and Cu(I)@bipy-CTF carried out	76
	at 77 K (a). The CO ₂ sorption isotherm of bipy-CTF (b) and	
	Cu(I)@bipy-CTF (c). Selective CO ₂ sorption isotherm of	
	Cu(I)@bipy-CTF (d).	
18.	(a) Recyclability test and (b) leaching test of Cu(I)@bipy-CTF.	82
19.	Simulated structure of P-COF (ball and stick model) (gray, Carbon;	97
	blue, Nitrogen).	
20.	(a) Experimental (blue) and simulated (purple) powder XRD plots of	100
	P-COF. (b) Powder XRD plots of Fe(III)@P-COF samples, pristine	
	(I), and recycled after catalysis (II). (c and d) SEM images of P-COF	
	and Fe(III)@P-COF, respectively.	
21.	XPS plot of Fe(III)@P-COF, (a) survey spectrum (b) N 1s, (c) Fe 2p,	101
	and (d) Cl 2p.	
22.	(a) N ₂ adsorption plot of P-COF and Fe(III)@P-COF. (b) The CO ₂	102
	sorption isotherms of P-COF (I, II) and Fe(III)@P-COF (III, IV) were	
	performed at 273 K and 298 K, respectively.	
23.	The optimization of catalytic reaction by varying temperature (a) and	106
	time (b). Reaction conditions: catalyst (10 mg), styrene (0.6 mmol),	
	TBAB (0.3 mmol), CO ₂ (0.1 MPa), PhIO (1.5 mmol), and	
	dichloromethane (2 mL).	
24.	Recyclability (a) and catalyst leaching (b) test of Fe(III)@P-COF.	109
25.	Simulated structure of Pybpy-COF.	128
26.	(a) Comparison of the experimental and simulated PXRD plots of	130
	Pybpy-COF. (b) PXRD pattern of Ag@Pybpy-COF (Ag NPs peaks	

	<u>, </u>	
	are represented by arrows). (c) Solid-state ¹³ C CP-MAS spectra of	
	Pybpy-COF. (d) Thermogravimetric analysis (TGA) plot of Pybpy-	
	COF (red) and Ag@Pybpy COF (blue).	
27.	FE-SEM images of Pybpy-COF, and Ag@Pybpy-COF (a, b). HR-	131
	TEM image of Ag@Pybpy-COF along with inset plot of particle size	
	distribution, (c) SAED pattern, (d) and lattice fringes of Ag (e).	
28.	(a) XPS survey spectra of Ag@Pybpy-COF, (I) and Pybpy-COF,	
	(II). (b) Ag 3d spectra of Ag@Pybpy-COF. (c and d) The N 1s	132
	spectra of Pybpy-COF, and Ag@Pybpy-COF.	
29.	(a) N ₂ adsorption isotherm collected at 77K for Pybpy-COF (I) and	133
	Ag@Pybpy-COF (II); (b) CO ₂ adsorption isotherms of Pybpy-COF (I	
	and III), and Ag@Pybpy-COF (II and IV) performed at 273 and 298	
	K, respectively.	
30.	Optimization of reaction conditions for the carboxylation of	134
	phenylacetylene with CO ₂ by varying temperature and time (a and b)	
	catalyzed by Ag@Pybpy-COF. Reaction conditions: Ag@Pybpy-	
	COF (10 mg), Phenylacetylene (1 mmol), base (1.5 mmol), CO ₂ (1	
	bar), and solvent (DMF, 5 mL).	
31.	Recyclability (a) and leaching test (b) of Ag@Pybpy-COF.	146



List of Schemes

S. No.	Scheme caption			
1.	A plausible reaction mechanism of CO ₂ coupling with epoxides to	19		
	synthesize cyclic carbonates through C-O bond formation catalyzed			
	by COF. AS represents Brønsted acidic active sites such as -SO ₃ H, -			
	COOH, and -OH.			
2.	A plausible reaction mechanism for CO ₂ coupling with propargylic	21		
	alcohol to synthesize α -alkylidene cyclic carbonates through C-O			
	bond formation catalyzed by COF. AS represents alkynophilic Ag(I),			
	or Cu(I) active site.			
3.	A plausible reaction mechanism for CO ₂ utilization to synthesize 2-	22		
	oxazolidinones through C-N bond formation catalyzed by COF. AS			
	represents alkynophilic Ag(I), or Cu(I) active site.			
4.	A plausible reaction mechanism of CO ₂ coupling with terminal	23		
	alkynes to synthesize alkynyl carboxylic acids through C-C bond			
	formation catalyzed by COF. AS represents alkynophilic Ag(I)/Cu(I),			
	or Ag(0)/Cu(0) active site.			
5.	The synthesis scheme of COF-SO ₃ H and COF-H, the structural	47		
	models (yellow, Sulfur; red, Oxygen; blue, Nitrogen; grey,			
	Carbon; white, Hydrogen).			
6.	A plausible mechanism for coupling CO ₂ with epoxides catalyzed by	55		
	TpPa-SO ₃ H (only part of the COF unit is shown for clarity).			
7.	Synthesis scheme of bipy-CTF and Cu(I)@bipy-CTF.	72		
8.	A plausible mechanism for the carboxylation of CO ₂ with propargylic	83		
	alcohol catalyzed by Cu(I)@bipy-CTF.			
9.	Synthesis scheme for P-COF and M@P-COF.	99		
10.	A proposed mechanism for the one-step styrene carbonate synthesis	110		
	from styrene and CO ₂ catalyzed by Fe(III)@P-COF.			
11.	The synthesis scheme of Pybpy-COF and Ag@Pybpy-COF.	128		
12.	(a) Plausible reaction mechanism for the carboxylation of terminal	142		
	alkynes with CO ₂ catalyzed by Ag@Pybpy-COF. (b) DFT energy			
	profile for the carboxylation of terminal alkynes with CO ₂ catalyzed			
	by Ag@Pybpy-COF (bond distances are in Å). Color code: grey, C;			

	blue, N; red, O; and pale blue, Ag. For clarity, only a fragment of	
	COF is shown, and hydrogen atoms are omitted.	
13.	(a) Plausible reaction mechanism for the carboxylative cyclization of	144
	propargylic amines with CO ₂ catalyzed by Ag@Pybpy-COF. (b) DFT	
	energy profile for the carboxylative cyclization of PAs with CO ₂	
	catalyzed by Ag@Pybpy-COF (bond distances are in Å). Color code:	
	grey, C; blue, N; red, O; and pale blue, Ag. For clarity, only a	
	fragment of COF is shown and hydrogen atoms are omitted.	

List of Tables

S. No.	Table caption	Page No.
1.	Representative examples of COFs with their CO2 uptake capacities	12
	and Q _{st} values.	
2.	Representative examples of COFs reported for cycloaddition of	20
	epichlorohydrin with CO ₂ .	
3.	Optimization of reaction parameters for cycloaddition reaction of	52
	CO ₂ with epichlorohydrin catalyzed by COF-SO ₃ H.	
4.	Metal/solvent-free fixation of CO ₂ catalyzed by COF-SO ₃ H as	53
	heterogeneous catalyst.	
5.	Optimization table for the carboxylation of 2-methyl-3-butyn-2-ol	78
	catalyzed by Cu(I)@bipyCTF.	
6.	Coupling of CO ₂ with propargylic alcohols catalyzed by	79
	Cu(I)@bipy-CTF.	
7.	Catalytic conversion of CO ₂ from dilute gas to α-aCCs.	81
8.	Optimization table for oxidation of styrene to styrene oxide.	103
9.	Epoxidation of olefins catalyzed by Fe(III)@P-COF.	104
10.	Optimization table for catalytic oxidative carboxylation of styrene	105
	to styrene carbonate.	
11.	One-step oxidative carboxylation of olefins with CO ₂ .	106
12.	Optimization table for the carboxylation of terminal alkynes with	135
	CO ₂ catalyzed by Ag@Pybpy-COF.	
13.	Carboxylation of various terminal alkynes with CO ₂ catalyzed by	137
	Ag@Pybpy-COF.	
14.	Optimization table for the carboxylic cyclization of CO ₂ with	139
	propargylic amines catalyzed by Ag@Pybpy-COF.	
15.	Carboxylative cyclization of propargylic amines with CO ₂ catalyzed	140
	by Ag@Pybpy-COF.	

Notations and Abbreviations

PDAN	1,4-phenylenediacetonitrile
DBU	1,8-diazabicyclo[5.4.0]undec-7-ene
DCbipy	2,2'-bipyridine-5,5'-dicarbonitrile
BDA	1,4-benzenedicarboxaldehyde
Py-NH2	4,4',4'',4'''-(pyrene-1,3,6,8-tetrayl)tetraniline
bpy-CHO	2,2'-bipyridyl-5,5'-dialdehyde
α-aCCs	Alpha-alkylidene cyclic carbonates
AS	Active sites
ACN	acetonitrile
AGE	Allyl glycidyl ether
Å	Angstrom
a. u.	Arbitrary unit
BA	Brønsted acid
BET	Brunauer-Emmett-Teller
BGE	Butyl glycidyl ether
BE	Binding energy
bpy	Bipyridine
CO ₂	Carbon dioxide
CCS	Carbon capture and storage
CCU	Carbon capture and utilization
CCs	Cyclic carbonates
COFs	Covalent-organic frameworks
CTFs	Covalent-triazine frameworks
Cu NPs	Copper nanoparticles
CP-MAS	Cross polarization magic angle spinning
¹³ C NMR	Carbon nuclear magnetic resonance
Cs ₂ CO ₃	Cesium carbonate
°C	Degree celsius
DCM	Dichloromethane
Et ₂ O	Diethyl ether
DMSO	Dimethyl sulfoxide
DFT	Density functional theory
ECH	Epichlorohydrin
eV	Electron volt
EDS	Energy dispersive X-ray spectroscopy
FT-IR	Fourier-transform infrared spectroscopy
¹⁹ F NMR	Fluorine nuclear magnetic resonance
g	Gram
HBD	Hydrogen bond donor

HNU	Henan Normal University
ННТР	Hexahydroxytriphenylene
HR-TEM	High-resolution transmission electron microscopy
肛	Ionic-liquid
PhIO	Iodosobenzene
Qst	Isosteric heat of adsorption
JLU	Jilin university
K	Kelvin
MOFs	Metal-organic frameworks
MPa	Megapascal
MgSO ₄	Magnesium sulphate
mg	Milligram
mL	milliliter
mmol	millimole
mTorr	Millitorr
MP-AES	Microwave-plasma atomic emission
	spectroscopy Nitrous oxide
NO ₂	
DMF	N, N'-Dimethylformamide
1D	One-dimension
OA	Oxidizing agent
PPM	Parts per million
POPs	Porous-organic polymers
PCPs	Porous-coordination polymers
BDBA	Phenyl diboronic acid
PMCR	Povarov multicomponet reaction
PSM	Post-synthetic modification
PXRD	Powder x-ray diffraction
KOH	Potassium hydroxide Potassium carbonate
K ₂ CO ₃ ¹ H NMR	
	Proton nuclear magnetic resonance
RT	Room temperature Round bottom flask
RBF	
P/Po	Relative pressure
SCs	Styrene carbonates
Ag NPs	Silver nanoparticles
SO	Styrene oxide
SEM	Scanning electron microscopy
NaHCO ₃	Sodium bicarbonate
SAED	Selected area electron diffraction
Na ₂ CO ₃	Sodium carbonate

2D	Two-dimension
3D	Three-dimension
Td	Tetrahedral
TBAB	Tetra-n-butylammonium bromide
TON	Turnover number
TGA	Thermogravimetric analysis
TPD	Temperature-programmed desorption
THF	Tetrahydrofuran
TS	Transition state
TAPP	Tetra(p-amino-phenyl)porphyrin
wt%	Weight percentage
XPS	X-ray photoelectron spectroscopy
ZnCl ₂	Zinc chloride

Chapter 1 Introduction

Chapter 1

Introduction

Chapter 1 Introduction

1.1 Carbon dioxide (CO₂), a greenhouse gas

The current energy demand for human activities is met primarily through fossil fuels and natural gas combustion. This process emits greenhouse gases such as CO₂, NO₂, and other fluorinated gases (Figure 1a). Hence, the level of CO₂ in the atmosphere is fast growing, and it has surpassed 425 ppm currently.² Figure 1b illustrates the overall CO₂ emissions across various economic sectors globally. The highest emissions originate from industry, electricity production, agriculture, and transportation, followed by other energy-related processes (Figure 1b).3 This rising concentration of CO₂ has caused a plethora of environmental concerns, including global warming, extreme weather conditions, and overall elevation of Earth's atmospheric temperature.^{4,5} To address the rising concentration of CO₂, extensive research endeavors are underway worldwide in the realms of carbon capture, storage (CCS), and utilization (CCU).⁶⁻¹⁰ However, current CCS technology demands significant energy for processes such as purification, separation, transportation, and storage. 11-13 A novel and valuable approach is carbon capture and utilization (CCU) as a C1 source for synthesizing valuable chemicals and fuels. The process of CCU offers numerous advantages, particularly in addressing energy-related issues.¹⁴

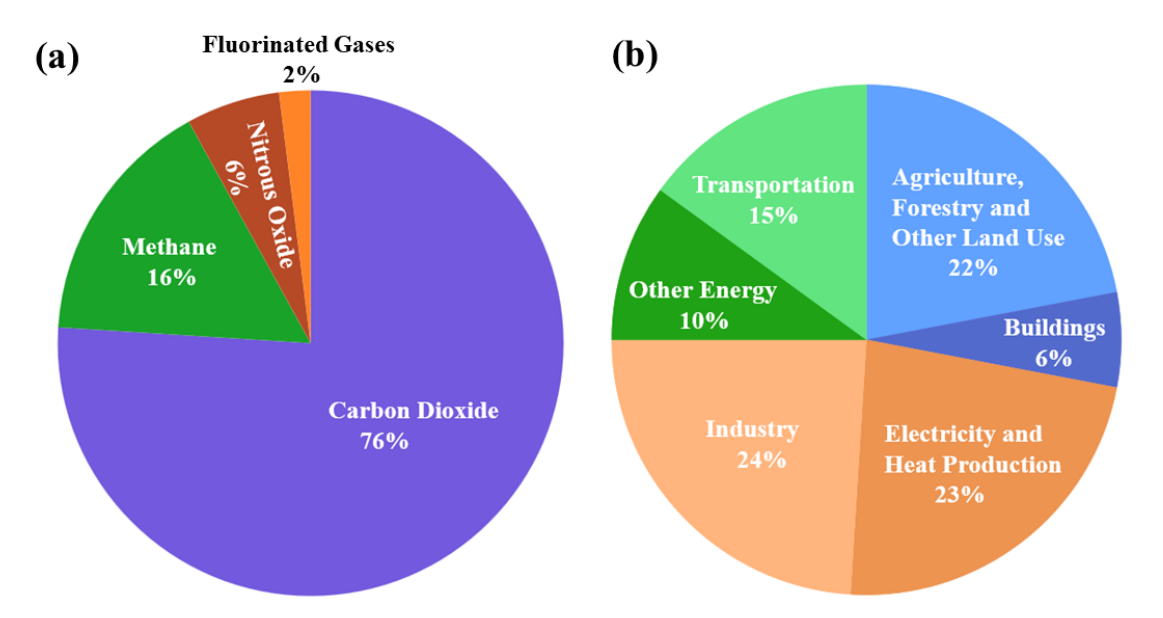


Figure 1. (a) Global greenhouse gas emissions. (b) Global greenhouse gas emission by different economic sectors.

1.2 Carbon capture and utilization

The exploitation of carbon dioxide (CO₂) as a C1 source offers the dual benefits of mitigating atmospheric CO₂ levels and generating value-added chemicals. 15-17 Carbon dioxide is an easily accessible, cheap, and harmless C1 source, making it an attractive candidate for chemical synthesis. The feasibility of coupling CO₂ with various organic molecules enables production of a diverse array of chemicals and fuels, as illustrated in Figure 2. Consequently, employing CO₂ as a C1 source to generate value-added compounds has become a significant area of research worldwide. At the same time, industrial applications of CO₂ include the production of useful chemicals, such as urea, methanol, and salicylic acid. Besides, carbon dioxide is utilized in the food and beverage sectors. Thus, it is imperative to explore new and efficient methods for utilizing CO₂ in the development of value-added compounds, especially cyclic carbonates, oxazolidinones, α-alkylidene cyclic carbonates (αCCs), formamides, alkynyl carboxylic acids, carbamates, etc., (Figure 2). In this regard, various synthetic pathways have been established to effectively convert CO₂ into important compounds. For example, Cyclic carbonates are produced via cycloaddition reaction of epoxides with CO₂. Oxazolidinones are formed through carboxylative cyclization of propargylic amines with CO₂. The α -Alkylidene cyclic carbonates (α -aCCs) are formed by coupling propargylic alcohols with CO₂. Formamides are generated by reacting amines with CO₂ and alkynyl carboxylic acids/phenylpropiolic acids are formed through carboxylative cyclization of terminal alkynes with CO₂. These compounds have broad applications in industry and pharmaceuticals synthesis. For example, cyclic carbonates are employed as electrolytes in batteries and polar aprotic liquid solvents. Oxazolidinones and alkynyl carboxylic acids have significant pharmaceutical applications, including the production of antibiotics and anticancer medications.

However, utilization of CO₂ at ambient conditions poses challenges due to its high C-O bond dissociation energy (805 kJ/mol) and kinetic inertness. Hence, there is significant scope for developing effective catalysts that efficiently adsorb CO₂ and transform it into valuable compounds under ambient conditions.¹⁸ It is worth noting that, for optimal catalytic activity, the catalyst should possess high CO₂-philic basic and catalytic sites along with high surface area, thermal/chemical stability.^{19,20} In search of ideal catalytic systems, researchers worldwide are making extensive research efforts to develop effective catalytic processes for carbon dioxide capture and

conversion to various value-added compounds.²¹⁻²⁷ However, heterogeneous catalysts are crucial in practical applications because they can eliminate the issues of product separation and catalyst recyclability.²⁸⁻³⁰ In the literature, there are various heterogeneous catalysts reported for transformation of CO₂ to high-value chemicals, including metal-oxides, metal-organic frameworks (MOFs), covalent organic frameworks (COFs), etc.³¹⁻³⁵ Considering the unique advantages of COF-based materials, their excellent ability to capture carbon dioxide has been utilized to design efficient, reusable catalysts for concurrent capture and transformation of CO₂ into useful compounds under ambient conditions.^{36,37}

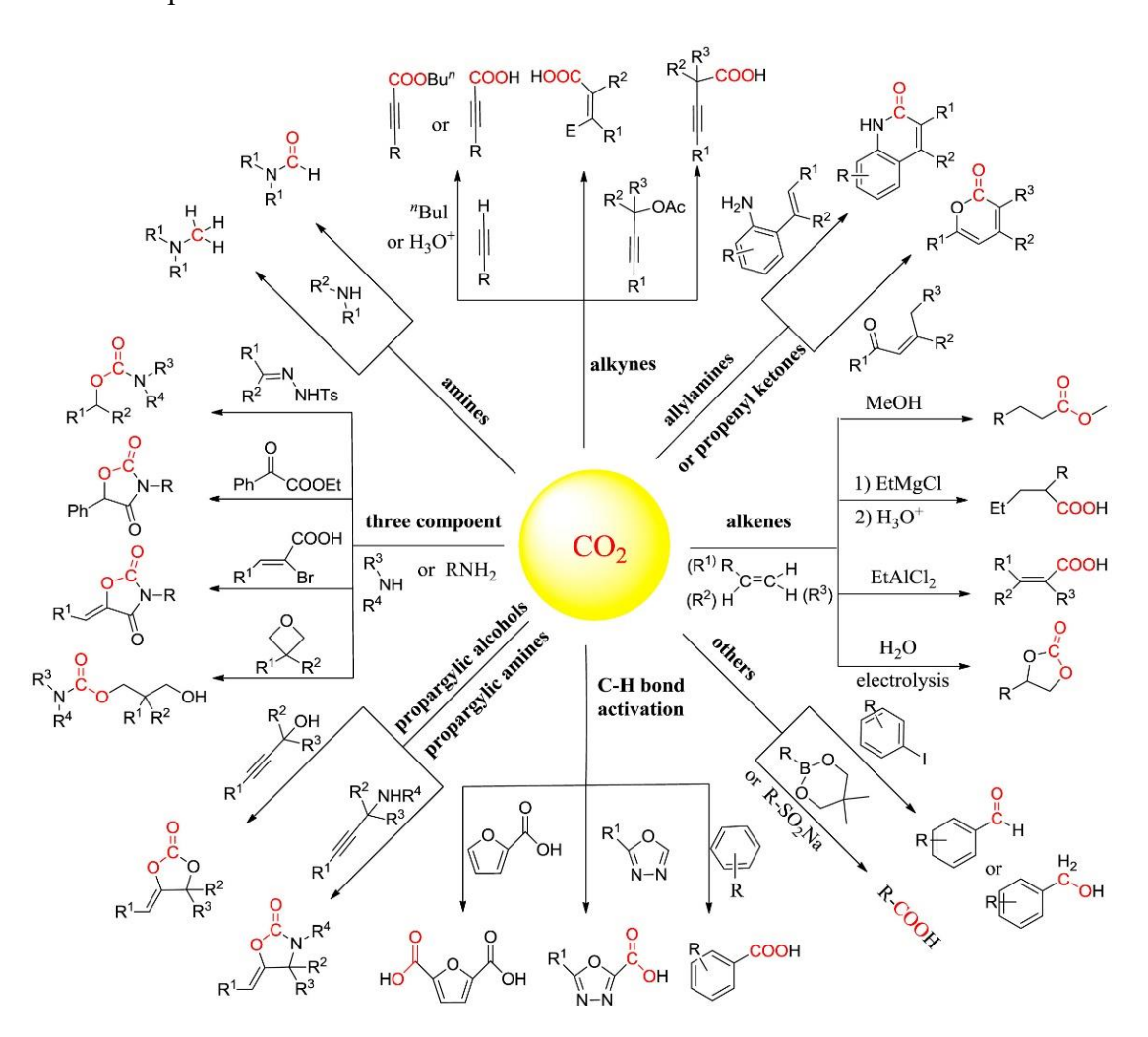


Figure 2. Schematic representation of CO₂ utilization as a C1 source in constructing various value-added compounds. Reproduced with permission from reference 38.

1.3 Framework-based materials

1.3.1. Metal-Organic Frameworks (MOFs)

MOFs, also known as porous coordination polymers (PCPs), represent an innovative genre of crystalline inorganic-organic hybrid porous materials. MOFs are synthesized by coordination bonds between metal nodes and multi-functional organic molecules, forming extended 1D, 2D, or 3D structures. 39,40 These frameworks exhibit remarkable attributes, including high crystallinity, excellent surface area, variable pore dimension, and functionality. 41,42 These exceptional properties enable MOFs to be utilized in various applications, including gas capture/separation, 43 catalysis, 44 sensing, 45 proton conduction, 46 energy storage 47,48, and drug delivery. 49 Among these applications, conversion of CO₂ into useful chemicals/fuels is of particular interest.⁵⁰ The rational integration of organic linkers with CO₂-philic sites and Lewis acidic metal nodes as catalytic sites renders them highly effective heterogeneous catalysts for specific CO₂ adsorption and transformation. The transformation of CO₂ to cyclic carbonates by coupling with epoxides has been widely investigated using MOFs as recyclable catalysts. 51,52 The Lewis acidic metal nodes in MOFs are potential sites for polarizing epoxides, which further couple with CO₂ to produce cyclic carbonates under ambient conditions. In addition, MOFs have been utilized as effective catalysts for transforming CO₂ into various commodity chemicals.

1.3.2. Covalent-Organic Frameworks (COFs)

COFs are an emerging class of crystalline porous organic polymers constructed from organic linkers composed of light elements (B, C, N, O, S, and F) through covalent bonding to form extended 2D or 3D framework structures.⁵³⁻⁵⁶ In COFs, the organic building units are generally connected via strong covalent bonds. The strong covalent connections within the building units are crucial in forming extended crystalline networks. The distinctive properties of COFs include large surface area, crystallinity, thermal/chemical stability, and tailored properties, making them ideal catalysts for various applications.^{57,58} These applications encompass gas adsorption/separation, sensing, proton conduction, catalysis, energy storage, etc.⁵⁹⁻⁶³ COFs are synthesized using various organic linkers to construct frameworks with diverse architectures. The pore dimensions and functionality can be finely modified by using appropriate linkers, rendering the creation of COFs with 1D, 2D, or 3D

structures, as illustrated in Figure 3. The 1D COFs are linear or rod-like structures where the covalent connectivity extends primarily in one dimension (Figure 3). 64 The 2D COFs are planar frameworks with covalent bonds extending in two directions, generating sheet-like networks. 65 These layers stack on top of one another through weak van der Waals interactions or π - π stacking. On the other hand, 3D COFs represent the most complex and fully interconnected networks, extending in three spatial dimensions. 66 These 3D covalent linking render rigid, highly porous structures featuring exceptional stability and large surface area. The synthesis of 1D, 2D, or 3D COFs can be achieved by rationally choosing organic building blocks. For instance, a $C_2 + C_2$ amalgamation of organic building units along a direction forms 1D COF. While a combination of $C_3 + C_2$ or $C_3 + C_3$ linkers results in hexagonal COFs, and $C_4 + C_2$ combination affords tetragonal COFs with an extended 2D structure. 53 It is important to highlight that formation of 3D COFs requires a minimum of one tetrahedral (Td) organic unit. 56 For example, a combination of tetrahedral node with a C_2 or C_3 organic building block renders 3D COFs, as depicted in Figure 3.

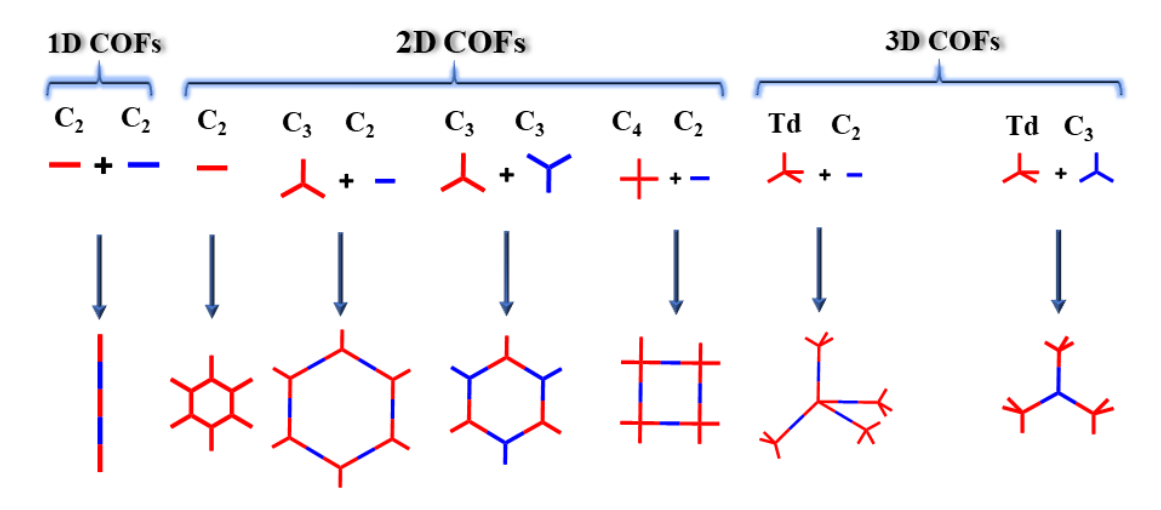


Figure 3. Construction of 1D chain, 2D sheet, and 3D framework of COFs connected through different linkers.

1.3.2.1. History of COFs

In 2005, Yaghi and co-workers developed the first 2D COF through a condensation reaction involving phenyl diboronic acid (BDBA).⁶⁷ Further, Yaghi's group constructed a second COF (COF-5) by condensation reaction of diboronic acid (BDBA) with hexahydroxytriphenylene (HHTP).⁶⁷ Notably, the COFs with boroxine and boronate linkages are known to exhibit remarkable thermal stability. In 2008,

Thomas and co-workers developed triazine-based frameworks.⁶⁸ Thus, the first covalent triazine framework (CTF) was constructed by cyclotrimerization of 1,4dicyanobenzene in molten ZnCl₂ at 400 °C. ⁶⁸ The synthesized CTF exhibited superior thermal stability compared to boron-based COFs. In 2009, Yaghi and co-workers prepared the first imine-based (C=N) 3D COF by employing tetrahedral tetra-(4anilyl)-methane and linear terephthalaldehyde through solvothermal method.⁶⁹ These imine-based COFs offer intriguing applications in numerous areas, including gas adsorption/separation, energy storage, catalysis, sensing, etc. 70-73 Baneriee, and coworkers synthesized β-ketoenamine-linked COFs in 2012 by Schiff-base condensation reaction of 1,3,5-triformylphloroglucinol with p-phenylenediamine. ¹⁰⁹ The synthesized COFs exhibited significant chemical endurance in both acidic and basic environments, owing to significant intramolecular (N-H...N) hydrogen bonding interactions within the framework layers. This advancement signifies a promising stride in COFs, presenting a gateway for global researchers to fabricate and employ chemically stable frameworks in diverse catalytic applications. Besides, several other research groups have developed COFs that exhibit high stability by employing various linkages, viz squaraine, azine, imide, and sp² carbon-linked COFs. 74-78 It has been demonstrated that sp² carbon-linked COFs (olefin/vinylene-based) synthesized through Knoevenagel condensation of aromatic aldehydes and nitriles have received great attention owing to presence of π-electron conjugated network. Thus, in 2019, Wang and co-workers successfully developed the first olefin-linked COF by employing phenylenediacetonitrile (PDAN) and porphyrin aldehyde via a base-catalyzed Knoevenagel condensation reaction.⁷⁹ Overall, the development of numerous COFs by utilizing different linkages has greatly broadened their scope for applications in several fields, including gas adsorption, separation, sensing, catalysis, and CCU. 80-82

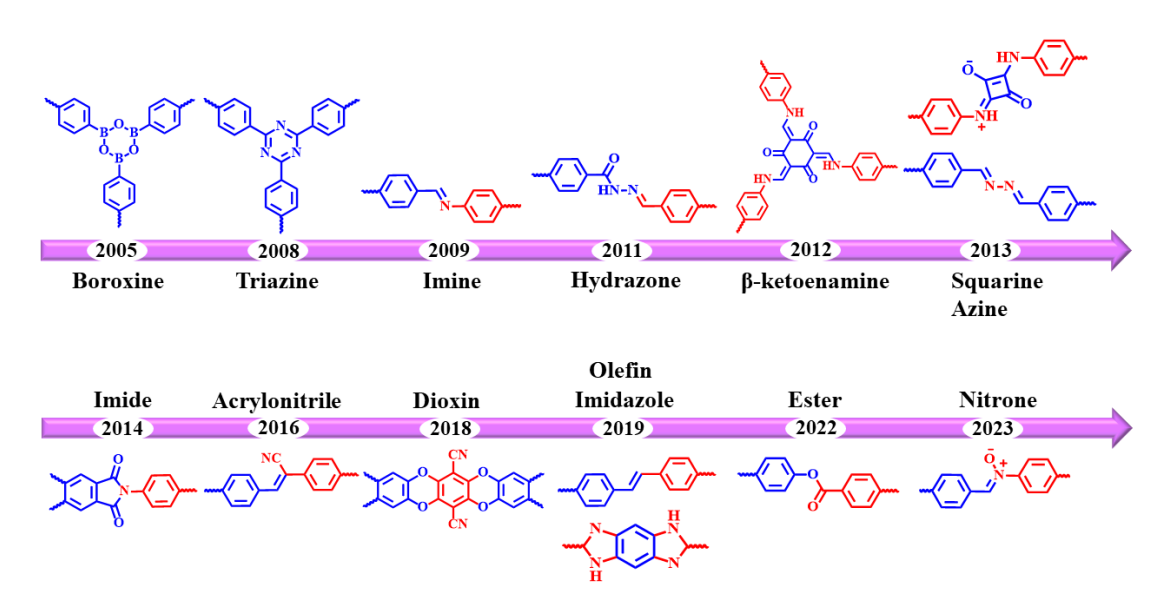


Figure 4. Development of COFs with different linkages.

1.4. Applications of COFs

The distinct properties of COF-based materials, especially large surface area, adjustable pore size, functionality, and chemical constancy, render them excellent catalysts for various applications including gas adsorption/separation, sensing, drug delivery, catalysis, and energy storage (Figure 5). 83-86 These innovative properties of COFs inspired us to develop efficient framework materials that can absorb CO₂ and simultaneously convert it into valuable chemicals under ambient conditions.

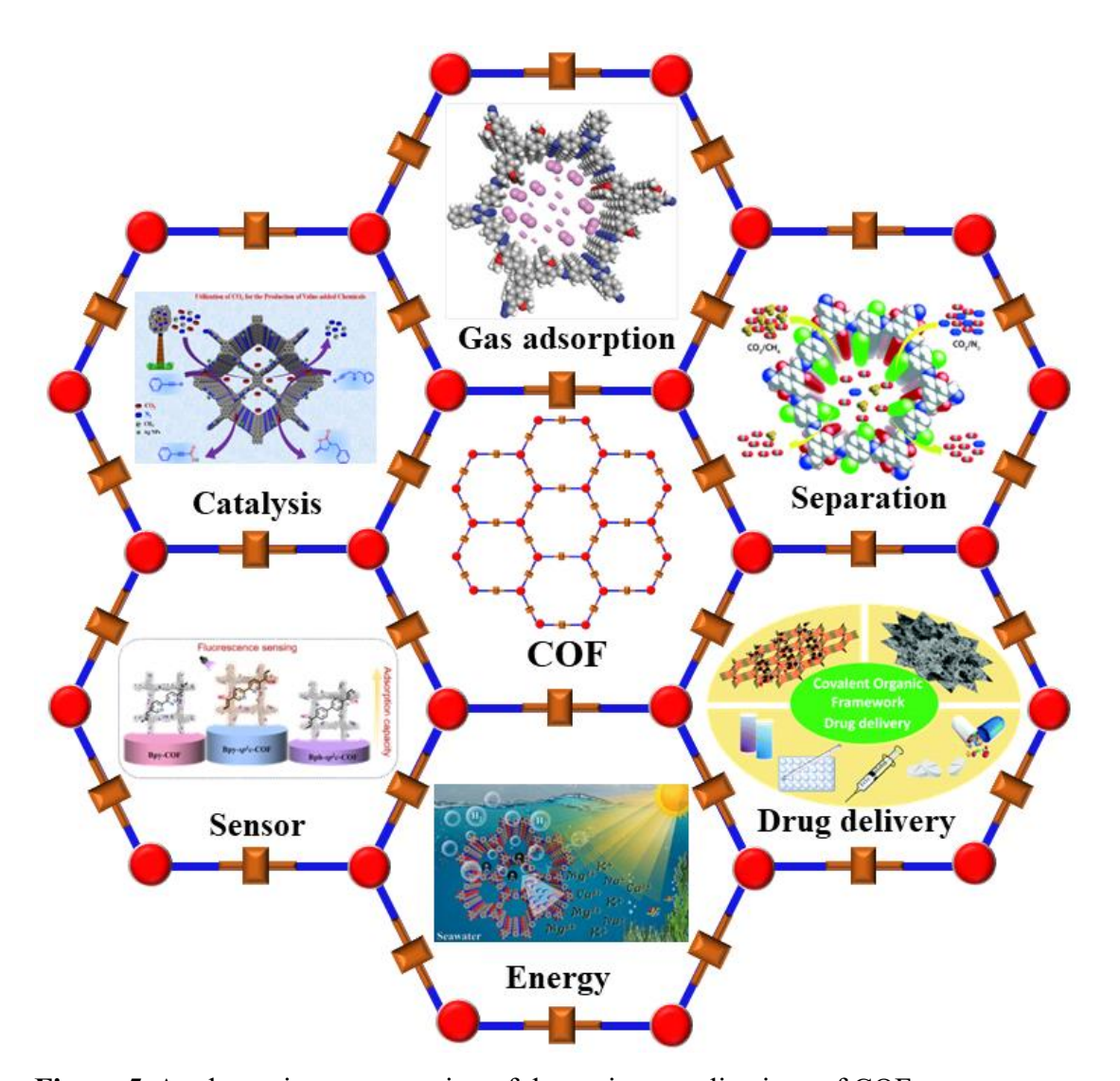


Figure 5. A schematic representation of the various applications of COFs.

1.5. COFs for CO₂ capture and utilization

1.5.1. COFs for CO₂ capture

The literature study demonstrated that COFs offer significant potential for CO₂ capture and storage (CCS) applications owing to their pre-designed structures and customized functions by incorporation of desired polar (-COOH, -OH, SO₃H), and basic imine (C=N), Azo (N=N) moieties within the framework.⁸⁷⁻⁸⁹ In the literature, several COFs have been described for applications in CO₂ capture and storage (CCS).⁹⁰⁻⁹² It has been extensively proven that incorporating polar functional groups viz -NH₂, -OH, SO₃H, -COOH, and CO₂-philic basic sites within the COF framework significantly enhances CO₂ uptake.⁹³⁻⁹⁵ These functional groups improve carbon dioxide adsorption capacity, facilitating efficient capture and storage.⁹⁶⁻⁹⁹ A few notable examples of COFs reported for substantial CO₂ adsorption at 273 K

temperature and 1 bar CO₂ pressure, together with their Q_{st} value, have been listed in Table 3. In 2015, Jiang and co-workers synthesized imine-based COF employing porphyrin amine [Tetra(p-amino-phenyl)porphyrin (TAPP)] and aromatic aldehydes [2,5-dihydroxyterephthalaldehyde (DHTA) + 1,4-phthalaldehyde (PA)] under solvothermal conditions, and it was further functionalized with succinic anhydride to introduce carboxylic acid groups onto the 1D channel walls of the framework.¹⁰¹ The fully functionalized COF ([COOH]_{100%}-H₂P-COF) showed significantly high CO₂ adsorption of 89 cc/g (Q_{st} value of 43.5 kJ/mol) in contrast to non-functionalized COF ([HO]_{100%}-H₂P-COF) with 32 cc/g (Q_{st} value of 36.6 kJ/mol) at 273 K and 1 bar pressure. The high CO₂ adsorption of carboxylic acid functionalized COF has been attributed to the availability of extensive binding sites for CO₂ molecules. Additionally, the carboxylic acid groups contribute to a higher isosteric heat of adsorption.^{101,108}

Further, in 2013, Han and co-workers synthesized two covalent triazine frameworks (CTFs) named CTF-1-600 and FCTF-1-600 by treating terephthalonitrile and tetrafluoroterephthalonitrile with ZnCl₂. ¹⁰⁴ Notably, the CTF (FCTF-1-600) constituted by fluorinated linker showed high CO₂ uptake of 124 cc/g over nonfluorinated CTF (80 cc/g) at 273 K and 1 bar CO₂ pressure. The enhanced CO₂ uptake of perfluorinated CTF (FCTF-1-600) is associated with greater interaction of CO₂ molecules ($Q_{st} = 32 \text{ kJ/mol}$) with the electronegative fluorine atoms exposed in the 1D channels of the framework. Further, basic nitrogen sites are known to support greater interaction of CO₂ molecules with the framework. For instance, Liu and co-workers reported azine-linked COF (ACOF-1), produced by reaction of 1,3,5-triformylbenzene with hydrazine hydrate using solvothermal method, which demonstrated improved CO₂ uptake of 90 cc/g at 273 K, 1 bar CO₂ owing to presence of basic azine groups. ¹⁰⁵ The increased CO₂ adsorption has been ascribed to favorable interaction of carbon dioxide with azine groups exposed within the COF. Further, Banerjee and co-workers conducted a CO₂ uptake study on triformylphloroglucinol (Tp) based COFs. They synthesized various Tp-based COFs using different functional amines, namely TpPa-1, TpPa-2, TpPa-NO₂, and TpPa-F₄. Notably, TpPa-1 demonstrated an impressive CO₂ uptake capacity of 78 cc/g at 273 K and atmospheric pressure (Table 1). 109,112 Several other examples have been reported in the literature utilizing functionalized COFs for achieving high CO₂ uptake, as summarized in Table 1. Thus, the advancement of

COFs as highly efficient adsorbent catalysts for substantial CO₂ adsorption under ambient pressure and temperature conditions is being extensively explored worldwide.

Table 1: Representative examples of COFs with their CO_2 uptake capacities and Q_{st} values.

S. No.	COFs	Bond type/	CO ₂ uptake	Q _{st} (kJ/mol)	References
		Functionality	(cc/g)		
1.	[COOH] _{100%} -	Imine/COOH	89	43.5	101
	H ₂ P-COF				
2.	TBICOF	-NH	68.89	42.8	100
3.	[OH] _{100%} -	Imine/OH	32	36.4	101
	H ₂ P-COF				
4.	FCTF-1-600	Triazine/F	124	32.0	104
5.	COF-SO ₃ H	Imine/-SO ₃ H	54.5	31.4	93
6.	COF-JLU-2	Azine	110	31.0	102
7.	COF-IL	Imidazolium-	106.04	30.2	103
		IL			
8.	CTF-1-600	triazine	80	30.0	104
9.	ACOF-1	Azine	90	27.6	105
10.	TDCOF-5	Boronate	47	21.8	106
11.	[EtNH ₂] ₁₀₀ -	Imine/ NH ₂	49	20.9	108
	H ₂ P-COF				
12.	[EtOH] ₁₀₀ -	Imine/OH	43	19.3	108
	H ₂ P-COF				
13.	[AcOH] ₁₀₀ -	Imine/COOH	49	18.8	108
	H ₂ P-COF				
14.	ILCOF-1	imine	31	18.3	107
15.	[MeOAc] ₁₀₀ -	Imine/COOMe	33	17.8	108
	H ₂ P-COF				
16.	[Et] ₁₀₀ -H ₂ P-	Imine/CH ₃	19	15.3	108
	COF				
17.	TpPa-1	Imine/H	78	-	109
18.	COF-DhaTab	Imine/OH	78	-	110
19.	TpPa-2	Imine/CH ₃	64	-	109
20.	DhaTph	Imine/OH	65	-	111

21.	TpPa-NO ₂	Imine/NO ₂	73	-	112
22.	COF-1	Boroxine	51	-	113
23.	DmaTph	Imine/OMe	37	-	111
24.	TpPa-F ₄	Imine/F	35	-	112

1.5.2. COFs for CO₂ utilization

COFs have gained significant interest as potential candidate materials for CCU because of their adjustable pore sizes and functional properties. COFs can be engineered to exhibit precise pore sizes and high surface areas, facilitating efficient CO₂ adsorption and transformation to value-added compounds. The inclusion of polar functional moieties, for instance, amines (-NH₂), carboxylic acids (-COOH), and sulfonic acids (-SO₃H) enhances their CO₂ uptake performance. The free amines within the framework react with CO₂ to generate carbamate species, whereas carboxylic acids and sulfonic acids interact with carbon dioxide through hydrogen bonding and other non-covalent interactions. ^{101,114} These interactions enhance the framework's affinity for CO₂ and its selective capture performance. ^{93,115} This enhances COFs performance to adsorb significant amounts of CO₂ even under ambient conditions.

Furthermore, the potential of COFs to integrate catalytic sites opens up avenues for converting captured CO₂ into valuable chemicals and fuels. Thus, CCU provides the combined advantage of decreasing rising carbon dioxide concentration and producing value-added chemicals at ambient conditions. Numerous transformations have been established in literature to employ CO₂ to produce important commodity compounds. Notable catalytic transformations include the generation of cyclic carbonates (CCs) through C-O bond formation between epoxides and CO₂. The coupling of propargylic amines with CO₂ to acquire 2-oxazolidinones, and carboxylation of propargylic alcohols with CO₂ to yield α-alkylidene cyclic carbonates (αCCs) and others (Figure 6). Additionally, carboxylation of terminal alkynes with CO₂ to synthesize bioactive alkynyl carboxylic acids, hydrogenation of CO₂ to generate valuable formic acid, and photo/electrocatalytic CO₂ reduction to generate various fuels are studied (Figure 6).

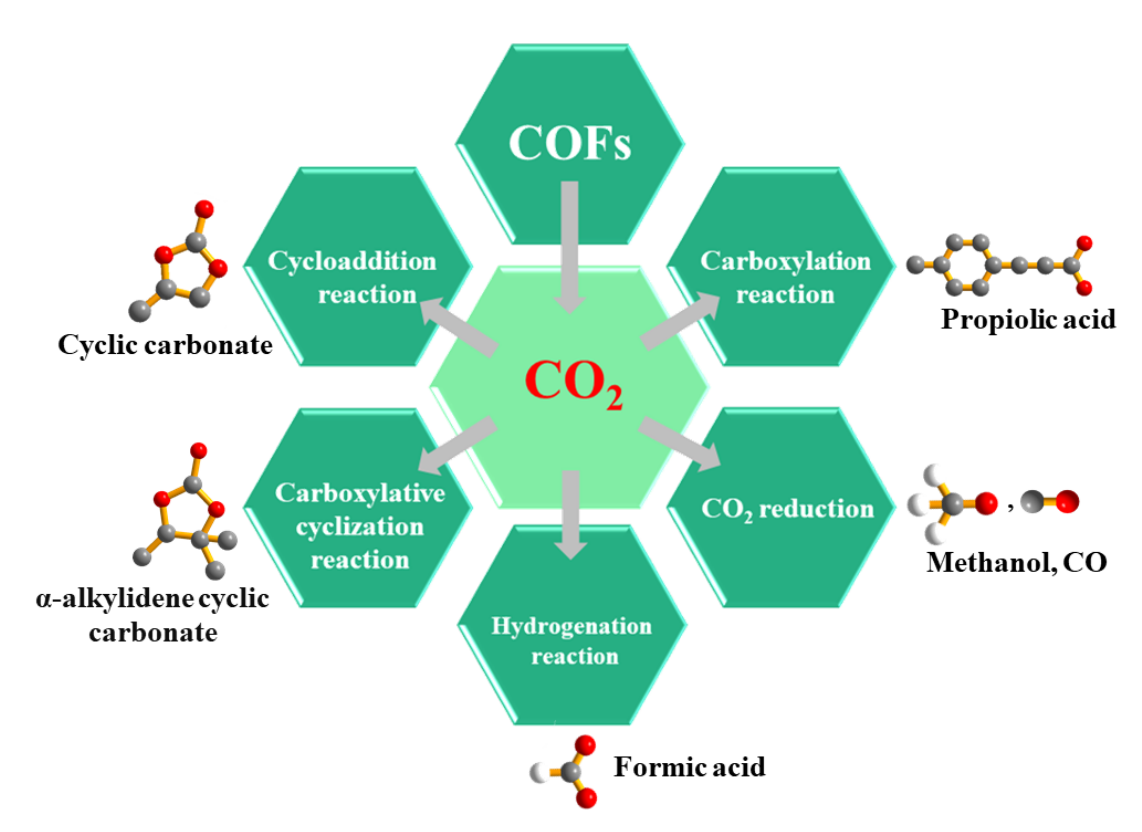


Figure 6. A schematic representation of CO₂ utilization catalyzed by COF catalysts.

Thus COFs offer great potential in CO₂ utilization for synthesis of various useful compounds and fuels. The desired CO₂ transformation determines the choice of active sites and functional groups within COFs, as different catalytic reactions require uniquely designed functionalities to ensure optimal performance and selectivity. Thus, the framework design and its post-synthetic modification processes need to be optimized to obtain COFs with improved structural and functional properties. These approaches are described in detail below (Figure 7).

1.5.2.1. Modification in the backbone of COFs

As reported in the literature, imine-based COFs are extensively utilized in several applications, including the chemical fixation of CO₂ to synthesize various commodity compounds, photocatalytic CO₂ reduction, hydrogen evolution from water, etc. ^{122,123} Despite their versatility, imine-based COFs often face challenges regarding stability when exposed to aqueous environments. It has been demonstrated that the chemical stability of imine-based COFs can be amended by reacting the imine bonds with styrene and epoxides, resulting in formation of stable aromatic linkages with phenyl ring through multicomponent Povarov reaction. ^{124,125} These functionalizations are

anticipated to render COFs with stronger backbone structures (Figure 7a). For instance, Thomas and co-workers constructed a COF (PMCR-1) under solvothermal conditions using triazine-based amine and aldehyde precursors. ¹²⁴ They employed a multicomponent Povarov reaction to generate quinoline-linked COF with enhanced framework stability. This modified aqueous stable COF (PMCR-1) was utilized for photocatalytic hydrogen peroxide (H₂O₂) production.

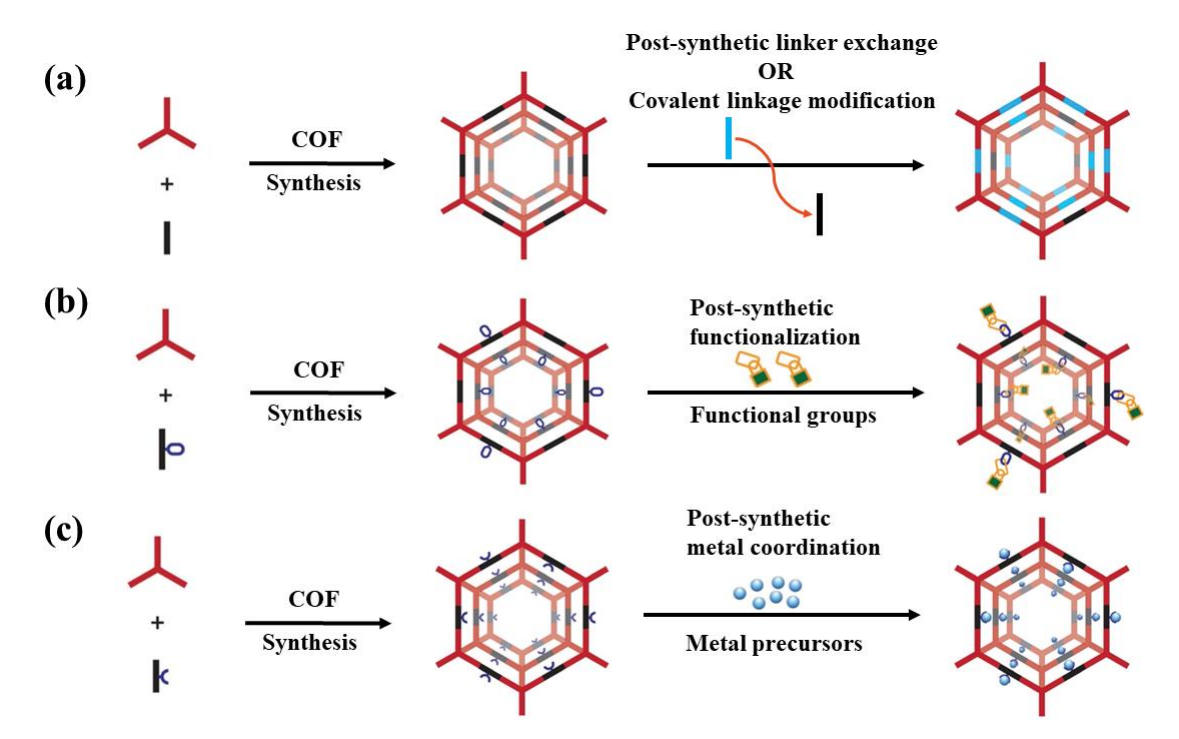


Figure 7. Representation of various strategies to incorporate catalytic active sites into a COF framework. Reproduced with permission from reference number 57.

1.5.2.2. Functionalization of COFs

The rationally functionalized COFs incorporating CO₂-philic and catalytic sites function as bifunctional materials for efficient CO₂ capture and further functionalization to value-added compounds. A key challenge is integrating specific functional groups into the COF skeleton, which is often hindered by rigorous conditions required for solvothermal synthesis. To address this issue, polar functional moieties can be introduced into the COF's framework via chemical reactions, ensuring the framework structure remains intact (Figure 7b).^{126,127} The functionalization of COFs can be accomplished by treating with various reagents which can introduce desired functional moieties like -NH₂, -OH, -SO₃H, -COOH, etc. In literature, various functionalization strategies of COFs and their applications for effective CCU to

synthesize value-added compounds are reported. For instance, Liu and co-workers reported synthesis of two triazine-based COFs (COF-JLU6, COF-JLU7) and their functionalization with hydroxyl groups. 146 These OH-functionalized COFs were subsequently employed for the cycloaddition of epoxides with CO2 to generate value-added cyclic carbonates. The hydroxyl groups in the COF framework promote polarizing the epoxide through hydrogen bonding, enabling the formation of cyclic carbonates. Wang and co-workers developed a hydroxyl-based COF, namely COF-HNU2. 128 The COF was further modified by reacting it with imidazolium-based ionic liquids (ILs) to obtain bifunctional imidazolium-anchored COF and utilized for the chemical functionalization of CO2 to cyclic carbonates. This post-synthetic modification approach enhanced the catalytic efficiency of the COFs. Here, the presence of polar hydroxyl groups functions as Brønsted acidic sites and serves as hydrogen bond donors, facilitating the activation of epoxides to undergo cycloaddition with CO2, resulting in the generation of cyclic carbonates.

1.5.2.3. Incorporation of catalytic active metal sites into COFs

The catalytic conversion efficiency of CO₂ to value-added compounds can significantly improve by strategically incorporating metal catalytic sites into the framework via post-synthetic modification (Figure 7c). Metals such as Zn, Mg, Co, Ag, Ru, Cu, Fe, etc., can be precisely integrated into the anchoring sites of the framework, such as bipyridine sites or free-base porphyrin cavities. 129,130 These metaldoped frameworks exhibit high efficacy in various catalytic conversions, including the generation of cyclic carbonates through the cycloaddition reaction of epoxides with CO₂, among other valuable transformations. For example, Yaghi and co-workers developed cobalt-doped porphyrin-based COFs via Schiff-base condensation reaction of porphyrin amine, tetra(p-amino-phenyl)porphyrin (TAPP) with various functionalized aromatic aldehydes under solvothermal conditions. 122 These synthesized COFs demonstrated potential application in electrocatalytic CO₂ reduction. In a related study, Wang and co-workers constructed porphyrin-based COFs and subsequently doped with various metal ions, including Co(II) and Zn(II). 131 The resulting metal-doped COFs were then employed to generate cyclic carbonates via cycloaddition reaction of CO₂ with epoxides. Further, incorporation of alkynophilic active sites (Ag(0)/Cu(0)) at the bipyridine anchoring sites of the framework considerably increases catalytic activity for the conversion of CO2 to important

compounds. ¹³² For example, the alkynophilic metal sites promote activation of the C \equiv C bond of alkynes and facilitate CO₂ coupling in generating value-added α -alkylidene cyclic carbonates (α CCs). In 2019, Wang and co-workers successfully synthesized an azine-linked three-dimensional COF (3D-HNU5). The synthesized COF was subsequently utilized to stabilize silver nanoparticles (NPs) within the framework. ¹³³ The resulting COF (Ag@3D-HNU5), demonstrated significant catalytic efficiency in functionalizing CO₂ with propargylic alcohols to generate value-added α -alkylidene cyclic carbonates (α CCs) under ambient reaction conditions. Thus, the post-synthetic modification method is useful for stabilizing catalytically active sites within the functionalized pores of the framework to obtain hybrid materials capable of converting CO₂ into valuable chemicals.

1.5.3. Utilization of CO_2 via C-X (X = O, N, and C) bond formation

The framework-based materials provide dual benefits of mitigating rising CO_2 concentration and producing new value-added compounds under mild conditions. Moreover, numerous value-added chemicals and fuels have been generated by the chemical fixation of CO_2 through C-X (X = O, N, and C) bond formation between CO_2 and substrate molecule under mild conditions (Figure 8). As a result, substantial research initiatives have been devoted to the rational creation of CO_2 -based catalysts for the chemical transformation of CO_2 into useful chemicals and fuels, as shown below.

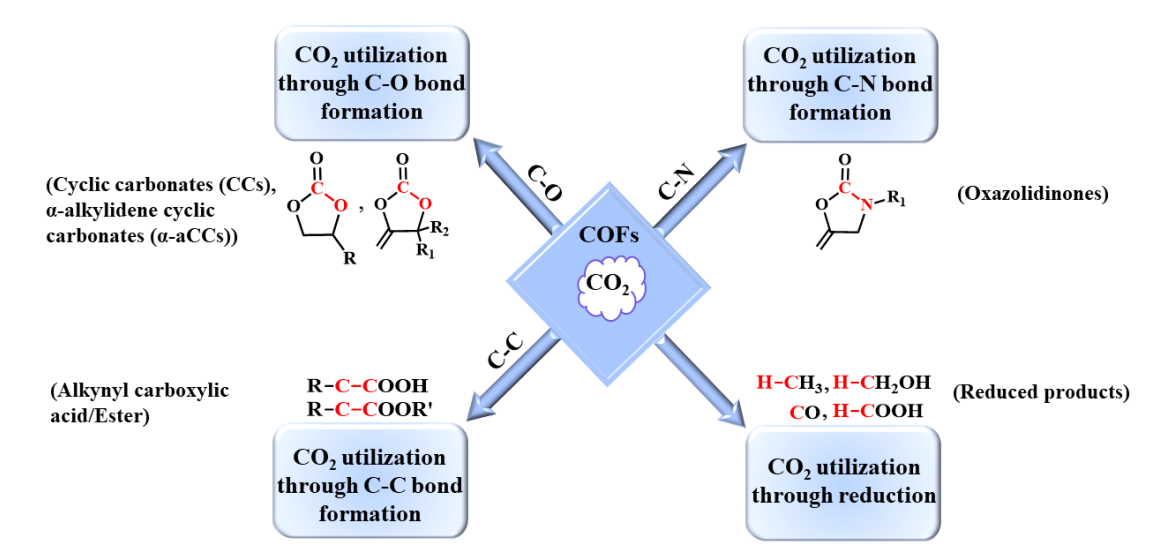


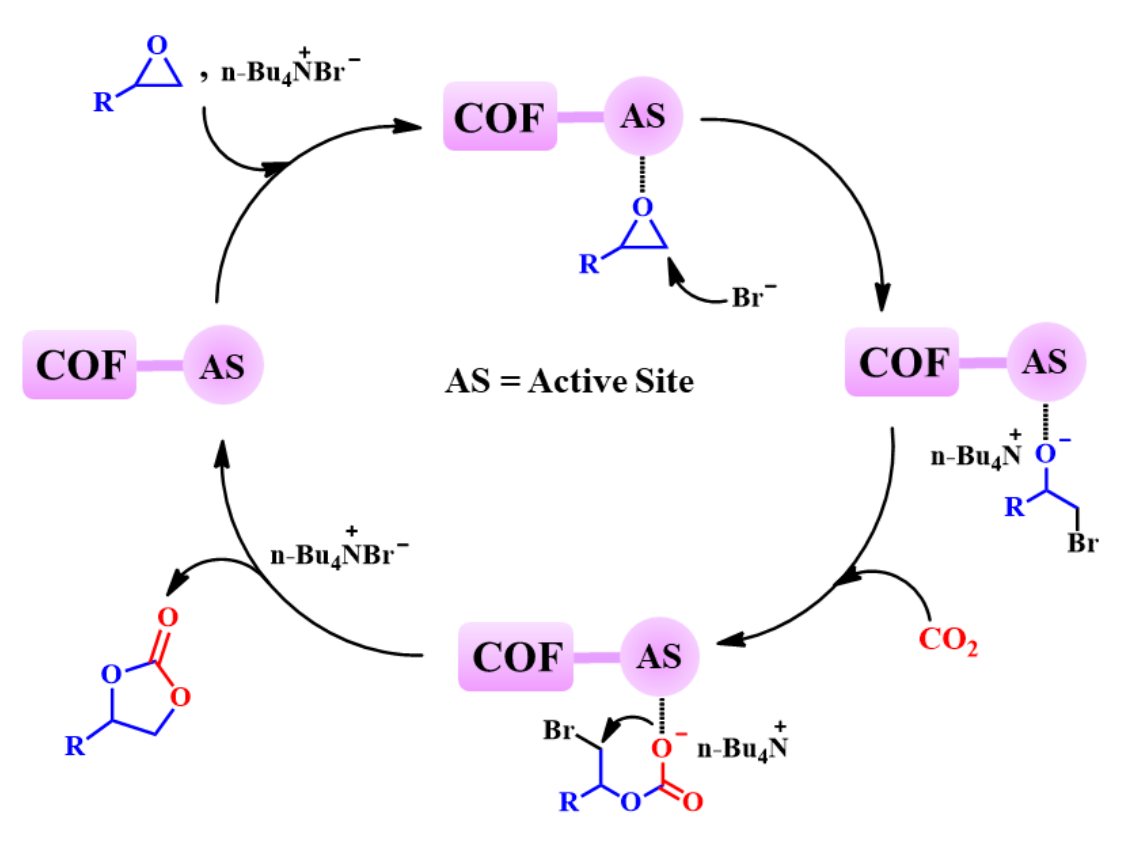
Figure 8. Utilization of CO₂ through C-X bond formation.

1.5.3.1. Utilization of CO₂ via C-O bond formation

The cycloaddition of epoxides with CO₂ via C-O bond formation has garnered significant attention lately because of its high atom efficacy, leading to cyclic carbonates with 100% selectivity. 135,136 The resulting cyclic carbonates offer extensive uses in the pharmaceutical and industrial fields. For instance, they are employed as electrolytes in lithium-ion batteries, substrates for polymer synthesis, and polar aprotic chemicals, etc. 137,138 Numerous homogeneous catalysts, including ionic liquids, 139 metal complexes, 140 and quaternary ammonium salts, 141 have been reported for the conversion of CO₂ to cyclic carbonates using epoxides. However, to facilitate product separation and catalyst recycling, heterogeneous catalysts, including carbon-based materials, 142 metal oxides, 143 zeolites, 144 metal-organic frameworks (MOFs), 145 covalent organic frameworks (COFs),93 and covalent triazine frameworks (CTFs)78 have been employed in functionalization of CO₂ with epoxides to generate CCs. Particularly, COFs show potential for fixation of carbon dioxide to cyclic carbonates (CCs) owing to their distinctive structural characteristics composed of significant CO₂philic basic and Lewis/Bronsted acidic sites. These features enhance the uptake of CO₂ and epoxide polarization, thereby promoting the efficient formation of cyclic carbonates. In some cases, COFs enable in reducing the necessity of metal ions employed to polarize epoxides in synthesizing cyclic carbonates. 100,146 Additionally, their stability under mild conditions further enhances their appeal for sustainable and environmentally friendly catalytic processes. The Brønsted acidic sites (-SO₃H, -COOH, -OH) within the framework support polarization of epoxides in cyclic carbonate synthesis.

The plausible reaction mechanism for the generation of cyclic carbonates via chemical reaction of CO₂ with epoxides through C-O bond formation is shown in Scheme 1. To accomplish effective coupling of CO₂ with epoxides, the catalyst should be composed of Brønsted acidic active sites (AS), which are utilized for the polarization of the epoxides, along with a nucleophilic co-catalyst such as tetra-n-butylammonium bromide (TBAB) for ring opening of polarized epoxide, thereby, promoting the generation of cyclic carbonates. The reaction proceeds with the polarization of epoxide using Brønsted acidic active sites (AS) present within the catalyst. Subsequently, nucleophilic attack of Br⁻ at the less sterically hindered carbon atom of polarized epoxides resulted in the generation of a bromoalkoxide intermediate. Further, CO₂ insertion occurs, leading to an alkyl carbonate anion that undergoes ring

closure to yield five-membered cyclic carbonate as the final product. 93,100 Simultaneously, regeneration of the catalyst takes place, which is reused for subsequent catalytic cycles. The selected examples of COFs known for production of cyclic carbonates are summarized in Table 2.



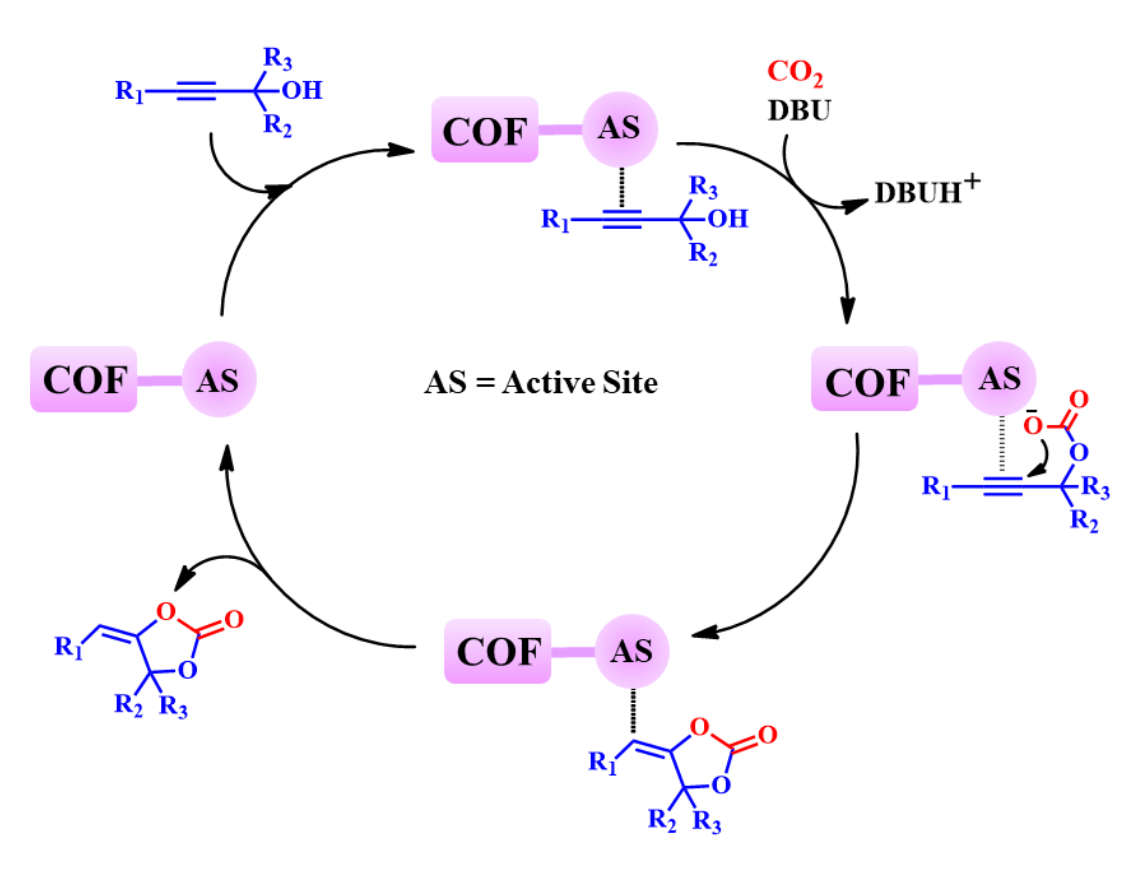
Scheme 1. A plausible reaction mechanism of CO₂ coupling with epoxides to synthesize cyclic carbonates through C-O bond formation catalyzed by COF. AS represents Brønsted acidic active sites such as -SO₃H, -COOH, and -OH.

Table 2: Representative examples of COFs reported for cycloaddition of epichlorohydrin with CO₂.

S. No.	Catalyst	Active sites	Pressure (bar)	Conversion (%)	References
1.	COF-JLU7	-OH	01	92	146
2.	COF-JLU6	-OH	01	86	146
3.	TBICOF	-NH-	01	95	100
4.	2,3-DhaTph COF	-ОН	01	77	147
5.	2,3-DmaTph COF	-OCH ₃	01	63	147
6.	COF-SO ₃ H	-SO ₃ H	01	>99	93
7.	Tp-BD-COF	-NH-	01	99	148
8.	Tp-PD-COF	-NH-	01	87	148
9.	Tp-PMD-COF	-NH-	01	85	148
10.	TFPB-DHBD- COF	-ОН	01	97	149
11.	OMe-TPBP- COF	-OCH ₃	01	48	150
12.	OMe-OH- TPBP-COF	-OCH ₃ /OH	01	91	150
13.	OH-TPBP-COF	-OH	01	89	150

Furthermore, another application of COFs for utilization of CO₂ via C-O bond formation is the production of α -alkylidene cyclic carbonates (α -aCCs) via carboxylation of propargylic alcohols with CO₂. The synthesized α -aCCs have potential utility in synthesis of polyurethanes, polycarbonates, and drugs. The literature study reveals that the transformation of propargylic alcohols to α -aCCs by utilization of greenhouse gas, carbon dioxide has been achieved using alkynophilic Cu(I)/Ag(I) active sites in the framework. A plausible mechanism for carboxylative cyclization of propargylic alcohol with CO₂ to α -aCCs catalyzed by COFs is shown in Scheme 2. In the initial step, the alkyne bond of the propargylic alcohol undergoes polarization through interaction with the active sites (AS) present in the COF. Then,

propargylic alcohol deprotonation occurs with a base, DBU (1,8-diazabicyclo[5.4.0]undec-7-ene). This deprotonation facilitates the insertion of CO_2 molecule, forming a carbamate species. Subsequently, intramolecular cyclization occurs, leading to the generation of α -alkylidene cyclic carbonates (α CCs). At last, the catalyst is regenerated and utilized for subsequent cycles.¹⁹

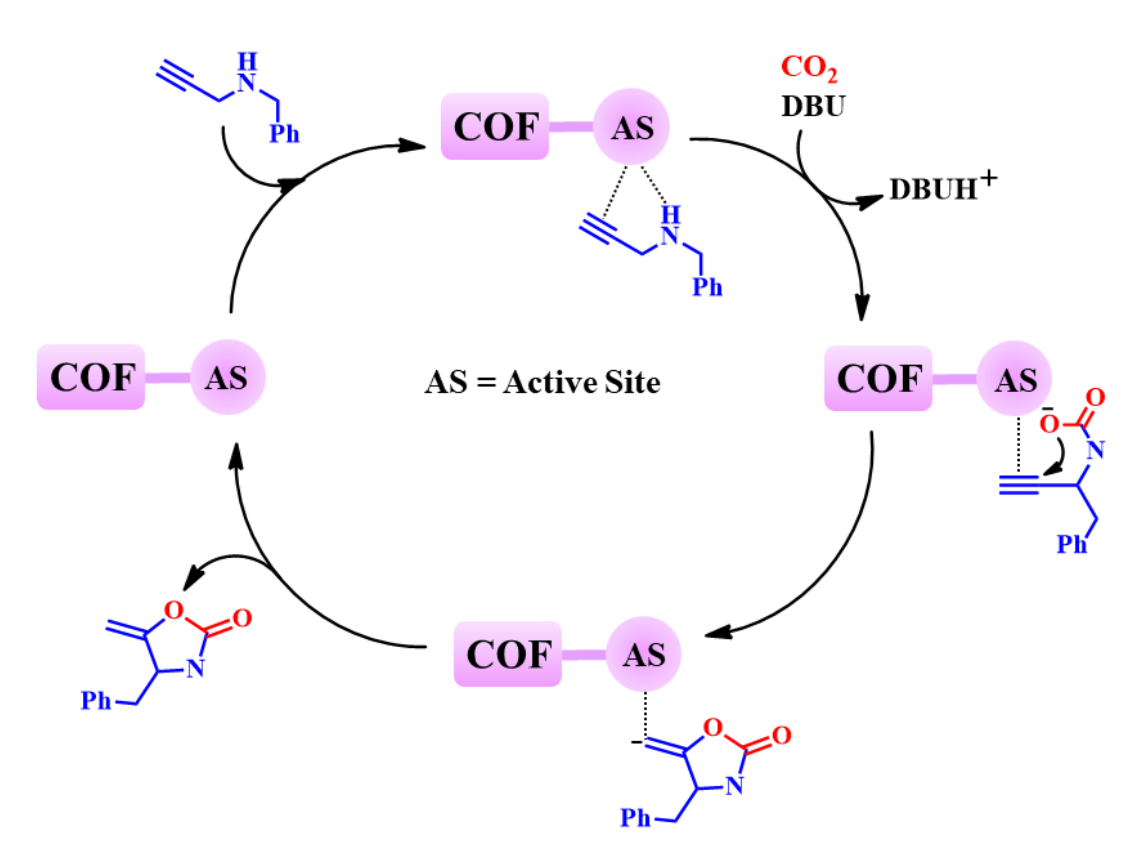


Scheme 2. A plausible reaction mechanism for CO_2 coupling with propargylic alcohol to synthesize α -alkylidene cyclic carbonates through C-O bond formation catalyzed by COF. AS represents alkynophilic Ag(I) or Cu(I) active site.

1.5.3.2. Utilization of CO₂ via C-N bond formation

The utilization of CO₂ through C-N bond formation offers the benefits of mitigating the rising CO₂ concentration and generating bioactive 2-oxazolidinones. This has been achieved by chemical fixation of propargylic amines with CO₂ through carboxylative cyclization. The oxazolidinones offer potential applications as building blocks for synthesis of antibiotics and other pharmaceuticals.¹⁵³ A literature study indicated that alkynophilic Cu(0)/Ag(0) or Cu(I)/Ag(I) are effective for converting propargylic amines to 2-oxazolidinones via carboxylative cyclization with CO₂.¹⁵⁴ The

literature study unveiled that the number of examples of COFs reported for synthesis of 2-oxazolidinones is relatively less compared to that of cyclic carbonates (CCs). Consequently, there is substantial scope for investigating synthesis of 2-oxazolidinones using functionalized COFs by utilization of CO₂. The plausible reaction mechanism for generation of 2-oxazolidinones by coupling propargylic amines with CO₂ through carboxylative cyclization is shown in Scheme 3.



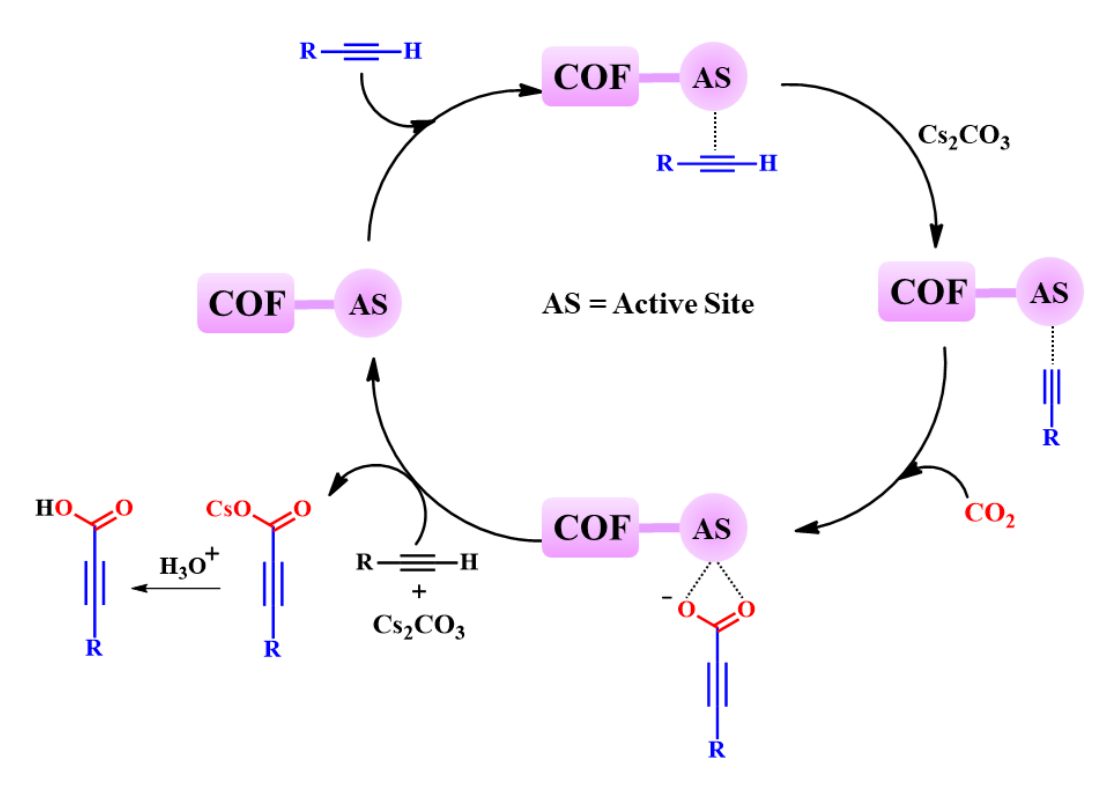
Scheme 3. A plausible reaction mechanism for CO_2 utilization to synthesize 2-oxazolidinones through C-N bond formation catalyzed by COF. AS represents alkynophilic Ag(I) or Cu(I) active site.

In the first step, the C \equiv C bond of propargylic amine is polarized by alkynophilic Cu(0)/Ag(0) or Cu(I)/Ag(I) active sites (AS) present in the framework. Following this activation, propargylic amine is deprotonated using DBU as a base. Subsequently, the insertion of CO₂ takes place, resulting in carbamate formation. The subsequent step involves an intramolecular cyclization process, wherein the carbamate intermediate undergoes rearrangement to form 2-oxazolidinones.¹¹⁷ Finally, 2-oxazolidinone

product is eliminated from the metal center, regenerating the catalyst for further catalytic cycles.

1.5.3.3. Utilization of CO₂ via C-C bond formation

The utilization of CO₂ via C-C bond formation by carboxylation of terminal alkynes to produce alkynyl carboxylic acids/esters has sparked substantial interest. ¹⁵⁵ This process finds potential application in synthesizing antibiotics and anticancer agents, such as flavones, coumarins, and other essential compounds. ¹⁵⁶ The literature reports have demonstrated the necessity of an alkynophilic metal center, such as Cu or Ag, to catalyze this transformation. The Cu/Ag metals play a vital role in facilitating the carboxylation of terminal alkynes with CO₂ to produce alkynyl carboxylic acids/esters. Thus extensive research efforts have been conducted worldwide to advance the carboxylation of terminal alkynes with CO₂ to obtain alkynyl carboxylic acids/esters. The detailed mechanism for the fixation of CO₂ to alkynyl carboxylic acids/phenylpropiolic acids via C-C bond formation through the carboxylation of terminal alkynes with CO₂ catalyzed by COFs is shown in Scheme 4.



Scheme 4. A plausible reaction mechanism of CO_2 coupling with terminal alkynes to synthesize alkynyl carboxylic acids through C-C bond formation catalyzed by COF. AS represents alkynophilic Ag(I)/Cu(I), or Ag(0)/Cu(0) active site.

As discussed before, the reaction proceeds with a polarization of C≡C bond of terminal alkynes at the alkynophilic (Ag/Cu) active site. This step is followed by deprotonation of the alkyne in presence of Cs₂CO₃, resulting in the formation of an Ag-acetylide intermediate. Then, CO₂ insertion occurs in the Ag/Cu-acetylide intermediate to form the corresponding Ag-carboxylate. Subsequently, transmetalation leads to the formation of cesium carboxylate, which, upon hydrolysis, results in the desired product (alkynyl carboxylic acid). The catalyst was regenerated for multiple cycles of reuse.

Overall, with the thesis objectives of CO_2 utilization as a C1 source for generating valuable chemicals using heterogeneous catalysts, we strategically synthesized functionalized COFs. Further, the COFs were utilized for effective CO_2 capture and conversion into valuable commodity compounds, viz cyclic carbonates (CCs), α -alkylidene cyclic carbonates (α -aCCs), 2-oxazolidinones, and bio-active alkynylcarboxylic acids/phenylpropiolic acids under ambient conditions, which are discussed in the subsequent chapters.

1.6. Summary

This chapter provided a brief overview of COFs, their distinctive features, and potential applications. Specifically, we explored the potential of COFs for CO_2 capture and utilization into several valuable chemicals through C-X (X = O, N, and C) bond formation. This discussion sets the stage for further exploration of COFs in the context of sustainable chemistry and green technology.

1.7. References

- (1) Meinshausen, M.; Meinshausen, N.; Hare, W.; Raper, S. C. B.; Frieler, K.; Knutti, R.; Frame, D. J.; Allen, M. R. Greenhouse-gas emission targets for limiting global warming to 2 °C. *Nature* **2009**, *458*, 1158-1162.
- (2) https://www.co2.earth/daily-co2.
- (3) Hernández, S.; Farkhondehfal, M. A.; Sastre, F.; Makkee, M.; Saracco, G.; Russo, N. Syngas production from electrochemical reduction of CO₂: current status and prospective implementation. *Green Chem.* **2017**, *19*, 2326-2346.
- (4) Jacobson, M. Z. Review of solutions to global warming, air pollution, and energy security. *Energy Environ. Sci.* **2009**, *2*, 148-173.

(5) Joos, F.; Plattner, G. -K.; Stocker, T. F.; Marchal, O.; Schmittner, A. Global Warming and Marine Carbon Cycle Feedbacks on Future Atmospheric CO₂. *Science* **1999**, *284*, 464-467.

- (6) Pires, J. C. M.; Martins, F. G.; Alvim-Ferraz, M. C. M.; Simões M. Recent developments on carbon capture and storage: An overview. *Chem. Eng. Res. Des.* **2011**, *89*, 1446-1460.
- (7) Bui, M.; Adjiman, C. S.; Bardow, A.; Anthony, E. J.; Boston, A.; Brown, S.; Fennell, P. S.; Fuss, S.; Galindo, A.; Hackett, L. A.; Hallett, J. P.; Herzog, H. J.; Jackson, G.; Kemper, J.; Krevor, S.; Maitland, G. C.; Matuszewski, M.; Metcalfe, I. S.; Petit, C.; Puxty, G.; Reimer, J.; Reiner, D. M.; Rubin, E. S.; Scott, S. A.; Shah, N.; Smit, B.; Trusler, J. P. M.; Webley, P.; Wilcoxx, J.; Dowell, N. M. Carbon capture and storage (CCS): the way forward. *Energy Environ. Sci.* **2018**, *11*, 1062-1176.
- (8) Al-Mamoori, A.; Krishnamurthy, A.; Rownaghi, A. A.; Rezaei, F. Carbon Capture and Utilization Update. *Energy Technol.* **2017**, *5*, 834-849.
- (9) Mikulčić, H.; Skov, I. R.; Dominković, D. F.; Alwi, S. R. W.; Manan, Z. A.; Tan, R.; Duić, N.; Mohamad, S. N. H.; Wang, X. Flexible Carbon Capture and Utilization technologies in future energy systems and the utilization pathways of captured CO₂. *Renew. Sustain. Energy Rev.* **2019**, *114*, 109338.
- (10) Yu, K. M. K.; Curcic, I.; Gabriel, J.; Tsang, S. C. E. Recent Advances in CO₂ Capture and Utilization. *Chem Sus Chem* **2008**, *1*, 893-899.
- (11) Kolster, C.; Mechleri, E.; Krevor, S.; Dowell, N. M. The role of CO₂ purification and transport networks in carbon capture and storage cost reduction. *Int. J. Greenhouse Gas Contr.* **2017**, *58*, 127-141.
- (12) Smith, E.; Morris, J.; Kheshgi, H.; Teletzke, G.; Herzog, H.; Paltsev. S. The cost of CO₂ transport and storage in global integrated assessment modeling. *Int. J. Greenhouse Gas Control* **2021**, 109, 103367.
- (13) Simonsen, K. R.; Hansen, D. S.; Pedersen, S. Challenges in CO₂ transportation: Trends and perspectives. *Renew. Sustain. Energy Rev.* **2024**, *191*, 114149.
- (14) Assen, N. V. D, Voll, P.; Peters, M.; Bardow, A. Life cycle assessment of CO₂ capture and utilization: a tutorial review. *Chem. Soc. Rev.* **2014**, *43*, 7982-7994.
- (15) Wu, J.; Zhou, X. -D. Catalytic conversion of CO₂ to value-added fuels: Current status, challenges, and future directions. *Chin. J. Catal.* **2016**, *37*, 999-1015.
- (16) Modak, A.; Bhanja, P.; Dutta, S.; Chowdhury, B.; Bhaumik, Asim. Catalytic reduction of CO₂ into fuels and fine chemicals. *Green Chem.* **2020**, *22*, 4002-4033.

(17) Quan, Y.; Zhu, J.; Zheng, G. Electrocatalytic Reactions for Converting CO₂ to Value-Added Products. *Small Sci.* **2021**, *1*, 2100043.

- (18) Dhankhar, S. S.; Nagaraja, C. M. Porous nitrogen-rich covalent organic framework for capture and conversion of CO₂ at atmospheric pressure conditions. *Micropor. Mesopor. Mat.* **2020**, *308*, 110314.
- (19) Singh, G.; Nagaraja, C. M. Rational Design of Cu(I)-Anchored Porous Covalent Triazine Framework (CTF) for Simultaneous Capture and Conversion of CO₂ at Ambient Conditions. *J. CO₂ Util.* **2022**, *63*, 102132.
- (20) Zhao, Z.; Zheng, D.; Guo, M.; Yu, J.; Zhang, S.; Zhang, Z.; Chen. Y. Engineering Olefin-Linked Covalent Organic Frameworks for Photoenzymatic Reduction of CO₂. *Angew. Chem. Int. Ed.* **2022**, *61*, 202200261.
- (21) Yusuf, N.; Almomani, F.; Qiblawey, H.; Catalytic CO₂ conversion to C1 value-added products: Review on latest catalytic and process developments. *Fuel*, **2023**, *345*, 128178.
- (22) Saini, N.; Malik, A.; Jain, S. L. Light-driven chemical fixation and conversion of CO₂ into cyclic carbonates using transition metals: A review on recent advancements. *Coord. Chem. Rev.* **2024**, *502*, 215636.
- (23) Guo, L.; Lamb, K. J.; North. M. Recent developments in organocatalyzed transformations of epoxides and carbon dioxide into cyclic carbonates. *Green Chem.* **2021**, *23*, 77-118.
- (24) Tounzoua, C. N.; Grignard, B.; Detrembleur, Christophe. Exovinylene Cyclic Carbonates: Multifaceted CO₂-Based Building Blocks for Modern Chemistry and Polymer Science. *Angew. Chem. Int. Ed.* **2022**, *61*, e202116066.
- (25) Lu, M.; Zhang, M.; Liu, J.; Chen, Y.; Liao, J. -P.; Yang, M. -Y.; Cai, Y. -P.; Li, S. -L.; Lan. Y. -Q. Covalent Organic Framework Based Functional Materials: Important Catalysts for Efficient CO₂ Utilization. *Angew. Chem. Int. Ed.* **2022**, *134*, 202200003.
- (26) Qiu, L. -Q.; Li, H. -R, He, L. -N. Incorporating Catalytic Units into Nanomaterials: Rational Design of Multipurpose Catalysts for CO₂ Valorization. *Acc. Chem. Res.* **2023**, *56*, 2225-2240.
- (27) Qin, L.; Ma, C.; Zhang, J.; Zhou T.; Structural Motifs in Covalent Organic Frameworks for Photocatalysis. *Adv. Funct. Mater.* **2024**, 2401562.
- (28) Guan, Q.; Zhou, L. -L.; Dong, Y. -B. Metalated covalent organic frameworks: from synthetic strategies to diverse applications. *Chem. Soc. Rev.* **2022**, *51*, 6307-6416.

(29) Luo, R.; Yang, Y.; Chen, K.; Liu, X.; Chen, M.; Xu, W.; Liu, B.; Ji, H.; Fang. Y. Tailored covalent organic frameworks for simultaneously capturing and converting CO₂ into cyclic carbonates. *J. Mater. Chem. A* **2021**, *9*, 20941-20956.

- (30) Singh, G.; Lee, J.; Karakoti, A.; Bahadur, R.; Yi, J.; Zhao, D.; AlBahilyc, K.; Vinu, A. Emerging trends in porous materials for CO₂ capture and conversion. *Chem. Soc. Rev.* **2020**, *49*, 4360-4404.
- (31) Singh, N.; Yadav, D.; Mulay, S. V.; Kim, J. Y.; Park, N. -J.; Baeg, J. -O. Band Gap Engineering in Solvochromic 2D Covalent Organic Framework Photocatalysts for Visible Light-Driven Enhanced Solar Fuel Production from Carbon Dioxide. *ACS Appl. Mater. Interfaces* **2021**, *13*, 14122-14131.
- (32) Zhang, Y.; Wu, M. -X.; Zhou, G.; Wang, X. -H.; Liu, X. A Rising Star from Two Worlds: Collaboration of COFs and Ils. *Adv. Funct. Mater.* **2021**, *31*, 2104996.
- (33) Dhankhar, S. S.; Ugale, B.; Nagaraja, C. M. Co-CatalystFree Chemical Fixation of CO₂ into Cyclic Carbonates by using Metal-Organic Frameworks as Efficient Heterogeneous Catalysts. *Chem. -Asian J.* **2020**, *15*, 2403-2427.
- (34) Sharma, N.; Dhankhar, S. S.; Nagaraja, C. M. Environment-friendly, co-catalyst-and solvent-free fixation of CO₂ using an ionic zinc(II) porphyrin complex immobilized in porous metal-organic frameworks. *Sustain. Energy Fuels* **2019**, *3*, 2977-2982.
- (35) Das, R.; Nagaraja, C. M. Highly Efficient Fixation of Carbon Dioxide at RT and Atmospheric Pressure Conditions: Influence of Polar Functionality on Selective Capture and Conversion of CO₂. *Inorg. Chem.* **2020**, *59*, 9765-9773.
- (36) Feng, X.; Ding, X.; Jiang, D. Covalent organic frameworks. *Chem. Soc. Rev.* **2012**, *41*, 6010-6022.
- (37) Kurisingal, J. F.; Kim, H.; Choe, J. H.; Hong, C. S. Covalent organic framework-based catalysts for efficient CO₂ utilization reactions. *Coord. Chem. Rev.* **2022**, *473*, 214835.
- (38) Yuan, G.; Qi, C.; Wu, W.; Jiang, H. Recent advances in organic synthesis with CO₂ as C1 synthon. *Curr. Opin. Green Sustain.* **2017**, *3*, 22-27.
- (39) Zhou, H. -C. J.; Kitagawa, S. Metal-Organic Frameworks (MOFs). *Chem. Soc. Rev.*, **2014**, *43*, 5415-5418.
- (40) Stock, N.; Biswas, S.; Synthesis of Metal-Organic Frameworks (MOFs): Routes to Various MOF Topologies, Morphologies, and Composites. *Chem. Rev.* **2012**, *112*, 933-969.

(41) Liu, C.; Wang, J.; Wan, J.; Yu, C. MOF-on-MOF hybrids: Synthesis and applications. *Coord. Chem. Rev.* **2021**, *432*, 213743.

- (42) Wang, K.; Li, Y.; Xie, L. -H.; Li, X.; Li, J. -R. Construction and application of base-stable MOFs: a critical review. *Chem. Soc. Rev.* **2022**, *51*, 6417-6441.
- (43) Li, J. -R.; Kuppler, R. J.; Zhou, H. -C. Selective gas adsorption and separation in metal-organic frameworks. *Chem. Soc. Rev.* **2009**, *38*, 1477-1504.
- (44) Ugale, B.; Kumar, S.; Kumar, T. J. D.; Nagaraja, C. M. Environmentally Friendly, Co-catalyst-Free Chemical Fixation of CO₂ at Mild Conditions Using Dual-Walled Nitrogen-Rich Three-Dimensional Porous Metal-Organic Frameworks. *Inorg. Chem.* **2019**, *58*, 3925-3936.
- (45) Lusti, W. P.; Mukherjee, S.; Rudd, N. D.; Desai, A. V.; Li, J.; Ghosh, S. K. Metalorganic frameworks: functional luminescent and photonic materials for sensing applications. *Chem. Soc. Rev.* **2017**, *46*, 3242-3285.
- (46) Shimizu, G. K. H.; Taylor, J. M.; Kim, A. Proton Conduction with Metal-Organic Frameworks. *Science* **2013**, *341*, 354-355.
- (47) Ding, M.; Cai, X.; Jiang, H. -L. Improving MOF stability: approaches and applications. *Chem. Sci.* **2019**, *10*, 10209-10230.
- (48) Qian, Y.; Zhang, F.; Pang. H. A Review of MOFs and Their Composites-Based Photocatalysts: Synthesis and Applications. *Adv. Funct. Mater.* **2021**, *31*, 2104231.
- (49) Lawson, H. D.; Walton, S. P.; Chan, C. Metal-Organic Frameworks for Drug Delivery: A Design Perspective. *ACS Appl. Mater. Interfaces* **2021**, *13*, 7004-7020.
- (50) Pal, T. K.; De, D.; Bharadwaj, P. K. Metal-organic frameworks for the chemical fixation of CO₂ into cyclic carbonates. *Coord. Chem. Rev.* **2020**, *408*, 213173.
- (51) Liang, J.; Huang, Y.-B.; Cao, R. Metal-organic frameworks and porous organic polymers for sustainable fixation of carbon dioxide into cyclic carbonates. *Coord. Chem. Rev.* **2019**, *378*, 32-65.
- (52) Das, R.; Dhankhar, S. S.; Nagaraja, C. M. Construction of a bifunctional Zn(II)—organic framework containing a basic amine functionality for selective capture and room temperature fixation of CO₂. *Inorg. Chem. Front.* **2020**, *7*, 72-81.
- (53) Geng, K.; He, T.; Liu, R.; Tan, K. T.; Li, Z.; Tao, S.; Gong, Y.; Jiang, Q.; Jiang, D. Covalent Organic Frameworks: Design, Synthesis, and Functions. *Chem. Rev.* **2020**, *120*, 8814-8933.
- (54) Ding, S. -Y. Wang, W. Covalent organic frameworks (COFs): from design to applications. *Chem. Soc. Rev.* **2013**, *42*, 548-568.

(55) Lohse, M. S.; Bein, T. Covalent Organic Frameworks: Structures, Synthesis, and Applications. *Adv. Funct. Mater.* **2018**, *28*, 1705553.

- (56) Gui, B.; Lin, G.; Ding, H.; Gao, C.; Mal, A.; Wang, C. Three-Dimensional Covalent Organic Frameworks: From Topology Design to Applications. *Acc. Chem. Res.* **2020**, *53*, 2225-2234.
- (57) Zhao, X.; Pachfule, P.; Thomas. A. Covalent organic frameworks (COFs) for electrochemical applications. *Chem. Soc. Rev.* **2021**, *50*, 6871-6913.
- (58) Gong, Y. -N.; Guan, X.; Jiang, H. -L. Covalent organic frameworks for photocatalysis: Synthesis, structural features, fundamentals and performance. *Coord. Chem. Rev.* **2023**, *475*, 214889.
- (59) Wang, J.; Zhuang. S. Covalent organic frameworks (COFs) for environmental applications. *Coord. Chem. Rev* **2019**, *400*, 213046.
- (60) Liu, X.; Huang, D.; Lai, C.; Zeng, G.; Qin, L.; Wang, H. Yi, H.; Li, B.; Liu, S.; Zhang, M.; Deng, R.; Fu, Y.; Li, L.; Xue, W.; Chen, S. Recent advances in covalent organic frameworks (COFs) as a smart sensing material. *Chen Chem. Soc. Rev.* **2019**, 48, 5266-5302.
- (61) Yang, Q.; Luo, M.; Liu, K.; Cao, H.; Yan, H. Covalent organic frameworks for photocatalytic applications. *Appl. Catal. B: Environ.* **2020**, *276*, 11917.
- (62) Zhan, X.; Chen, Z.; Zhang, Q. Recent progress in two-dimensional COFs for energy-related applications. *J. Mater. Chem. A* **2017**, *5*, 14463-14479.
- (63) Li, J.; Zhou, X.; Wang, J.; Li, X. Two-Dimensional Covalent Organic Frameworks (COFs) for Membrane Separation: a Mini Review. *Ind. Eng. Chem. Res.* **2019**, *58*, 15394-15406.
- (64) Chen, Z.; Wang, K.; Hu, X.; Shi, P.; Guo, Z.; Zhan, H. Novel One-Dimensional Covalent Organic Framework as a H⁺ Fluorescent Sensor in Acidic Aqueous Solution. *ACS Appl. Mater. Interfaces* **2021**, *13*, 1145-1151.
- (65) Zhang, T.; Zhang, G.; Chen. L. 2D Conjugated Covalent Organic Frameworks: Defined Synthesis and Tailor-Made Functions. *Acc. Chem. Res.* **2022**, *55*, 795-808.
- (66) Huang, W.; Zhang, W.; Yang, S.; Wang, L.; Yu. G. 3D Covalent Organic Frameworks from Design, Synthesis to Applications in Optoelectronics. *Small* **2024**, *20*, 2308019.
- (67) Cote, A. P.; Benin, A. I.; Ockwig, N. W.; Keeffe, M. O.; Matzger, A. J.; Yaghi, O. M. Porous, Crystalline, Covalent Organic Frameworks. *Science* **2005**, *310*, 1166-1170.

(68) Kuhn, P.; Antonietti, M.; Thomas, A. Porous, Covalent Triazine-Based Frameworks Prepared by Ionothermal Synthesis. *Angew. Chem. Int. Ed.* **2008**, *47*, 3450-3453.

- (69) Uribe-Romo, F. J.; Hunt, J. R.; Furukawa, H.; Klock, C.; Keeffe, M. O.; Yaghi, O. M. A Crystalline Imine-Linked 3-D Porous Covalent Organic Framework. *J. Am. Chem. Soc.* **2009**, *131*, 4570-4571.
- (70) Singh, G.; Prakash, K.; Nagaraja, C. M. Fe(III)-Anchored Porphyrin-Based Nanoporous Covalent Organic Frameworks for Green Synthesis of Cyclic Carbonates from Olefins and CO₂ under Atmospheric Pressure Conditions. *Inorg. Chem.* **2023**, *62*, 13058-13068.
- (71) Zhao, Z.; Zheng, Y.; Wang, C.; Zhang, S.; Song, J.; Li, Y.; Ma, S.; Cheng, P.; Zhang, Z.; Chen, Y. Fabrication of Robust Covalent Organic Frameworks for Enhanced Visible-Light-Driven H₂ Evolution. *ACS Catal.* **2021**, *11*, 2098-2107.
- (72) Wang, Y.; Sun, T.; Zheng, T.; Ding, X.; Zhang, P.; Xu, Q.; Li, T.; Zhang, S.; Wang, K.; Xu, L.; Jiang J. Two-Dimensional Kagome Covalent Organic Frameworks with Single Atomic Co Sites for Superior Photocatalytic CO₂ Reduction. *ACS Materials Lett.* **2024**, *6*, 140-152.
- (73) Liu, Y. -H.; Chu, X.; Jiang, Y.; Han, W.; Wang, Y.; Shao, L. -H.; Zhang, G.; Zhang, F. -M. Self-Accelerating H₂ Evolution Activity by In Situ Transformation on Noble-Metal-Free Photocatalyst of Covalent Organic Framework and Cu₂O Composite. *Adv. Funct. Mater.* **2024**, *34*, 2316546.
- (74) Chen, Q.; Wang, Y.; Luo, G. Photoenzymatic CO₂ Reduction Dominated by Collaborative Matching of Linkage and Linker in Covalent Organic Frameworks. *J. Am. Chem. Soc.* **2024**, *146*, 586-598.
- (75) Stegbauer, L.; Schwinghammer, K.; Lotsch, B. V. A hydrazone-based covalent organic framework for photocatalytic hydrogen production. *Chem. Sci.* **2014**, **5**, 2789-2793.
- (76) Stegbauer, L.; Zech, S.; Savasci, G.; Banerjee, T.; Podjaski, F.; Schwinghammer, K.; Ochsenfeld, C.; Lotsch, B. V. Tailor-Made Photoconductive Pyrene-Based Covalent Organic Frameworks for Visible-Light Driven Hydrogen Generation. *Adv. Energy Mater.* **2018**, *8*, 1703278.
- (77) Li, G.; Ye, J.; Fang, Q.; Liu, F. Amide-based covalent organic frameworks materials for efficient and recyclable removal of heavy metal lead (II). *Chem. Eng. J.* **2019**, *370*, 822-830.

(78) Buyukcakir, O.; Je, S. H.; Talapaneni, S. N.; Kim, D.; Coskun. A. Charged Covalent Triazine Frameworks for CO₂ Capture and Conversion. *ACS Appl. Mater. Interfaces* **2017**, *9*, 7209-7216.

- (79) Chen, R.; Shi, J. L.; Ma, Y.; Lin, G.; Lang, X.; Wang. C. Designed Synthesis of a
- 2D Porphyrin-Based sp² Carbon-Conjugated Covalent Organic Framework for Heterogeneous Photocatalysis. *Angew. Chem. Int. Ed.* **2019**, *58*, 6430-6434.
- (80) Wang, D. -G.; Qiu, T.; Guo, W.; Liang, Z.; Tabassum, H.; Xia D.; Zou R. Covalent organic framework-based materials for energy applications. *Energy Environ. Sci.* **2021**, *14*, 688-728.
- (81) Li, X.; Yang, C.; Sun, B.; Cai, S.; Chen, Z.; Lv, Y.; Zhang J.; Liu. Y. Expeditious synthesis of covalent organic frameworks: a review. *J. Mater. Chem. A* **2020**, *8*, 16045-16060.
- (82) Cui, D.; Perepichka, D. F.; MacLeod, J. M.; Rosei. F. Surface-confined single-layer covalent organic frameworks: design, synthesis, and application. *Chem. Soc. Rev.* **2020**, *49*, 2020-2038.
- (83) Duan, K.; Wang, J.; Zhang, Y.; Liu, J. Covalent organic frameworks (COFs) functionalized mixed matrix membrane for effective CO₂/N₂ separation. *J. Membr Sci.* **2019**, *572*, 588-595.
- (84) Chandra, S.; Kundu, T.; Dey, K.; Addicoat, M.; Heine, T.; Banerjee, R. Interplaying intrinsic and extrinsic proton conductivities in covalent organic frameworks. *Chem. Mater.* **2016**, *28*, 1489-1494.
- (85) Bai, L.; Phua, S. Z. F.; Lim, W. Q.; Jana, A.; Luo, Z.; Tham, H. P.; Zhao, L.; Gao, Q.; Zhao. Y. Nanoscale covalent organic frameworks as smart carriers for drug delivery. *Chem. Commun.* **2016**, *52*, 4128-4131.
- (86) Liang, Z.; Shen, R.; Ng, Y. H.; Fu, Y.; Ma, T.; Zhang, P.; Li, Y.; Li, X. Covalent organic frameworks: Fundamentals, mechanisms, modification, and applications in photocatalysis. *Chem Catal.* **2022**, *2*, 2157-2228.
- (87) Ge, R.; Hao, D.; Shi, Q.; Dong, B.; Leng, W.; Wang, C.; Gao, Ya. Target Synthesis of an Azo (N=N) Based Covalent Organic Framework with High CO₂-over-N₂ Selectivity and Benign Gas Storage Capability. *J. Chem. Eng. Data* **2016**, *61*, 1904-1909.
- (88) Maia, R. A.; Oliveira, F. L.; Ritleng, V.; Wang, Q.; Louis, B.; Esteves, P. M. CO₂ Capture by Hydroxylated Azine-Based Covalent Organic Frameworks. *Chem. Eur. J.* **2021**, *27*, 8048-8055.

(89) Wang, Y.; Kang, C.; Zhang, Z.; Usadi, A. K.; Calabro, D. C.; Baugh, L. S.; Yuan, Y. D.; Zhao D. Evaluation of Schiff-Base Covalent Organic Frameworks for CO₂ Capture: Structure-Performance Relationships, Stability, and Performance under Wet Conditions. *ACS Sustainable Chem. Eng.* **2022**, *10*, 332-341.

- (90) Zeng, Y.; Zou, R.; Zhao, Y. Covalent Organic Frameworks for CO₂ Capture. *Adv. Mater.* **2016**, *28*, 2855-2873.
- (91) Olajire, A. A. Recent advances in the synthesis of covalent organic frameworks for CO₂ capture. *J. CO₂ Util.* **2017**, *17*, 137-161.
- (92) Lyu, H.; Li, H.; Hanikel, N.; Wang, K.; Yaghi. O. M. Covalent Organic Frameworks for Carbon Dioxide Capture from Air. *J. Am. Chem. Soc.* 2022, **144**, *28*, 12989-12995.
- (93) Singh, G.; Nagaraja, C. M. Highly Efficient Metal/Solvent-Free Chemical Fixation of CO₂ at Atmospheric Pressure Conditions using Functionalized Porous Covalent Organic Frameworks. *J. CO₂ Util.* **2021**, *53*, 101716.
- (94) Sarkar, P.; Chowdhury, I. H.; Das, S.; Islam, S. M. Recent trends in covalent organic frameworks (COFs) for carbon dioxide reduction. *Mater. Adv.* **2022**, *3*, 8063-8080.
- (95) He, N.; Liu, B.; Jiang, B.; Li, X.; Jia, Z.; Zhang, J.; Long, H.; Zhang, Y.; Zou, Y.; Yang, Y.; Xiong, S.; Cao, K.; Li, Y.; Ma. L. Monomer Symmetry-Regulated Defect Engineering: In Situ Preparation of Functionalized Covalent Organic Frameworks for Highly Efficient Capture and Separation of Carbon Dioxide. *ACS Appl. Mater. Interfaces* **2023**, *15*, 16975-16983.
- (96) Zhang, M.; Zheng, R.; Ma, Y.; Chen, R.; Sun, X.; Sun. X. N-rich covalent organic frameworks with different pore size for high-pressure CO₂ adsorption. *Micropor. Mesopor. Mat.* **2019**, *285*, 70-79.
- (97) Wang, K.; Huang, H.; Liu, D.; Wang, C.; Li, J.; Zhong. C.; Covalent Triazine-Based Frameworks with Ultramicropores and High Nitrogen Contents for Highly Selective CO₂ Capture. *Environ. Sci. Technol.* **2016**, *50*, 4869-4876.
- (98) Hug, S.; Stegbauer, L.; Oh, H.; Hirscher, M.; Lotsch. B. V. Nitrogen-Rich Covalent Triazine Frameworks as High-Performance Platforms for Selective Carbon Capture and Storage. *Chem. Mater.* **2015**, *27*, 8001-8010.
- (99) Sang, Y.; Cao, Y.; Wang, L.; Yan, W.; Chen, T.; Huang, J.; Liu Y. -N. N-rich porous organic polymers based on Schiff base reaction for CO₂ capture and mercury(II) adsorption. *J. Colloid Interface Sci.* **2021**, *587*, 121-130.

(100) Das, P.; Mandal, S. K. In-depth experimental and Computational Investigations for Remarkable Gas/Vapor Sorption, Selectivity, and Affinity by a Porous Nitrogen-Rich Covalent Organic Framework. *Chem. Mater.* **2019**, *31*, 1584-1596.

- (101) Huang, N.; Chen, X.; Krishna, R.; Jiang, D. Two-Dimensional Covalent Organic Frameworks for Carbon Dioxide Capture through Channel-Wall Functionalization. *Angew. Chem. Int. Ed.* **2015**, *54*, 2986-2990.
- (102) Li, Z.; Zhi, Y.; Feng, X.; Ding, X.; Zou, Y.; Liu, X.; Mu, Y.; An Azine-Linked Covalent Organic Framework: Synthesis, Characterization and Efficient Gas Storage *Chem. Eur. J.* **2015**, *21*, 12079.
- (103) Ding, L. -G.; Yao, B. -J.; Li, F.; Shi, S. -C.; Huang, N. Yin, H. -B.; Guan, Q.; and Dong, Y. -B. Ionic liquid-decorated COF and its covalent composite aerogel for selective CO₂ adsorption and catalytic conversion. *J. Mater. Chem. A*, **2019**, *7*, 4689-4698.
- (104) Zhao, Y.; Yao, K. X.; Teng, B.; Zhang, T.; Han, Y. A perfluorinated covalent triazine-based framework for highly selective and water-tolerant CO₂ capture. *Energy Environ. Sci.* **2013**, *6*, 3684.
- (105) Li, Z.; Feng, X.; Zou, Y.; Zhang, Y.; Xia, H.; Liu, X.; Mu, Y. A 2D azine-linked covalent organic framework for gas storage applications *Chem. Commun.* **2014**, *50*, 13825-13828.
- (106) Kahveci, Z.; Islamoglu, T.; Shar, G. A.; Ding, R.; El-Kaderi, H. M. Targeted synthesis of a mesoporous triptycene-derived covalent organic framework. *CrystEngComm* **2013**, *15*, 1524-1527.
- (107) Rabbani, M. G.; Sekizkardes, A. K.; Kahveci, Z.; Reich, T. E.; Ding, R.; El-Kaderi, H. M. A 2D Mesoporous Imine-Linked Covalent Organic Framework for High-Pressure Gas Storage Applications. *Chem. Eur. J.* **2013**, *19*, 3324-3328.
- (108) Huang, N.; Krishna, R.; Jiang, D. Tailor-Made Pore Surface Engineering in Covalent Organic Frameworks: Systematic Functionalization for Performance Screening. *J. Am. Chem. Soc.* **2015**, *137*, 7079-7082.
- (109) Kandambeth, S.; Mallick, A.; Lukose, B.; Mane, M. V.; Heine, T. Banerjee, R. Construction of Crystalline 2D Covalent Organic Frameworks with Remarkable Chemical (Acid/Base) Stability via a Combined Reversible and Irreversible Route. *J. Am. Chem. Soc.* **2012**, *134*, 19524-19527.

(110) Kandambeth, S.; Venkatesh, V.; Shinde, D. B.; Kumari, S.; Halder, A.; Verma, S.; Banerjee, R. Self-templated chemically stable hollow spherical covalent organic framework. *Nat. Commun.* **2015**, *6*, 6786.

- (111) Kandambeth, S.; Shinde, D. B.; Panda, M. K.; Lukose, B.; Heine, T. Banerjee, R. Enhancement of Chemical Stability and Crystallinity in Porphyrin Containing Covalent Organic Frameworks by Intramolecular Hydrogen Bonds. *Angew. Chem. Int. Ed.* **2013**, *52*, 13052-13056.
- (112) Chandra, S.; Kandambeth, S.; Biswal, B. P.; Lukose, B.; Kunjir, S. M.; Chaudhary, M.; Babarao, R.; Heine, T.; Banerjee, R. Chemically Stable Multilayered Covalent Organic Nanosheets from Covalent Organic Frameworks via Mechanical Delamination. *J. Am. Chem. Soc.* **2013**, *135*, 17853-17861.
- (113) Furukawa, H.; Yaghi, O. M. Storage of Hydrogen, Methane, and Carbon Dioxide in Highly Porous Covalent Organic Frameworks for Clean Energy Applications. *J. Am. Chem. Soc.* **2009**, *131*, 8875-8883.
- (114) Dhankhar, S. S.; Sharma, N.; Kumar, S.; Kumar, T. J. D.; Nagaraja, C. M. Rational Design of a Bifunctional, Two-Fold Interpenetrated Zn^{II}-Metal-Organic Framework for Selective Adsorption of CO₂ and Efficient Aqueous Phase Sensing of 2,4,6-Trinitrophenol. *Chem. Eur. J.* **2017**, *23*, 16204-16212.
- (115) Mahmood, J.; Ahmad, I.; Jung, M.; Seo, J. -M.; Yu, S. -Y.; Noh, H. -J.; Kim, Y. H.; Shin H. -J.; Baek, J. -B. Two-dimensional amine and hydroxy functionalized fused aromatic covalent organic framework. *Commun Chem.* **2020**, *3*, 31.
- (116) Sengupta, M.; Bag, A.; Ghosh, S.; Mondal, P.; Bordoloi, A.; Islam, S. M. CuxOy@ COF: An efficient heterogeneous catalyst system for CO₂ cycloadditions under ambient conditions. *J. CO₂ Util.* **2019**, *34*, 533-542.
- (117) Li, H.; Deng, G.; Wang, Z.; Cheng, K.; Li, Z.; Luo, X.; Yang, Y.; Sun, Y.; Li, P.-Z.; Wang, Z. Effective CO₂ Catalytic Conversion by Nitrogen-Rich Covalent Organic Framework-Immobilized Ag Nanoparticles. *ACS Appl. Nano Mater.* **2023**, *6*, 16424-16432.
- (118) Roy, A.; Haque, N.; Chatterjee, R.; Biswas, S.; Bhaumik, A.; Sarkar M.; Islam. S. M. AgNPs supported over porous organic polymers for the fixation of CO₂ on propargyl alcohols and amines under solvent-free conditions. *New J. Chem.* **2023**, *47*, 6673-6684.

(119) Dang, Q. -Q.; Liu, C. -Y.; Wang, X. -M.; Zhang, X. -M. Novel Covalent Triazine Framework for High-Performance CO₂ Capture and Alkyne Carboxylation Reaction. *ACS Appl. Mater. Interfaces* **2018**, *10*, 27972-27978.

- (120) Cui, J. -X.; Wang, L -J.; Feng, L.; Meng, B.; Zhou, Z -Y.; Su, Z. -M.; Wang, K.; and Liu. S. A metal-free covalent organic framework as a photocatalyst for CO₂ reduction at low CO₂ concentration in a gas-solid system. *J. Mater. Chem. A*, **2021**, *9*, 24895-24902.
- (121) Nguyen, H. L.; Alzamly, A. Covalent Organic Frameworks as Emerging Platforms for CO₂ Photoreduction. *ACS Catal.* **2021**, *11*, 9809-9824.
- (122) Diercks, C. S.; Lin, S.; Kornienko, N.; Kapustin, E. A.; Nichols, E. M.; Zhu, C.; Zhao, Y.; Chang, C. J.; Yaghi. O. M. Reticular Electronic Tuning of Porphyrin Active Sites in Covalent Organic Frameworks for Electrocatalytic Carbon Dioxide Reduction. *J. Am. Chem. Soc.* **2018**, *140*, 1116-1122.
- (123) Yu, H.; Zhang, J.; Yan, X.; Wu, C.; Zhu, X.; Li, B.; Li, T.; Guo, Q.; Gao, J.; Hu, M.; Yang, J. Donor–acceptor covalent organic framework hollow submicrospheres with a hierarchical pore structure for visible-light-driven H₂ evolution. *J. Mater. Chem. A* **2022**, *10*, 11010-11018.
- (124) Das, P.; Roeser, J.; Thomas. A. Solar Light Driven H₂O₂ Production and Selective Oxidations Using a Covalent Organic Framework Photocatalyst Prepared by a Multicomponent Reaction. *Angew. Chem. Int. Ed.* **2023**, *62*, e202304349.
- (125) Das, P.; Chakraborty, G.; Friese, N.; Roeser, J.; Prinz, C.; Emmerling, F.; Schmidt, J.; Thomas. A. Heteropolyaromatic Covalent Organic Frameworks via One-Pot Multicomponent Reactions. *J. Am. Chem. Soc.* **2024**, *146*, 17131-17139.
- (126) Sekizkardes, A. K.; Wang, P.; Hoffman, J.; Budhathoki S.; Hopkinson. D. Amine-functionalized porous organic polymers for carbon dioxide capture. *Mater. Adv.* **2022**, *3*, 6668-6686.
- (127) Wang, X.; Liu, H.; Zhang, J.; Chen. S. Covalent organic frameworks (COFs): a promising CO₂ capture candidate material. *Polym. Chem.* **2023**, *14*, 1293-1317.
- (128) Qiu, J.; Zhao, Y.; Li, Z.; Wang, H.; Shi, Y.; Wang, J. Imidazolium Salts Functionalized Covalent Organic Frameworks for Highly Efficient Catalysis of CO₂ Conversion. *Chem Sus Chem* **2019**, *12*, 2421-2427.
- (129) Feng, X.; Chen, L.; Dong, Y.; Jiang. D. Porphyrin-based two-dimensional covalent organic frameworks: synchronized synthetic control of macroscopic structures and pore parameters. *Chem. Commun.* **2011**, *47*, 1979-1981.

(130) Yang, S.; Hu, W.; Zhang, X.; He, P.; Pattengale, B.; Liu, C.; Cendejas, M.; Hermans, I.; Zhang, X.; Zhang, J.; et al. 2D Covalent Organic Frameworks as Intrinsic Photocatalysts for Visible Light-Driven CO₂ Reduction. *J. Am. Chem. Soc.* **2018**, *140*, 14614-14618.

- (131) Xu, K.; Dai, Y.; Ye, B.; Wang, H. Two dimensional covalent organic framework materials for chemical fixation of carbon dioxide: excellent repeatability and high selectivity. *Dalton Trans.* **2017**, *46*, 10780-10785.
- (132) Wu, J.; Ma, S.; Cui, J.; Yang, Z.; Zhang. J. Nitrogen-Rich Porous Organic Polymers with Supported Ag Nanoparticles for Efficient CO₂ Conversion. *Nanomater*. **2022**, *12*, 3088.
- (133) Guan, P.; Qiu, J.; Zhao, Y.; Wang, H.; Li, Z.; Shi, Y.; Wang, J.; A novel crystalline azine-linked three-dimensional covalent organic framework for CO₂ capture and conversion. *Chem. Commun.* **2019**, *55*, 12459-12462.
- (134) Luo, R.; Chen, M.; Liu, X.; Xu, W.; Li, J.; Liu, B.; Fang, Y. Recent advances in CO₂ capture and simultaneous conversion into cyclic carbonates over porous organic polymers having accessible metal sites. *J. Mater. Chem. A* **2020**, *8*, 18408-18424.
- (135) Sani, R.; Dey, T. K.; Sarkar, M.; Basu, P.; Islam, S. M. A study of contemporary progress relating to COF materials for CO₂ capture and fixation reactions. *Mater. Adv.* **2022**, *3*, 5575-5597.
- (136) Ding, M.; Flaig, R. W.; Jiang, H. -L.; Yaghi, O. M. Carbon capture and conversion using metal-organic frameworks and MOF-based materials. *Chem. Soc. Rev.* **2019**, *48*, 2783-2828.
- (137) Scrosati, B.; Hassoun, J.; Sun, Y. -K. Lithium-ion batteries. A look into the future *Energy Environ. Sci.* **2011**, *4*, 3287-3295.
- (138) Besse, V.; Camara, F.; Voirin, C.; Auvergne, R.; Caillol, S.; Boutevin, B. Synthesis and applications of unsaturated cyclocarbonates. *Polym. Chem.* **2013**, *4*, 4545-4561.
- (139) Ghazali-Esfahani, S.; Song, H.; Păunescu, E.; Bobbink, F. D.; Liu, H.; Fei, Z.; Laurenczy, G.; Bagherzadeh, M.; Yan N.; Dyson. P. J. Cycloaddition of CO₂ to epoxides catalyzed by imidazolium-based polymeric ionic liquids. *Green Chem.* **2013**, *15*, 1584-1589.
- (140) Wani, M. Y.; Kumar, S.; Arranja, C. T.; Dias, C. M. F.; Sobral. A. J. F. N. Cycloaddition of CO₂ to epoxides using di-nuclear transition metal complexes as catalysts. *New J. Chem.* **2016**, *40*, 4974-4980.

(141) Wang, J. -Q.; Dong, K.; Cheng, W. -G.; Sun, J.; Zhang. S. -J. Insights into quaternary ammonium salts-catalyzed fixation carbon dioxide with epoxides. *Catal. Sci. Technol.* **2012**, *2*, 1480-1484.

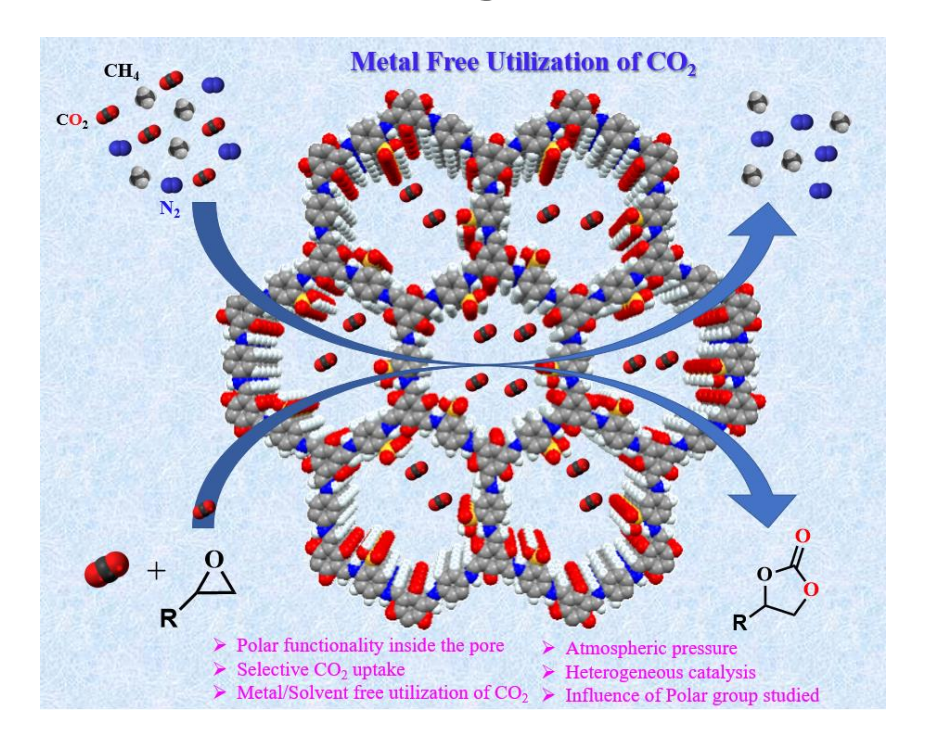
- (142) Gorji, Z. E.; Khodadadi, A. A.; Riahi, S.; Repo, T.; Mortazavi, Y.; Kemell. M. Functionalization of nitrogen-doped graphene quantum dot: A sustainable carbon-based catalyst for the production of cyclic carbonate from epoxide and CO₂. *J. Environ. Sci.* **2023**, *126*, 408-422.
- (143) Ma, R.; He, L. N.; Zhou, Y. B. An efficient and recyclable tetraoxo-coordinated zinc catalyst for the cycloaddition of epoxides with carbon dioxide at atmospheric pressure. *Green Chem.* **2016**, *18*, 226-231.
- (144) Duan, R.; Hu, C.; Zhou, Y.; Huang, Y.; Sun, Z.; Zhang, H.; Pang X. Propylene Oxide Cycloaddition with Carbon Dioxide and Homopolymerization: Application of Commercial Beta Zeolites. *Ind. Eng. Chem. Res.* **2021**, *60*, 1210-1218.
- (145) Ugale, B.; Dhankhar, S. S.; Nagaraja, C. M. Interpenetrated Metal-Organic Frameworks of Cobalt(II): Structural Diversity, Selective Capture, and Conversion of CO₂. *Cryst. Growth. Des.* **2017**, *17*, 3295-3305.
- (146) Zhi, Y.; Shao, P.; Feng, X.; Xia, H.; Zhang, Y.; Shi, Z.; Mu, Y.; Liu, X. Covalent organic frameworks: efficient, metal-free, heterogeneous organocatalysts for chemical fixation of CO₂ under mild conditions. *J. Mater. Chem. A* **2018**, *6*, 374-382.
- (147) Saptal, V.; Shinde, D. B.; Banerjee, R.; Bhanage, B. M. State-of-the-art catechol porphyrin COF catalyst for chemical fixation of carbon dioxide via cyclic carbonates and oxazolidinones. *Catal. Sci. Technol.* **2016**, *6*, 6152-6158.
- (148) Wang, Q.; Li, Y.; Zhou, M.; Zhou, J.; Liu, X.; Yu, X.; Gao, J.; Liang, E.; Chen, X.; Zhang, Y.; Han, B.; Fan, J.; Li, J. N-doping of β-ketoenamine based covalent organic frameworks for catalytic conversion of CO₂ to cyclic carbonate and Knoevenagel condensation. *Micropor. Mesopor. Mat.* **2024**, *364*, 112872.
- (149) Pang, Y.; Wang, B.; Gu, X.; Shen, H.; Yan, X.; Li, Y.; Chen, L. Hydroxy-Rich Covalent Organic Framework for the Efficient Catalysis of the Cycloaddition of CO₂. *Langmuir* **2023**, *39*, 16721-16730.
- (150) Yang, F.; Li, Y.; Zhang, T.; Zhao, Z.; Xing, G.; Chen, L. Docking Site Modulation of Isostructural Covalent Organic Frameworks for CO₂ Fixation. *Chem. Eur. J.* **2020**, *26*, 4510-4514.
- (151) Haque, N.; Biswas, S.; Ghosh, S.; Chowdhury, A. H.; Khan, A.; Islam S. M. Zn(II)-Embedded Nanoporous Covalent Organic Frameworks for Catalytic

Conversion of CO₂ under Solvent-Free Conditions. *ACS Appl. Nano Mater.* **2021**, *4*, 7663-7674.

- (152) Gennen, S.; Grignard, B.; Tassaing, T.; Jerome, C.; Detrembleur, C. CO₂-sourced α-alkylidene cyclic carbonates: a step forward in the quest for functional regioregular poly(urethane)s and poly(carbonate)s. *Angew. Chem. Int. Ed.* **2017**, *129*, 10530-10534.
- (153) Shinabarger, D. L.; Marotti, K. R.; Murray, R. W.; Lin, A. H.; Melchior, E. P.; Swaney, S. M.; Dunyak, D. S.; Demyan, W. F.; Buysse, J. M. Mechanism of Action of Oxazolidinones: Effects of Linezolid and Eperezolid on Translation Reactions. *Antimicrob. Agents Chemother.* **1997**, *41*, 2132-2136.
- (154) Yoshida, M.; Mizuguchi, T.; Shishido, K. Synthesis of Oxazolidinones by Efficient Fixation of Atmospheric CO₂ with Propargylic Amines by using a Silver/1,8 Diazabicyclo[5.4.0]undec-7-ene (DBU) Dual-Catalyst System. *Chem. Eur. J.* **2012**, *18*, 15578-15581.
- (155) Zhang, Y.; Lan, X.; Yan, F.; He, X.; Wang, J.; -Sandoval, L. R.; Chen, L.; Bai, G. Controllable Encapsulation of Silver Nanoparticles by Porous Pyridine-Based Covalent Organic Frameworks for Efficient CO₂ Conversion using Propargylic Amines. *Green Chem.* **2022**, *24*, 930-940.
- (156) Trost, B. M.; Toste, F. D.; Greenman, K. Atom Economy. Palladium-Catalyzed Formation of Coumarins by Addition of Phenols and Alkynoates via a Net C-H Insertion. *J. Am. Chem. Soc.* **2003**, *125*, 4518-4526.

Chapter 2

Highly efficient metal/solvent-free chemical fixation of CO₂ at atmospheric pressure conditions using functionalized porous covalent organic frameworks



❖ Reference: "Singh, G.; Nagaraja, C. M. J. CO₂ Util. 2021, 53, 101716."

2.1. Introduction

Carbon dioxide (CO₂) is one of the major contributors to global warming, resulting in the greenhouse effect and climate change. 1-4 However, CO₂ can be utilized as a harmless, abundant, cheap, and renewable feedstock to synthesize high-value chemicals or fuels.⁵⁻⁹ Among the various chemical functionalizations, coupling CO₂ with epoxides to produce cyclic carbonates has attracted significant attention due to its 100% atom competence. 10-16 Further, cyclic carbonates offer numerous applications in various fields, such as precursors for synthesizing polymeric materials and pharmaceuticals, electrolytes in lithium-ion batteries, and so on.¹⁷ In this regard, various homogeneous ¹⁸⁻²² and heterogeneous catalysts ²³⁻³⁰ have been utilized for the cycloaddition of epoxide with CO₂. However, most of these catalysts require costly metal ions, high pressure, and temperature conditions to efficiently convert CO2 into cyclic carbonates.³¹⁻³⁶ On the other hand, towards green and sustainable chemistry practices, the development of heterogeneous catalysts for metal-free utilization of CO₂ under mild conditions has gained the significant interest of researchers.³⁷⁻⁴¹ In this context, covalent organic frameworks (COFs), a new class of crystalline porous organic polymers (POPs) have gained tremendous attention. 42-44 Further, COFs can be rationally designed with tailored chemical and physical properties, suitable for various applications, like selective gas storage/separation, catalysis, proton conductivity, and so on. 45-50 Particularly, COFs composed of CO₂-philic basic sites such as azo (N=N), azine (C-N-N-C), and imine (C=N), based organic linkers are of potential significance for selective capture and conversion of CO₂.51-55 Further, most of the COFs reported for catalytic conversion of CO₂ required additional steps for catalyst preparation. ⁵⁶⁻⁵⁹ On the other hand, it has been observed that catalyst-bearing hydrogen bond donor (HBD) groups can activate the epoxides through hydrogen bonding interaction.⁶⁰

Keeping these aspects, in Chapter 2, we report the utilization of sulfonic acidfunctionalized COF name COF-SO₃H for the chemical fixation of CO₂ into valueadded cyclic carbonate.⁶¹ Further, to evaluate the role of the polar group (-SO₃H) towards CO₂ capture and conversion, an analogous COF, COF-H, which lacks the -SO₃H group was synthesized. Interestingly, COF-SO₃H showed about 10.8 kJ/mol higher heat of interaction energy for CO₂ than that of COF-H. The high value of Q_{st} observed for COF-SO₃H highlights the crucial role of polar functionality (-SO₃H) towards enhanced capture and conversion of CO₂. Further, the presence of a high density of basic -NH and polar Brønsted acid (BA) sites provided a suitable platform for metal/solvent-free chemical fixation of CO₂ with epoxides under mild conditions. Indeed, COF-SO₃H showed higher catalytic activity than most of the COF-based catalysts reported for the coupling of CO₂ to epoxides. Besides, the catalyst could be recycled for multiple cycles without loss of catalytic activity and framework rigidity. Overall, this chapter demonstrates the utilization of polar functionalized COF for selective capture and fixation of CO₂ under atmospheric pressure conditions.

2.2. Experimental section

2.2.1. Materials

All the reagents used in this work were commercially available and employed as provided without any further purification. 1,3,5- trimethyl benzene, 1,4-dioxane, N-butyl alcohol, and o-dichlorobenzene were purchased from TCI chemicals Ltd. Acetic acid (99%) was obtained from Merck and Co. 2,5-diamino benzene sulfonic acid, and 1,4-phenylenediamine utilized for COF synthesis were obtained from Alfa Aesar Chemical Co. 1,3,5-Triformyl phloroglucinol was prepared by following the previously reported procedure.⁶²

2.2.2. Physical measurements

Powder X-ray diffraction measurements were conducted in the 2θ range of 3-50° on PAN analytical's X'PERT PRO X-Ray diffractometer with a scan rate of 2°/min using Cu-Kα radiation (λ = 1.54184 Å, 40 kV, 20 mA) for confirming phase purity of as-synthesized samples. Thermogravimetric analyses of the as-synthesized samples were carried out using a Metler Toledo thermogravimetric analyzer under a nitrogen atmosphere with a flow rate of 30 mL/min from 25-600 °C (heating rate of 5 °C/min). Fourier transform infrared (FT-IR) spectra of the samples were recorded on a Bruker Tensor-F27 instrument in ATR mode. The products of catalytic reactions were identified, and the catalytic conversions were determined by ¹H NMR spectra recorded on a JEOL JNM-ECS-400 spectrometer operating at a frequency of 400 MHz using CDCl₃ solvent. ¹³C CP-MAS (Cross Polarization Magic Angle Spinning) solid-state NMR (400MHz) spectra were recorded on Bruker Advance 400 (DRX400) instrument.

2.2.3. Synthesis

2.2.3.1. Synthesis of COF-SO₃H

COF-SO₃H was synthesized following the previously reported procedure with modification.⁶³ Briefly, little pyrex tube charged with 1,3,5is Triformylphloroglucinol (0.3 mmol), 2,5-diaminobenzenesulfonic acid (0.45 mmol), 3 mL solvent mixture of N-butyl alcohol and o-dichlorobenzene, and 0.5 mL of 3 M glacial acetic acid. The mixture was sonicated for 10 minutes to get a homogeneous dispersion of the solution. Then, the Pyrex tube was flash-frozen using a liquid N₂ bath (77 K) and degassed by three freeze-pump-thaw cycles. Subsequently, the pyrex tube was sealed off using a flame torch and heated in an oven at 120 °C for 72 h. After completion of the reaction, a dark red-colored precipitate was collected by filtration and washed with acetone. The crystalline solid obtained was then subjected to solvent exchange with acetone 5-6 times to remove unreacted reactants and dried at 120 °C under vacuum for 12 h to get a fine crystalline red powder of COF-SO₃H in ~70 % isolated yield.

2.2.3.2. Synthesis of COF-H

COF-H was synthesized by following the previously reported procedure with little modification. ⁶⁴ Briefly, a pyrex tube was charged with Triformylphloroglucinol (0.3 mmol), 1,4-phenylenediamine (0.45 mmol), and a 3 mL solvent mixture of mesitylene and dioxane (1:1), and 0.5 mL of 3 M aqueous acetic acid. Then, the mixture was sonicated for 10 minutes to get a homogeneous dispersion of the solution. Subsequently, the pyrex tube was flash-frozen using a liquid N₂ bath (77 K) and degassed by three freeze-pump-thaw cycles. Later, the tube was sealed and maintained in an oven at 120 °C for 72 h. After the reaction was completed, the red-colored precipitate was collected by centrifugation and washed with acetone. The powder was kept in acetone for solvent exchange to remove the high boiling solvent in the material and dried at 120 °C under vacuum for 12 h to get a fine crystalline red powder of COF-H in ~80 % isolated yield.

2.2.4. Metal-free cycloaddition of CO₂ with epoxides

The cycloaddition reaction of CO₂ with various epoxides was carried out in a stainless steel reactor (50 mL) with a magnetic stirrer at 80 °C and 1 bar pressure of CO₂. The catalyst, COF-SO₃H, was activated at 373 K for 12 h under vacuum to

remove the guest solvents. The reactants were taken in the reactor at room temperature, and it was flushed with CO₂ twice, the required pressure, 0.1 MPa was introduced, and the contents were kept stirring for 24 h. After the reaction, the reactor was allowed to cool down, excess CO₂ gas was released from the reactor, and the catalyst, COF-SO₃H was separated from the reaction mixture by filtration. The catalytic conversion was determined by recording the ¹H NMR spectra of the filtrate. The recovered catalyst was washed with acetone thrice, activated at 373 K under vacuum for 12 h, and reused for further catalytic cycles. The catalytic conversions were quantified by ¹H NMR analysis. The TON was calculated using the relation given below.

TON = Moles of product formed (mmol g^{-1})/total number of active acidic sites on the catalyst (mmol g^{-1}).

2.2.5. Structure simulation and modeling of COF-SO₃H and COF-H

To elucidate the structure of COF-SO₃H/COF-H and to calculate the unit cell parameters, a possible 2D model was constructed. The experimental PXRD pattern matches well with the simulated pattern for an eclipsed model of COF-SO₃H and COF-H. Refinement of PXRD patterns was carried out using the Pseudo-Voigt function. The simulated optimized structure of COF-SO₃H/H is shown in Figures 1 and 2.

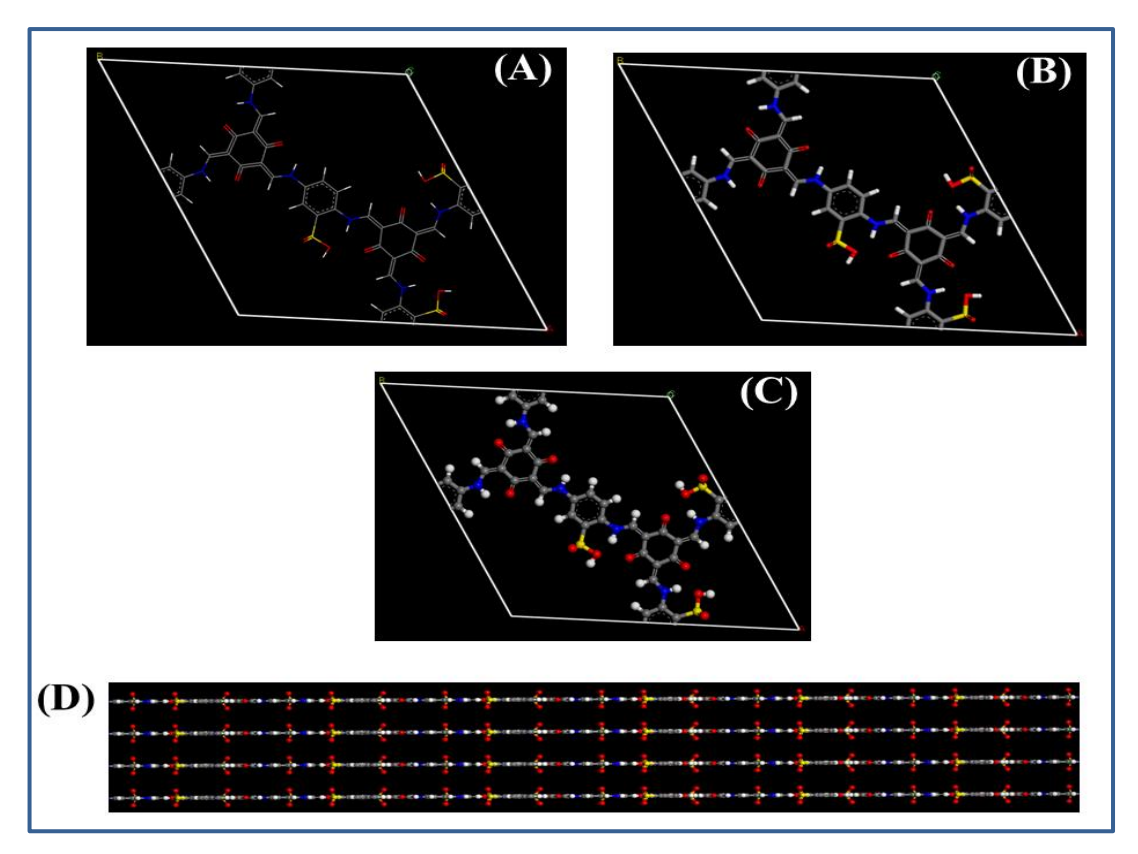


Figure 1. The unit cell of COF-SO₃H in different display style representation, (A) Line, (B) stick, (C) ball and stick, and (D) stacked 2D layers of COF-SO₃H.

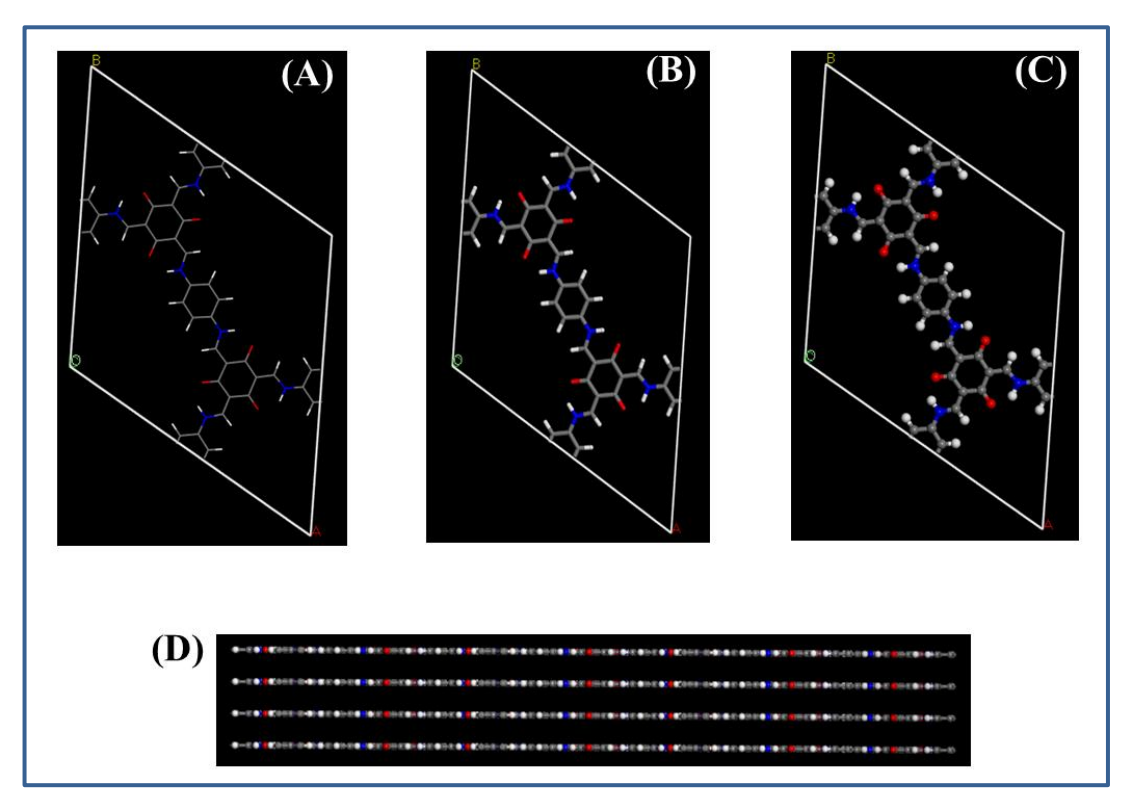


Figure 2. The unit cell of COF-H in different display style representation, (A) Line, (B) stick, (C) ball and stick, and (D) stacked 2D layers of COF-H.

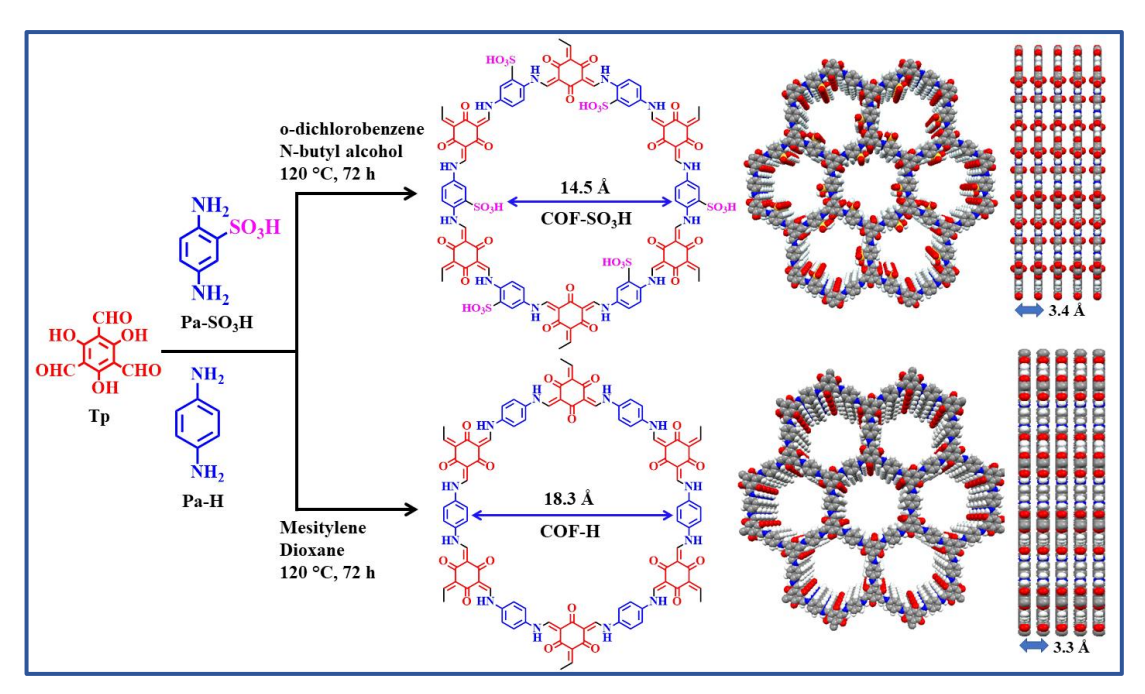
2.2.6. Gas adsorption measurements

N₂ adsorption-desorption studies were carried out at 77 and 273 K, while CO₂ adsorption-desorption measurements were carried out at 273 and 298 K using QUANTACHROME Quadrasorb SI automated surface area and pore size analyzer instrument. Ultrapure (99.995%) N₂, CO₂, and CH₄ gases were used for the adsorption-desorption measurements. Prior to adsorption measurements, the sample (~0.050 g) was evacuated at 393K under vacuum (20 mTorr) for 12 h on QUANTACHROME Flovac degasser and further purged with ultrapure N₂ (99.995%) gas on cooling. The BET surface area of the COFs was estimated from N₂ sorption isotherms carried out at 77 K. The gas selectivity experiments were carried out at 273 K. The dead volume of the sample cell was measured using Helium gas (99.995%).

2.3. Results and discussion

2.3.1. Synthesis and structural description

The COF-SO₃H and COF-H were synthesized by following the previously reported procedure with a slight modification (Scheme 1). The FT-IR spectra of assynthesized COF-SO₃H showed the absence of characteristic stretching peaks around 3335-3425 cm⁻¹ and 1650 cm⁻¹ corresponding to free N-H and C=O groups from precursors, 2,5-diaminobenzenesulfonic acid and 1,3,5-triformylphloroglucinol, respectively. In addition, the appearance of two new peaks at 1578 cm⁻¹ and 1233 cm⁻¹ corresponding to C=C and C-N stretching frequencies, respectively, supporting the COF formation by Schiff-base condensation of the aldehyde and amine precursors (Figure A1a). Similarly, new peaks at 1572 and 1252 cm⁻¹ corresponding to C=C and C-N stretching frequencies were observed in support of COF-H formation (Figure A1b). In the case of COF-SO₃H, the appearance of an additional peak at 1005 cm⁻¹ due to S-OH stretching supports the presence of free sulfonic acid (-SO₃H) groups decorated in the 1D channels of the COF (Figure A1a).⁶⁵



Scheme 1. The synthesis scheme of COF-SO₃H, COF-H, and their structural models (yellow, Sulfur; red, Oxygen; blue, Nitrogen; grey, Carbon; white, Hydrogen).

Moreover, the ¹³C CP-MAS solid-state NMR spectrum of COF-SO₃H/H showed the absence of a C=O resonance peak, confirming the complete consumption of starting material. 66,67 Further, the appearance of new resonance peaks at δ, 145-150 ppm corresponding to the C-N bond formed by Schiff-base condensation supports the formation of COF-SO₃H/H (Figure 3a and 3b). It is worth mentioning that the peaks due to C-N and C=C in COF-SO₃H are relatively downfield shifted compared to those of COF-H, which has been attributed to the presence of electron-withdrawing group (-SO₃H).^{66,67} Moreover, the PXRD pattern of as-synthesized COF-SO₃H showed a predominant peak at low angle range, $2\Theta =$ 4.8° assigned to (100) plane supporting the long-range ordering in the structure and appearance of a broad peak in the range of $2\Theta = 26.8-27.2^{\circ}$ is assigned to (001) plane corresponding to π - π stacking between the planes of COF-SO₃H. It is worth noting that the experimental PXRD pattern is well-matched with that of the simulated pattern (Figure 3c). The PXRD pattern of COF-H showed an intense peak at $2\Theta = 4.7^{\circ}$ corresponding to the (100) plane supporting the long-range ordering in the structure. Besides, minor peaks were observed at $2\Theta = 8.3^{\circ}$, 11.1° , and 27° , which are assigned to (200), (210), and (001) planes (Figure 3d). The d-spacing calculated for COF-SO₃H and COF-H was found to be 3.4 Å and 3.3 Å, respectively (Scheme 1). Further, the most probable 2D model of COF-SO₃H was envisaged in an eclipsed structure with a Triclinic crystal system in the PI space group. The unit cell parameters for COF-SO₃H are a=22.83 Å, b=22.94 Å, c=6.87 Å, $\alpha=89.85^{\circ}$, $\beta=89.79^{\circ}$ and $\gamma=120.54^{\circ}$. Whereas the probable 2D model of COF-H in an eclipsed form was simulated with a hexagonal crystal structure in the P6/m space group and the unit cell parameters are a=b=22.82 Å, c=3.34 Å, $\alpha=\beta=90^{\circ}$ and $\gamma=120^{\circ}$. Further, COF-SO₃H possesses 1D channels with a diameter of 14.5 Å decorated with a high density of polar (-SO₃H) groups. Whereas, COF-H has 1D channels with a dimension of 18.3 Å free from polar functional groups (Scheme 1).

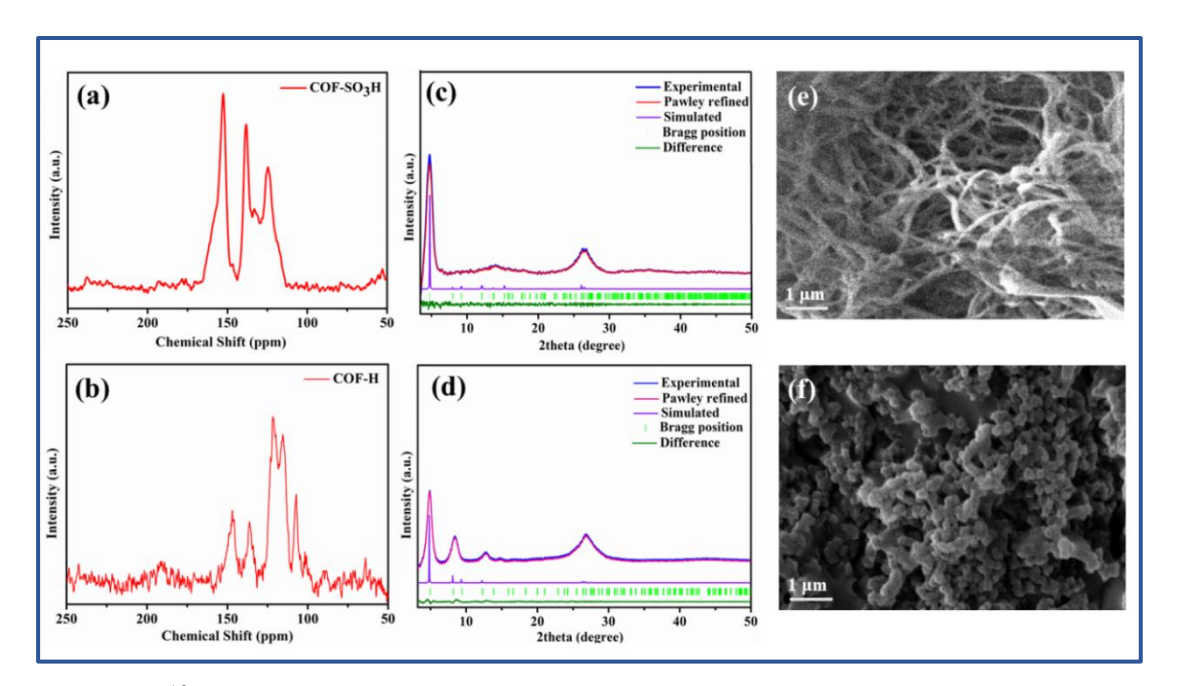


Figure 3. ¹³C CP-MASS solid-state NMR spectrum of COF-SO₃H (a) and COF-H (b). Comparison of theoretical and experimental PXRD patterns of COF-SO₃H, (c) and COF-H (d). SEM images of COF-SO₃H (e) and COF-H (f).

The SEM images of COF-SO₃H showed nanofiber-like morphology, while COF-H showed aggregated particles (Figures 3e and 3f).⁶⁸ Further, to test the thermal stability of the samples, thermogravimetric analysis (TGA) of the COFs was carried out as shown in Figure A2. The TGA plot of the COFs show a weight loss in the temperature range of 50-100 °C, which can be attributed to the loss of adsorbed solvent molecules. The desolvated COFs were stable up to 300 °C, and at higher temperatures, the frameworks undergo disintegration (Figure A2a and A2b).

2.3.3. Gas adsorption studies

The permanent porosity of COF-SO₃H and COF-H was determined by N₂

adsorption measurements at 77 K. Prior to the adsorption measurements, the assynthesized samples were activated at 120 °C under vacuum for 12h. From N₂ adsorption measurements, the BET surface area (S_{BET}) of COF-SO₃H and COF-H were determined to be 185 m²g⁻¹ and 498.7 m²g⁻¹, respectively (Figure 4a). The relatively higher surface area of the COF-H sample could be attributed to its relatively smaller particle size in comparison to that of COF-SO₃H. The pore size distribution plot of COF-SO₃H confirms the microporous (~ 14.2 Å) nature of the material. Further, CO₂ adsorption isotherms of COF-SO₃H/H follow a type-I profile with the uptake of 75.2/58.5 cc/g and 54.5/38.5 cc/g at 273 and 298 K, respectively (Figure 4b and 4c). Furthermore, the adsorption isotherms were fitted with the Freundlich-Langmuir equation⁶⁹ (Figure A3 and A4), and the value of heat of interaction (Q_{st}) determined using the Clausius-Clayperon equation ⁷⁰ was 42.2 kJ/mol and 31.4 kJ/mol for COF-SO₃H and COF-H, respectively (Figure A5a and A5b). The high heat of interaction energy of COF-SO₃H over COF-H supports stronger interaction of CO₂ with polar (-SO₃H) groups lined in the 1D channels of the framework. A similar observation of enhanced CO₂ interaction with frameworks in the presence of polar SO₃H groups is reported in the literature.⁷¹ Moreover, COF-SO₃H shows selective adsorption of CO₂ over N₂ and CH₄ at 273 K (Figure 4d) with a Henry selectivity constant of 49.3 and 86.8 for K_{CO2}/_{CH4} and K_{CO2}/_{N2}, respectively (Figure A6).

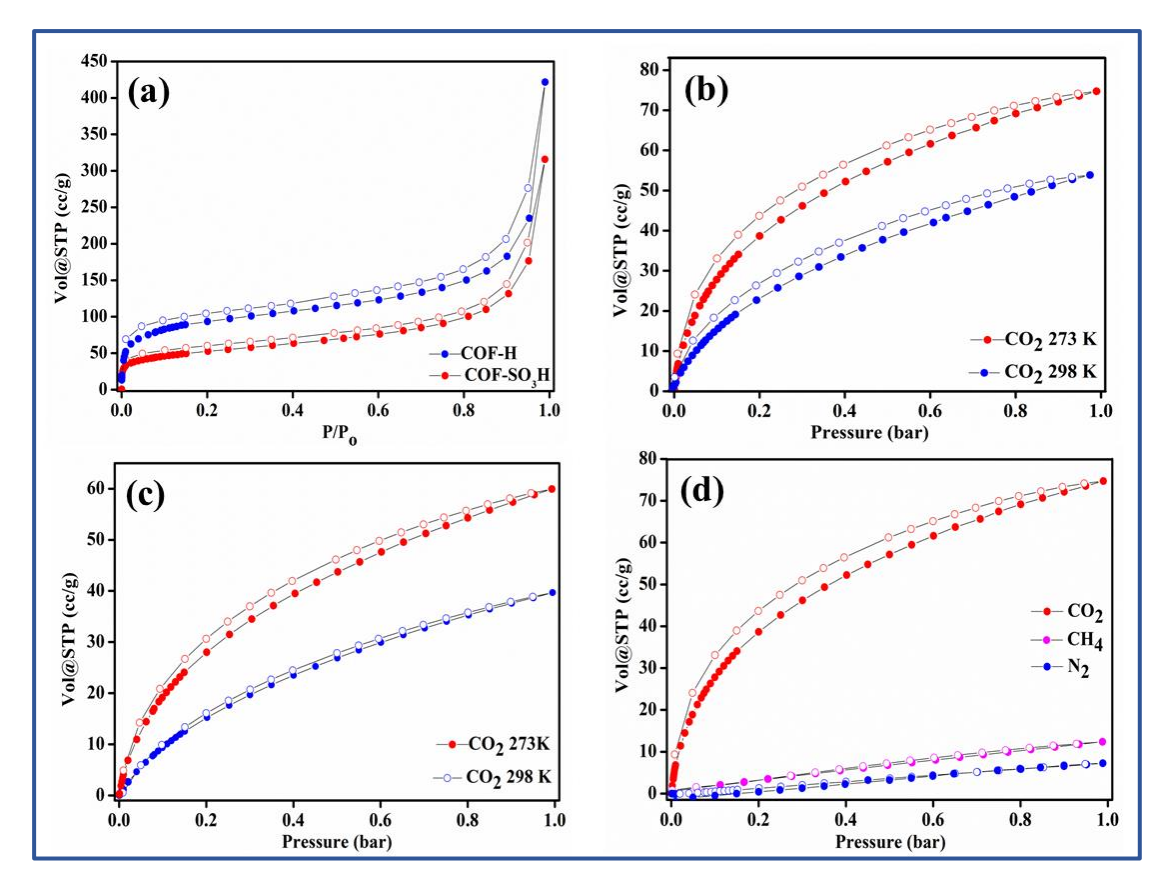


Figure 4. N₂ adsorption isotherms for COF-SO₃H and COF-H carried out at 77 K (a). The CO₂ adsorption-desorption isotherms of COF-SO₃H (b) and COF-H (c). Selective CO₂ adsorption isotherms of COF-SO₃H (d).

Furthermore, the amount of acidic sites present in COF-SO₃H was determined by the temperature-programmed desorption (TPD) technique. The NH₃-TPD analysis was carried out to quantify the acidity of the COF-SO₃H. As shown in Figure A7, the NH₃-TPD analysis revealed that NH₃ is desorbed with peaks maxima around 140 and 360 °C. The amount of acidity in COF-SO₃H was calculated to be 3.46 mmol g⁻¹, which can be attributed to the presence of sulfonic acid (-SO₃H) groups. Thus, the -SO₃H groups introduce Brønsted acid sites in the COF, which facilitate the catalytic conversion of CO₂ with epoxides to obtain value-added cyclic carbonates.

2.3.4. Metal-free utilization of CO₂

The high heat of CO₂ interaction and the presence of Brønsted acid (BA) sites in COF-SO₃H motivated us to explore its catalytic activity towards the cycloaddition of CO₂ with epoxides under metal/solvent-free conditions. To start with, the catalytic reactions were carried out using epichlorohydrin (ECH) as the model substrate, and

the catalytic conditions were optimized (Table 1) by varying the temperature and time of the reaction, as shown in Figure 5.

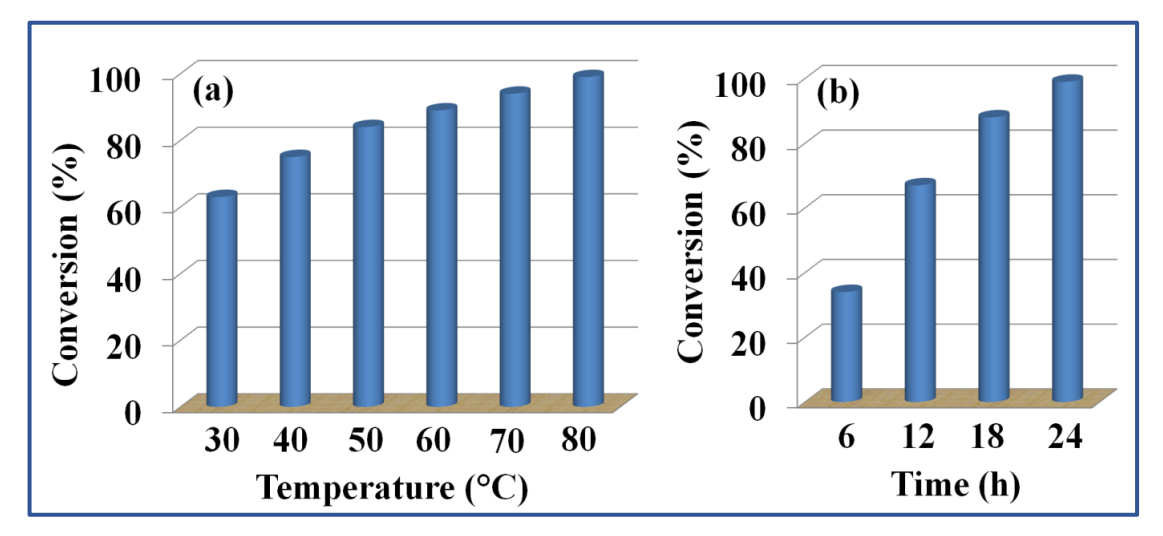


Figure 5. The catalytic optimization performed by varying reaction temperature (a) and time (b). Conditions: Epoxide (20 mmol), COF-SO₃H (0.01 mmol), TBAB (2.5 mol%), and 1 bar CO₂.

The catalytic reaction carried out with COF-SO₃H as a catalyst at RT and 1 bar CO₂ resulted in 63% conversion of ECH into cyclic carbonate (CC) in 24 h (Table 1). Further, with an increase in reaction temperature to 80 °C, the conversion of ECH to corresponding cyclic carbonate increased by >99% (Table 1). Moreover, a control experiment carried out using TBAB (tetrabutylammonium bromide) as a catalyst showed only 27% conversion of ECH to CC under the optimized conditions, highlighting the importance of COF-SO₃H towards the conversion of CO₂ (Table 1).

Table 1. Optimization of reaction parameters for cycloaddition reaction of CO₂ with epichlorohydrin catalyzed by COF-SO₃H.

Entry	Catalyst	Co-	Pressure	Time	Temperature	Conversion	
No.	(mol%)	catalyst	(bar)	(h)	(°C)	%	
		(mol%)					
1.	-	-	1	12	r.t.	-	
2.	-	-	1	12	60	-	
3.	COF-	-	1	12	80	-	
	SO ₃ H						
4.	COF-	TBAB	1	24	30	63	
	SO_3H						
5.	COF-	TBAB	1	24	80	>99	
	SO_3H						
6.	COF-H	TBAB	1	24	80	75	
7.	-	TBAB	1	24	80	27	

This high catalytic activity motivated us to extend the substrate scope for various other epoxides. The epoxides, 1,2-epoxypropane, 1,2-epoxybutane, 1,2epoxyhexane, and 1,2-epoxydecane were found to undergo conversion to the corresponding cyclic carbonates with >99, 85, 71, and 66% yield, respectively (Table 2). The decrease in the catalytic conversion of the longer epoxides can be attributed to the confinement of the pore channels, which results in the restricted diffusion of larger epoxides to the BA sites lined in the 1D channels of the framework.⁷² Whereas, butyl glycidyl ether (BGE) and allyl glycidyl ether (AGE) undergo relatively higher catalytic conversion with 89 and 80% conversion, respectively, which can be ascribed to the electron-donating nature of glycidyl ether (Table 2).73 Besides, aromatic epoxide, viz styrene oxide (SO), was found to convert 75% to styrene carbonate (Table 2). Further, to evaluate the role of Brønsted acid (-SO₃H) sites towards the catalytic conversion of CO₂, the catalytic activity of analogs COF having no -SO₃H sites was studied at the optimized conditions. Interestingly, COF-H catalyzed only 75% conversion of ECH to CC at the optimized conditions (Table 1). This relatively lower catalytic activity of COF-H highlights the importance of -SO₃H groups for enhanced capture and conversion of CO₂. It is

worth emphasizing that COF-SO₃H showed higher catalytic activity than various COF-based catalysts reported in the literature (Table A1).

Table 2. Metal/solvent-free fixation of CO₂ catalyzed by COF-SO₃H as heterogeneous catalyst.^a

	<u> </u>	F-SO ₃ H, TBAB OC, 1 bar CO ₂	o o		
S. No.	Substrate	Product	Conversion (%) ^b	Selec tivity (%)	TON
1	CI	CI	>99	100	248
2			>99	100	248
3			85	100	213
4			71	99	178
5			66	100	165
6			80	100	200
7			89	100	223
8			75	99	188

^aReaction conditions: Epoxide (20 mmol), COF-SO₃H (0.01 mmol), TBAB (2.5 mol%), Temperature (80 °C), 1 bar CO₂, 24 h, and ^bThe catalytic conversions were determined by ¹H NMR analysis.

2.3.5. Recyclability and catalyst leaching test

The recyclability of a heterogeneous catalyst is an essential parameter for practical applications. To test the recyclability, the COF-SO₃H was separated from the reaction mixture by filtration, washed with acetone, dried, and reused for subsequent cycles. Remarkably, no significant loss in the catalytic activity was observed even after reusing for five consecutive cycles (Figure 6a). Further, the recycled COF was characterized by various techniques to confirm its structural stability and morphology. Indeed, the PXRD pattern, FT-IR spectra, and morphology of the recycled sample matched well with an as-synthesized sample, confirming retaining the original framework structure even after catalysis (Figure A8-A10). Furthermore, the N₂ adsorption isotherm of COF-SO₃H recovered after catalysis showed a slight reduction in BET surface area (151 m²/g) in comparison to that of pristine COF (185 m²/g) (Figure A11). To rule out the leaching of the active catalyst, a control experiment was carried out for cycloaddition of ECH in which the catalytic reaction was stopped after 6 h, the COF was separated by filtration, and the filtrate was allowed to stir for an additional period of 18 h. Interestingly, only a slight increase (~6%) in the conversion of ECH was observed, which can be attributed to the presence of a co-catalyst (TBAB) in the reaction mixture. The significant reduction in the conversion of ECH upon removal of COF catalyst supports the absence of leaching of active catalyst into the reaction mixture (Figure 6b).

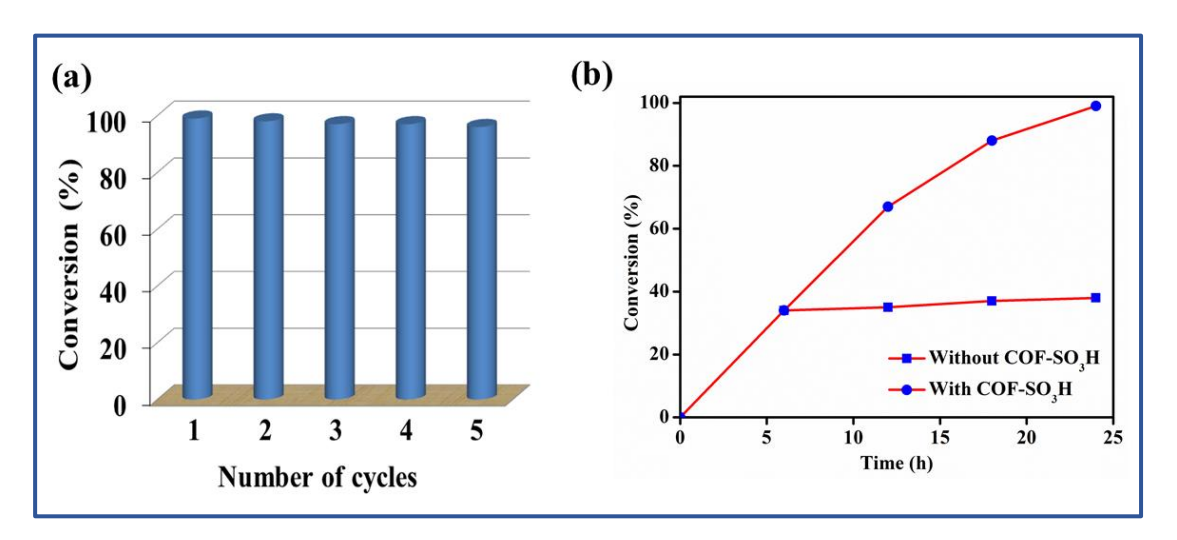
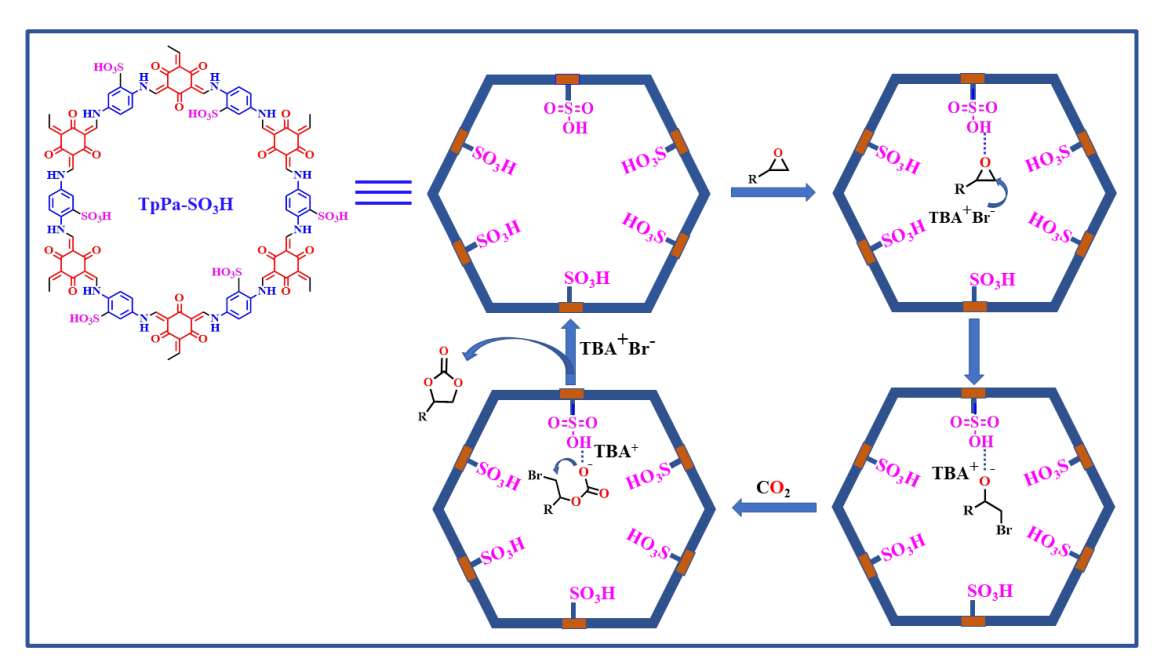


Figure 6. (a) Recyclability test and (b) leaching test of COF-SO₃H.

2.3.6. Plausible mechanism

A plausible mechanism for the cycloaddition reaction of CO₂ with epoxide using COF-SO₃H is shown in Scheme 2. The sulfonic acid groups lined in the 1D channels act as Brønsted acid sites at which polarization of epoxide takes place through H-bonding interactions. To confirm this step, COF-SO₃H was treated with ECH for 2 h followed by washing with methanol. The FT-IR spectra (Figure A12) of the recovered COF show characteristic peaks around 3000-2900 cm⁻¹ corresponding to C-H stretching frequencies of the epoxide, supporting polarization of the epoxide by COF-SO₃H. This step is followed by nucleophilic attack of the Br⁻ ion of TBAB at the less hindered carbon atom of epoxide, facilitating ring-opening of the epoxide and leading to the formation of oxyanion intermediate. Subsequent insertion of the CO₂ molecule results in forming an alkyl carbonate anion, which undergoes ring closure to form cyclic carbonate, and its elimination regenerates the COF-SO₃H catalyst for further cycles.



Scheme 2. A plausible mechanism for coupling CO₂ with epoxides catalyzed by TpPa-SO₃H (only part of the COF unit is shown for clarity).

2.4. Conclusion

In summary, the present work demonstrates the utilization of a polar functionalized COF (COF-SO₃H) for selective capture and conversion of CO₂ into high-value cyclic carbonates under metal and solvent-free mild conditions of RT and

an atmospheric pressure of CO₂. The presence of the polar group not only enhanced the CO₂ affinity of the framework but also promoted higher catalytic activity over the analogs COF, which lacks the polar group. More importantly, the COF-SO₃H catalyst was highly recyclable for up to five cycles without loss of catalytic activity and framework stability. Overall, this study can pave the way for the development of metal-free heterogeneous catalysts functionalized with polar Brønsted acid sites for the fixation of CO₂ into value-added chemicals under mild conditions.

2.5. References

- (1) Jacobson, M. Z. Review of solutions to global warming, air pollution, and energy security. *Energy Environ. Sci.* **2009**, *2*, 148-173.
- (2) Tiba, S.; Omri, A. Literature survey on the relationships between energy, environment and economic growth. *Renew. Sust. Energ. Rev.* **2017**, *69*, 1129-1146.
- (3) Joos, F.; Plattner, G. -K.; Stocker, T. F.; Marchal O.; Schmittner, Global Warming and Marine Carbon Cycle Feedbacks on Future Atmospheric CO₂. A. *science* **1999**, 284, 464-467.
- (4) Glikson, A. The lungs of the Earth: Review of the carbon cycle and mass extinction of species. *Energy Procedia* **2018**, *146*, 3-11.
- (5) (a) Sakakura, T.; Choi, J. -C.; Yasuda, H. Transformation of carbon dioxide. *Chem. Rev.* 2007, **107**, 2365-2387; (b) Liu, Q.; Wu, L.; Jackstell, R.; Beller, M. Using carbon dioxide as a building block in organic synthesis. *Nat Commun.* **2015**, 6, 5933.
- (6) Ding, M.; Flaig, R. W.; Jiang, H. -L.; Yaghi, O. M. Carbon capture and conversion using metal-organic frameworks and MOF-based materials. *Chem. Soc. Rev.* **2019**, *48*, 2783-2828.
- (7) Omodolor, I. S.; Otor, H. O.; Andonegui, J. A.; Allen, B. J.; -Rubio, A. Dual-Function Materials for CO₂ Capture and Conversion: A Review. *Ind. Eng. Chem. Res.* **2020**, *59*, 17612-17631.
- (8) Liang, J.; Huang, Y. -B.; Cao R. Metal-organic frameworks and porous organic polymers for sustainable fixation of carbon dioxide into cyclic carbonates. *Coord. Chem. Rev.* **2019**, *378*, 32-65.
- (9) North, M.; Pasquale, R.; Young, C. Synthesis of cyclic carbonates from epoxides and CO₂. *Green Chem.* **2010**, *12*, 1514-1539.

- (10) Calabrese, C.; Giacalone, F.; Aprile, C. Hybrid Catalysts for CO₂ Conversion into Cyclic Carbonates. *Catalyst* **2019**, *9*, 325.
- (11) Yu, K.; Puthiaraj, P.; Ahn, W. -S. One-pot catalytic transformation of olefins into cyclic carbonates over an imidazolium bromide-functionalized Mn(III)-porphyrin metal-organic framework. *Appl. Catal. B* **2020**, *273*, 119059.
- (12) Dhankhar, S. S.; Ugale, B.; Nagaraja, C. M. Co-Catalyst-Free Chemical Fixation of CO₂ into Cyclic Carbonates by using Metal-Organic Frameworks as Efficient Heterogeneous Catalysts. *Chem. Asian J.* **2020**, *15*, 2403-2427.
- (13) Pal, T. K.; De, D.; Bhardwaj, P. K. Metal-organic frameworks for the chemical fixation of CO₂ into cyclic carbonates. *Coord. Chem. Rev.* **2020**, *408*, 213173.
- (14) Dhakshinamoorthy, A.; Asiri, A. M.; Alvaro, M.; Garcia, H. Metal organic frameworks as catalysts in solvent-free or ionic liquid assisted conditions. *Green Chem.* **2018**, *20*, 86-107.
- (15) Dhakshinamoorthy, A.; Li, Z.; Garcia, H. Catalysis and photocatalysis by metal-organic frameworks. *Chem. Soc. Rev.* **2018**, *47*, 8134-8172.
- (16) Ding, M.; Flaig, R. W.; Jiang, H. -L.; Yaghi, O. M. Carbon capture and conversion using metal-organic frameworks and MOF-based materials. *Chem. Soc. Rev.* **2019**, *48*, 2783-2828.
- (17) (a) Scrosati, B.; Hassoun, J.; Sun, Y. -K. Lithium-ion batteries. A look into the future. *Energy Environ. Sci.* **2011**, *4*, 3287-3295; (b) Besse, V.; Camara, F.; Voirin, C.; Auvergne, R.; Caillol, S.; Boutevin, B. Synthesis and applications of unsaturated cyclocarbonates. *Polym. Chem.* **2013**, *4*, 4545-4561; (c) Fukuoka, S.; Kawamura, M.; Komiya, K.; Tojo, M.; Hachiya, H.; Hasegawa, K.; Aminaka, M.; Okamoto, H.; Fukawa, I.; Konno, S. A novel non-phosgene polycarbonate production process using by-product CO₂ as starting material. *Green Chem.* **2003**, *5*, 497-507.
- (18) (a) Martin, C.; Fiorani, G.; Kleij, A. W. Recent advances in the catalytic preparation of cyclic organic carbonates. *ACS Catal.* **2015**, *5*, 1353-1370; (b) Comerford, J. W.; Ingram, I. D. V.; North, M.; Wu, X. Sustainable metal-based catalysts for the synthesis of cyclic carbonates containing five-membered rings. *Green Chem.* **2015**, *17*, 1966-1987.
- (19) (a) Kohrt, C.; Werner, T. Recyclable Bifunctional Polystyrene and Silica Gel-Supported Organocatalyst for the Coupling of CO₂ with Epoxides. *ChemSusChem.* **2015**, 8, 2031-2034; (b) Toda, Y.; Komiyama, Y.; Kikuchi, A.; Suga, H. Tetraarylphosphonium salt-catalyzed carbon dioxide fixation at atmospheric

pressure for the synthesis of cyclic carbonates. ACS Catal. 2016, 6, 6906-6910.

- (20) Ren, Y.; Shim, J. -J. Efficient Synthesis of Cyclic Carbonates by MgII/Phosphine-Catalyzed Coupling Reactions of Carbon Dioxide and Epoxides. *ChemCatChem* **2013**, *5*, 1344-1349.
- (21) Dagorne, S.; Wehmschulte, R. Recent Developments on the Use of Group 13 Metal Complexes in Catalysis. *ChemCatChem* **2018**, *10*, 2509-2520.
- (22) Pescarmona, P. P. Cyclic carbonates synthesized from CO₂: Applications, challenges, and recent research trends. *Curr. Opin. Green Sustain.* **2021**, 29, 100457.
- (23) (a) Wu, P.; Li, Y.; Zheng, J. -J., Hosono, N.; Otake, K. -I.; Wang, J.; Liu, Y.; Xia, L.; Jiang, M.; Sakaki, S.; Kitagawa, S. Carbon dioxide capture and efficient fixation in a dynamic porous coordination polymer. Nature Commun. 2019, 10, 4362; (b) Das, R.; Nagaraja, C. M. Highly Efficient Fixation of Carbon Dioxide at RT and Atmospheric Pressure Conditions: Influence of Polar Functionality on Selective Capture and Conversion of CO₂. *Inorg. Chem.* **2020**, *59*, 9765-9773; (c) Bhanja, P.; Modak, A.; Bhaumik, A. Porous Organic Polymers for CO₂ Storage and Conversion Reactions. ChemCatChem 2019, 11, 244-257; (d) Sharma, N.; Dhankhar, S. S.; Nagaraja, C. M. Environment-friendly, co-catalyst-and solvent-free fixation of CO₂ using an ionic zinc(II)-porphyrin complex immobilized in porous metal-organic frameworks. Sustain. Energy Fuels 2019, 3, 2977-2982; (e) Olajire, A. A. Synthesis chemistry of metal-organic frameworks for CO₂ capture and conversion for sustainable energy future. Renew. Sustain. Energy Rev. 2018, 92, 570-607; (f) Huh, S. Direct Catalytic Conversion of CO₂ to Cyclic Organic Carbonates under Mild Reaction Conditions by Metal-Organic Frameworks. Catalyst **2019**, 9, 34.
- (24) (a) He, H.; Perman, J. A.; Zhu, G.; Ma, S. Metal-Organic Frameworks for CO₂ Chemical Transformations. *Small* **2016**, *12*, 6309-6324; (b) Ugale, B.; Kumar, S.; Kumar, T. J. D.; Nagaraja, C. M. Environmentally Friendly, Co-catalyst-Free Chemical Fixation of CO₂ at Mild Conditions Using Dual-Walled Nitrogen-Rich Three-Dimensional Porous Metal-Organic Frameworks. *Inorg. Chem.* **2019**, *58*, 3925-3936; (c) Trickett, C. A.; Helal, A.; -Maythalony, B. A. A.; Yamani, Z. H.; Cordova, K. E.; Yaghi, O. M. The chemistry of metal-organic frameworks for CO₂ capture, regeneration and conversion. *Nat. Rev. Mater.* **2017**, *2*, 17045; (d) Ugale, B.; Dhankhar, S. S.; Nagaraja, C. M. Interpenetrated Metal-Organic Frameworks of

- Cobalt(II): Structural Diversity, Selective Capture, and Conversion of CO₂. *Cryst. Growth. Des.* **2017**, *17*, 3295-3305; (e) Sharma, N.; Dhankhar, S. S.; Kumar, S.; Kumar, T. J. D.; Nagaraja, C. M. Rational Design of a 3D Mn^{II}-Metal-Organic Framework Based on a Nonmetallated Porphyrin Linker for Selective Capture of CO₂ and One-Pot Synthesis of Styrene Carbonates. *Chem. Eur. J.* **2018**, *24*, 16662-16669; (f) Ugale, B.; Dhankhar, S. S.; Nagaraja, C. M. Construction of 3-Fold-Interpenetrated Three-Dimensional Metal-Organic Frameworks of Nickel(II) for Highly Efficient Capture and Conversion of Carbon Dioxide. *Inorg. Chem.* **2016**, *55*, 9757-9766; (g) Ugale, B.; Dhankhar, S. S. Nagaraja, C. M. Exceptionally Stable and 20-Connected Lanthanide Metal-Organic Frameworks for Selective CO₂ Capture and Conversion at Atmospheric Pressure. *Cryst. Growth. Des.* **2018**, *18*, 2432-2440.
- (25) Singh, G.; Lee, J.; Karakoti, A.; Bahadur, R.; Yi, J.; Zhao, D.; AlBahilyc, K.; Vinu, A. Emerging trends in porous materials for CO₂ capture and conversion. *Chem. Soc. Rev.* **2020**, *49*, 4360-4404.
- (26) Marciniak, A. A.; Lamb, K. J.; Ozorio, L. P.; Mota, C. J. A.; North. M. Heterogeneous catalysts for cyclic carbonate synthesis from carbon dioxide and epoxides. *Curr. Opin. Green Sustain.* **2020**, *26*, 10035.
- (27) He, H.; Sun, Q.; Gao, W.; Perman, J. A.; Sun, F.; Zhu, G.; Aguila, B.; Forrest, K.; Space, B.; Ma. S. A stable metal-organic framework featuring a local buffer environment for carbon dioxide fixation. *Angew. Chem. Int. Ed.* **2018**, *57*, 4657-4662.
- (28) Chakraborty, G.; Das, P.; Mandal, S. K. Efficient and Highly Selective CO₂ Capture, Separation, and Chemical Conversion under Ambient Conditions by a Polar-Group-Appended Copper(II) Metal-Organic Framework. *Inorg. Chem.* **2021**, *60*, 5071-5080.
- (29) Cao, C. -S.; Xia, S. -M.; Song, Z. -J.; Xu, H.; Shi, Y.; He, L. -N.; Cheng, P.; Zhao, B. Highly Efficient Conversion of Propargylic Amines and CO₂ Catalyzed by Noble-Metal-Free [Zn116] Nanocages. *Angew. Chem. Int. Ed.* **2020**, *59*, 8586-8593.
- (30) Hou, S. -L.; Dong, J.; Zhao, B. Formation of C-X Bonds in CO₂ Chemical Fixation Catalyzed by Metal-Organic Frameworks. *Adv. Mater.* **2020**, *32*, 1806163. (31) (a) Kohrt, C.; Werner, T. Recyclable Bifunctional Polystyrene and Silica Gel-Supported Organocatalyst for the Coupling of CO₂ with Epoxides. *ChemSusChem*

2015, *8*, 2031-2034; (b) Toda, Y.; Komiyama, Y.; Kikuchi, A.; Suga, H. Tetraarylphosphonium salt-catalyzed carbon dioxide fixation at atmospheric pressure for the synthesis of cyclic carbonates. *ACS Catal.* **2016**, *6*, 6906-6910; (c) Miralda, C. M.; Macias, E. E.; Zhu, M.; Ratnasamy P.; Carreon, M. A. Zeolitic Imidazole Framework-8 Catalysts in the Conversion of CO₂ to Chloropropene Carbonate. *ACS Catal.* **2012**, *2*, 180-183; (d) Kuruppathparambil, R. R.; Babu, R.; Jeong, H. M.; Hwang, G. -Y.; Jeong, G. S.; Kim, M. -I.; Kim, D. -W.; Park, D. -W. A solid solution zeolitic imidazolate framework as a room temperature efficient catalyst for the chemical fixation of CO₂. *Green Chem.* **2016**, *18*, 6349-6356. (e) Das, P.; Mandal, S. K. Efficient and Highly Selective CO₂ Capture, Separation, and Chemical Conversion under Ambient Conditions by a Polar-Group-Appended Copper(II) Metal-Organic Framework. *Inorg. Chem.* **2021**, *60*, 5071-5080.

(32) (a) Wang, J. -Q.; Kong, D. -L.; Chen, J. -Y.; Cai, F.; He, L. -N. Synthesis of cyclic carbonates from epoxides and carbon dioxide over silica-supported quaternary ammonium salts under supercritical conditions. *J. Mol. Catal. A Chem.* **2006**, *249*, 143-148; (b) Sun, Q.; Jin, Y.; Aguila, B.; Meng, X.; Ma, S.; Xiao, F. -S. Porous Ionic Polymers as a Robust and Efficient Platform for Capture and Chemical Fixation of Atmospheric CO₂. *ChemSusChem.* **2017**, *10*, 1160-1165; (c) Wang, J.; Yang, J. G. W.; Yi, G.; Zhang, Y. Phosphonium salt incorporated hyper crosslinked porous polymers for CO₂ capture and conversion. *Chem. Commun.* **2015**, *51*, 15708-15711.

(33) (a) He, H.; Perman, J. A.; Zhu, G.; Ma, S. Metal-Organic Frameworks for CO₂ Chemical Transformations. *Small* **2016**, *12*, 6309-6324; (b) Gao, W. -Y.; Chen, Y.; Niu, Y.; Williams, K.; Cash, L.; Perez, P. J.; Wojtas, L.; Cai, J.; Chen, Y. -S.; Ma, S. Crystal Engineering of an nbo Topology Metal-Organic Framework for Chemical Fixation of CO₂ under Ambient Conditions. *Angew. Chem. Int. Ed.* **2014**, *53*, 2615-2619; (c) Zhou, Z.; He, C.; Xiu, J.; Yang, L.; Duan, C. Metal-organic polymers containing discrete single-walled nanotube as a heterogeneous catalyst for the cycloaddition of carbon dioxide to epoxides. *J. Am. Chem. Soc.* **2015**, *137*, 15066-15069; (d) Beyzavi, M. H.; Klet, R. C.; Tussupbayev, S.; Borycz, J.; Vermeulen, N. A.; Cramer, C. J.; Stoddart, J. F.; Hupp, J. T.; Farha, O. K. A Hafnium-Based Metal-Organic Framework as an Efficient and Multifunctional Catalyst for Facile CO₂ Fixation and Regioselective and Enantioretentive Epoxide Activation. *J. Am. Chem. Soc.* **2014**, *136*, 15861-15864; (e) Li, P. -Z.; Wang, X. -J.; Liu, J.; Lim, J. S.;

- Zou, R.; Zhao, Y. A Triazole-Containing Metal-Organic Framework as a Highly Effective and Substrate Size-Dependent Catalyst for CO₂ Conversion. *J. Am. Chem. Soc.* **2016**, *138*, 2142-2145; (f) Ma, D.; Li, B.; Liu, K.; Zhang, X.; Zou, X.; Yang, Y.; Li, G.; Shi, Z.; Feng, S. Bifunctional MOF heterogeneous catalysts based on the synergy of dual functional sites for efficient conversion of CO₂ under mild and co-catalyst free conditions. *J. Mater. Chem. A* **2015**, *3*, 23136-23142.
- (34) Zhu, Q. -Q.; Zhang, W. -W.; Zhang, H. -W.; Yuan, Y.; Yuan, R.; Sun, F.; He, H. A Double-Walled Porous Metal-Organic Framework as a Highly Efficient Catalyst for Chemical Fixation of CO₂ with Epoxides. *Inorg. Chem.* **2019**, *58*, 15637-15643.
- (35) Xu, H.; Cao, C. -S.; Hu, H. -S.; Wang, S. -B.; Liu, J. -C.; Cheng, P.; Kaltsoyannis, N.; Li, J.; Zhao, B. High Uptake of ReO₄⁻ and CO₂ Conversion by a Radiation-Resistant Thorium-Nickle [Th₄₈Ni₆] Nanocage-Based Metal-Organic Framework. *Angew. Chem. Int. Ed.* **2019**, *58*, 6022-6027.
- (36) Seong, W.; Hahm, H.; Kim, S.; Park, J.; Abboud, K. -A.; Hong, S.; Self-Assembled Bimetallic Aluminum-Salen Catalyst for the Cyclic Carbonates Synthesis. *Molecules* **2021**, *26*, 4097.
- (37) Das, P.; Mandal, S. K. In-Depth Experimental and Computational Investigations for Remarkable Gas/Vapor Sorption, Selectivity, and Affinity by a Porous Nitrogen-Rich Covalent Organic Framework. *Chem. Mater.* **2019**, *31*,1584-1596.
- (38) Yang, F.; Li, Y.; Zhang, T.; Zhao, Z.; Xing, G.; Chen, L. Docking Site Modulation of Isostructural Covalent Organic Frameworks for CO₂ Fixation. *Chem. Eur. J.* **2020**, *26*, 4510-4514.
- (39) Saptal, V.; Shinde, D. B.; Banerjee, R.; Bhanage, B. M. State-of-the-art catechol porphyrin COF catalyst for chemical fixation of carbon dioxide via cyclic carbonates and oxazolidinones. *Catal. Sci. Technol.* **2016**, *6*, 6152-6158.
- (40) He, H. Zhu, Q. -Q.; Zhang, W. -W.; Zhang, H. -W.; Chen, J.; Li, C. -P.; Du, M.; Metal and Co-Catalyst Free CO₂ Conversion with a Bifunctional Covalent Organic Framework (COF). *ChemCatChem* **2020**, *12*, 5192-5199.
- (41) Hou, S. -L.; Dong, J.; Jiang, X. -L.; Jiao, Z. -H.; Zhao, B. A Noble-Metal-Free Metal-Organic Framework (MOF) Catalyst for the Highly Efficient Conversion of CO₂ with Propargylic Alcohols. *Angew. Chem. Int. Ed.* **2019**, *58*, 577-581.
- (42) Geng, K.; He, T.; Liu, R.; dalapati, S.; Tan, K. T.; Li, Z.; Tao, S.; Gong, Y.;

- Jiang, Q.; Jiang, D. Covalent organic frameworks: design, synthesis, and functions. *Chem. Rev.* **2020**, *16*, 8814-8933.
- (43) Wang, J.; Zhuang, S. Covalent organic frameworks (COFs) for environmental applications. *Coord. Chem. Rev.* **2019**, *400*, 213046.
- (44) Q. Guan, Wang, G. -B.; Zhou, L. L.; Li, W. -Y.; Dong, Y. -B. Nanoscale covalent organic frameworks as theranostic platforms for oncotherapy: synthesis, functionalization, and applications. *Nanoscale Adv.* **2020**, *2*, 3656-3733.
- (45) Ding, S. -Y.; Wang, W. Covalent organic frameworks (COFs): from design to applications. *Chem. Soc. Rev.* **2013**, *42*, 548-568.
- (46) (a) Xu, H.; Tao, S.; Jiang, D. *Nat. Mater.* **2016**, *15*, 722-726; (b) Ma, H.; Liu, B.; Li, B.; Zhang, L.; Li, Y. -G.; Tan, H. -Q.; Zang, H. -Y.; Zhu, G. *J. Am. Chem. Soc.* **2016**, *138*, 5897-5903.
- (47) (a) Deblase, C. R.; Silberstein, K. E.; Truong, T. -T.; Abruna, H. D.; Dichtel, W. R. β-Ketoenamine-linked covalent organic frameworks capable of pseudocapacitive energy storage. *J. Am. Chem. Soc.* **2013**, *135*, 16821-16824; (b) Xu, F.; Xu, H.; Chen, X.; Wu, D.; Wu, Y.; Liu, H.; Gu, C.; Fu, R.; Jiang, D. Radical covalent organic frameworks: a general strategy to immobilize open-accessible polyradicals for high-performance capacitive energy storage. *Angew Chem.* **2015**, *127*, 6918-6922; (c) Wang, S.; Wang, Q.; Shao, P.; Han, Y.; Gao, X.; Ma, L.; Yuan, S.; Ma, X.; Zhou, J.; Feng, X.; Wang, B. Exfoliation of covalent organic frameworks into few-layer redox-active nanosheets as cathode materials for lithiumion batteries. *J. Am. Chem. Soc.* **2017**, *139*, 4258-4261; (d) Bhanja, P.; Bhunia, K.; Das, S. K.; Pradhan, D.; Kimura, R.; Hijikat, Y.; Irle, S.; Bhaumik, A. A new triazine-based covalent organic framework for high-performance capacitive energy storage. *ChemSusChem* **2017**, *10*, 921-929.
- (48) Geng, K.; He, T.; Liu, R.; Tan, K. T.; Li, Z.; Tao, S.; Gong, Y.; Jiang, Q.; Jiang, D. Covalent organic frameworks: design, synthesis, and functions. *Chem. Rev.* **2020**, *120*, 8814-8933.
- (49) Wang, J.; Zhuang, S.; Covalent organic frameworks (COFs) for environmental applications. *Coord. Chem. Rev.* **2019**, *400*, 213046.
- (50) Sharma, R. K.; Yadav, P.; Yadav, M.; Gupta, R.; Rana, P.; Srivastava, A.; Zboril, R.; Varma, R. S.; Antonietti, M.; Gawande, M. B. *Mater. Horiz.* **2020**, *7*, 411-454.
- (51) Ge, R.; Hao, D.; Shi, Q.; Dong, B.; Leng, W.; Wang, C.; Gao, Y. Target

- Synthesis of an Azo (N=N) Based Covalent Organic Framework with High CO₂-over-N₂ Selectivity and Benign Gas Storage Capability. *J. Chem. Eng. Data* **2016**, *61*, 1904-1909.
- (52) Li, Z.; Feng, X.; Zou, Y.; Zhang, Y.; Xia, H.; Liu, X.; Mu, Y. A 2D azine-linked covalent organic framework for gas storage applications. *Chem. Commuun.* **2014**, *50*, 13825-13828.
- (53) (a) Huang, N.; Chen, X.; Krishna, R.; Jiang, D. Two-dimensional covalent Organic Frameworks for Carbon Dioxide Capture through Channel-Wall Functionalization. *Angew. Chem. Int. Ed.* **2015**, *127*, 3029-3033; (b) Huang, N.; Krishna, R.; Jiang, D. Tailor-made pore surface engineering in covalent organic frameworks: systematic functionalization for performance screening. *J. Am. Chem. Soc.* **2015**, *137*, 7079-7082; (c) Rabbani, M. G.; Sekizkardes, A. K.; Kahveci, Z.; Reich, T. E.; Ding, R.; Kaderi, H. M. E. A 2D mesoporous imine-linked covalent organic framework for high-pressure gas storage applications. *Chem. Eur. J.* **2013**, *19*, 3324-3328.
- (54) Dhankhar, S. S.; Nagaraja, C. M. Porous nitrogen-rich covalent organic framework for capture and conversion of CO₂ at atmospheric pressure conditions. *Micropor. Mesopor. Mat.* **2020**, *308*, 110314.
- (55) He, H.; Zhu, Q. -Q.; Zhang, W. -W.; Zhang, H. -W. J. Chen, C. -P. Li, M. Du, Metal and Co-Catalyst Free CO₂ Conversion with a Bifunctional Covalent Organic Framework (COF). *ChemCatChem* **2020**, *12*, 5192-5199.
- (56) (a) Qiu, J.; Zhao, Y.; Li, Z.; Wang, H.; Shi, Y.; Wang, J. Imidazolium-Salt-Functionalized Covalent Organic Frameworks for Highly Efficient Catalysis of CO₂ Conversion. *ChemSusChem* **2019**, *12*, 2421-2427; (b) Sengupta, M.; Bag, A.; Ghosh, S.; Mondal, P.; Bordoloi, A.; Islam, S. M. CuxOy@ COF: An efficient heterogeneous catalyst system for CO₂ cycloadditions under ambient conditions. *J. CO₂ Util.* **2019**, *34*, 533-542; (c) Sun, Q.; Aguila, B.; Perman, J.; Nguyen, N.; Ma, S. Flexibility matters: cooperative active sites in covalent organic framework and threaded ionic polymer. *J. Am. Chem. Soc.* **2016**, *138*, 15790-15796; (d) Guan, P.; Qiu, J.; Zhao, Y.; Wang, H.; Li, Z.; Shi, Y.; Wang, J.; A novel crystalline azine-linked three-dimensional covalent organic framework for CO₂ capture and conversion. *Chem. Commun.* **2019**, *55*, 12459-12462.
- (57) Li, H.; Feng, X.; Shao, P.; Chen, J.; Li, C.; Jayakumar, S.; Yang, Q.; Synthesis of covalent organic frameworks via in situ salen skeleton formation for catalytic

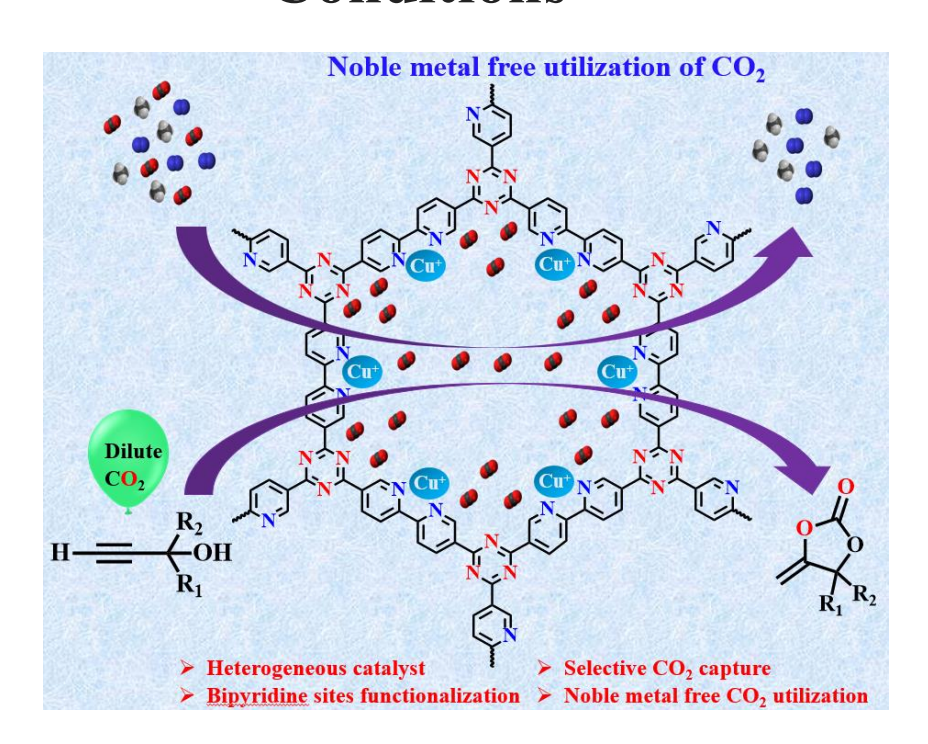
- applications. J. Mater. Chem. A 2019, 7, 5482-5492.
- (58) Puthiaraj, P.; Kim, H. S.; Yu, K.; Ahn, W. S. Triphenylamine-based covalent imine framework for CO₂ capture and catalytic conversion into cyclic carbonates. *Micropor. Mesopor. Mat.* **2020**, *297*, 110011.
- (59) Wang, J.; Zhang, Y. Facile synthesis of N-rich porous azo-linked frameworks for selective CO₂ capture and conversion. *Green Chem.* **2016**, *18*, 5248-5253.
- (60) Ravi, S.; Kang, D. H.; Roshan, R.; Tharun, J.; Kathalikkattil, A. C.; Park, D. W. Organic sulphonate salts tethered to mesoporous silicas as catalysts for CO₂ fixation into cyclic carbonates. *Catal. Sci. Technol.* **2015**, *5*, 1580-1587.
- (61) (a) Ravi, S.; Roshan, R.; Tharun, J.; Kathalikkattil, A. C.; Park, D. W. Sulfonic acid functionalized mesoporous SBA-15 as catalyst for styrene carbonate synthesis from CO₂ and styrene oxide at moderate reaction conditions. *J. CO₂ Util.* **2015**, 10, 88-94; (b) Xiao, L.; Lv, D.; Wu, W. Brønsted acidic ionic liquids mediated metallic salts catalytic system for the chemical fixation of carbon dioxide to form cyclic carbonates. *Catal. Lett.* **2011**, *141*, 1838-1844.
- (62) Chong, J. H.; Sauer, M.; Patrick, B. O.; MacLachlan, M. J. Highly stable keto-enamine Salicylideneanilines. *Org. Lett.* **2003**, *5*, 3823-3826.
- (63) Li, J. H.; Yu, Z. W.; Gao, Z.; Li, J. Q.; Tao, Y.; Xiao, Y. X.; Yin, W. H.; Fan, Y. L.; Jiang, h.; Sun, L. J.; Luo, F. Ultralow-Content Palladium Dispersed in Covalent OrganicFramework for Highly Efficient and Selective Semihydrogenation of Alkynes. *Inorg. Chem.*, **2019**, *58*, 10829-10836.
- (64) Kandambeth, S.; Mallick, A.; Lukose, B.; Mane, M. V.; Heine, T.; Banerjee, R. Construction of crystalline 2D covalent organic frameworks with remarkable chemical (acid/base) stability via a combined reversible and irreversible route. *J. Am. Chem. Soc.* **2012**, *48*, 19524-19527.
- (65) Chandra, S.; Kundu, T.; Dey, K.; Addicoat, M.; Heine, T.; Banerjee, R. Interplaying intrinsic and extrinsic proton conductivities in covalent organic frameworks. *Chem. Mater.* **2016**, *28*, 1489-1494.
- (66) Karak, S.; Kandambeth, S.; Biswal, B. P.; Sasmal, H. S.; Kumar, S.; Pachfule, P.; Banerjee, R. Constructing ultra porous covalent organic frameworks in seconds via an organic terracotta process. *J. Am. Chem. Soc.* **2017**, *139*, 1856-1862.
- (67) Gao, Z.; Yu, Z.; Huang, Y.; He, X.; Su, X.; Xiao, L.; Yu, Y.; Huang, X.; Luo, F. Flexible and robust bimetallic covalent organic frameworks for the reversible switching of electrocatalytic oxygen evolution activity. *J. Mater. Chem. A* **2020**, 8,

5907-5912.

- (68) Wei, H.; Chai, S.; Hu, N.; Yang, Z.; Wei, L.; Wang, L. The microwave-assisted solvothermal synthesis of a crystalline two-dimensional covalent organic framework with high CO₂ capacity. *Chem. Commun.* **2015**, *51*, 12178-12181.
- (69) Yang, R. T. Gas Separation by Adsorption Processes, Butterworth, Boston, 1997.
- (70) Pan, H.; Ritter, J. A.; Balbuena, P. B. Examination of the approximations used in determining the isosteric heat of adsorption from the Clausius-Clapeyron equation. *Langmuir* **1998**, *14*, 6323-6327.
- (71) (a) Gu, C.; Liu, Y.; Wang, W.; Liu, J.; Hu, J. Effects of functional groups for CO₂ capture using metal-organic frameworks. *Front. Chem. Sci. Eng.* **2021**, *15*, 437-449; (b) Zeng, Y.; Zou, R.; Zhao, Y.; Covalent Organic Frameworks for CO₂ Capture. *Adv. Mater.* **2016**, *28*, 2855-2873; (c) Liu, R.; Tan, K. T.; Gong, Y.; Chen, Y.; Li, Z.; Xie, S.; He, T.; Lu, Z.; Yang, H.; Jiang, D. Covalent organic frameworks: an ideal platform for designing ordered materials and advanced applications. *Chem. Soc. Rev.* **2021**, *50*, 120-242.
- (72) (a) Das, R.; Dhankhar, S. S.; Nagaraja, C. M. Construction of a bifunctional Zn (II)-organic framework containing a basic amine functionality for selective capture and room temperature fixation of CO₂. *Inorg. Chem. Front.* **2020**, *7*, 72-81; (b) Das, R.; Muthukumar, D.; Pillai, R. S.; Nagaraja, C. M. Rational Design of a Zn^{II} MOF with Multiple Functional Sites for Highly Efficient Fixation of CO₂ under Mild Conditions: Combined Experimental and Theoretical Investigation. *Chem. Eur. J.* **2020**, *26*, 17445-17454.
- (73) Dhankhar, S. S.; Das, R.; Ugale, B.; Pillai, R. S.; Nagaraja, C. M. Chemical Fixation of CO₂ Under Solvent and Co-Catalyst-free Conditions Using a Highly Porous Two-fold Interpenetrated Cu(II)-Metal-Organic Framework. *Cryst. Growth Des.* **2021**, *21*, 1233-1241.

Chapter 3

Rational Design of Cu(I)-anchored Porous Covalent Triazine Framework (CTF) for Simultaneous Capture and Conversion of CO₂ at Ambient Conditions



❖ Reference: "Singh, G.; Nagaraja, C. M. J. CO₂ Util. 2022, 63, 102132."

3.1. Introduction

The concentration of CO₂ is increasing rapidly in the atmosphere, resulting in various environmental issues.¹⁻³ Therefore, it is necessary to extenuate the rising concentration of CO₂ by utilizing it as a C1 source for synthesizing valuable chemicals and fuels.⁴⁻⁹ However, owing to the high C-O bond energy (805 kJ/mol) and inert nature of CO₂, efficient catalysts capable of selectively capturing and converting carbon dioxide into fine chemicals at ambient conditions are highly desired. 10-21 In this regard, researchers worldwide are making significant research efforts to develop efficient catalytic systems.²²⁻³⁰ Among the various functionalization strategies developed so far, the formation of α -aCCs by fixation of CO₂ with alkyne molecules has gained much attention due to their potential utilization as commodity chemicals for polycarbonates, polyurethanes, pharmaceuticals, and so on. 31-38 Hence design of highly active catalytic systems composed of high density of CO₂-philic and catalytic sites capable of functionalizing CO₂ to α-aCCs at mild conditions is of significant interest. In this regard, covalent organic frameworks (COFs) have received significant interest because of their highly exposed surface and modular nature, enabling rational tuning of pore size and functionality for desired applications. 39-47 Therefore, the strategic design of COFs composed of CO₂ philic basic and Bronsted acidic functionalities is of potential significance to utilize as promising transition metal-free heterogeneous catalysts for the chemical functionalization of CO₂. Further, the literature survey revealed that production of α -aCCs has been mostly achieved using Ag(I)/Ag(0) as a catalyst owing to alkynophilicity of silver promoting activation of alkyne C≡C bonds. 56-59 However, from the point of green and sustainable synthesis, the use of non-noble metal-based catalysts is highly preferred over noble metal-based ones.60

Keeping these objectives, in Chapter 3, we report the strategic utilization of the covalent triazine framework (CTF) owing to its advantages of high thermal/chemical stability and large pore channels decorated with CO₂-philic basic nitrogen sites. 61-63 More importantly, the functionalized CTFs with the 1D channels decorated with bipyridine coordination sites can serve as ideal supports for anchoring catalytic metal/complex ions to carry out various catalytic transformations. 64-67 In this regard, CTF-anchored metal-based heterogeneous catalysts are gaining increasing attention because of the advantages of high catalyst stability towards recycling. 68-70 Hence, in

this chapter, we demonstrate the application of CTF with pores functionalized with bipyridine sites as the ideal support for anchoring noble metal-free Cu(I) ions to obtain Cu(I)@bipy-CTF.

3.2. Experimental section

3.2.1. Materials

All the reagents used in this work are commercially available and employed as provided without any further purification. 2,2'-bipyridine-5,5'-dicarbonitrile (DCbipy) utilized for CTF synthesis was obtained from the alfa Aeser chemical co. The CuI and ZnCl₂ were purchased from Sigma Aldrich.

3.2.2. Physical measurements

Powder X-ray diffraction measurements were conducted in the 2θ range of 5-80° on PAN analytical's X'PERT PRO X-ray diffractometer with a scan rate of 2°/min using Cu-K α radiation (λ = 1.54184 Å, 40 kV, 20 mA) for confirming phase purity of as-synthesized samples. Fourier transform infrared (FT-IR) spectra of the samples were recorded on a Bruker Tensor-F27 instrument in ATR mode. The products of catalytic reactions were identified, and the catalytic conversions were determined by 1 H NMR spectra recorded on a JEOL JNM-ECS-400 spectrometer operating at a frequency of 400 MHz using CDCl₃ solvent.

3.2.3. Synthesis

3.2.3.1. Synthesis of bipy-CTF

The bipy-CTF was synthesized by following the reported procedure with little modifications. ⁷¹ 2,2'-bipyridine-5,5'-dicarbonitrile (0.10 g, 0.04 mmol) and ZnCl₂ (0.33 g, 2.4 mmol) were charged into 1 mL sealed tube under N₂ atmosphere. After that, the tube was sealed under a vacuum with flame and kept in the furnace for 48 h at 400 °C with a heating rate of 60 °C/h. After the reaction, the furnace was cooled down to room temperature, and the resulting black powder was ground and stirred in 250 mL of water for 3 h. After washing with water and acetone, the resulting solid was refluxed with 1 M HCl (250 mL) for 16 h. Further, the black powder was kept for drying at 200 °C for 6 h after washing with 1 M HCl (150 mL), H₂O (150 mL), THF (150 mL), and acetone (150 mL).

3.2.3.2. Synthesis of Cu(I)@bipy-CTF

The bipy-CTF (0.036 mmol) and an acetonitrile solution of CuI (0.18 mmol) were taken in a 50 mL two-neck RB under N_2 atmosphere and incubated at 60 °C for 12 h. The resulting powder was separated from the reaction mixture by centrifugation, washed with a copious amount of acetonitrile, and used for further characterization after vacuum drying.

3.2.4. Catalytic cycloaddition reactions of CO₂ with propargylic alcohol

The catalytic cyclic carboxylation of propargylic alcohol was carried out in a Schlenk tube (30 mL) at 40 °C under 1 atm CO₂ (balloon). Prior to the catalytic study, the catalyst was activated by treating at 373 K under vacuum for 12 h. In a typical procedure, catalyst Cu(I)@bipy-CTF (0.02 mmol), propargylic alcohol (4 mmol), and DBU (0.4 mmol) were taken in a Schlenk tube with 2 mL DMF at room temperature. The CO₂ was introduced at 1 atm using a balloon, and the contents were stirred at 40 °C for 24 h. Then, the catalyst was separated by centrifugation, and the conversion was determined by ¹H NMR analysis of the filtrate in CDCl₃ solvent. The recovered catalyst was washed in acetone, activated for 12 h at 100 °C, and then used for subsequent catalytic cycles. A similar procedure was used for the catalytic reactions carried out with dilute gas (13% CO₂), except that the reaction temperature was maintained at 60 °C.

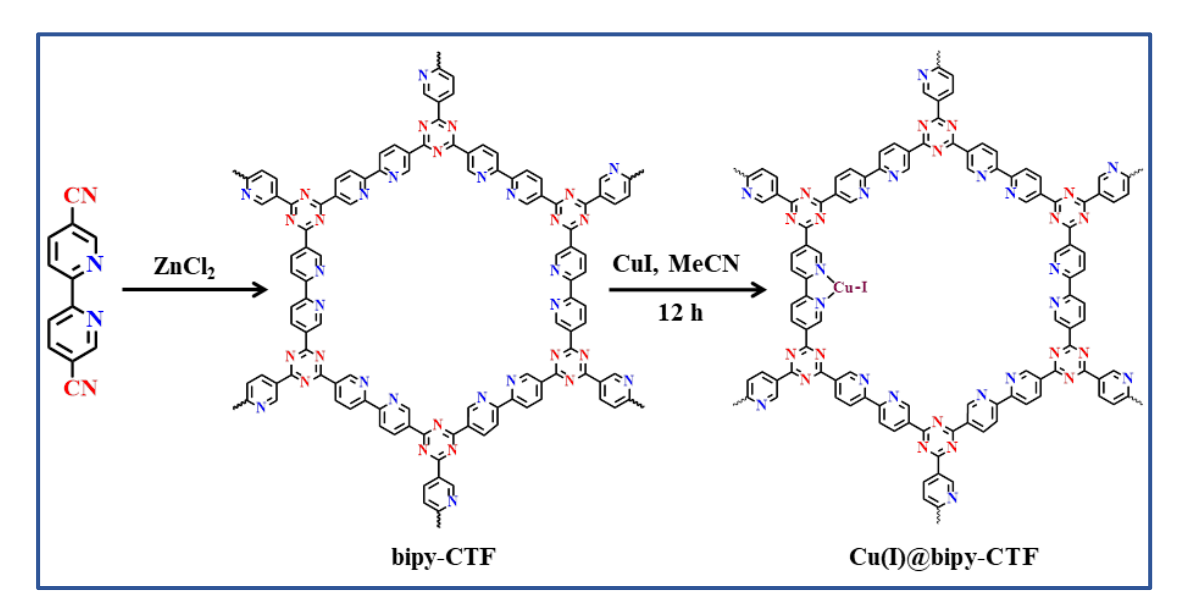
3.2.5. Adsorption measurements

N₂ adsorption-desorption studies were carried out at 77 and 273 K, while CO₂ adsorption-desorption measurements were carried out at 273 and 298 K using QUANTACHROME Quadrasorb SI automated surface area and pore size analyzer instrument. Ultrapure (99.995%) N₂, CO₂, and CH₄ gases were used for the adsorption-desorption measurements. Before the adsorption measurements, the sample (~0.100 g) was evacuated at 393 K under vacuum (20 mTorr) for 12 h on QUANTACHROME Flovac degasser and further purged with ultrapure N₂ (99.995%) gas on cooling. The BET surface area of the COFs was estimated from N₂ sorption isotherms carried out at 77 K, respectively. The gas selectivity experiments were carried out at 273 K.

3.3. Results and discussion

3.3.1. Synthesis and Characterizations

The synthesis of bipy-CTF with pores functionalized with bipyridine moieties was achieved by adopting the previously reported procedure with a slight modification and characterized by various techniques (Scheme 1). The FT-IR spectra of as-prepared bipy-CTF depicted stretching frequencies at 1506 and 822 cm⁻¹ corresponding to the triazine ring and absence of peaks at 2300-2200 cm⁻¹ corresponding to C \equiv N (nitrile) group of precursor, 5,5'-dicyano-2,2'-bipyridine supporting the complete conversion of nitrile group into triazine ring (Figure 1a). Furthermore, the appearance of bands at 1600-1550 cm⁻¹ and 740 cm⁻¹ corresponds to C \equiv N and C-H stretching vibrations of the bipyridine ring, respectively.⁶⁵ Furthermore, the solid-state ¹³C CP-MAS NMR spectrum of bipy-CTF showed characteristic peaks at 120-170 ppm corresponding to the ¹³C resonance from carbon atoms of the triazine and bipyridine rings supporting the formation of bipy-CTF (Figure 1b).^{65,72} Further, the powder X-ray diffraction (PXRD) pattern of bipy-CTF showed a broad peak at $2\Theta = 25^{\circ}$ which is assigned to the (001) plane, indicating the structural ordering of the bipy-CTF (Figure A13).^{65,73}



Scheme 1. Synthesis scheme of bipy-CTF and Cu(I)@bipy-CTF.

The anchoring of Cu(I) at the bipyridine sites of CTF was achieved through a post-synthetic approach by treating as-synthesized bipy-CTF with acetonitrile (ACN) solution of CuI for 12 h at 60 °C. The FT-IR spectra of Cu(I)@bipy-CTF showed a shift in the C=N stretching frequency of the bipyridine ring supporting the embedding

of Cu(I) ions at the bipy sites lined in the 1D channels of the COF (Figure 1a).⁷⁰ The PXRD pattern of Cu(I)@bipy-CTF is in accordance with that of pristine COF, suggesting that the framework is retained even after metalation (Figure A13). The scanning electron microscopy (SEM) images of bipy-CTF show irregular block-shaped morphology of the sample and the morphology was retained even after embedding of Cu(I) at the bipy sites of the framework (Figure 1c and 1d). Further support for anchoring of Cu(I) in CTF was obtained from energy dispersive spectroscopy (EDS) analysis (Figure A14a and A14b). Besides, the percentage loading of Cu(I) determined by microwave-plasma atomic emission spectroscopy (MP-AES) analysis was 7.5% (Figure A15).

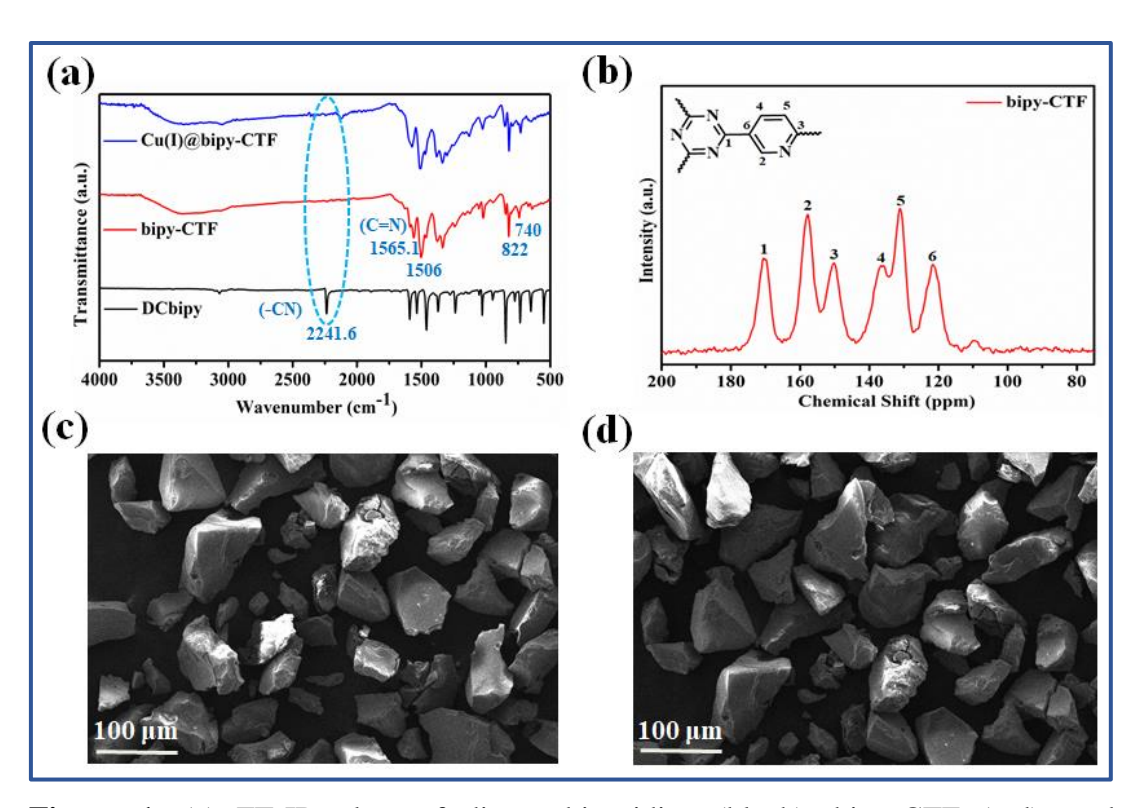


Figure 1. (a) FT-IR plots of dicyanobipyridine (black), bipy-CTF (red), and Cu(I)@bipy-CTF (blue). (b) ¹³C CP-MAS solid-state NMR spectrum of bipy-CTF. The SEM images of bipy-CTF (c) and Cu(I)@bipy-CTF (d).

The X-ray photoelectron spectroscopy (XPS) analysis was performed for bipy-CTF and Cu(I)@bipy-CTF to determine the elemental composition. Figure 2a shows the N 1s spectra of bipy-CTF with two BE peaks at 398.7 and 399.2 eV corresponding to triazine and pyridine N, respectively. Whereas the deconvoluted N 1s spectra (Figure 2b) of Cu(I)@bipy-CTF showed BE peaks not only for triazine

and pyridine Ns but also for the Cu(I) bound bipy N at 400.2 eV.^{71,74} Figure 2c shows Cu(I) spectra with binding energy (BE) peaks at 933.1 and 952.9 eV assigned to $2P_{3/2}$ and $2P_{1/2}$, respectively, which is in line with the XPS spectra of Cu(I) reported before.⁶⁰ Hence, the XPS analysis confirmed the Cu(I) anchoring at the bipyridine sites decorated in the pore walls of bipy-CTF.

Thermogravimetric analysis (TGA) of bipy-CTF revealed high thermal stability of the sample up to 550 °C (Figure 2d) with an initial weight loss of ~11% corresponding to guest water molecules. Meanwhile, the TGA plot of Cu(I)@bipy-CTF showed thermal stability up to 400 °C, and at higher temperatures, the framework undergoes disintegration (Figure 2d).

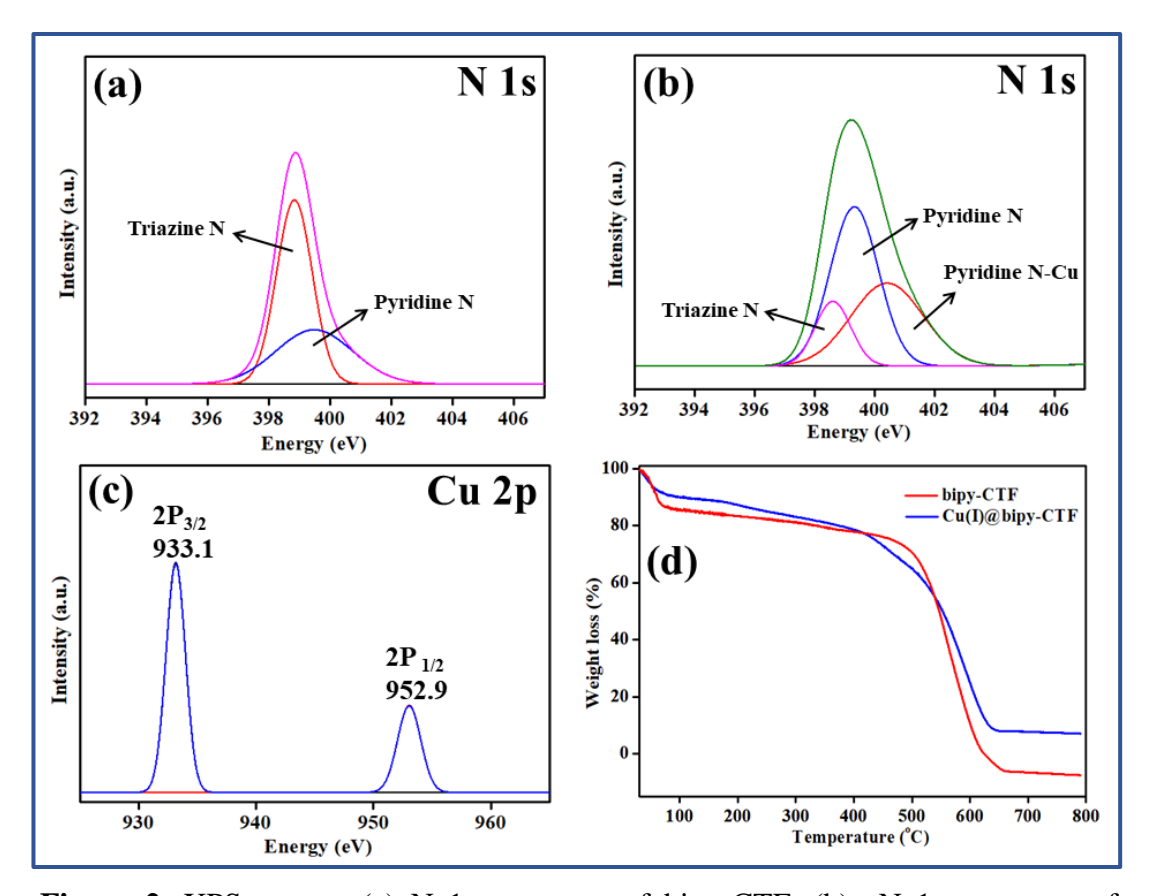


Figure 2. XPS spectra (a) N 1s spectrum of bipy-CTF, (b) N 1s spectrum of Cu(I)@bipy-CTF, (c) Cu 2p spectrum of Cu(I)@bipy-CTF, and (d) Thermogravimetric analysis (TGA) plots for bipy-CTF (red) and Cu(I)@bipy-CTF (blue).

3.3.2. Gas sorption analysis

To test the permanent porosity of Cu(I)@bipy-CTF, the N₂ sorption studies

were carried out. The as-prepared bipy-CTF and Cu(I)@bipy-CTF were activated at 120 °C for 12 h under vacuum prior to gas sorption measurements. As shown in Figure 3a, N₂ sorption isotherms display a type-I plot indicating the microporous nature of CTF. The calculated BET (Brunauer-Emmett-Teller) surface area of bipy-CTF and Cu(I)@bipy-CTF were found to be 538.3 m²g⁻¹ and 348.6 m²g⁻¹, respectively. The reduction in surface area of Cu(I)@bipy-CTF can be ascribed to a partial loss of porosity upon embedding of Cu(I) ions at the bipy sites lined in the 1D channels of CTF. Further, CO₂ sorption measurements of bipy-CTF and Cu(I)@bipy-CTF show type-I plots with the uptake of 48.13/29.48 cc/g and 32.15/21.26 cc/g at 273/298 K, respectively (Figure 3b and 3c). The CO₂ sorption isotherms were fitted with the Freundlich-Langmuir equation to accurately predict the CO₂ uptake (Figures A16 and A17).⁷⁵ Moreover, the heat of interaction energy (Q_{st}) estimated from the Clausius-Clayperon equation was 34.94 and 44.09 kJ/mol for bipy-CTF and Cu(I)@bipy-CTF, respectively (Figure A16 and A17). The high value of interaction energy indicates preferential interaction of CO₂ with basic nitrogen sites of Cu(I)@bipy-CTF. As shown in Figure 3d, gas selectivity measurements revealed negligible uptake of N2 and CH4 over CO2 with a Henry gas selectivity constant of 29.32 for K_{CO2}/_{CH4} and 51.94 for K_{CO2}/_{N2}, respectively (Figure A18).

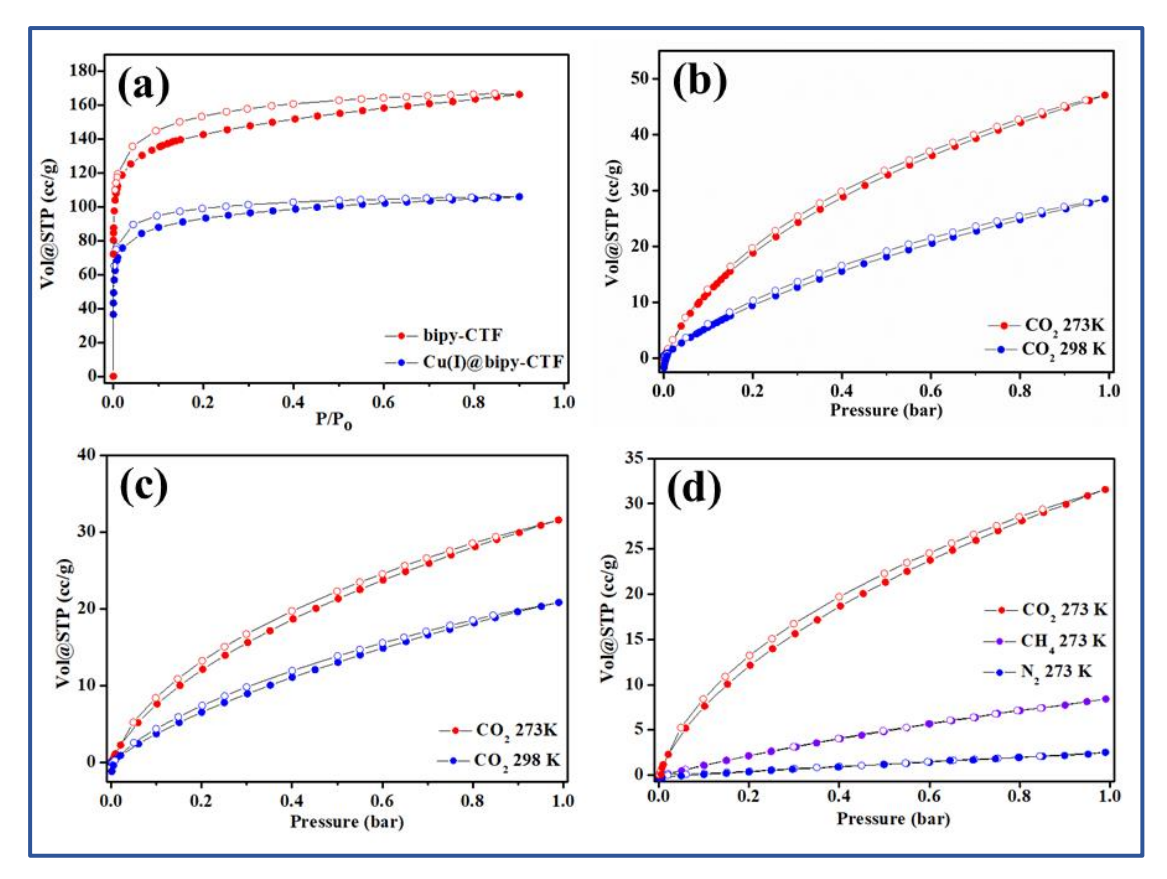


Figure 3. N₂ sorption isotherm for bipy-CTF and Cu(I)@bipy-CTF carried out at 77 K (a). The CO₂ sorption isotherm of bipy-CTF (b) and Cu(I)@bipy-CTF (c). Selective CO₂ sorption isotherm of Cu(I)@bipy-CTF (d).

3.3.3. Coupling of CO₂ with propargylic alcohol at atmospheric conditions

The presence of CO_2 philic triazine nitrogen and catalytic Cu(I) sites in Cu(I)@bipy-CTF encouraged us to investigate its catalytic performance for coupling of CO_2 with propargylic alcohol to produce α -alkylidene cyclic carbonate (Table 1). To begin with, the activity was checked at RT and 1 atm (balloon) of CO_2 using 2-methyl-3-butyne-2-ol as a model substrate with the addition of DBU (1,8-diazabicyclo[5.4.0]underc-7-ene) which facilitates the deprotonation of propargylic alcohol. Indeed, Cu(I)@bipy-CTF catalyzed about 80% conversion of propargylic alcohol into α -alkylidene cyclic carbonate within 24 h with high selectivity (> 99%) at room temperature (Table 1). Further, upon increasing the temperature up to 40 °C, the catalytic conversion was enhanced to 96% in 24 h, supporting the promising catalytic activity of Cu(I)@bipy-CTF for the conversion of CO_2 to valuable chemicals (Table 1). Moreover, control experiments performed using $Cu(NO_3)_2.6H_2O$, and bipy-CTF as catalysts showed no conversion of propargylic alcohol into α -alkylidene cyclic

carbonate. This observation clearly highlights the importance of Cu(I) catalytic sites in activating and functionalizing the alkynes with CO_2 to yield α -aCC (Table 1). More interestingly, Cu(I)@bipy-CTF showed high catalytic activity as compared to the homogeneous counterpart, CuI which showed about 70% conversion of propargylic alcohol to α -aCC. At this juncture, it is worth mentioning that, although the catalytic reaction carried out using CuI (homogeneous) showed a moderate conversion of propargylic alcohol, it has limits in terms of catalyst recycling and product separation. Further, the higher catalytic activity of Cu(I)@bipy-CTF can be ascribed to the presence of CO_2 philic basic sites and catalytic Cu(I) sites in the framework. To confirm the role of CO_2 in the catalytic conversion of propargylic alcohol to α -aCC, we carried out the catalytic reaction in the absence of carbon dioxide using Ar gas at the optimized conditions. To our delight, no conversion of propargylic alcohol was observed which unambitiously proves the role of CO_2 in the formation of α -aCC (Table 1).

Table 1. Optimization table for the carboxylation of 2-methyl-3-butyn-2-ol catalyzed by Cu(I)@bipyCTF.^a

"Reactions Conditions: 2-methyl-3-butyn-2-ol (4 mmol), catalyst (0.02 mmol), DBU (0.4 mmol), DMF (2 mL), time (24 h), b: the percentage conversions were determined by ¹H NMR analysis, c: under argon atmosphere, d: without DBU and e: time (12 h)

Further, the superior catalytic activity of Cu(I)@bipy-CTF encouraged us to explore the coupling of CO₂ with other alcohol substrates under the optimized conditions (Table 2). As can be seen from the entries in Table 2, as the alkyl chain length of epoxide increases, the catalytic conversion decreases, which could be correlated to the restricted diffusion of larger alcohols to the Cu(I) active sites inside the 1D channels of the framework.^{60,76} Interestingly, a comparison of the catalytic activity of Cu(I)@bipy-CTF with literature examples of COF-based heterogeneous systems revealed its higher catalytic activity for coupling CO₂ with propargylic alcohols to afford valuable chemicals under mild conditions (Table A2).

Table 2. Coupling of CO₂ with propargylic alcohols catalyzed by Cu(I)@bipy-CTF.^a

^aReaction conditions: propargylic alcohol (4 mmol), catalyst (0.02 mmol), DBU (0.4 mmol), DMF (2 mL), temperature (40 °C), CO₂ (1 atm, balloon), 24 h. ^bThe catalytic conversions were determined by ¹H NMR analysis. ^cTON = no. of moles of product formed / no. of moles of catalytic Cu(I) sites

3.3.4. Coupling of propargylic alcohol with dilute CO₂ (13%)

Encouraged by the high catalytic activity of Cu(I)@bipy-CTF for coupling of CO_2 with propargylic alcohols, the activity was checked using dilute CO_2 gas ($CO_2:N_2$ = 13:87%) as a carbon dioxide source. The catalysis performed at the optimized

conditions resulted in a 60% conversion of the propargylic alcohol to α -aCC (Table 3). Further, to increase the yield of α -aCC, the reaction temperature was increased to 60 °C, leading to an increase in the product yield to 85% in 24 h (Table 3). To achieve quantitative conversion of propargylic alcohol, the catalytic reaction was extended for an additional time, and about 97% conversion of propargylic alcohol to α -aCC was observed in 36 h (Table 3). The enhanced catalytic conversion of propargylic alcohol even at a low concentration of CO_2 (13%) prompted us to extend the catalytic activity to other derivatives of propargylic alcohols. Interestingly, the catalyst Cu(I)@bipy-CTF showed good activity for the catalytic conversion of various propargylic alcohols to α -aCCs as shown in Table 3.

Table 3. Catalytic conversion of CO₂ from dilute gas to α-aCCs.^a

	$H = \begin{cases} R_2 \\ OH \end{cases} + \begin{cases} d \\ C \end{cases}$	Cu(I)@bipy-CTI	R_1	
S. No.	Substrate	Product	Conversion (%) ^d	TON ^e
1 ^b	н———		60	120
2	н———		85	170
3	н——		67	134
4	н		58	116
5	н — ОН		54	108
6	н—— ОН	O Ph	48	96
7 ^c	н———		97	194

^aReaction conditions: propargylic alcohol (4 mmol), catalyst (0.02 mmol), DBU (0.4 mmol), DMF (2 mL), temperature (60 °C), CO₂ (1 atm, dilute gas), 24 h. ^bTemperature (40 °C). ^cTime (36 h). ^dThe catalytic conversions were determined by ¹H NMR

analysis. ^eTON = no. of moles of product formed / no. of moles of active catalytic Cu(I) sites.

3.3.5. Recyclability and catalyst leaching test

To test the recyclability of Cu(I)@bipy-CTF, the catalyst was recovered after the reaction and reused for further catalytic cycles with prior activation at 100 °C for 12 h. Interestingly, Cu(I) anchored bipy-CTF was recyclable up to eight cycles with no substantial reduction in the yield of α -aCC formed (Figure 4a). Further, the stability of the recycled catalyst was confirmed by PXRD and FT-IR analysis (Figures A19 and A20). Moreover, SEM analysis revealed that the morphology of recycled COF is almost similar to that of the pristine sample (Figure A21). Further, the leaching test was carried out to rule out any catalysis from the homogeneous phase. To do this, the reaction was stopped after 6 h at which the conversion of propargylic alcohol into α -alkylidene cyclic carbonate was found to be 33%. Then the catalyst was separated and the reaction was continued for a further period. Interestingly, no significant increase in the conversion of propargylic alcohol into α -alkylidene cyclic carbonate was observed, which unambiguously rules out the absence of leaching of active catalyst (Figure 4b).

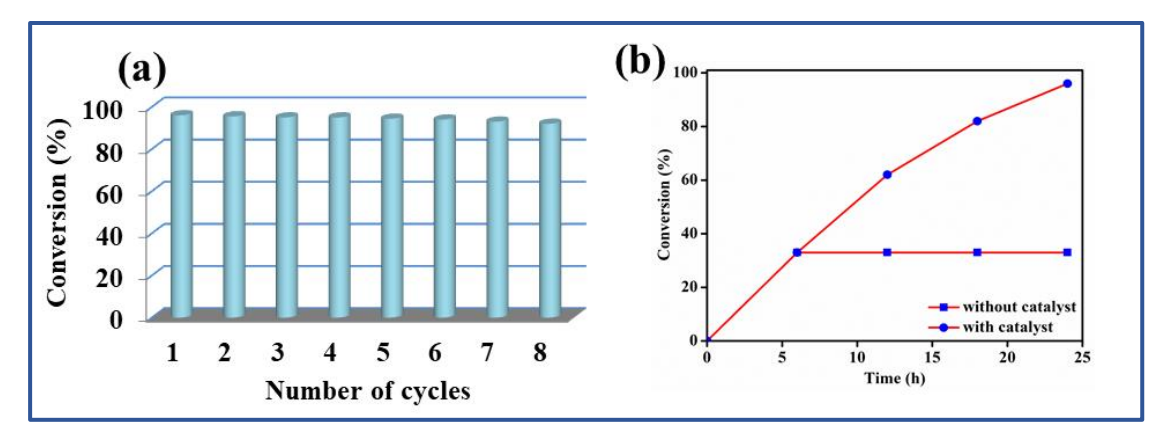


Figure 4. (a) Recyclability test and (b) leaching test of Cu(I)@bipy-CTF.

3.3.6. Plausible mechanism

A plausible mechanism for Cu(I)@bipy-CTF catalyzed functionalization of CO_2 with propargylic alcohols resulting in the formation of α -aCC as shown in Scheme 2. It involves the polarization of the alkyne bond upon interaction with Cu(I) sites. To confirm this alkyne bond polarization, the alcohol was treated with bipy-CTF and Cu(I)@bipy-CTF for 2 h, and then the catalyst was recovered, followed by washing

with methanol and dried. The FT-IR spectra of Cu(I)@bipy-CTF recovered showed stretching bands at 2120 cm⁻¹ corresponding to alkyne coordinated to Cu(I) sites. Whereas no stretching bands corresponding to alkyne were observed in the case of metal-free bipy-CTF (Figure A22), supporting the polarization of alkyne bond by Cu(I) sites in the framework. This step is followed by the deprotonation of alcohol by DBU and the subsequent addition of CO_2 results in α -aCC formation. Then the catalyst was recycled for further cycles after activation at 100 °C for 12 h.

Scheme 2. A plausible mechanism for the carboxylation of CO₂ with propargylic alcohol catalyzed by Cu(I)@bipy-CTF.

3.4. Conclusion

In summary, a Cu(I) anchored covalent triazine framework is demonstrated for

selective capture and functionalization of carbon dioxide to synthesize α-alkylidene cyclic carbonate at the mild conditions of 1 atm (balloon) of CO₂. The presence of basic triazine moiety provided good CO₂-philicity to the framework with a high binding energy of 44.09 kJ/mol. Consequently, the combined effect of CO₂-philic triazine and Cu(I) catalytic sites rendered promising activity for the fixation of CO₂ to α-alkylidene cyclic carbonate even with dilute gas (13% CO₂) at atmospheric pressure conditions. Besides, Cu(I)@bipy-CTF showed very good recyclability and chemical stability for several cycles of reuse. This work represents a rare example of a CTF-based noble-metal-free recyclable catalyst for the chemical fixation of CO₂ into high-value chemicals under mild conditions.

3.5. References

- (1) Tiba, S.; Omri, A. Literature survey on the relationships between energy, environment, and economic growth. *Renew. Sust. Energ. Rev.* **2017**, *69*, 1129-1146.
- (2) Jacobson, M. Z. Review of solutions to global warming, air pollution, and energy security. *Energy Environ. Sci.* **2009**, *2*, 148-173.
- (3) Joos, F.; Plattner, G. -K.; Stocker, T. F.; Marchal, O.; Schmittner, A. Global Warming and Marine Carbon Cycle Feedbacks on Future Atmospheric CO₂. A. *Science* **1999**, 284, 464-467.
- (4) Ding, M.; Flaig, R. W.; Jiang, H. -L.; Yaghi, O. M. Carbon capture and conversion using metal-organic frameworks and MOF-based materials. *Chem. Soc. Rev.* **2019**, *48*, 2783-2828.
- (5) Liang, J.; Huang, Y. -B.; Cao, R. Metal-organic frameworks and porous organic polymers for sustainable fixation of carbon dioxide into cyclic carbonates. *Coord. Chem. Rev.* **2019**, *378*, 32-65.
- (6) Liu, Q.; Wu, L.; Jackstell, R.; Beller, M. Using carbon dioxide as a building block in organic synthesis. *Nat Commun.* **2015**, *6*, 5933.
- (7) Singh, G.; Lee, J.; Karakoti, A.; Bahadur, R.; Yi, J.; Zhao, D.; Albahily, K.; Vinu, A. Emerging trends in porous materials for CO₂ capture and conversion. *Chem. Soc. Rev.* **2020**, *49*, 4360-4404.
- (8) Chu, S. Carbon Capture and Sequestration, Science 2009, 325, 1599.
- (9) Das, R.; Muthukumar, D.; Pillai, R. S.; Nagaraja, C. M. Rational Design of a Zn^{II} MOF with Multiple Functional Sites for Highly Efficient Fixation of CO₂ under Mild

- Conditions: Combined Experimental and Theoretical Investigation. *Chem. Eur. J.* **2020**, *26*, 17445-17454.
- (10) Ugale, B.; Kumar, S.; Kumar, T. J. D.; Nagaraja, C. M. Environmentally Friendly, Co-catalyst-Free Chemical Fixation of CO₂ at Mild Conditions Using Dual-Walled Nitrogen-Rich Three-Dimensional Porous Metal-Organic Frameworks. *Inorg. Chem.* **2019**, *58*, 3925-3936.
- (11) Liu, Q.; Wu, L.; Jackstell, R.; Beller, M. Using carbon dioxide as a building block in organic synthesis. *Nat. Commun*, **2015**, *6*, 5933.
- (12) Yun, D.; Park, S. D.; Lee, K. R.; Yun, Y. S.; Kim, T. Y.; Park, H.; Lee, H.; Yi, J.; A new energy saving catalytic system: carbon dioxide activation by a metal/carbon catalyst. *ChemSusChem* **2017**, *10*, 3671-3678.
- (13) Wilson, M.; -Palomo, S. N. B.; Stevens, P. C.; Mitchell, N. L.; Oswald, G.; Nagaraja, C. M.; Badyal, J. P. S. Substrate-independent epitaxial growth of the metalorganic framework MOF-508a, *ACS Appl. Mater. Interfaces* **2018**, *10*, 4057-4065.
- (14) Liu, Q.; Wu, L.; He, L. -N. Efficient, selective, and sustainable catalysis of carbon dioxide. *Green. Chem.* **2017**, *19*, 3707-3728.
- (15) Omae, I. Recent developments in carbon dioxide utilization for the production of organic chemicals. *Coord. Chem. Rev.* **2012**, *256*, 1384-1405.
- (16) Sneddon, G.; Rath, D.; Parida, K. M. A mechanistic approach towards the photocatalytic organic transformations over functionalized metal-organic frameworks: a review. *Catal. Sci. Technol.* **2018**, *8*, 679-696.
- (17) Bhanja, P.; Modak, A.; A. Bhaumik, Supported porous nanomaterials as efficient heterogeneous catalysts for CO₂ fixation reactions. *Chem. -Eur. J.* **2018**, *24*, 7278-7297.
- (18) Yang, H.; Zhang, X.; Zhang, G.; Fei, H. An alkaline-resistant Ag(I)-anchored pyrazolate-based metal-organic framework for chemical fixation of CO₂. *Chem. Commun.* **2018**, *54*, 4469-4472.
- (19) Zhu, Q. -Q.; Zhang, W. -W.; Zhang, H. -W.; Yuan, Y.; Yuan, R.; Sun, F.; He, H. A double-walled porous metal-organic framework as a highly efficient catalyst for the chemical fixation of CO₂ with epoxides. *Inorg. Chem.* **2019**, *58*, 15637-15643.
- (20) North, M.; Pasquale, R.; Young, C. Synthesis of cyclic carbonates from epoxides and CO₂. *Green. Chem.* **2010**, *12*, 1514-1539.
- (21) Sharma, N.; Dhankhar, S. S.; Nagaraja, C. M. Environment-friendly, co-catalystand solvent-free fixation of CO₂ using an ionic zinc(II)–porphyrin complex

- immobilized in porous metal-organic frameworks. *Sustain. Energy Fuels* **2019**, 3, 2977-2982.
- (22) Dhakshinamoorthy, A.; Li, Z.; Garcia, H. Catalysis and photocatalysis by metal organic frameworks. *Chem. Soc. Rev.* **2018**, *47*, 8134-8172.
- (23) Dhankhar, S. S.; Ugale, B.; Nagaraja, C. M. Co-Catalyst-Free Chemical Fixation of CO₂ into Cyclic Carbonates by using Metal-Organic Frameworks as Efficient Heterogeneous Catalysts. *Chem. Asian J.* **2020**, *15*, 2403-2427.
- (24) Sharma, N.; Dhankhar, S. S.; Kumar, S.; Kumar, T. J. D.; Nagaraja, C. M. Rational Design of a 3D Mn^{II}-Metal-Organic Framework Based on a Nonmetallated Porphyrin Linker for Selective Capture of CO₂ and One-Pot Synthesis of Styrene Carbonates. *Chem. Eur. J.* **2018**, *24*, 16662-16669.
- (25) Qiu, J.; Zhao, Y.; Li, Z.; Wang, H.; Fan, M.; Wang, J. Efficient ionic-liquid-promoted chemical fixation of CO₂ into α-alkylidene cyclic carbonates. *ChemSusChem* **2017**, *10*, 1120-1127.
- (26) Jones, W. D. Carbon capture and conversion. *J. Am. Chem. Soc.* **2020**, *142*, 4955-4957.
- (27) Sen, R.; Goepperts, A.; Karand, S.; Parkash, G. K. S. Hydroxide-based integrated CO₂ capture from air and conversion to methanol. *J. Am. Chem. Soc.* **2020**, *142*, 4544-4549.
- (28) Pal, T. K.; De, D.; Bhardwaj, P. K.; Metal-organic frameworks for the chemical fixation of CO₂ into cyclic carbonates. *Coord. Chem. Rev.* **2020**, *408*, 213173.
- (29) Das, P.; Mandal, S. K. In-depth experimental and Computational Investigations for Remarkable Gas/Vapor Sorption, Selectivity, and Affinity by a Porous Nitrogen-Rich Covalent Organic Framework. *Chem. Mater.* **2019**, *31*,1584-1596.
- (30) Dhankhar, S. S.; Nagaraja, C. M. Construction of a 3D porous Co(II) metalorganic framework (MOF) with Lewis acidic metal sites exhibiting selective CO₂ capture and conversion under mild conditions. *New J. Chem.* **2019**, *43*, 2163-2170.
- (31) Li, M.; Abdolmohamadi, S.; -Namin, M. S. H.; Behmagham, F.; Vassally, E.; Carboxylative cyclization of propargylic alcohols with carbon dioxide: a facile and green route to α-methylene cyclic carbonates. *J. CO*₂ *Util.* **2020**, *38*, 220-231.
- (32) Zhang, G.; Yang, H.; Fei, H.; Unusual missing linkers in an organosulfonate-based primitive-cubic (pcu)-type metal-organic framework for CO₂ capture and conversion under ambient conditions. *ACS Catal.* **2018**, *8*, 2519-2525.

- (33) Yu, K.; Puthiaraj, P.; Ahn, W. -S. One-pot catalytic transformation of olefins into cyclic carbonates over an imidazolium bromide-functionalized Mn(III)-porphyrin metal-organic framework. *Appl. Catal. B* **2020**, 273, 119059.
- (34) Sharma, N.; Dhankhar, S. S.; C. M. Nagaraja. A Mn(II)-porphyrin-based metalorganic framework (MOF) for visible-light-assisted cycloaddition of carbon dioxide with epoxides. *Micropor. Mesopor. Mat.* 2019, **280**, 372-378.
- (35) Fukuoka, S.; Kawamura, M.; Komiya, K.; Tojo, M.; Hachiya, H.; Hasegawa, K.; Aminaka, M.; Okamoto, H.; Fukawa, I.; Konno, S. A novel non-phosgene polycarbonate production process using by-product CO₂ as starting material. *Green. Chem.* **2003**, *5*, 497-507.
- (36) Gennen, S.; Grignard, B.; Tassaing, T.; Jerome, C.; Detrembleur, C. CO₂-sourced α-alkylidene cyclic carbonates: a step forward in the quest for functional regionegular poly(urethane)s and poly(carbonate)s. *Angew. Chem. Int. Ed.* **2017**, *129*, 10530-10534.
- (37) Ninokata, R.; Yamahira, T.; Onodera, G.; Kimura, M. Nickel-catalyzed CO_2 rearrangement of enol metal carbonates for the efficient synthesis of β -keto carboxylic acids. *Angew. Chem. Int. Ed.* **2017**, *56*, 208-211.
- (38) Das, R.; Parihar, V.; Nagaraja, C. M. Strategic design of a bifunctional Ag(I)-grafted NHC-MOF for efficient chemical fixation of CO₂ from a dilute gas under ambient conditions. *Inorg. Chem. Front.* **2022**, *9*, 2583-2593.
- (39) Feng, X.; Ding, X.; D. Jiang, Covalent organic frameworks. *Chem. Soc. Rev.* **2012**, *41*, 6010-6022.
- (40) Ding, S. -Y.; Wang, W. Covalent organic frameworks (COFs): from design to applications, *Chem. Soc. Rev.* **2013**, *42*, 548-568.
- (41) Xu, F.; Xu, H.; Chen, X.; Wu, D.; Wu, Y.; Liu, H.; Gu, C.; Fu, R. Jiang, D. Radical covalent organic frameworks: a general strategy to immobilize open-accessible polyradicals for high-performance capacitive energy storage. *Angew. Chem. Int. Ed.* **2015**, *127*, 6918-6922.
- (42) Wang, J.; Zhuang, S. Covalent organic frameworks (COFs) for environmental applications. *Coord. Chem. Rev.* **2019**, *400*, 213046.
- (43) Sharma, R. K.; Yadav, P.; Yadav, M.; Gupta, R.; Rana, P.; Srivastava, A.; Zboril, R.; Varma, R. S.; Antonietti, M.; Gawande, M. B. Recent development of covalent organic frameworks (COFs): synthesis and catalytic (organic-electro-photo) applications. *Mater. Horiz.* **2020**, *7*, 411-454.

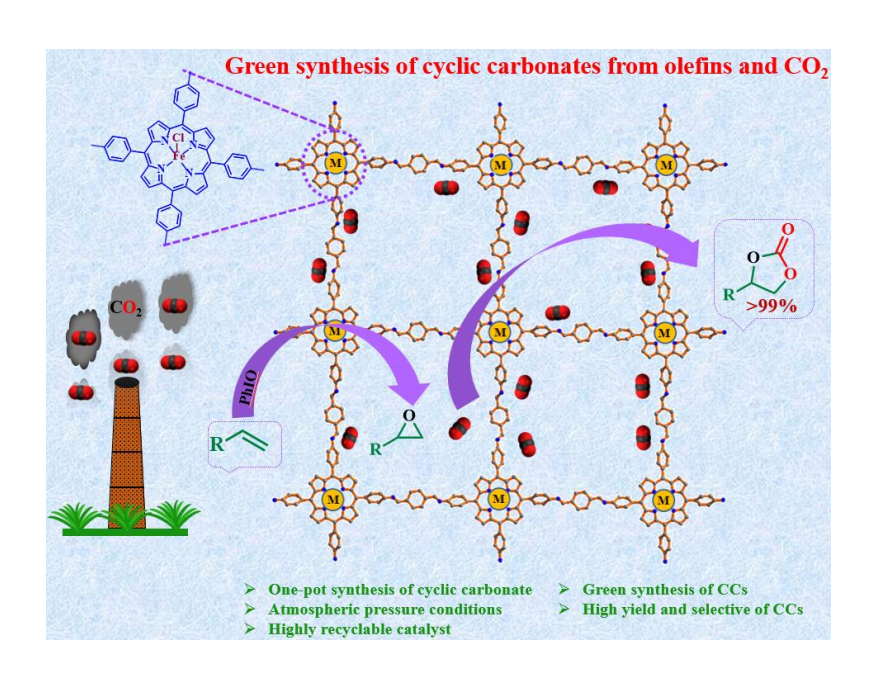
- (44) Liang, Z.; Wang, H. -Y.; Zheng, H.; Zhang, W.; R. Cao, Porphyrin-based frameworks for oxygen electrocatalysis and catalytic reduction of carbon dioxide. *Chem. Soc. Rev.* **2021**, *50*, 2540-2581.
- (45) Guan, X.; Chen, F.; Fang, Q.; Qiu, S.; Design and applications of three-dimensional covalent organic frameworks. *Chem. Soc. Rev* **2020**, *49*, 1357-1384.
- (46) Cote, A. P.; Benin, A. I.; Ockwig, N. W.; O'Keeffee, M.; Matzger, A. J.; Yaghi, O. M. Porous, crystalline, covalent organic frameworks. *Science* **2005**, *310*, 1166-1170.
- (47) Chen, X.; Geng, K.; Liu, R.; Tan, K. T.; Gong, Y.; Li, Z.; Tao, S.; Jiang, Q.; Jiang, D. Covalent organic framework: chemical approaches to designer structure and built-in functions. *Angew. Chem. Int. Ed.* **2020**, *59*, 5050-5091.
- (48) Li, Z.; Feng, X.; Zou, Y.; Zhang, Y.; Xia, H.; Liu, X.; Mu, Y. A 2D azine-linked covalent organic framework for gas storage applications. *Chem. Commun.* **2014**, *50*, 13825-13828.
- (49) Dhankhar, S. S; Nagaraja, C. M. Porous nitrogen-rich covalent organic framework for capture and conversion of CO₂ at atmospheric pressure conditions. *Micropor. Mesopor. Mat..* **2020**, *308*, 110314.
- (50) Li, H.; Feng, X.; Shao, P.; Chen, J.; Li, C.; Jayakumar, S.; Yang, Q. Synthesis of covalent organic frameworks via in situ salen skeleton formation for catalytic applications. *J. Mater. Chem. A* **2019**, *7*, 5482-5492.
- (51) Wang, J.; Zhang, Y.; Facile synthesis of N-rich porous azo-linked frameworks for selective CO₂ capture and conversion. *Green. Chem.* **2016**, *18*, 5248-5253.
- (52) Sengupta, M.; Bag, A.; Ghosh, S.; Mondal, P.; Bordoloi, A.; Islam, S. M. CuxOy@COF: An efficient heterogeneous catalyst system for CO₂ cycloadditions under ambient conditions. *J. CO₂ Util.* **2019**, *34*, 533-542.
- (53) Singh, G.; Nagaraja, C. M. Highly efficient metal/solvent-free chemical fixation of CO₂ at atmospheric pressure conditions using functionalized porous covalent organic frameworks. *J. CO₂ Util.* **2021**, *53*, 101716.
- (54) Luo, R.; Chen, M.; Liu, X.; Xu, W.; Li, J.; Liu, B.; Fang, Y. Recent advances in CO₂ capture and simultaneous conversion into cyclic carbonates over porous organic polymers having accessible metal sites. *J. Mater. Chem. A* **2020**, *8*, 18408-18424.
- (55) Luo, R.; Yang, Y.; Chen, K.; Liu, X.; Chen, M.; Xu, W.; Liu, B.; Ji, H.; Fang, Y. Tailored covalent organic frameworks for simultaneously capturing and converting CO₂ into cyclic carbonates. *J. Mater. Chem. A* **2021**, *9*, 20941-20956.

- (56) Chakraborty, D.; Shekhar, P.; Singh, H. D.; Kushwaha, R.; Vinod, C. P.; Vaidhyanathan, R. Ag nanoparticles supported on a resorcinol-phenylenediamine based covalent organic framework for chemical fixation of CO₂. *Chem. Asian J.* **2019**, *14*, 4767-4773.
- (57) Haque, N.; Biswas, S.; Ghosh, S.; Chowdhury, A. H.; Khan, A.; Islam, S. M. Zn(II)- embedded nanoporous covalent organic frameworks for catalytic conversion of CO₂ under solvent-free conditions. *ACS Appl. Nano Mater.* **2021**, *4*, 7663-7674.
- (58) Guan, P.; Qiu, J.; Zhao, Y.; Wang, H.; Li, Z.; Shi, Y.; Wang, J. A novel crystalline azine linked three-dimensional covalent organic framework for CO₂ capture and conversion. *Chem. Commun.* **2019**, *55*, 12459-12462.
- (59) Yang, Z.; Yu, B.; Zhang, H.; Zhao, Y.; Chen, Y.; Ma, Z.; Ji, G.; Gao, X.; Han, B.; Liu, Z. Metalated mesoporous poly(triphenylphosphine) with azo functionality: efficient catalysts for CO₂ conversion. *ACS Catal.* **2016**, *6*, 1268-1273.
- (60) Das, R.; Nagaraja, C. M. Noble metal-free Cu(I)-anchored NHC-based MOF for highly recyclable fixation of CO₂ under RT and atmospheric pressure conditions. *Green. Chem.* **2021**, *23*, 5195-5204.
- (61) Kuhn, P.; Antonietti, M.; Thomas, A. Porous, covalent triazine-based frameworks prepared by ionothermal synthesis. *Angew. Chem., Int. Ed.* **2008**, *47*, 3450-3453.
- (62) Bojdys, M. J.; Jeromenok, J.; Thomas, A.; Antonietti, M. Rational extension of the family of layered, covalent, triazine-based frameworks with regular porosity. *Adv. Mater.* **2010**, 22, 2202-2205.
- (63) Qian, Z.; Wang, Z. J.; Zhang, K. A. I. Covalent triazine frameworks as emerging heterogeneous photocatalysts. *Chem. Mater.* **2021**, *33*, 1909-1926.
- (64) -Thaw, C. E. C.; Villa, A.; Katekomol, P.; Dangsheng, S.; Thomas, A.; Prati, L. Covalent triazine framework as catalytic support for liquid phase reaction. *Nano Lett.* **2010**, *10*, 537-541.
- (65) Hug, S.; Tauchert, M. E.; Li, S.; Pachmayr, U. E.; Lotsch, B. V. A functional triazine framework based on *N*-heterocyclic building blocks. *J. Mater. Chem.* **2012**, 22, 13956-13964.
- (66) Luo, R.; Xu, W.; Chen, M.; Liu, X.; Fang, Y.; Ji, H. Covalent triazine frameworks obtained from nitrile monomers for sustainable CO₂ catalysis. *ChemSusChem* **2020**, *13*, 6509-6522.
- (67) Krishnaraj, C.; Jena, H. S.; Leus, K.; Voort, P. V. D. Covalent triazine frameworks-a sustainable perspective. *Green. Chem.* **2020**, 22, 1038-1071.

- (68) Gunasekar, G. H.; Park, K.; Ganesan, V.; Lee, K.; Kim, N. -K.; Jung, K. -D.; Yoon, S. A covalent triazine framework, functionalized with Ir/N-heterocyclic carbene sites, for the efficient hydrogenation of CO₂ to formate. *Chem. Mater.* **2017**, 29, 6740-6748.
- (69) Wang, H.; Jiang, D.; Huang, D.; Zeng, G.; Xu, P.; Lai, C.; Chen, M.; Cheng, M.; Zhang, C. Wang, Z. Covalent triazine frameworks for carbon dioxide capture. *J. Mater. Chem. A* **2019**, *7*, 22848-22870.
- (70) Sudakar, P.; Gunasekar, G. H.; Baek, I. H.; Yoon, S. Recyclable and efficient heterogenized Rh and Ir catalysts for the transfer hydrogenation of carbonyl compounds in aqueous medium. *Green. Chem.* **2016**, *18*, 6456-6461.
- (71) Padmanaban, S.; Gunasekar, G. H.; Lee, M.; Yoon, S. Recyclable covalent triazine framework-based Ru catalyst for transfer hydrogenation of carbonyl compounds in water. *ACS Sustain. Chem. Eng.* **2019**, *7*, 8893-8899.
- (72) Jurgens, B.; Irran, E.; Senker, J.; Kroll, P.; Muller, H.; Schnick, W.; Melem (2,5,8-Triamino-tri-s-triazine), an important intermediate during condensation of melamine rings to graphitic carbon nitride: synthesis, structure determination by X-ray powder diffractometry, solid-state NMR, and theoretical studies. *J. Am. Chem. Soc.* **2003**, *34*, 10288-10300.
- (73) Tahir, N.; -Miranda, F. M.; Everaert, J.; Tack, P.; Heugebaert, T.; Leus, K.; Vincze, L.; Stevens, C. V.; Speybroeck, V. V.; Voort, P. V. D. Immobilization of Ir(I) complex on covalent triazine frameworks for C-H borylation reactions: a combined experimental and computational study. *J. Catal.* **2019**, *371*, 135-143.
- (74) Xu, N.; Diao, Y.; Xu, Z.; Ke, H.; Zhu, X. Covalent triazine frameworks embedded with Ir complexes for enhanced photocatalytic hydrogen evolution. *ACS Appl. Energy Mater.* **2022**, *5*, 7473-7478
- (75) Yang, R. T. Gas Separation by Adsorption Processes, Butterworth, Boston, 1997.
- (76) Das, R.; Nagaraja, C. M. Highly efficient fixation of carbon dioxide at RT and atmospheric pressure conditions: influence of polar functionality on selective capture and conversion of CO₂. *Inorg. Chem.* **2020**, *59*, 9765-9773.

Chapter 4

Fe(III)-Anchored Porphyrin-Based Nanoporous Covalent Organic Frameworks for Green Synthesis of Cyclic Carbonates from Olefins and CO₂ under Atmospheric Pressure Conditions



❖ Reference: "Singh, G.; Prakash, K.; Nagaraja, C. M. Inorg. Chem. 2023, 62, 13058-13068."

4.1. Introduction

The gradual increase in the atmospheric CO₂ concentration has resulted in climate change, a rise in global average temperature, and other potentially harmful environmental issues.¹⁻³ Towards contending this rise in atmospheric CO₂ level, its selective capture/storage and utilization has been studied by researchers worldwide. Especially carbon capture and its subsequent utilization as a C1 source for generating useful chemicals/fuels is a promising and valuable approach with the dual benefits of lowering atmospheric carbon dioxide concentration and producing commodity chemicals. 4-8 In this direction, various strategies have been employed by researchers in functionalizing CO₂, a greenhouse gas, into valuable compounds. 9-21 Particularly, the transformation of CO₂ to cyclic carbonates via cycloaddition reaction with epoxides is of much interest owing to its 100% atom efficiency. 22-33 Additionally, cyclic carbonates find applications as polar solvents, electrolytes, and commodity chemicals for polymers. 34-38 Various strategies have been employed by researchers in developing catalytic systems for efficient coupling of CO2 to epoxides for cyclic carbonate production.³⁹⁻⁵⁰ However, the synthesis of cyclic carbonates by a green, one-pot oxidative carboxylation of olefins is highly preferred over the two-step process involving the utilization of epoxides.

In this regard, significant efforts are being made toward designing catalytic systems suitable for the one-step preparation of cyclic carbonates from readily accessible olefins and CO₂.⁵¹⁻⁵⁵ Particularly styrene carbonates have received special interest due to their potential applications as precursors for the synthesis of styrene carbamates, vicinal diols, polymers, etc.^{56,57} However, most of the reports known for styrene carbonate (SC) synthesis utilize a two-step process involving the conversion of styrene to styrene oxide (SO) and its subsequent coupling with CO₂ to generate styrene carbonate.⁵⁸⁻⁶¹ Towards developing a green and sustainable approach, it is desirable to carry out the synthesis via a one-pot cascade process by utilizing styrene and CO₂ under mild conditions.^{62,63} This one-step process offers advantages over the two-step synthesis in terms of easy handling, low cost, and minimum use of solvents. However, examples of recyclable catalysts known for the one-pot cascade synthesis of styrene carbonates are scarce.

The rational construction of covalent organic frameworks (COFs) as heterogeneous catalysts for selective CO₂ functionalization to valuable chemicals has

recently gained tremendous interest owing to their high surface area, ordered structure, tailored pore size, and functionality.⁶⁴⁻⁷¹ Especially, COFs with pores functionalized with polar groups are ideal candidate materials for CO₂ capture/utilization applications.⁷²⁻⁸¹ In this context, porphyrin-based frameworks have received a special interest owing to the presence of a free-base macrocyclic cavity that acts as a nanoreactor to promote selective CO₂ adsorption.^{82,83} At the same time, the free-base porphyrin ring can also serve as a potential site for anchoring catalytic metal ions suitable for various organic transformations, including CO₂ conversion to high-value chemicals.⁸⁴⁻⁸⁸ However, to date, there are no reports on the utilization of porphyrin-based COFs for an environmentally friendly, one-pot preparation of cyclic carbonates from readily available precursors, i.e. olefins and CO₂ under mild conditions.

Thus in Chapter 4, we demonstrate the application of Fe(III)-doped porphyrin COF, (Fe(III)@P-COF) as a recyclable catalyst for one-step preparation of CCs by utilizing olefins and CO₂ under atmospheric pressure conditions. A Schiff-base reaction of tetra(p-amino-phenyl)porphyrin with (TAPP) 1,4benzenedicarboxaldehyde (BDA) was employed to obtain the porphyrin-COF (P-COF). The Lewis acidic Fe(III) ions were anchored at the free-base porphyrin ring of P-COF by treating with FeCl₃. The resultant Fe(III)@P-COF was characterized by various techniques. Further, catalytic investigations of Fe(III) embedded P-COF revealed excellent activity for the one-step CC preparation from readily accessible olefins and CO₂ through in situ formation of epoxides. Indeed, various olefins, including substituted styrenes and linear alkenes, were transformed to their respective CCs in good yield and selectivity under atmospheric pressure conditions. Further, the catalyst was reusable for multiple cycles, retaining its network structure and catalytic performance. More importantly, Fe(III)@P-COF exhibited superior catalytic performance over several heterogeneous catalysts reported in the literature. This is a rare demonstration of applying porphyrin-COF-based catalysts for one-step CCs synthesis under mild conditions.

4.2. Experimental section

4.2.1. Materials

All the reagents used in this work were commercially available and employed as received without any further purification. The 1,3,5-trimethyl benzene was

purchased from TCI Chemicals Ltd. Acetic acid (99%) was obtained from Merck and Co. 1,4-benzenedicarboxaldehyde (BDA) utilized for COF synthesis was obtained from Sigma Aldrich Chemicals Co. Tetra(p-amino-phenyl)porphyrin (TAPP) was prepared by following the previously reported procedure.⁸⁹

4.2.2. Physical measurements

Powder X-ray diffraction measurements were recorded in the 2Θ range of 2-50° on PAN analytical's X'PERT PRO X-Ray diffractometer with a scan rate of 2°/min using Cu-K α radiation (λ = 1.54184 Å, 40 kV, 20 mA) for confirming phase purity of as-synthesized samples. Fourier transform infrared (FT-IR) spectra of the samples were recorded on a Bruker Tensor-F27 instrument in ATR mode. The products of catalytic reactions were identified and the catalytic conversions were determined by 1 H NMR spectra recorded on a JEOL JNM-ECS-400 spectrometer operating at a frequency of 400 MHz using CDCl₃ solvent.

4.2.3. Synthesis

4.2.3.1. Synthesis of porphyrin COF (P-COF)

In a typical synthesis, a pyrex tube was charged with terephthalaldehyde (5.6 mg, 0.04 mmol), tetra(p-aminophenyl)porphyrin (13.5 mg, 0.02 mmol), and to which absolute ethanol (0.5 mL), mesitylene (0.5 mL), and 6 M aqueous acetic acid (0.1 mL) were added. The tube was flash frozen at 77 K, evacuated, flame sealed, and heated at 120 °C for 72 h in an oven. After completion of the reaction, a purple crystalline solid was separated by centrifugation, washed with 1,4-dioxane, THF, and acetone, and dried under a vacuum. FT-IR (KBr, cm⁻¹) 3426 (br), 1620 (s), 1512 (m), 1466 (m), 1420 (w), 1381 (m), 1288 (m), 1249 (m), 1180 (s), 1118 (w), 802 (s), 733 (w), 656 (w), 556 (w).

4.2.3.2. Synthesis of Fe(III)@P-COF

The activated sample of P-COF (0.06 mmol) at 120 °C was treated with the solution of FeCl₃ (0.6 mmol) in DMF (10 mL) and the mixture was refluxed for 12 h. After completion of the reaction, the solid was separated by centrifugation, washed with a copious amount of methanol to remove unreacted FeCl₃, and dried under a vacuum. The percentage loading of Fe^{III} in P-COF was determined by MP-AES elemental analysis.

4.2.3.3. Synthesis of Fe(II)/Zn(II)@P-COF

This Fe(II)@P-COF was prepared following a procedure similar to that of the Fe(III)@P-COF. The activated sample of P-COF (0.06 mmol) was treated with a solution of Fe(OAc)₂ (0.6 mmol) in DMF (10 mL) and refluxed for 12 h. After completion of the reaction, the solid was separated by centrifugation and washed with a copious amount of methanol to remove unreacted Fe(OAc)₂ and dried under a vacuum. In addition, we used Zn(OAc)₂.2H₂O in methanol for Zn doping and the process remained the same. The loading of Fe(II)/Zn(II) was determined by MP-AES analysis.

4.2.4. Catalytic epoxidation of styrenes

The catalytic reaction was carried out as follows, the Zn/Fe@P-COF (10 mg), styrene (0.6 mmol), and oxidant PhIO (1.5 mmol) were mixed in dichloromethane (5 mL) in RB at RT and the reaction mixture was heated with stirring for 18 h. After that, the catalyst was separated by centrifugation, and the filtrate was evaporated. The yield of styrene carbonate formed was determined by ¹H NMR spectroscopic analysis.

4.2.5. One-pot oxidative carboxylation of styrene

In a 50 mL stainless steel reactor, the oxidative carboxylation reaction of styrene with CO₂ was performed using Fe(III)@P-COF as a catalyst in the presence of PhIO and TBAB as oxidant and co-catalyst, respectively. Before the reaction, the catalyst was activated at 373 K for 10 h under a vacuum to eliminate the guest solvent molecules. Then the activated catalyst Fe(III)@P-COF (10 mg), styrene (0.6 mmol), oxidant, PhIO (1.5 mmol), and TBAB (0.3 mmol) in dichloromethane (2 mL) were taken in a 50 mL glass reactor with a stainless steel jacket and flushed three times with CO₂ to eliminate the air inside the glass reactor. After introducing the required CO₂ pressure (0.1 MPa), the reaction mixture was stirred at 80 °C for 24 h. After that time, the CO₂ was released slowly, the catalyst was separated by centrifugation, the filtrate was evaporated, and the catalytic conversion of styrene was determined by ¹H NMR spectroscopy. The recovered catalyst was washed with methanol, activated for 12 h at 100 °C, and then reused for subsequent catalytic cycles.

4.2.6. Structure simulation and modeling of P-COF

To elucidate the structure of P-COF and to calculate the unit cell parameters, a

possible 2D model was constructed. The experimental PXRD pattern matches well with that of the simulated pattern for an eclipsed model of P-COF. Refinement of PXRD patterns was carried out using the Pseudo-Voigt function. The optimized structural parameters are given below. The simulated optimized structure of P-COF is shown in Figure 1.

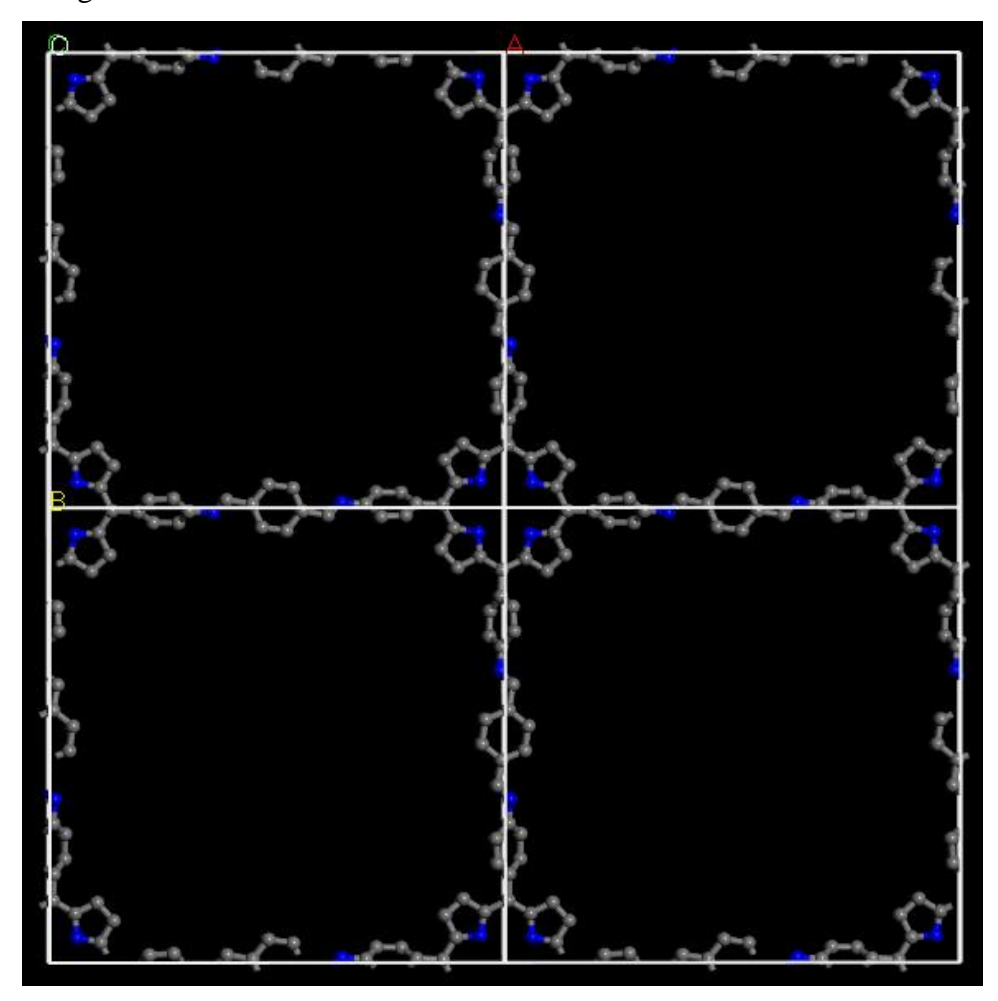


Figure 1. Simulated structure of P-COF (ball and stick model) (gray, Carbon; blue, Nitrogen).

4.2.7. Gas adsorption measurements

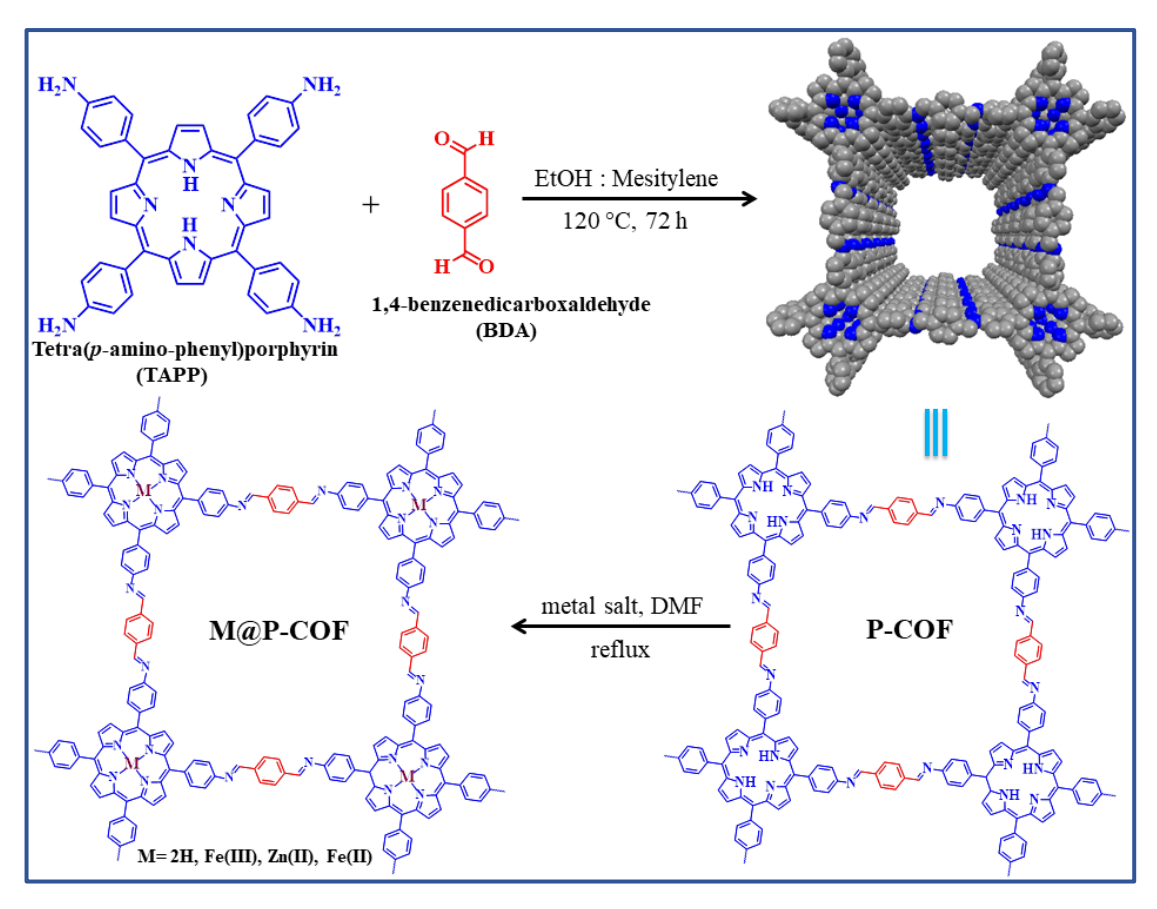
N₂ adsorption-desorption studies were carried out at 77 and 273 K, while CO₂ adsorption-desorption measurements were carried out at 273 and 298 K using QUANTACHROME Quadrasorb SI automated surface area and pore size analyzer instrument. Ultrapure (99.995%) N₂ gas was used for the adsorption-desorption measurements. Priorto adsorption measurements, the sample (~0.070g) was evacuated at 393 K under vacuum (20 mTorr) for 12 h on QUANTACHROME Flovac degasser and further purged with ultrapureN₂ (99.995%) gas on cooling. The BET surface area

of the COFs was estimated from N_2 sorption isotherms carried out at 77 K, respectively. The dead volume of the sample cell was measured using Helium gas (99.995%).

4.3. Results and discussion

4.3.1. Synthesis and structural description

The preparation of porphyrin-based COFs has been achieved by employing various synthetic routes. ^{76,90} Particulary, the solvothermal approach is generally followed to obtain COFs with high crystallinity. ^{67,68,91} The porphyrin-COF (P-COF) was prepared by adopting the reported solvothermal procedure with minor modifications ⁹² (Scheme 1) and characterized by different techniques. The FTIR spectra of P-COF depicted the disappearance of characteristic stretching frequencies due to the -NH₂ group of tetra(p-amino-phenyl)porphyrin (TAPP) and also the carbonyl group (C=O) of 1,4-benzenedicarboxaldehyde (BDA) indicating complete consumption of the precursors during the COF synthesis. Besides, a new stretching frequency at 1620 cm⁻¹ corresponding to the C=N group was observed, supporting the formation of P-COF by Schiff base condensation (Figure A23a). Furthermore, the solid-state ¹³C CP-MAS NMR spectra of P-COF showed a characteristic peak at 159.0 ppm assigned to the ¹³C resonance of the C=N group formed between the precursors (Figure A24). ⁹³



Scheme 1. Synthesis scheme for P-COF and M@P-COF.

Moreover, the crystalline nature of P-COF was revealed from the XRD analysis. The powder XRD pattern (Figure 2a) showed an intense peak at a lower Bragg angle of 3.54° corresponding to the (100) plane and a relatively lower intense peak at 7.14° due to the (200) plane, indicating the presence of long-range ordering in the material. In addition, the broad peak around 20° (001) corresponds to π - π stacking amongst the 2D COF sheets. Furthermore, the XRD pattern of P-COF matches well with the simulated pattern (Figure 2a). The most probable 2D model of P-COF was conceived of as an eclipsed form having a tetragonal system with space group, P4/m with unit cell parameters of a = b = 25.41 Å, c = 12.37 Å, $\alpha = \beta = \gamma = 90^{\circ}$. Further, SEM images of P-COF and Fe(III)@P-COF showed a flower-like hierarchical structure (Figures 2c and 2d). Further, the porphyrin COF (P-COF) was treated with FeCl₃ to obtain Fe(III)@P-COF, which was isolated and washed with methanol to remove free metal salt. Various characterizations further confirmed the incorporation of Fe^{III} at the freebase porphyrin ring. For instance, the FTIR spectra (Figure A23b and A23c) of Fe(III)@P-COF showed the disappearance of stretching frequency at 3327 cm⁻¹ corresponding to the pyrrole -N-H bond of porphyrin ring supporting the anchoring of Fe(III) in P-COF as illustrated in Scheme 1. Further, the PXRD plot of Fe(III)@P-COF displays a diffraction pattern similar to that of pristine P-COF, suggesting the retention of network structure even after the incorporation of Fe^{III} ion (Figure 2b). Furthermore, EDS analysis proved the presence of Fe^{III} ion in the framework (Figures A25 and A26), and the % loading determined by MP-AES (microwave plasma atomic emission spectroscopy) analysis was 6.9 wt % (Figure A27a).

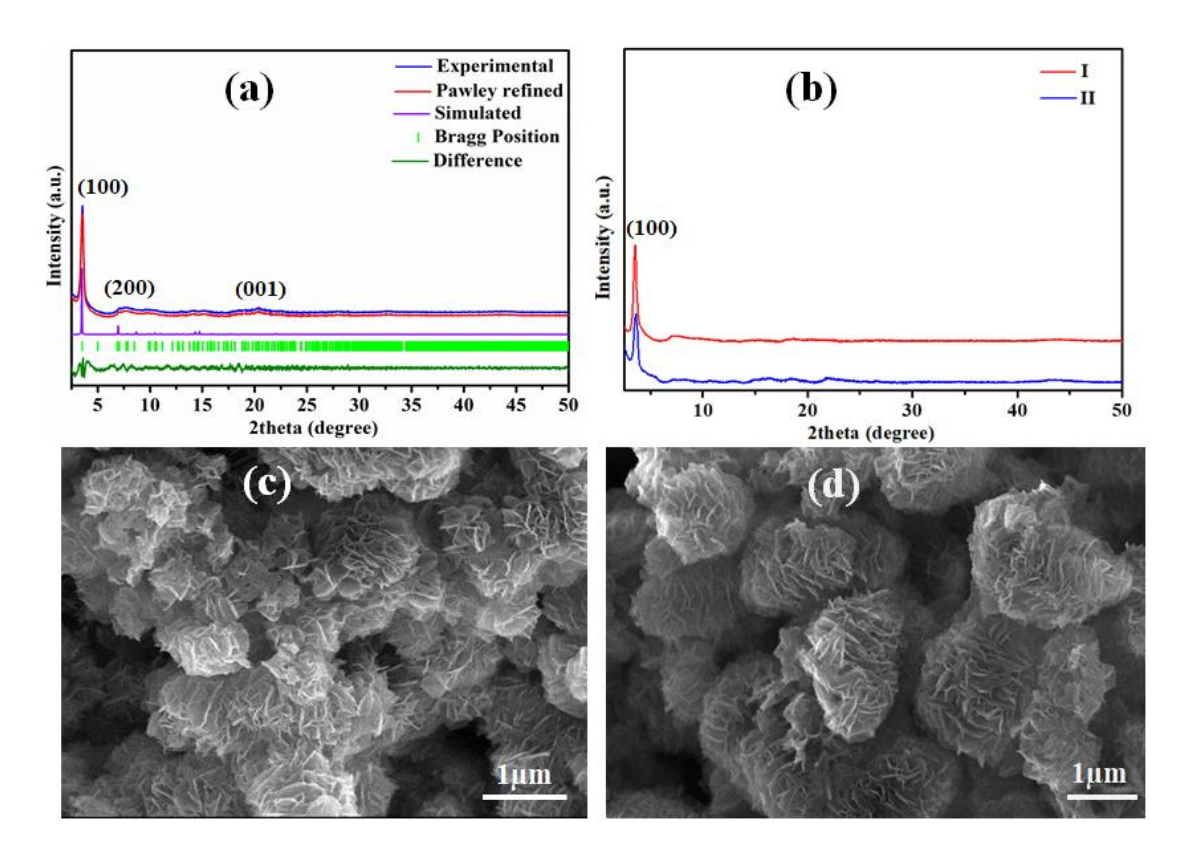


Figure 2. (a) Experimental (blue) and simulated (purple) powder XRD plots of P-COF. (b) Powder XRD plots of Fe(III)@P-COF samples, pristine (I), and recycled after catalysis (II). (c and d) SEM images of P-COF and Fe(III)@P-COF, respectively.

The XPS analysis of pristine P-COF and Fe^{III}-anchored COF was performed to confirm the elemental composition of the samples. The survey scan (Figures 3a and A28a) showed the presence of constituent elements. The N 1s spectra of P-COF show two binding energy (BE) bands at 398.2 and 400.2 eV corresponding to -C=N- and pyrrolic N, respectively (Figure A28b). ^{95,96} While a new band was observed at 398.8 eV in the N 1s spectra of Fe(III)@P-COF corresponding to the pyrrole N of the porphyrin ring coordinated to Fe^{III} (Fe-N) (Figure 3b). Further, the Fe^{III} 2p spectra (Figure 3c) show two peaks due to 2p_{3/2} and 2p_{1/2} at BE of 710.7 and 724.6 eV,

respectively. This observation is in line with the XPS spectra of Fe^{III} compounds reported before. ⁹⁷⁻⁹⁹ Besides, the deconvoluted spectra of Cl 2p (Figure 3d) show the presence of two BE bands at 197.9 and 199.6 eV attributed to $2p_{3/2}$ and $2p_{1/2}$, respectively, which further asserted the +3 oxidation state of Fe. Thus, XPS analysis supports the embedding of Fe^{III} in the porphyrin pyrrole ring.

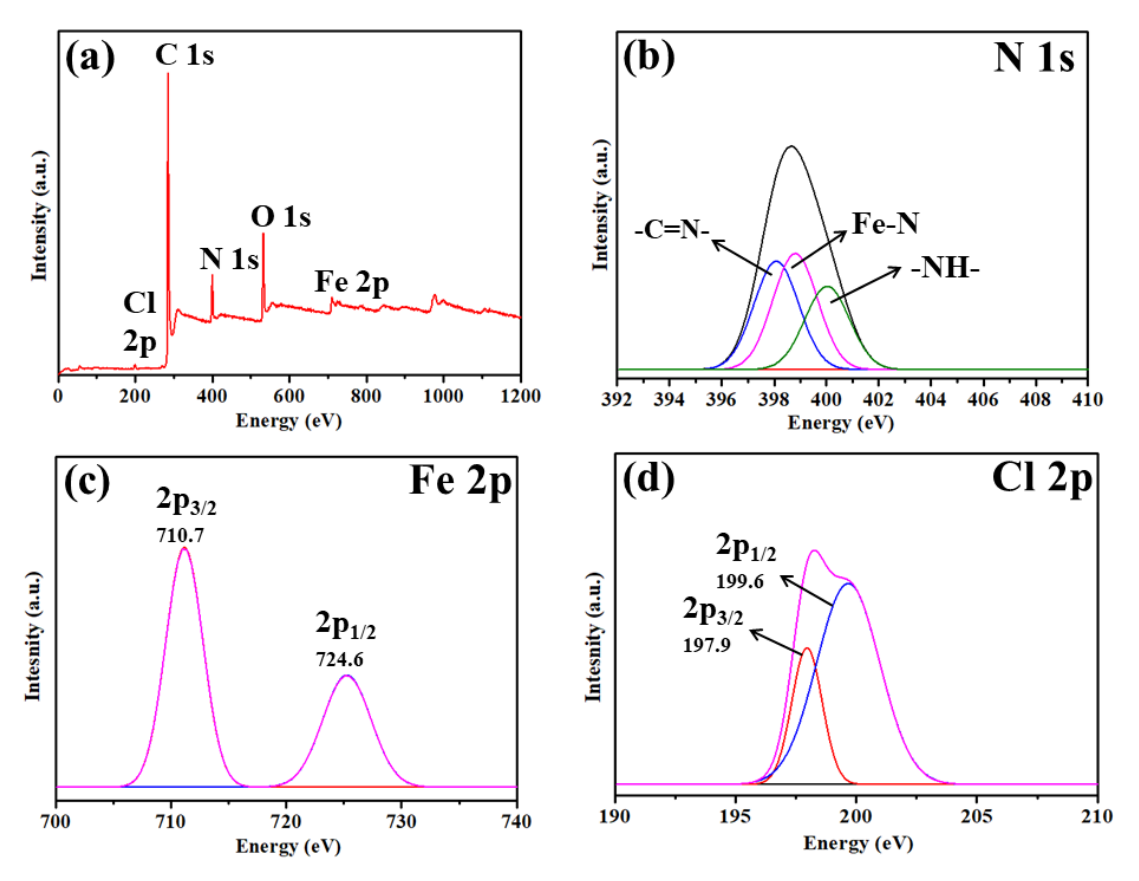


Figure 3. XPS plot of Fe(III)@P-COF, (a) survey spectrum (b) N 1s, (c) Fe 2p, and (d) Cl 2p.

Furthermore, to establish the role of oxophilic Fe^{III} ion in catalyzing the one-step oxidative carboxylation of olefins to CCs, analogous COFs based on Zn(II)/Fe(II) were prepared and characterized. The FT-IR spectra of Zn(II)/Fe(II)@P-COF showed the absence of peaks at 3327 cm⁻¹ due to pyrrole N-H of the porphyrin ring, indicating anchoring of Fe(II)/Zn(II) at the porphyrin ring (Figure A29a). Further, the PXRD plot of the metal-embedded COFs matches well with that of parent P-COF, with diffraction peaks at 20 of 3.5, and 7.1 corresponding to the (100) and (200) plane, respectively supporting the isostructural nature of Zn(II)/Fe(II) and Fe(III)@P-COFs (Figure A29b). Further, the % loading of the metal was determined by MP-AES (microwave plasma atomic emission spectroscopy) analysis (Figure A27b and A27c).

4.3.2. Gas adsorption analysis

The N_2 sorption isotherms performed to assess the porosity of P-COF and Fe(III)@P-COF are shown in Figure 4. The samples were activated prior to adsorption measurements. The BET surface area (S_{BET}) of pristine P-COF was determined to be 686 m²g⁻¹ which was decreased to 382 m²g⁻¹ upon the incorporation of Fe^{III} in the porphyrin ring (Fe(III)@COF) owing to loss of porosity on metallation (Figure 4a). Further, CO₂ sorption isotherms of P-COF and Fe(III)@P-COF show typical type-1 profiles with the uptake of 27.13/16.91 cc/g and 18.43/10.47 cc/g at 273/298 K, respectively (Figure 4b). The accurate determination of CO₂ uptake was performed by fitting the isotherms adopting the Freundlich-Langmuir equation (Figure A30), and the adsorption energy (Q_{st}) determined from Clausius-Clayperon equation were 28.08 and 37.76 kJ/mol for P-COF and Fe(III)@P-COF, respectively (Figure A31). The high heat of adsorption of CO₂ with Fe(III) anchored COF can be attributed to their enhanced interaction aided by the presence of imine (-C=N-) linkages and unsaturated Fe(III) ion through Lewis acid/base and/or metal ion/quadrupole interactions. 100,101,104

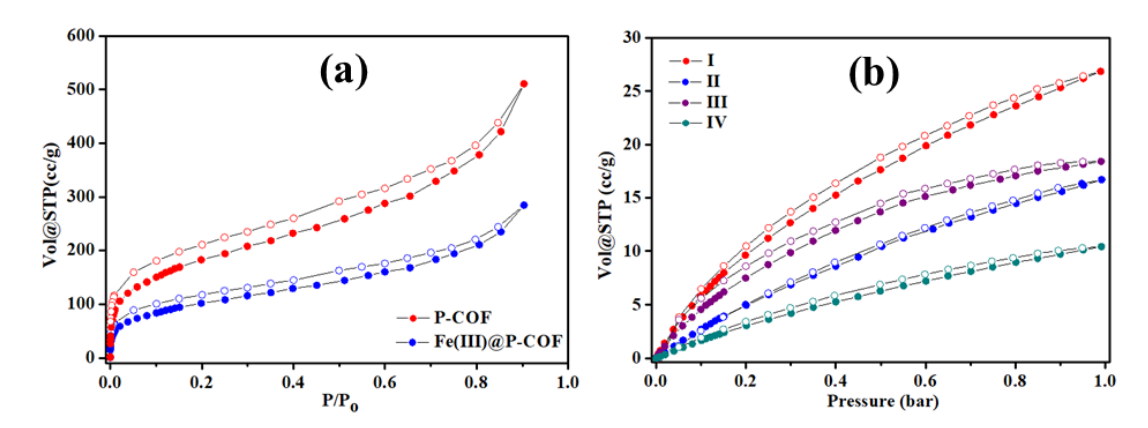


Figure 4. (a) N₂ adsorption plot of P-COF and Fe(III)@P-COF. (b) The CO₂ sorption isotherms of P-COF (I, II) and Fe(III)@P-COF (III, IV) were performed at 273 K and 298 K, respectively.

4.3.3. Catalytic epoxidation of styrenes

The nanoporous Fe(III)@P-COF with 1D channels decorated with Lewis acidic, oxophilic Fe^{III} ions motivated us to investigate its catalytic performance for the one-step reaction of CO₂ with olefins. To start with, the catalysis was tested for the oxidation of olefins to epoxides. The catalytic reaction performed for the epoxidation of styrene using P-COF as a catalyst and PhIO as an oxidizing agent (OA) showed no styrene oxide (SO) formation. Whereas the use of Fe(III)@P-COF as a catalyst at the

optimized conditions (Table 1) resulted in >99% SO formation with 100% selectivity, highlighting the requirement of Fe^{III} ions for selective oxidation of styrene (Table 1). Further, to examine the critical role of Fe^{III} ions in catalyzing the epoxidation of olefins, the reaction was tested with Zn(II)/Fe(II)@P-COF as a catalyst. Interestingly, negligible conversion of styrene was observed with Zn(II)-COF, while about 38.2% styrene was converted to SO using Fe(II)@P-COF as a catalyst at the optimized conditions (Table 1). These results unambiguously confirm the necessity of Lewis acidic, oxophilic Fe^{III} in catalyzing the epoxidation of olefins.

Table 1: Optimization table for oxidation of styrene to styrene oxide.^a

S. No.	Catalyst	Oxidant	Conversion (%) ^b
1	_	PhIO	2
2	P-COF	NO	-
3	FeCl ₃	PhIO	4
4	TAPP	PhIO	2
5	FeCl ₂	PhIO	3
6	Zn(II)@P-COF	PhIO	4
7	P-COF	PhIO	3
8	Fe(II)@P-COF	PhIO	38.2
9	Fe(III)@P-COF	No	-
10^c	Fe(III)@P-COF	PhIO	55.6
11	Fe(III)@P-COF	PhIO	>99
12 ^d	Fe(III)@P-COF	PhIO	53.2

^aReaction conditions: catalyst (10 mg), styrene (0.6 mmol), PhIO (1.5 mmol), CH₂Cl₂, and time (18 h) at 40 °C. ^bThe percentage conversion was determined by ¹H NMR analysis. ^cTemperature (RT). ^dTime (9h).

Further, various control experiments were performed to arrive at the optimum conditions required for the epoxidation of styrene to styrene oxide (Table 1). The enhanced catalytic activity of Fe(III)@P-COF has been ascribed to the facile formation of Fe^{IV}-oxo species, a key intermediate in SO (epoxide) formation. ^{102,103} This superior catalytic performance of Fe(III)@P-COF encouraged us to test the epoxidation of various olefins, such as substituted styrenes and linear olefins. Notably,

most olefins were transformed to respective epoxides in good conversion and selectivity (Table 2). More interestingly, the catalytic performance of Fe(III)@P-COF is comparable to or better than reported heterogeneous catalysts (Table A3).

Table 2: Epoxidation of olefins catalyzed by Fe(III)@P-COF. a

	R^	Fe(III)@P-COF	\sim R $^{\circ}$	
	R= Ph, Ph-F, Ph-Cl, (CH ₂) ₄ etc.			
S. No.	Substrate	Product	Conversion (%) ^b	
1		O O	>99	
2	F	F O	91.2	
3	CI	CI	86.2	
4	O_2N	O_2N	76.3	
5			70.2	
6	\		65.3	
7	\\\\		52.5	
8	\\\\	√	39.4	
9		0	38.2	

^aReaction conditions: catalyst (10 mg), olefin (0.6 mmol), PhIO (1.5 mmol), CH₂Cl₂, and time (18 h) at 40 °C. ^bThe conversions were determined by ¹H NMR analysis.

4.3.4. One-pot cyclic carboxylation of olefins

The enhanced catalytic performance of Fe(III)@P-COF for the epoxidation of olefins encouraged us to test their catalytic activity for the one-pot CCs synthesis from readily accessible olefins and carbon dioxide. Hence, the catalysis was carried out in the presence of an oxidant (PhIO) and a nucleophilic cocatalyst, tetrabutylammonium bromide (TBAB), to promote the ring-opening of the epoxide. To start with, the catalytic performance was studied using styrene as a model reagent, and optimization of reaction conditions was performed by varying the temperature and time of the reaction. The best catalytic performance was achieved at 80 °C in 24 h (Figure 5 and Table 3).

Table 3: Optimization table for catalytic oxidative carboxylation of styrene to styrene carbonate.^a

S. No.	Catalyst	Oxidant	Conversion (%) ^b
1	FeCl ₃	PhIO	3
2	_	PhIO	1
3	P-COF	No	-
4 ^c	P-COF	No	-
5	FeCl ₂	PhIO	2
6	Fe(III)@P-COF	No	-
7	TAPP	PhIO	1
8	TABB	PhIO	3
9	P-COF	PhIO	4
10	Zn(II)@P-COF	PhIO	5
11	Fe(II)@P-COF	PhIO	40
12^d	Fe(III)@P-COF	PhIO	60.3
13	Fe(III)@P-COF	PhIO	>99
14 ^e	Fe(III)@P-COF	PhIO	58.9
15 ^f	Fe(III)@P-COF	No	>99

^aReaction conditions: catalyst (10 mg), styrene (0.6 mmol), PhIO (1.5 mmol), TBAB (0.3 mmol), CO₂ (0.1 MPa), CH₂Cl₂ (2 mL) and time (24 h) at 80 °C. ^bThe percentage conversion was determined by ¹H NMR analysis. ^cwithout TBAB. ^dTemperature (RT). ^eTime (12 h). ^fconversion for styrene oxide.

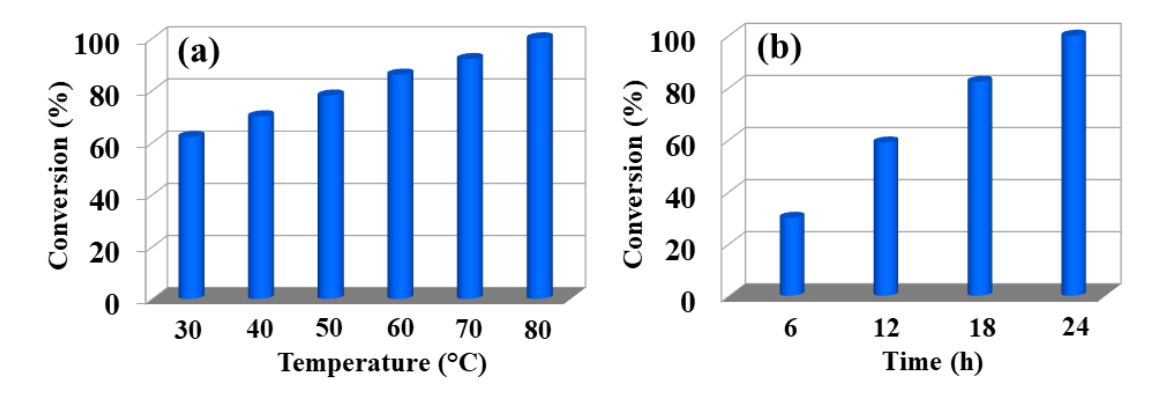


Figure 5. The optimization of catalytic reaction by varying temperature (a) and time (b). Reaction conditions: catalyst (10 mg), styrene (0.6 mmol), TBAB (0.3 mmol), CO₂ (0.1 MPa), PhIO (1.5 mmol), and dichloromethane (2 mL).

The catalytic reaction performed at RT and 1 bar CO₂ using Fe(III)@P-COF (10 mg) as a catalyst along with PhIO (1.5 mmol), and TBAB (0.3 mmol) led to a 60.3% conversion of styrene to SC within 24 h (Table 4). Further, the effect of temperature on catalysis was studied. As can be seen from Figure 5a, the reaction carried out at 60 °C resulted in 86.2% conversion of styrene to SC. Upon increasing the temperature further, the conversion of styrene was found to increase. The best catalytic performance with >99% conversion of styrene to styrene carbonate (98.5% selectivity) along with styrene oxide (1.5 %) as a minor product was observed at 80 °C in 24 h (Table 3). These results suggest that the SO formed in situ undergoes cycloaddition with CO₂ in the presence of TBAB to form SC. This was further supported by the control experiment carried out in the absence of catalyst and PhIO, which showed no SC formation (Table 3). On the contrary, the catalytic reactions performed with pristine P-COF as a catalyst under the optimized conditions led to negligible formation of SC (Table 3). While the application of TBAB as a catalyst showed negligible conversion (~3%) of styrene to SC (Table 3). In addition, the reaction carried out with Zn(II)@P-COF did not yield SC (Table 3), whereas the use of Fe(II)@P-COF rendered a 40% conversion of styrene (Table 3). These experiments further highlight the necessity of Lewis acidic, oxophilic Fe^{III}-anchored COF for the one-pot synthesis of SCs from styrene and CO₂ (Table 3).

Table 4: One-step oxidative carboxylation of olefins with CO₂.

		Fee + CO ₂ —	(III)@P-COF PhIO	0
	R= P	h, Ph-F, Ph-Cl, (CH ₂) ₄ etc.	TBAB R	, o
S.			Conversion	Selectivity of
No.	Substrate	Product	$(\%)^b$	SC (%)
1			>99	98.5 ^c
2	F	F O	92.3	91.5 ^d
3	H ₃ C	H ₃ C	85.1	89.7 ^e
4	CI	CI	88.3	90.7 ^f
5	O ₂ N	O ₂ N	78.2	87.8 ^g
6	XCX		72.3	85.4 ^h
7	>		69.2	74.2^{i}
8	>>>>		56.3	62.3^{j}
9	\\\\		41.6	49.4 ^k
10	\bigcirc	0 =0	40	56.6 ^l

^aReaction conditions: catalyst (10 mg), olefin (0.6 mmol), TBAB (0.3 mmol), PhIO (1.5 mmol), CO₂ (0.1 MPa), CH₂Cl₂ (2 mL) and time (24 h) at 80 °C. ^bThe conversions were

determined by ¹H NMR analysis. Selectivity of styrene oxide: ^c1.5, ^d8.5, ^e10.3, ^f9.3, ^g12.2, ^h14.6, ⁱ25.8, ^j37.7, ^k50.6 and ^l43.4.

This promising catalytic performance of Fe(III)@P-COF for one-pot synthesis of SCs further motivated us to investigate the scope of the process for the transformation of substituted styrenes using the optimized conditions (Table 4). As shown in Table 4, most styrenes were found to transform to respective SCs in quantitative yield (72.3-99.5%) along with SO intermediate as a minor product at 1 atm of CO₂. This one-pot synthesis strategy was also extended for oxidative carboxylation of linear olefins. Interestingly, the catalytic conversions were found to decrease with an increase in the alkyl chain length of the olefins from 1-hexene to 1decene (Table 4). 106 This can be ascribed to the lower reactivity and restricted diffusion of higher alkenes in the pore channels of COF. Moreover, the internal alkene, cyclohexene, was transformed to the corresponding CC in a moderate yield (Table 4). This lower conversion of cyclohexene has been attributed to its intrinsic low reactivity and bulkiness, limiting its diffusion to the catalytic Fe(III) site. Further, the catalytic reaction performed using an epoxide/SO instead of olefin/styrene under the optimized conditions resulted in >99% SC formation within 18 h with a selectivity of 100%. This experiment supports the in situ formation of SO/epoxide intermediate en route to the SC formation (Table 4). A control experiment was performed to further characterize the intermediate in which Fe(III)@P-COF was treated with styrene oxide for 2 h. Then the catalyst was retrieved, and its FT-IR spectra recorded showed the appearance of peaks at 3100-2900 cm⁻¹ corresponding to the C-H stretching frequencies of SO, affirming its interaction with the Fe^{III} center in the COF (Figure A32). Notably, the performance of Fe(III)@P-COF for one-pot synthesis of SCs was found to be superior in comparison to various framework-based catalysts reported before (Table A4). Overall, this work highlights the CO₂ utilization at atmospheric pressure conditions for the one-step CC synthesis from olefins and CO₂.

4.3.5. Catalyst recycling and leaching test

To test the catalyst's recyclability, Fe(III)@P-COF was separated from the reaction mixture, and after suitable activation, it was reused for subsequent catalytic cycles. Notably, the catalyst was reusable for up to eight cycles without loss of catalytic performance (Figure 6a). The XRD and FT-IR plots of the recycled COF

support the structural rigidity of the recycled catalyst even after multiple cycles of reuse (Figure 2b and A33). Furthermore, SEM images of recycled COF showed that the original morphology was almost retained (Figure A34).

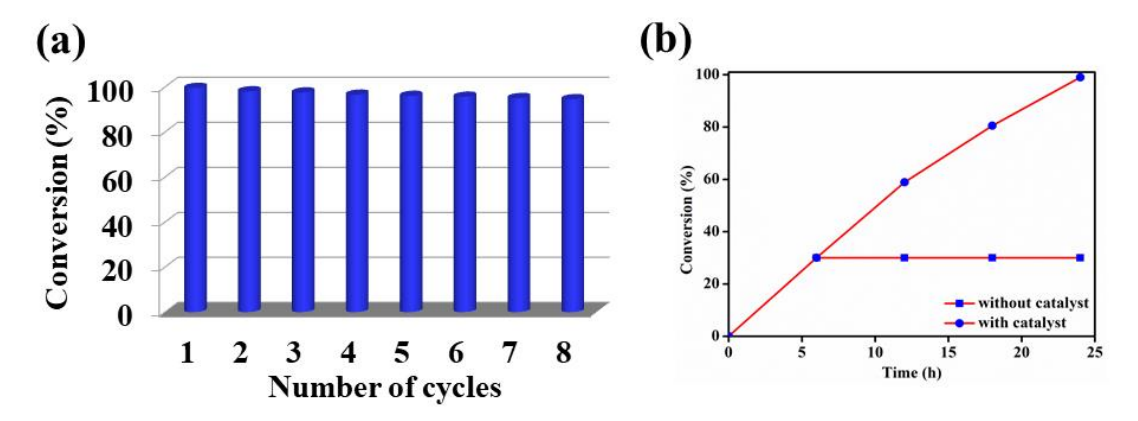


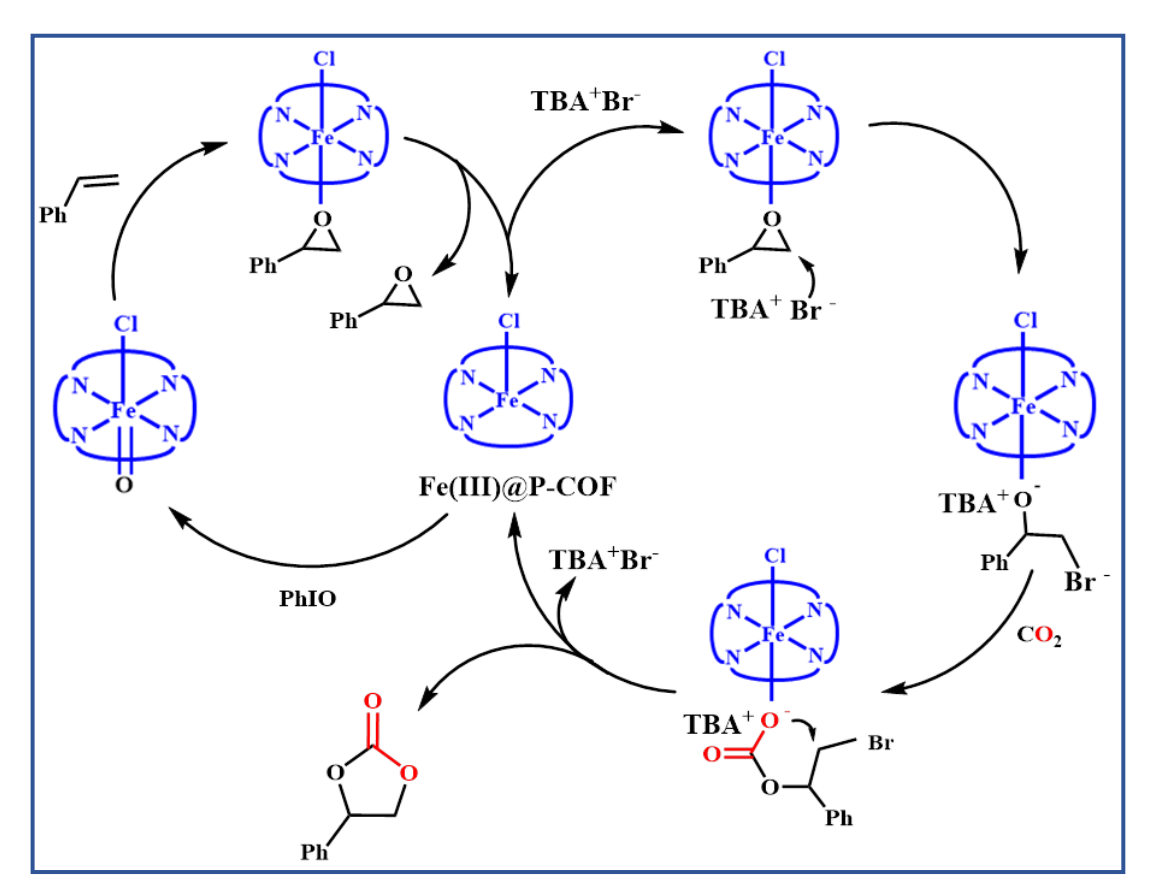
Figure 6. Recyclability (a) and catalyst leaching (b) test of Fe(III)@P-COF.

Moreover, to rule out any catalytic activity originating from the homogeneous phase, the catalyst leaching test was performed in which the Fe(III)@P-COF was stopped after 6 h with a 30% yield of SC. Then Fe(III)@P-COF was separated, and the filtrate was continued for an additional time. Interestingly, there was no substantial rise in the SC yield, supporting the absence of catalyst leaching (Figure 6b).

4.3.6. Plausible mechanism

A plausible reaction pathway for Fe(III)@P-COF catalyzed one-pot preparation of CCs from readily accessible styrene and CO₂ is shown in Scheme 2. The reaction proceeds with the *in situ* formation of epoxide by olefin oxidation catalyzed by Fe^{III} in the presence of the oxidizing agent PhIO. To get further support on this step, a time-dependent ¹H NMR study was undertaken for the oxidation of styrene as a model substrate. As can be seen from the stack plot (Figure A35), the ¹H NMR spectra of the aliquot taken after 18 h of catalytic reaction show peaks corresponding to styrene and the product, SC, along with the intermediate, SO. Further, with an increase in reaction time from 18 to 24 h, the intensity of the peaks due to SO decreases, and those of SC increase, supporting the transformation of SO to SC. The SO formed undergoes a ring-opening step by the attack of the Br⁻ ion of TBAB, resulting in bromo-alkoxide formation. The subsequent CO₂ insertion into the metal-alkoxide intermediate led to

SC formation, which upon intramolecular ring-closer reaction, yields SC. The elimination of SC regenerates the catalyst for successive catalytic cycles.



Scheme 2. A proposed mechanism for the one-step styrene carbonate synthesis from styrene and CO₂ catalyzed by Fe(III)@P-COF.

4.4. Conclusion

In summary, the one-step synthesis of CCs, valuable feedstock chemicals, was achieved by utilization of greenhouse gas, CO₂, and readily available olefins at atmospheric pressure conditions using Fe(III)@P-COF as a highly recyclable catalyst. The Fe(III)@P-COF showed good CO₂ affinity and catalytic activity for direct cascade preparation of various CCs from CO₂ and olefins. Notably, the catalyst was recycled for eight cycles without substantial loss in activity and structural rigidity. Overall the catalytic strategy developed here presents an eco-friendly route for generating valuable chemicals by utilizing abundant CO₂ and styrenes under mild atmospheric pressure conditions and paves the way for the rational design of catalysts for carbon capture and utilization under mild conditions.

4.5. References

- (1) Jacobson, M. Z. Review of solutions to global warming, air pollution, and energy security. *Energy Environ. Sci.* **2009**, *2*, 148-173.
- (2) Glikson, A. The lungs of the Earth: Review of the carbon cycle and mass extinction of Species. *Energy Procedia* **2018**, *146*, 3-11.
- (3) Joos, F.; Plattner, G. -K.; Stocker, T. F.; Marchal, O.; Schmittner, A. Global Warming and Marine Carbon Cycle Feedbacks on Future Atmospheric CO₂. *Science* **1999**, 284, 464-467.
- (4) North, M.; Pasuale, R.; Young, C. Synthesis of cyclic carbonates from epoxides and CO₂. *Green Chem.* **2010**, *12*, 1514-1539.
- (5) Chu, S. Carbon Capture and Sequestration. Science 2009, 325, 1599.
- (6) Saravanan, A.; Kumar, P. S.; Vo, D. -V. N.; Jeevanantham, S.; Bhuvaneswari, V.; Narayanan, V. A.; Yaashika, P. R.; Swetha, S.; Reshma, B. A comprehensive review on different approaches for CO₂ utilization and conversion pathways. *Chem. Eng. Sci.* **2021**, *236*, 116515.
- (7) Mustafa, A.; Lougou, B. G.; Shuai, Y.; Wang, Z.; Tan, H. Current technology development for CO₂ utilization into solar fuels and chemicals: A review. *J. Energy Chem.* **2020**, *49*, 96-123.
- (8) Nagaraja, C. M.; Haldar, R.; Maji, T. K.; Rao, C. N. R. Chiral Porous Metal-Organic Frameworks of Co(II) and Ni(II): Synthesis, Structure, Magnetic Properties, and CO₂ Uptake. *Cryst. Growth Des.* **2012**, *12*, 975-981.
- (9) Dai, W. -L.; Luo, S. -L.; Yin, S. -F.; Au, C. -T. The direct of carbon dioxide to organic carbonates over heterogeneous catalysts. *Appl. Catal. A* **2009**, *366*, 2-12.
- (10) Jones, W. D. Carbon Capture and Conversion. J. Am. Chem. Soc. **2020**, 142, 4955-4957.
- (11) Dhakshinamoorthy, A.; Li, Z.; Garcia, H. Catalysis and photocatalysis by metalorganic Frameworks. *Chem. Soc. Rev.* **2018**, *47*, 8134-8172.
- (12) Liu, Q.; Wu, L.; Jackstell, R.; Beller, M. Using carbon dioxide as a building block in organic synthesis. *Nat. Commun.* **2015**, *6*, 5933.
- (13) Ding, M.; Flaig, R. W.; Jiang, H. -L.; Yaghi, O. M. Carbon capture and conversion using metal-organic frameworks and MOF-based materials. *Chem. Soc. Rev.* **2019**, *48*, 2783-2828.
- (14) Subramanian, S.; Song, Y.; Kim, D.; Yavuz, C. T. Redox and Nonredox CO₂

- Utilization: Dry Reforming of Methane and Catalytic Cyclic Carbonate Formation. *ACS Energy Lett.* **2020**, *5*, 1689-1700.
- (15) Nam, D. -H.; Luna, P. D.; Hernandez, A. R.; Thevenon, A.; Li, F.; Agapie, T.; Peters, J. C.; Shekhah, O.; Eddaoudi, M.; Sargent, E. H. Molecular enhancement of heterogeneous CO₂ reduction. *Nat. Mater.* **2020**, *19*, 266-276.
- (16) Singh, G.; Nagaraja, C. M. Rational design of Cu(I)-anchored porous covalent triazine framework (CTF) for simultaneous capture and conversion of CO₂ at ambient conditions. *J. CO*₂ *Util.* **2022**, *63*, 102132.
- (17) Das, R.; Muthukumar, D.; Pillai, R. S.; Nagaraja, C. M. Rational Design of a Zn^{II} MOF with Multiple Functional Sites for Highly Efficient Fixation of CO₂ under Mild Conditions: Combined Experimental and Theoretical Investigation. *Chem. -Eur. J.* **2020**, *26*, 17445-17454.
- (18) Das, R.; Nagaraja, C. M. Noble metal-free Cu(I)-anchored NHC-based MOF for highly recyclable fixation of CO₂ under RT and atmospheric pressure conditions. *Green Chem.* **2021**, *23*, 5195-5204.
- (19) Das, R.; Nagaraja, C. M. Highly Efficient Fixation of Carbon Dioxide at RT and Atmospheric Pressure Conditions: Influence of Polar Functionality on Selective Capture and Conversion of CO₂. *Inorg. Chem.* **2020**, *59*, 9765-9773.
- (20) Nath, K.; Karan, C. K.; Biradha, K. Metal-Organic Frameworks and Metal-Organic Framework Derived N-Doped Porous Carbon Materials as Heterogeneous Catalysts: Chemical Fixation of Carbon Dioxide under Mild Conditions and Electrochemical Hydrogen Evolution. *Cryst. Growth Des.* **2019**, *19*, 6672-6681.
- (21) Das, R.; Parihar, V.; Nagaraja, C. M. Strategic design of a bifunctional Ag(I)-grafted NHC-MOF for efficient chemical fixation of CO₂ from a dilute gas under ambient conditions. *Inorg. Chem. Front.* **2022**, *9*, 2583-2593.
- (22) Dhankhar, S. S.; Ugale, B.; Nagaraja, C. M. Co-Catalyst-Free Chemical Fixation of CO₂ into Cyclic Carbonates by using Metal Organic Frameworks as Efficient Heterogeneous Catalysts. *Chem. -Asian J.* **2020**, *15*, 2403-2427.
- (23) Dhakshinamoorthy, A.; Asiri, A. M.; Alvaro, M.; Garcia, H. Metal organic frameworks as catalysts in solvent-free or ionic liquid assisted conditions. *Green Chem.* **2018**, *20*, 86-107.
- (24) Song, Q. -W.; Zhou, Z. -H.; He, L. -N. Efficient, selective, and sustainable catalysis of carbon dioxide. *Green Chem.* **2017**, *19*, 3707-3728.
- (25) Zhu, Q. -Q.; Zhang, W. -W.; Zhang, H. -W.; Yuan, Y.; Yuan, R.; Sun, F.; He, H.

- A. Double-Walled Porous Metal-Organic Framework as a Highly Efficient Catalyst for Chemical Fixation of CO₂ with Epoxides. *Inorg. Chem.* **2019**, *58*, 15637-15643.
- (26) Zhi, Y.; Shao, P.; Feng, X.; Xia, H.; Zhang, Y.; Shi, Z.; Mu, Y.; Liu, X. Covalent organic frameworks: efficient, metal-free, heterogeneous organocatalysts for chemical fixation of CO₂ under mild conditions. *J. Mater. Chem. A* **2018**, *6*, 374-382.
- (27) Das, P.; Mandal, S. K. In-Depth Experimental and Computational Investigations for Remarkable Gas/Vapor Sorption, Selectivity, and Affinity by a Porous Nitrogen-Rich Covalent Organic Framework. *Chem. Mater.* **2019**, *31*, 1584-1596.
- (28) Yang, F.; Li, Y.; Zhang, T.; Zhao, Z.; Xing, G.; Chen, L. Docking Sites Modulation of Isostructural Covalent Organic Frameworks for CO₂ Fixation. *Chem. Eur. J.* **2020**, *26*, 4510-4514.
- (29) Wang, J.; Zhang, Y. Facile synthesis of N-rich porous azo-linked frameworks for selective CO₂ capture and conversion. *Green Chem.* **2016**, *18*, 5248-5253.
- (30) Das, R.; Ezhil, T.; Palakkal, A. S.; Muthukumar, D.; Pillai, R. S.; Nagaraja, C. M. Efficient chemical fixation of CO₂ from direct air under environment-friendly co-catalyst and solvent-free ambient conditions. *J. Mater. Chem. A* **2021**, *9*, 23127-23139.
- (31) He, W.; Wen, M.; Shi, L.; Wang, R.; Li, F. Porous polymeric metalloporphyrin obtained through Sonogashira coupling: Catalytic performance at CO₂ cycloaddition to epoxides. *J. Solid State Chem.* **2022**, *309*, 122965.
- (32) Tsai, C. -Y.; Chen, Y. -H.; Lee, S.; Lin, C. -H.; Chang, C. -H.; Dai, W. -T.; Liu, W. -L. Uniform Core-Shell Microspheres of SiO₂@MOF for CO₂ Cyclo addition Reactions. *Inorg. Chem.* **2022**, *61*, 2724-2732.
- (33) Sharma, N.; Dhankhar, S. S.; Nagaraja, C. M. Environment-friendly, co-catalyst-and solvent-free fixation of CO₂ using an ionic zinc(II) porphyrin complex immobilized in porous metal-organic frameworks. *Sustain. Energy Fuels* **2019**, *3*, 2977-2982.
- (34) Ninokata, R.; Yamahira, T.; Onodera, G.; Kimura, M. Nickel-Catalyzed CO_2 Rearrangement of Enol Metal Carbonates for the Efficient Synthesis of β Ketocarboxylic Acids. *Angew. Chem., Int. Ed.* **2017**, *56*, 208-211.
- (35) Pal, T. K.; De, D.; Bhardwaj, P. K. Metal-organic frameworks for the chemical fixation of CO₂ into cyclic carbonates. *Coord. Chem. Rev.* **2020**, *408*, 213173.
- (36) Liu, H.; Lin, S.; Feng, Y.; Theato, P. CO₂-Responsive polymer materials. *Polym. Chem.* **2017**, *8*, 12-23.
- (37) Zhang, S. S. A review on electrolyte additives for lithium-ion batteries. J. Power

- Sources 2006, 162, 1379-1394.
- (38) Kamphuis, A. J.; Picchioni, F.; Pescarmona, P. P. CO₂ fixation into cyclic and polymeric carbonates: principles and applications. *Green Chem.* **2019**, *21*, 406-448.
- (39) Wang, J. Q.; Kong, D. L.; Chen, J. Y.; Cai, F.; He, L. N. J. M. Synthesis of cyclic carbonates from epoxides and carbon dioxide over silica-supported quaternary ammonium salts under supercritical conditions. *J. Mol. Catal. A: Chem.* **2006**, 249, 143-148.
- (40) Wang, S.; Song, K.; Zhang, C.; Shu, Y.; Li, T.; Tan, B. A novel metalloporphyrin-based microporous organic polymer with high CO₂ uptake and efficient chemical conversion of CO₂ under ambient conditions. *J. Mater. Chem. A* **2017**, *5*, 1509-1515.
- (41) Alkordi, M. H.; Weselinski, L. J.; Elia, V. D.; Barman, S.; Cadiau, A.; Hedhili, M. N.; Cairns, A. J.; AbdulHalim, R. G.; Basset, J. M.; Eddaoudi, M. CO₂ conversion: the potential of porous-organic polymers (POPs) for catalytic CO₂-epoxide insertion. *J. Mater. Chem. A* **2016**, *4*, 7453-7460.
- (42) Li, P. -Z.; Wang, X. -J.; Liu, J.; Lim, J. S.; Zou, R.; Zhao, Y. A Triazole-Containing Metal-Organic Framework as a Highly Effective and Substrate Size-Dependent Catalyst for CO₂ Conversion. *J. Am. Chem. Soc.* **2016**, *138*, 2142-2145.
- (43) Wang, J.; Yang, J.; Yi, G.; Zhang, Y. Phosphonium salt incorporated hyper-crosslinked porous polymers for CO₂ capture and conversion. *Chem. Commun.* **2015**, *51*, 15708-15711.
- (44) Cao, C. -S.; Xia, S. -M.; Song, Z. -J.; Xu, H.; Shi, Y.; He, L. -N.; Cheng, P.; Zhao, B. Highly Efficient Conversion of Propargylic Amines and CO₂ Catalyzed by Noble-Metal-Free [Zn₁₁₆] Nanocages. *Angew. Chem., Int. Ed.* **2020**, *59*, 8586-8593.
- (45) Singh, G.; Lee, J.; Karakoti, A.; Bahadur, R.; Yi, J.; Zhao, D.; Albahily, K.; Vinu, A. Emerging trends in porous materials for CO₂ capture and conversion. *Chem. Soc. Rev.* **2020**, *49*, 4360-4404.
- (46) Singh, G.; Nagaraja, C. M. Highly efficient metal/solvent-free chemical fixation of CO₂ at atmospheric pressure conditions using functionalized porous covalent organic frameworks. *J. CO₂ Util.* **2021**, *53*, 101716.
- (47) Liang, J.; Huang, Y. -B.; Cao, R. Metal-organic frameworks and porous organic polymers for sustainable fixation of carbon dioxide into cyclic carbonates. *Coord. Chem. Rev.* **2019**, *378*, 32-65.
- (48) Qiu, J.; Zhao, Y.; Li, Z.; Wang, H.; Shi, Y.; Wang, J. Imidazolium Salts

- Functionalized Covalent Organic Frameworks for Highly Efficient Catalysis of CO₂ Conversion. *ChemSusChem* **2019**, *12*, 2421-2427.
- (49) Liu, X.; Yang, Y.; Chen, M.; Xu, W.; Chen, K.; Luo, R. High Surface-Area Metalloporphyrin-Based Porous Ionic Polymers by the Direct Condensation Strategy for Enhanced CO₂ Capture and Catalytic Conversion into Cyclic Carbonates. *ACS Appl. Mater. Interfaces* **2023**, *15*, 1085-1096.
- (50) Lv, H.; Fan, L.; Hu, T.; Jiao, C.; Zhang, X. A highly robust cluster-based indium(III)-organic framework with efficient catalytic activity in cycloaddition of CO₂ and Knoevenagel condensation. *Dalton Trans.* **2023**, *52*, 3420-3430.
- (51) Eghbali, N.; Li, C. -J. Conversion of carbon dioxide and olefins into cyclic carbonates in water. *Green Chem.* **2007**, *9*, 213-215.
- (52) Wang, J. -L.; Wang, J. -Q.; He, L. -N.; Dou, X. -Y.; Wu, F. A CO₂/H₂O₂-tunable reaction: direct conversion of styrene into styrene carbonate catalyzed by sodium phosphotungstate/n-Bu₄NBr. *Green Chem.* **2008**, *10*, 1218-1223.
- (53) Bai, D.; Jing, H. Aerobic oxidative carboxylation of olefins with metalloporphyrin catalysts. *Green Chem.* **2010**, *12*, 39-41.
- (54) Han, F.; Li, H.; Zhuang, H.; Hou, Q.; Yang, Q.; Zhang, B.; Miao, C. Direct synthesis of cyclic carbonates from olefins and CO₂: Single- or multi-component catalytic systems via epoxide or halohydrin intermediate. *J. CO₂ Util.* **2021**, *53*, 101742.
- (55) Ramidi, P.; Felton, C. M.; Subedi, B. P.; Zhou, H.; Tian, Z. R.; Gartia, Y.; Pierce, B. S.; Ghosh, A. Synthesis and characterization of manganese(III) and high-valent manganese-oxo complexes and their roles in conversion of alkenes to cyclic carbonates. *J. CO*₂ *Util.* **2015**, *9*, 48-57.
- (56) Sun, J.; Yao, X.; Cheng, W.; Zhang, S. 1,3-Dimethylimidazolium-2-carboxylate: a zwitterionic salt for the efficient synthesis of vicinal diols from cyclic carbonates. *Green Chem.* **2014**, *16*, 3297-3304.
- (57) Gan, H.; Takeuchi, E. S. US Patent 5753389 A, **1998**.
- (58) Yu, K.; Puthiaraj, P.; Ahn, W. -S. One-pot catalytic transformation of olefins into cyclic carbonates over an imidazolium bromide-functionalized Mn(III)-porphyrin metal-organic framework. *Appl. Catal.*, *B* **2020**, *273*, 119059.
- (59) Dias, L. D.; Carrilho, R. M. B.; Henriques, C. A.; Calvete, M. J. F.; Bulto, A. M. M.; Claver, C.; Rossi, L. M.; Pereira, M. M. Hybrid Metalloporphyrin Magnetic Nanoparticles as Catalysts for Sequential Transformation of Alkenes and CO₂ into

- Cyclic Carbonates. ChemCatChem 2018, 10, 2792-2803.
- (60) Jin, H. -G.; Chen, F.; Zhang, H.; Xu, W.; Wang, Y.; Fanand, J.; Chao, Z.-S. Postmetalation of a new porphyrin ligand-based metalorganic framework for catalytic oxidative carboxylation of olefins. *J. Mater. Sci.* **2020**, *55*, 16184-16196.
- (61) Nguyen, P. T. K.; Nguyen, H. T. D.; Nguyen, H. N.; Trickett, C. A.; Ton, Q. T.; Puebla, E. G.; Monge, M. A.; Cordova, K. E.; Gandara, F. New Metal-Organic Frameworks for Chemical Fixation of CO₂. *ACS Appl. Mater. Interfaces* **2018**, *10*, 733-744.
- (62) Maksimchuk, N. V.; Ivanchikova, I. D.; Ayupov, A. B.; Kholdeeva, O. A. Onestep solvent-free synthesis of cyclic carbonates by oxidative carboxylation of styrenes over a recyclable Ti-containing catalyst. *Appl. Catal. B* **2016**, *181*, 363-370.
- (63) Nguyen, H. T. D.; Tran, Y. B. N.; Nguyen, H. N.; Nguyen, T. C.; Gandara, F.; Nguyen, P. T. K. A Series of Metal-Organic Frameworks for Selective CO₂ Capture and Catalytic Oxidative Carboxylation of Olefins. *Inorg. Chem.* **2018**, *57*, 13772-13782.
- (64) Sharma, R. K.; Yadav, P.; Yadav, M.; Gupta, R.; Rana, P.; Srivastava, A.; Zboril, R.; Varma, R. S.; Antonietti, M.; Gawande, M. B. Recent development of covalent organic frameworks (COFs): synthesis and catalytic (organic-electro-photo) applications. *Mater. Horiz.* **2020**, *7*, 411-454.
- (65) Wang, J.; Zhuang, S. Covalent organic frameworks (COFs) for environmental applications. *Chem. Rev.* **2019**, *400*, 213046.
- (66) Feng, X.; Ding, X.; Jiang, D. Covalent organic frameworks. *Chem. Soc. Rev.* **2012**, *41*, 6010-6022.
- (67) Cote, A. P.; Benin, A. I.; Ockwig, N. W.; Keeffee, M. O.; Matzger, A. J.; Yaghi, O. M. Porous, Crystalline, Covalent Organic Frameworks. *Science* **2005**, *310*, 1166-1170.
- (68) Ding, S. -Y.; Wang, W. Covalent organic frameworks (COFs): from design to applications. *Chem. Soc. Rev.* **2013**, *42*, 548-568.
- (69) Guan, X.; Chen, F.; Fang, Q.; Qiu, S. Design and applications of three-dimensional covalent organic frameworks. *Chem. Soc. Rev.* **2020**, *49*, 1357-1384.
- (70) Huang, K.; Zhang, J.-Y.; Liu, F.; Dai, S. Synthesis of Porous Polymeric Catalysts for the Conversion of Carbon Dioxide. *ACS Catal.* **2018**, *8*, 9079-9102.
- (71) Luo, R.; Chen, M.; Liu, X.; Xu, W.; Li, J.; Liu, B.; Fang, Y. Recent advances in CO₂ capture and simultaneous conversion into cyclic carbonates over porous organic

- polymers having accessible metal sites. J. Mater. Chem. A 2020, 8, 18408-18424.
- (72) Haung, N.; Chen, X.; Krishna, R.; Jiang, D. Two-Dimensional Covalent Organic Frameworks for Carbon Dioxide Capture through Channel-Wall Functionalization. *Angew. Chem., Int. Ed.* **2015**, *127*, 3029-3033.
- (73) Chandra, S.; Kundu, T.; Kandambeth, S.; Babarao, R.; Marathe, Y.; Kunjir, S. M.; Banerjee, R. Phosphoric Acid Loaded Azo (-N-N-) Based Covalent Organic Framework for Proton Conduction. *J. Am. Chem. Soc.* **2014**, *136*, 6570-6573.
- (74) Dhankhar, S. S.; Nagaraja, C. M. Porous nitrogen-rich covalent organic framework for capture and conversion of CO₂ at atmospheric pressure conditions. *Micropor. Mesopor. Mat.* **2020**, *308*, 110314.
- (75) Luo, R.; Yang, Y.; Chen, K.; Liu, X.; Chen, M.; Xu, W.; Liu, B.; Ji, H.; Fang, Y. Tailored covalent organic frameworks for simultaneously capturing and converting CO₂ into cyclic carbonates. *J. Mater. Chem. A* **2021**, *9*, 20941-20956.
- (76) Chen, M.; Li, H.; Liu, C.; Liu, J.; Feng, Y.; Wee, A. G. H.; Zhang, B. Porphyrin and porphyrinoid-based covalent organic frameworks (COFs): From design, synthesis to applications. *Coord. Chem. Rev.* **2021**, *435*, 213778.
- (77) Dhankhar, S. S.; Sharma, N.; Kumar, S.; Kumar, T. J. D.; Nagaraja, C. M. Rational Design of a Bifunctional, Two-Fold Interpenetrated Zn^{II}-Metal-Organic Framework for Selective Adsorption of CO₂ and Efficient Aqueous Phase Sensing of 2,4,6-Trinitrophenol. *Chem. -Eur. J.* **2017**, *23*, 16204-16212.
- (78) Torrisi, A.; Bell, R. G.; Draznieks, C. M. Functionalized MOFs for Enhanced CO₂ Capture. *Cryst. Growth Des.* **2010**, *10*, 2839-2841.
- (79) Saptal, V.; Shinde, D. B.; Banerjee, R.; Bhanage, B. M. State of the Art Catechol Porphyrin COF Catalyst for Chemical Fixation of Carbon Dioxide *via* Cyclic Carbonates and Oxazolidinones. *Catal. Sci. Technol.* **2016**, *6*, 6152-6158.
- (80) Kurisingal, J. F.; Kim, H.; Choe, J. H.; Hong, C. S. Covalent organic framework-based catalysts for efficient CO₂ utilization reactions. *Coord. Chem. Rev.* **2022**, *473*, 214835.
- (81) Bhanja, P.; Modak, A.; Bhaumik, A. Porous Organic Polymers for CO₂ Storage and Conversion Reactions. *ChemCatChem* **2019**, *11*, 244-257.
- (82) Kumar, S.; Wani, M. Y.; Arranja, C. T.; Silva, J. D. A.; Avula, B.; Sobral, A. J. F. N. Porphyrins as nanoreactors in the carbon dioxide capture and conversion: a review. *J. Mater. Chem. A* **2015**, *3*, 19615-19637.
- (83) Sharma, N.; Dhankhar, S. S.; Kumar, S.; Kumar, T. J. D.; Nagaraja, C. M.

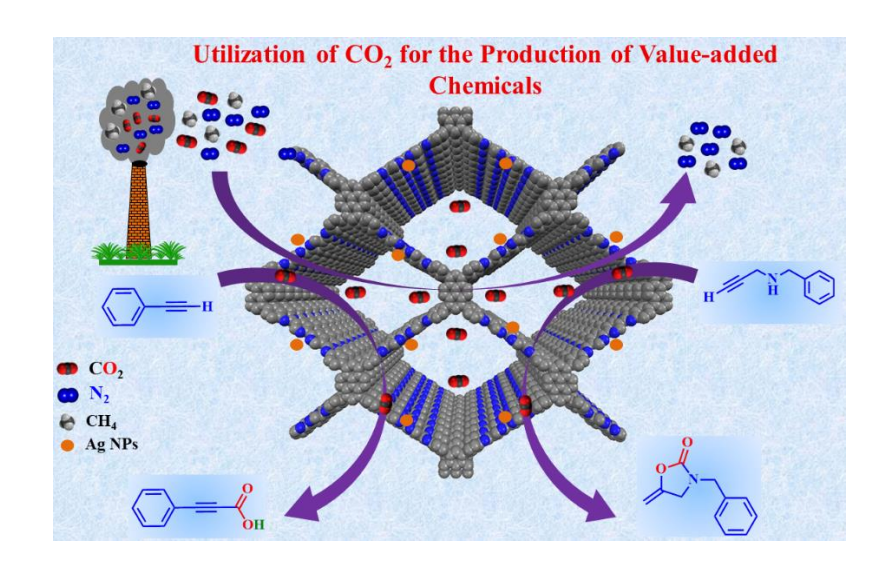
- Rational Design of a 3D Mn^{II}-Metal-Organic Framework Based on a Nonmetallated Porphyrin Linker for Selective Capture of CO₂ and One-Pot Synthesis of Styrene Carbonates. *Chem. -Eur. J.* **2018**, *24*, 16662-16669.
- (84) Cheung, P. L.; Lee, S. K.; Kubiak, C. P. Facile Solvent-Free Synthesis of Thin Iron Porphyrin COFs on Carbon Cloth Electrodes for CO₂ Reduction. *Chem. Mater.* **2019**, *31*, 1908-1919.
- (85) Xu, K.; Dai, Y.; Ye, B.; Wang, H. Two dimensional covalent organic framework material for chemical fixation of carbon dioxide: excellent repeatability and high selectivity. *Dalton Trans.* **2017**, *46*, 10780-10785.
- (86) Chen, A.; Zhang, Y.; Chen, J.; Chen, L.; Yu, Y. Metalloporphyrin-based organic polymers for carbon dioxide fixation to cyclic carbonate. *J. Mater. Chem. A* **2015**, *3*, 9807-9816.
- (87) Harvey, P. D. Porphyrin-based metal- and covalent-organic frameworks as heterogeneous nanosized photocatalysts in organic synthesis. *J. Mater. Chem. C* **2021**, *9*, 16885-16910.
- (88) Luo, R.; Chen, M.; Zhou, F.; Zhan, J.; Deng, Q.; Yu, Y.; Zhang, Y.; Xu, W.; Fang, Y. Synthesis of metalloporphyrin-based porous organic polymers and their functionalization for conversion of CO₂ into cyclic carbonates: recent advances, opportunities and challenges. *J. Mater. Chem. A* **2021**, *9*, 25731-25749.
- (89) Yuasa, M.; Oyaizu, K.; Yamaguchi, A.; Kuwakado, M. Micellar Cobaltporphyrin Nanorods in Alcohols. *J. Am. Chem. Soc.* **2004**, *126*, 11128-11129.
- (90) Liu, R.; Tan, K. T.; Gong, Y.; Chen, Y.; Li, Z.; Xie, S.; He, T.; Lu, Z.; Yanga, H.; Jiang, D. Covalent organic frameworks: an ideal platform for designing ordered materials and advanced applications. *Chem. Soc. Rev.* **2021**, *50*, 120-242.
- (91) Gong, Y. -N.; Guan, X.; Jiang, H. -L. Covalent organic frameworks for photocatalysis: Synthesis, structural features, fundamentals, and performance. *Coord. Chem. Rev.* **2023**, *475*, 214889.
- (92) Hu, J.; Zanca, F.; McManus, G. J.; Riha, I. A.; Nguyen, H. G. T.; Shirley, W.; Borcik, C. G.; Wylie, B. J.; Benamara, M.; Zee, R. D.; Moghadam, P. Z.; Beyzavi, H. Catalyst-Enabled *In Situ* Linkage Reduction in Imine Covalent Organic Frameworks. *ACS Appl. Mater. Interfaces* **2021**, *13*, 21740-21747.
- (93) Wang, B.; Yang, F.; Dong, Y.; Cao, Y.; Wang, J.; Yang, B.; Yang, B.; Wei, Y.; Wan, W.; Chen, J.; Jiang, H. Cu@porphyrin-COFs nanorods for efficiently photoelectrocatalytic reduction of CO₂. *Chem. Eng. J.* **2020**, *396*, 125255.

- (94) Wan, S.; Gandara, F.; Asano, A.; Furukawa, H.; Saeki, A.; Dey, S. K.; Liao, L.; Ambrogio, M. W.; Botros, Y. Y.; Duan, X.; Seki, S.; Stoddart, J. F.; Yaghi, O. M. Covalent Organic Frameworks with High Charge Carrier Mobility. *Chem. Mater.* **2011**, *23*, 4094-4097.
- (95) Gottfried, J. M.; Flechtner, K.; Kretschmann, A.; Lukasczyk, T.; Steinruck, H.-P. Direct Synthesis of a Metalloporphyrin Complex on a Surface. *J. Am. Chem. Soc.* **2006**, *128*, 5644-5645.
- (96) Xie, Y.; Xu, M.; Wang, L.; Liang, H.; Wang, L.; Song, Y. Ironporphyrin-based covalent-organic frameworks for electrochemical sensing H₂O₂ and pH. *Mater. Sci. Eng.*, C **2020**, 112, 110864.
- (97) Bajnóczi, É. G.; Balázs, N.; Mogyorósi, K.; Srankó, D. F.; Pap, Z.; Ambrus, Z.; Canton, S. E.; Norén, K.; Kuzmann, E.; Vértes, A.; Homonnay, Z.; Oszkó, A.; Pálinkó, I.; Sipos, P. The influence of the local structure of Fe(III) on the photocatalytic activity of doped TiO₂ photocatalysts-An EXAFS, XPS, and Mössbauer spectroscopic study. *Appl. Catal.*, *B* **2011**, *103*, 232-239.
- (98) Liu, Y.; Yan, X.; Li, T.; Zhang, W. -D.; Fu, Q. -T.; Lu, H. -S.; Wang, X.; Gu, Z. -G. Three-dimensional porphyrin-based covalent organic frameworks with tetrahedral building blocks for single-site catalysis. *New J. Chem.* **2019**, *43*, 16907-16914.
- (99) Yao, X.; Chen, K.; Qiu, L. -Q.; Yang, Z. -W.; He, L. -N. Ferric Porphyrin-Based Porous Organic Polymers for CO₂ Photocatalytic Reduction to Syngas with Selectivity Control. *Chem. Mater.* **2021**, *33*, 8863-8872.
- (100) Eder, G. M.; Pyles, D. A.; Wolfson, E. R.; McGrier, P. L. A ruthenium porphyrin-based porous organic polymer for the hydrosilylative reduction of CO₂ to formate. *Chem. Commun.* **2019**, *55*, 7195-7198.
- (101) Qin, J. -H.; Xu, P.; Huang, Y. -D.; Xiao, L. -Y.; Lu, W.; Yang, X.- G.; Ma, L. -F.; Zang, S. -Q. High loading of Mn(II)-metalated porphyrin in a MOF for photocatalytic CO₂ reduction in gas-solid conditions. *Chem. Commun.* **2021**, *57*, 8468-8471.
- (102) Silva, A. R.; Freire, C.; Castro, B. D. Modulation of the catalytic activity of manganese(III) salen complexes in the epoxidation of styrene: influence of the oxygen source. *New J. Chem.* **2004**, *28*, 253-260.
- (103) Groves, J. T.; Nemo, T. E.; Myers, R. S. Hydroxylation and Epoxidation Catalyzed by Iron-Porphine Complexes. Oxygen Transfer from Iodosylbenzene. *J. Am. Chem. Soc.* **1979**, *101*, 1032-1033.

- (104) Singh, M. K.; Bandhyopadhyay, D. Design and synthesis of nanoporous perylene bis imide linked metalloporphyrin frameworks and their catalytic activity. *J. Chem. Sci.* **2016**, *128*, 1-8.
- (105) Das, R.; Manna, S. S.; Pathak, B.; Nagaraja, C. M. Strategic Design of Mg-Centered Porphyrin Metal-Organic Framework for Efficient Visible Light-Promoted Fixation of CO₂ under Ambient Conditions: Combined Experimental and Theoretical Investigation. *ACS Appl. Mater. Interfaces* **2022**, *14*, 33285-33296.
- (106) Das, R.; Kamra, S.; Nagaraja, C. M. Ionic Fe(III)-porphyrin frameworks for the one-pot synthesis of cyclic carbonates from olefins and CO₂. *Inorg. Chem. Front.* **2023**, *10*, 2088-2099.

Chapter 5

Pyrene-Based Nanoporous Covalent Organic Framework for Carboxylation of C-H Bonds with CO₂ and ValueAdded 2-Oxazolidinones Synthesis under Ambient Conditions



Reference: "Singh, G.; Duhan, N.; Kumar, T. J. D.; Nagaraja, C. M. ACS Appl. Mater. Interfaces 2024, 16, 5857-5868."

5.1 Introduction

The rising concentration of CO₂ in the earth's atmosphere has resulted in global warming, climate change, unpredictable weather patterns, and so on.¹⁻³ To overcome these undesirable environmental issues, it is essential to mitigate the atmospheric CO₂ content by its selective capture and storage/utilization. In this regard, selective carbon capture and utilization (CCU) has been considered a promising route for generating value-added chemicals/fuels by utilizing abundant greenhouse gas, CO₂. as a one-carbon (C1) source.⁴⁻⁹ To date, extensive research efforts are being accomplished for the selective capture and transformation of carbon dioxide into various value-added chemicals and fuels. 10-18 Among them, the conversion of carbon dioxide into value-added cyclic carbonates (CCs) is well studied owing to its atom efficiency and potential utility as precursors for the synthesis of polymeric materials, pharmaceuticals, and so on. 19-24 Whereas the transformation of CO₂ into other valuable commodity chemicals such as alkynyl carboxylic acids/phenylpropiolic acids and 2oxazolidinones is relatively less studied. Hence, there is a significant scope to investigate the transformation of CO₂ to valuable alkynyl carboxylic acids by carboxylation of terminal alkynes through C-H bond functionalization. Further, alkynyl carboxylic acids are essential commodity compounds used in the synthesis of high-value medicinal molecules like flavones, and coumarins. 25-27 On the other hand, the production of 2-oxazolidinones, essential building blocks for antibacterial drugs, such as linezolid, eperezolid, and radezolid via carboxylative cyclization of propargylic amines with CO₂ is of high significance. ²⁸⁻³⁰ The literature study revealed that the synthesis of alkynyl carboxylic acids and 2-oxazolidinones by coupling CO₂ with terminal alkynes/amines has been achieved using homogeneous catalysts under harsh conditions. 31-33 However, green chemistry practices prefer the application of heterogeneous catalysts to overcome the limitations of product separation and catalyst recycling associated with homogeneous catalysts.^{34,35} Consequently, developing effective heterogeneous catalysts for CO₂ fixation to valuable alkynyl carboxylic acids and 2-oxazolidinones at ambient conditions is highly significant in the sustainable generation of high-value chemicals. 36-39

In this regard, covalent organic frameworks (COFs), an emerging class of crystalline porous organic polymers (POPs) have gained special interest due to their high surface area, chemical/thermal stability, and tunable functionality.⁴⁰⁻⁴² These

unique features enable COFs to be employed in heterogeneous catalysis, energy storage, proton conductivity, gas storage/separation, etc.⁴³⁻⁵² Especially functionalized COFs composed of heteroatom (N, F, Cl,) and polar (-COOH, -SO₃H, -OH) groups offer potential advantageous for selective CO₂ capture and conversion.^{44,53,54} In this regard, the COFs constituted by organic linkers containing bipyridine (bpy) moiety have gained significant interest as these bipyridine groups can serve as potential sites for anchoring of catalytic metal/complex ions or metal nanoparticles to bring out numerous catalytic transformations.^{15,55,56}

In light of these observations, in Chapter 5, we synthesized highly porous pyrene-based COF (Pybpy-COF) with 1D channels functionalized with bipyridine moieties by Schiff-base condensation of pyrene amine (Py-NH₂) with bipyridine aldehyde (bpy-CHO) under solvothermal conditions. Further, the bipyridine sites exposed in the 1D channels of the COF were utilized for stable anchoring of Ag(0) nanoparticles by treating with AgNO₃ followed by reduction with hydrazine. Notably, the Ag@Pybpy-COF showed excellent catalytic performance for the fixation of CO₂ with diverse terminal alkynes and propargylic amines to produce alkynyl carboxylic acids and 2-oxazolidinones in high-yield (99%) and selectivity (100%) under atmospheric conditions. The catalyst was recyclable for several cycles without losing substantial catalytic activity. Thus, this study showcases the importance of bipyridine functionalized porous COF for developing highly recyclable Ag NPs anchored COF for efficient utilization of atmospheric CO₂ to produce two value-added commodity chemicals, alkynyl carboxylic acids and 2-oxazolidinones under ambient conditions.

5.2. Experimental section

5.2.1. Materials

All the reagents used in this work were commercially available and employed as received without further purification. The 1,3,5-trimethyl benzene and 1,4-dioxane were purchased from TCI Chemicals Ltd. Acetic acid (99%) was obtained from Merck and Co. 2,2'-bipyridyl-5,5'-dialdehyde (bpy-CHO) utilized for COF synthesis was obtained from alfa Aeser chemical Co. 4,4',4",4"'-(pyrene-1,3,6,8tetrayl)tetraaniline (Py-NH₂) was prepared by following the previously reported procedure.⁵⁷

5.2.2. Physical measurements

Powder X-ray diffraction measurements were recorded in the 2Θ range of 2-50° on PAN analytical's X'PERT PRO X-Ray diffractometer with a scan rate of 2°/min using Cu-K α radiation ($\lambda = 1.54184$ Å, 40 kV, 20 mA) for confirming phase purity of as-synthesized samples. Fourier transform infrared (FT-IR) spectra of the samples were recorded on a Bruker Tensor-F27 instrument in ATR mode. Gas adsorption measurements of the samples were performed on a Quantachrome's QUADRASORB-SI automatic volumetric instrument using ultrapure (99.995%) N₂, CO₂, and CH₄ gases. The SEM images and EDAX patterns were recorded on the FEI Nova SEM-450 instrument. The metal content of Ag in the COF was determined by Agilent's microwave-plasma atomic emission spectrometer (MP-AES). The X-ray photoelectron spectroscopy (XPS) analyses were performed on a Thermo Fisher Scientific NEXSA photoemission spectrometer using Al Kα (1486.6 eV) X-ray radiation, and analysis of the obtained data was performed using Avantage software. The products of catalytic reactions were identified and catalytic conversions were determined by ¹H and ¹³C NMR spectra recorded in DMSO-d₆/CDCl₃ on a JEOL JNM-ECS-400 spectrometer operating at a frequency of 400 MHz and 100 MHz, respectively. First-principles calculations were performed using Material Studio's DMol³ module.⁵⁸

5.2.3. Synthesis Procedures

5.2.3.1. Synthesis of Pybpy-COF

In a typical synthesis, a pyrex tube was charged with bpy-CHO (0.04 mmol, 8.5 mg), Py-NH₂ (0.02 mmol, 11.3 mg), and subsequently dioxane (0.5 mL), mesitylene (0.5 mL), and 6 M aqueous acetic acid (0.1 mL) were added. The tube was flash-frozen at 77 K, evacuated, flame-sealed, and heated at 120 °C for three days in an oven. After completion of the reaction, the orange crystalline solid was separated by centrifugation, washed with THF and acetone, and dried under a vacuum.

5.2.3.2. Synthesis of Ag@Pybpy-COF

In a typical procedure, 0.03 mmol of Pybpy-COF was dispersed in 5 mL water, and in a separate vial, 0.13 mmol of AgNO₃ was dissolved in water in the dark. An aqueous solution of AgNO₃ was added dropwise to the dispersed solution of Pybpy-COF at room temperature with constant stirring for 1h. The solid was isolated from the reaction mixture and thoroughly washed with water. The dried powder was re-

dispersed in water, $500 \,\mu\text{L}$ hydrazine hydrate was added, and the reaction mixture was stirred for an additional 1 h. Then the solid was separated, washed with water, and dried under a vacuum.

5.2.4. Catalytic carboxylation of terminal alkynes

The carboxylation of terminal alkynes with CO₂ catalyzed by Ag@Pybpy-COF was carried out in a glass reactor (50 mL) with a magnetic stirrer at 50 °C and 1 bar CO₂ pressure. Prior to catalytic reactions, the catalyst was activated at 393 K for 12 h under a vacuum to remove the adsorbed solvent molecules. The activated sample of Ag@Pybpy-COF (10 mg) and DMF (5 mL) were taken in the reactor, then Cs₂CO₃ (1.5 mmol) and terminal alkyne (1 mmol) were added into the reaction mixture, and the reactor was flushed with CO₂ twice. Then, 0.1 MPa of CO₂ was introduced and the reaction was maintained at 50 °C for 12 h under stirring. After 12 h, the reactor was cooled down, and excess CO2 was released. The catalyst was separated from the reaction mixture by filtration followed by washing with acetone. The filtrate was washed with CH_2Cl_2 , acidified with 1 M HCl to pH = 1, and then extracted with ethyl acetate. The combined organic fraction was washed with saturated NaCl solution and dried over anhydrous MgSO₄. The solvent was removed under vacuum to obtain the carboxylic acid product. The isolated yield was calculated based on the reactant used. The products were characterized by ¹H and ¹³C NMR spectroscopic analysis. The recovered catalyst after the catalysis was washed with acetone followed by drying under a vacuum at 373 K for 12 h and reused for subsequent catalytic cycles.

5.2.5. Synthesis of propargylic amines

The reported procedure was followed for the synthesis of propargylic amine derivatives.⁵⁹

$$H$$
 + RNH₂ $\frac{\text{rt.}}{\text{over night}}$ H H R

In a typical experiment, propargylic bromide (3 mL, 27 mmol) was added into amine (162 mmol) dropwise over 30 minutes using an addition funnel. The mixture was allowed to be stirred overnight at ambient temperature. Then, the mixture was diluted with 20 mL Et₂O and washed with saturated aqueous NaHCO₃ (3 ×10 mL). The organic phases were collected and dried over anhydrous MgSO₄. The

concentrated mixture was purified by column chromatography on silica gel (petroleum ether/ethyl acetate = 9:1 as eluent) to afford the corresponding product as pale-yellow liquids.

5.2.6. Carboxylative cyclization of propargylic amines

The carboxylative cyclization of synthesized propargylic amines with CO₂ catalyzed by Ag@Pybpy-COF was carried out in a glass reactor (50 mL) with a magnetic stirrer at 50 °C and 1 bar CO₂ pressure. The catalyst was activated at 393 K for 12 h under a vacuum to remove guest solvent molecules. In a typical procedure, Ag@Pybpy-COF (10 mg) and DMSO (2 mL) were taken in a reactor, then propargylic amine (1 mmol) was added into the reaction mixture during stirring, followed by DBU (0.1 mmol) was added. Flushed the reactor with CO₂ twice. Later, 0.1 MPa of CO₂ was introduced and it was maintained at 50 °C for 0.5 h under stirring. After the required time, the reactor was cooled down and excess CO₂ was released. The catalyst was separated from the reaction mixture by filtration and the product was extracted from filtrate with DCM, washed with saturated NaCl solution, and dried over anhydrous MgSO₄. The product was further purified by column chromatography on silica gel, and the isolated yield was calculated based on the starting reactants utilized. The characterization of the product was performed by ¹H and ¹³C NMR analysis.

5.2.7. Structure simulation and modeling of Pybpy-COF

To elucidate the structure of Pybpy-COF and to calculate the unit cell parameters, a possible 2D model was constructed in the material studio software. The experimental PXRD pattern matches well with the simulated pattern for an eclipsed model of Pybpy-COF. Refinement of PXRD patterns was carried out using the Pseudo-Voigt function. The optimized structure of Pybpy-COF is given below.

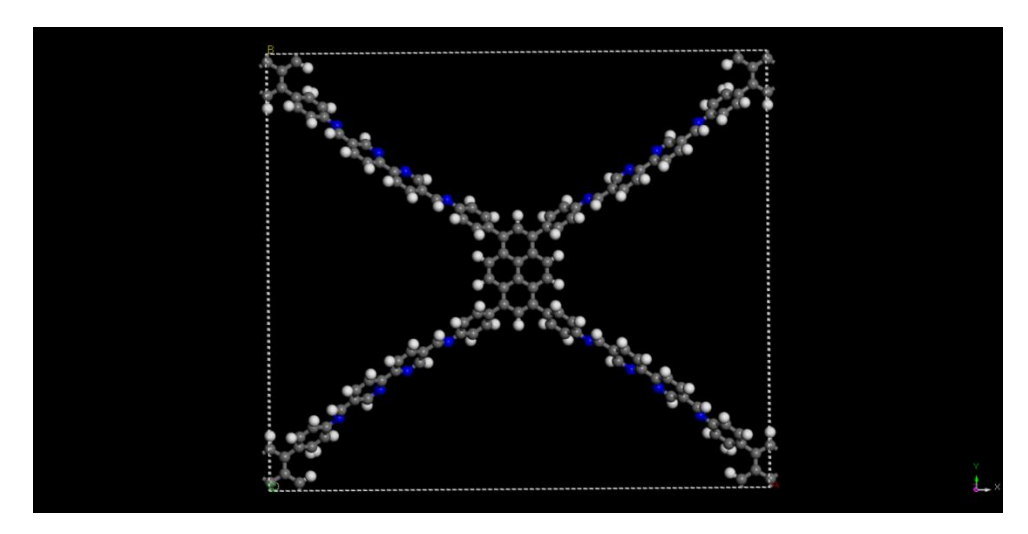
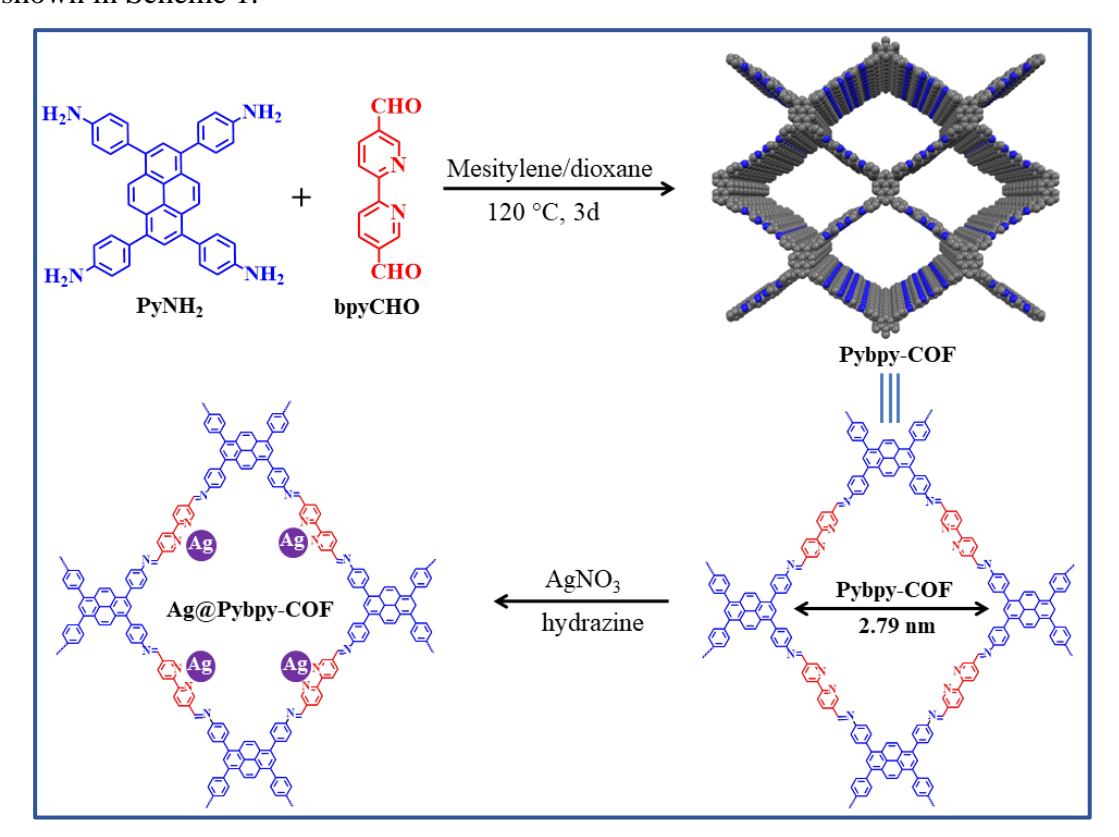


Figure 1. Simulated structure of Pybpy-COF.

5.3 Results and Discussion

The Pybpy-COF was synthesized by Schiff-base reaction of 4,4',4'',4'''-(pyrene-1,3,6,8-tetrayl)tetraaniline (Py-NH₂) with 2,2'-bipyridyl-5,5'-dialdehyde (bpy-CHO) in the presence of mesitylene/dioxane/6M AcOH at 120 °C (Scheme 1).⁶⁰ Further, the anchoring of Ag(0) at the bipy sites exposed in the 1D channels of Pybpy-COF was achieved by treating the COF with AgNO₃ followed by reduction with hydrazine, as shown in Scheme 1.



Scheme 1. The synthesis scheme of Pybpy-COF and Ag@Pybpy-COF.

The as-synthesized COFs were characterized by various techniques. The Fourier transform infrared (FT-IR) spectra of Pybpy-COF showed the disappearance of characteristic peaks due to the amine group of Py-NH₂ and the carboxyl group of bpy-CHO precursor. Besides, a new peak at 1624 cm⁻¹ was observed corresponding to the imine (-C=N-) bond formed by Schif-base condensation of the reactants supporting the Pybpy-COF formation, as depicted in Figure A36a.⁶¹ In addition, stretching bands corresponding to C=N and C-C bonds of the bipyridine ring were observed at 1600-1550 cm⁻¹ and 740 cm⁻¹, respectively. 15 Further, the FT-IR spectra of Ag(0) anchored Pybpy-COF showed the characteristic stretching band due to imine (-C=N-) bond, indicating retaining of the framework structure even after embedding of silver NPs, and a slight shift was observed in the C=N stretching frequency of the bipyridine ring supporting the interaction of Ag NPs at the bipy sites align in the 1D channel of the Pybpy-COF (Figure A36b). Moreover, the powder X-ray diffraction (XRD) pattern of the sample established the phase purity of as-synthesized Pybpy-COF. The XRD pattern shows an intense peak at a Bragg's angle (20) of 3.16° corresponding to 110 plane, supporting the presence of log-range ordering in the structure (Figure 2a). Besides, additional diffraction peaks with lower intensity were observed at $2\Theta = 4.58^{\circ}$, 6.38°, 9.74°, 12.98°, and 23.86° assigned to (020), (220), (330), (440), and (001) planes, respectively (Figure 2a).⁶² The (001) facet supports the structural ordering and π - π stacking between the 2D layers of COF. Additionally, the experimental XRD pattern matches well with that of the simulated pattern (Figure 2a). Further, the Ag(0) incorporated sample showed appearance of new diffraction peaks at $2\Theta = 38.1$, 44.2, 64.5, and 77.3 assigned to (111), (200), (220), and (311) planes of anchored Ag NPs (JCPDS no. 04-0783), supporting its successful embedding in the framework (Figure 2b). 63 The most probable 2D model of Pybpy-COF was optimized with an eclipsed structure in the *PMM2* space group, and the unit cell parameters are a = 42.10 Å, b =36.80 Å, C = 4.29 Å and $\alpha = \beta = \gamma = 90^{\circ}.^{62}$ Further, carbon cross-polarization magic angle spinning (¹³C CP-MAS) solid-state nuclear magnetic resonance (NMR) spectra of Pybpy-COF showed a resonance peak at 154.1 ppm corresponding to imine (-C=N) carbon, supporting the formation of COF (Figure 2c).⁶⁴ Besides, the spectrum shows resonance peaks corresponding to the pyridine, phenyl, and pyrene carbons of the framework.

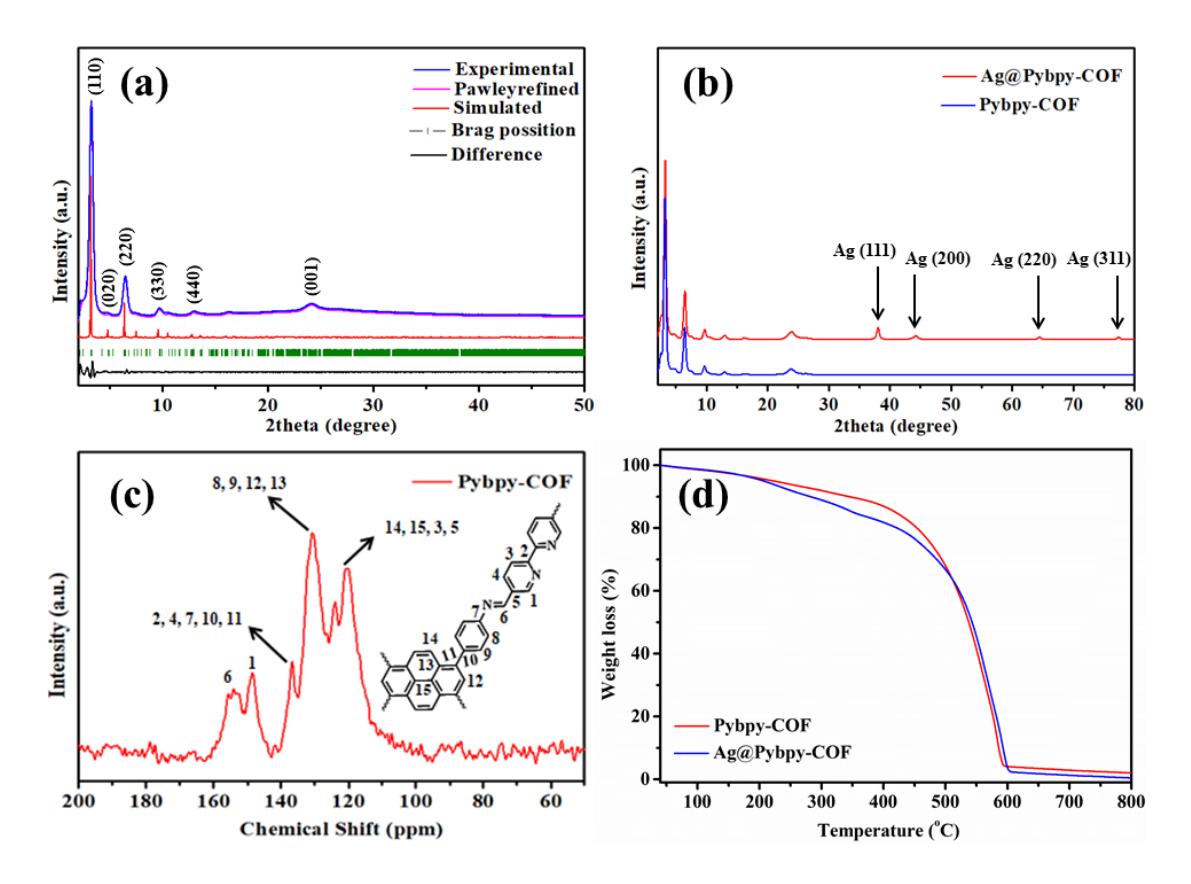


Figure 2. (a) Comparison of the experimental and simulated PXRD plots of Pybpy-COF. (b) PXRD pattern of Ag@Pybpy-COF (Ag NPs peaks are represented by arrows). (c) Solid-state ¹³C CP-MAS spectra of Pybpy-COF. (d) Thermogravimetric analysis (TGA) plot of Pybpy-COF (red) and Ag@Pybpy COF (blue).

Further, field-emission scanning electron microscopy (FE-SEM) analysis showed a flake-like morphology of pristine Pybpy-COF (Figure 3a).⁶⁵ The morphology was almost retained even after Ag NPs were anchored at the bipyridine sites of the COF (Figure 3b). Energy-dispersive X-ray spectroscopy (EDS) plots confirmed the presence of Ag NPs (Figure A37). Additionally, elemental mapping supports the uniform distribution of C, N, and Ag in the pristine and Ag-loaded COF(Figures A38a and A38b). Moreover, high-resolution transmission electron microscopy (HR-TEM) analysis of Ag@Pybpy COF unambiguously confirms the presence of Ag NPs on the surface of the COF with an average particle size of ~15 nm (Figure 3c). The selected area electron diffraction (SAED) pattern supports the crystalline nature of the Ag nanoparticles (Figure 3d).⁶⁶ Additionally, the lattice fringes with 0.23 nm spacing correspond to the (111) plane of Ag, supporting the embedding of Ag NPs in the COF (Figure 3e).⁶⁷ Besides, microwave plasma atomic

emission spectroscopy MP-AES analysis revealed 2.4 wt % loading of Ag in COF (Figure A39).

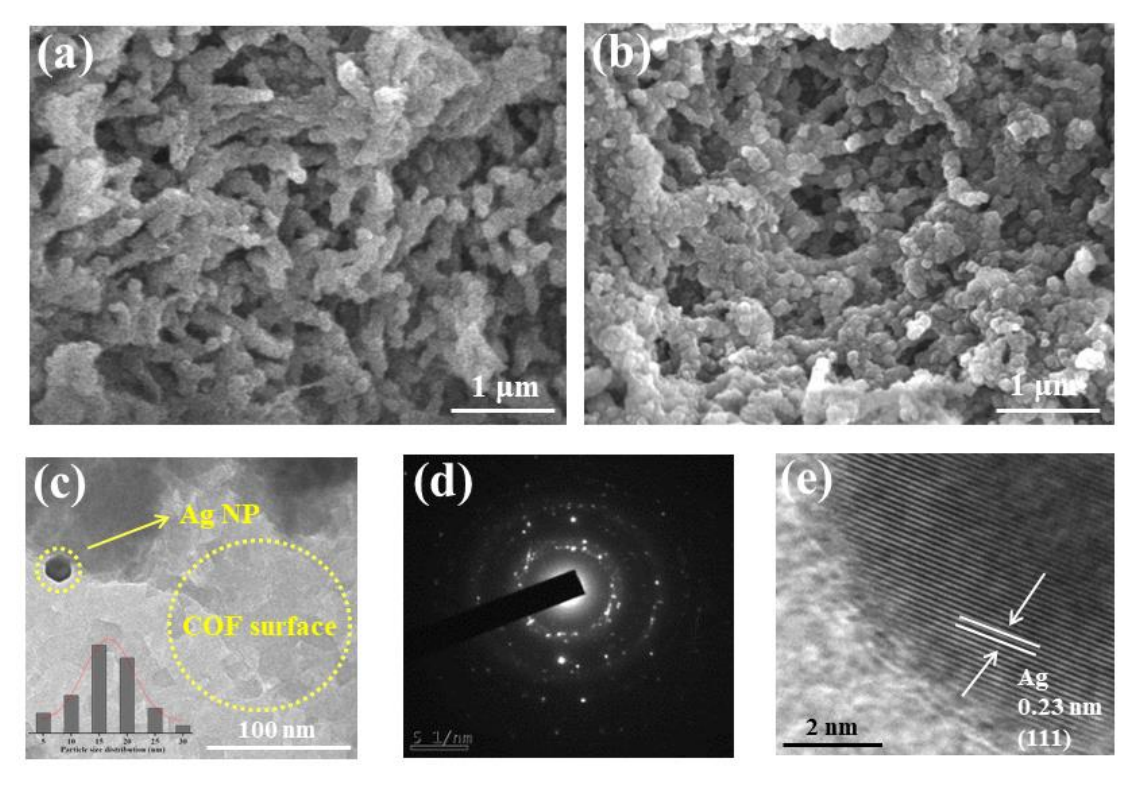


Figure 3. FE-SEM images of Pybpy-COF, and Ag@Pybpy-COF (a, b). HR-TEM image of Ag@Pybpy-COF along with inset plot of particle size distribution, (c) SAED pattern, (d) and lattice fringes of Ag (e).

X-ray photoelectron spectroscopy (XPS) study confirmed the presence of constituent (C, N, and Ag) elements (Figure 4a). The XPS spectra of Ag showed two characteristic bands at binding energy (BE) of 374.0 eV and 368.0 eV with a spacing of 6 eV corresponding to 3d_{3/2} and 3d_{5/2}, respectively, supporting its metallic Ag(0) state (Figure 4b).⁶⁸ A slight bathochromic shift observed with respect to BE reported for free Ag NPs (3d_{5/2} = 368.3 and 3d_{3/2} = 374.3) could be ascribed to its interaction with highly exposed bipy nitrogen sites in the 1D channels of the framework.⁶⁸ A similar observation of a shift in the BE of Ag has been reported upon the coordination of Ag NPs with bipyridine N-sites.^{68,69} The N 1s spectra of pristine COF showed two bands at BE of 398.3 eV and 399.7 eV corresponding to pyridyl nitrogen and imine nitrogen, respectively (Figure 4c).⁷⁰ On the other hand, the deconvoluted N 1s spectra of Ag@Pybpy-COF showed a new band at 399.2 eV corresponding to Ag-bound bipyridine-N (Figure 4d). Thus, XPS results confirm the anchoring of Ag at the bipyridine sites. Thus, COF plays a vital role in stabilizing Ag NPs at the bipyridine

sites lined in the pore walls. Further, the thermal stability of as-synthesized Pybpy-COF and Ag@Pybpy-COF was investigated by thermogravimetric analysis (TGA), and the COFs were found to exhibit high thermal stability up to 400 °C (Figure 2d). Further, the framework undergoes disintegration at temperatures higher than 400 °C.

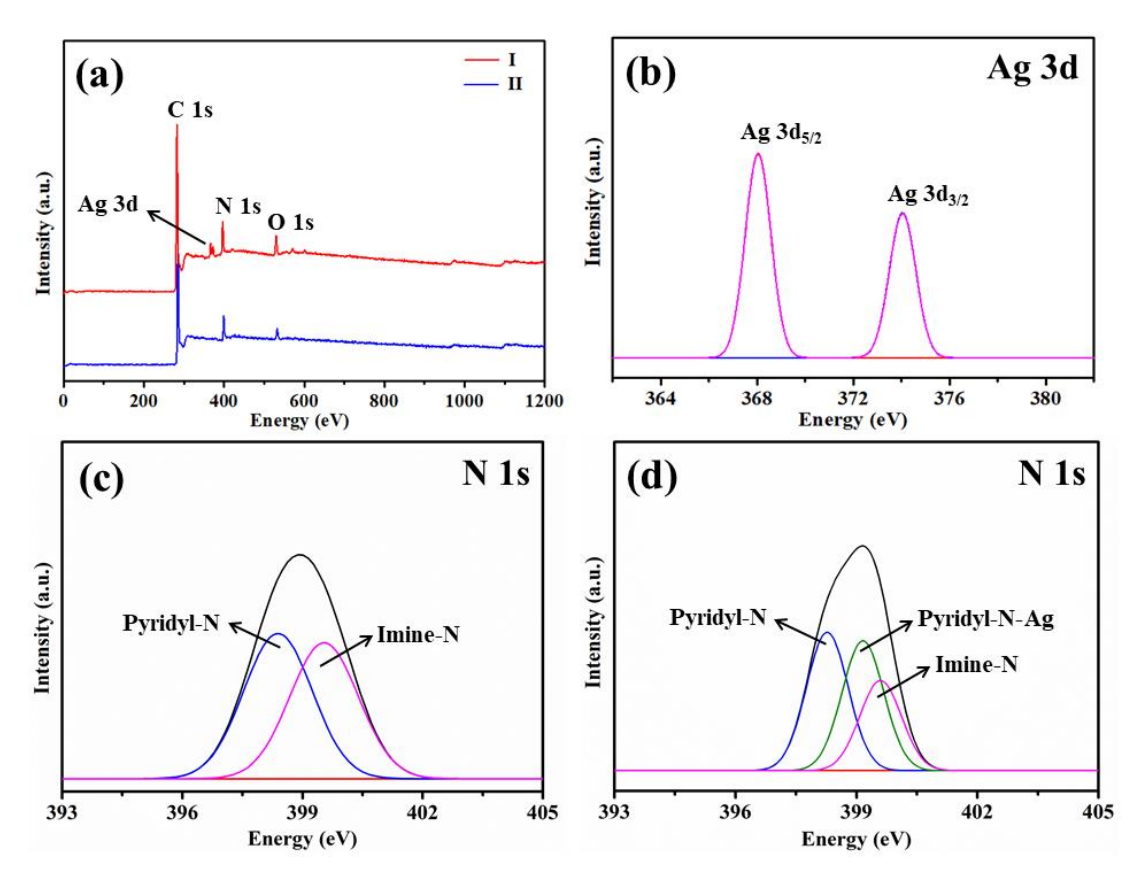


Figure 4. (a) XPS survey spectra of Ag@Pybpy-COF, (I) and Pybpy-COF, (II). (b) Ag 3d spectra of Ag@Pybpy-COF. (c and d) The N 1s spectra of Pybpy-COF, and Ag@Pybpy-COF.

5.3.1. Gas adsorption analysis

The N₂ adsorption measurements of Pybpy-COF and Ag@Pybpy-COF were carried out to test the permanent porosity of COFs. The BET (Brunauer-Emmett-Teller) surface area of Pybpy-COF and Ag@Pybpy-COF were estimated to be 1408 m²g⁻¹ and 787 m²g⁻¹, respectively (Figure 5a). The reduction in the surface area of Ag@Pybpy-COF can be attributed to a partial loss of porosity on incorporating Ag NPs in Pybpy-COF.⁷¹ Further, the CO₂ sorption isotherms of Pybpy-COF and Ag@Pybpy-COF showed type-1 plot with the uptake of 47.6/33.4 and 37.4/23.2 cc/g at 273 and 298 K, respectively (Figure 5b).⁶² The adsorption isotherms were suited

with the Freundlich-Langmuir equation, and the heat of adsorption value (Q_{st}) was calculated using the Clausius-Clayperson equation, and the value is 22.14 and 30.89 kJ/mol for Pybpy-COF and Ag@Pybpy-COF, respectively (Figure A40 and A41). The high Q_{st} value of Ag@Pybpy-COF could be ascribed to the interaction of CO₂ with Ag NPs embedded at the bipyridine sites of the COF. Further, gas selectivity measurements of Ag@Pybpy-COF revealed selective adsorption of CO₂ over N₂ and CH₄ with Henry gas selectivity constant of 66.25 for $K_{CO2/N2}$ and 35.50 for $K_{CO2/CH4}$, respectively (Figure A42).

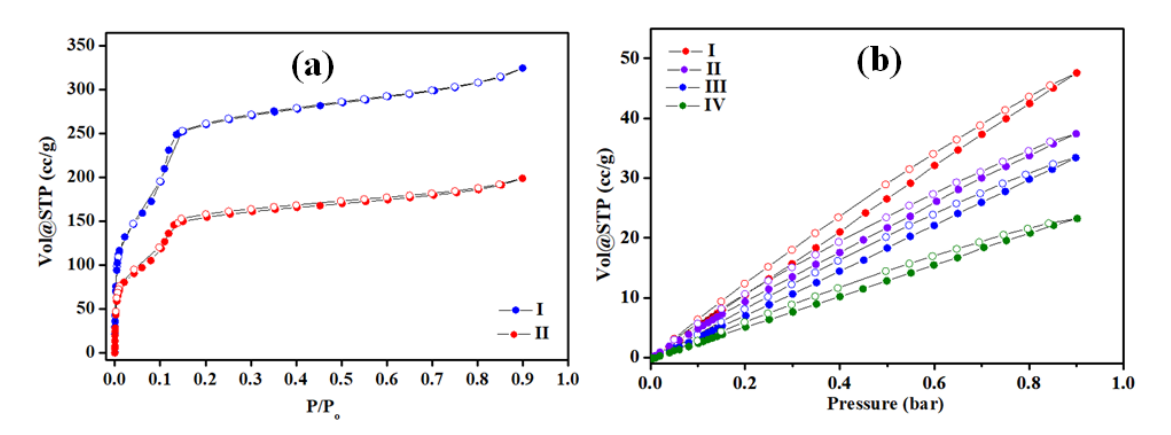


Figure 5. (a) N_2 adsorption isotherm collected at 77K for Pybpy-COF (I) and Ag@Pybpy-COF (II); (b) CO_2 adsorption isotherms of Pybpy-COF (I and III), and Ag@Pybpy-COF (II and IV) performed at 273 and 298 K, respectively.

5.3.2. Carboxylation of terminal alkynes with CO₂ catalyzed by Ag@Pybpy-COF

Owing to the presence of basic bipyridine and catalytic Ag(0) sites, the catalytic activity of Ag@Pybpy-COF was investigated for carboxylation of terminal alkynes to alkynyl carboxylic acids. To begin with, reaction conditions were optimized using phenylacetylene as a model substrate for alkynes (Table 1 and Figure 6).

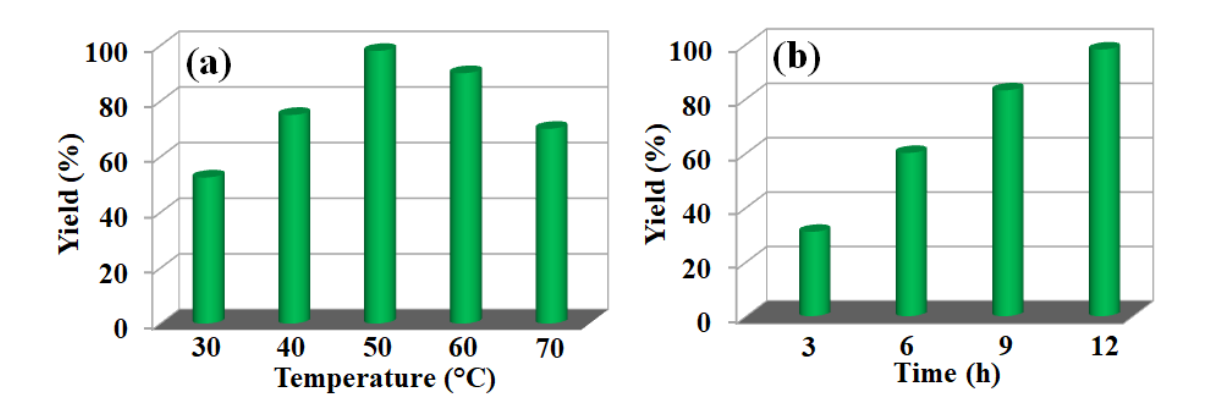


Figure 6. Optimization of reaction conditions for the carboxylation of phenylacetylene with CO₂ by varying temperature and time (a and b) catalyzed by Ag@Pybpy-COF. Reaction conditions: Ag@Pybpy-COF (10 mg), Phenylacetylene (1 mmol), base (1.5 mmol), CO₂ (1 bar), and solvent (DMF, 5 mL).

The effect of solvent on the catalytic performance was studied by screening various solvents (Table 1), and the reaction performed in dimethylformamide (DMF) afforded a higher product yield over other solvents [(Toluene, tetrahydrofuran (THF), and dimethyl sulfoxide (DMSO)] employed (Table 1). This higher catalytic activity could be due to better solubility of quadrupolar CO₂ and ionic Cs₂CO₃ in DMF. The effect of a base on the catalytic performance was also studied by screening various bases like KOH, Na₂CO₃, Triethylamine, K₂CO₃, and Cs₂CO₃ under the optimized conditions (Table 1). Notably, the catalytic reaction with Cs₂CO₃ (Table 1) showed a higher conversion of phenylacetylene to the product, 3-phenylpropargylic acid. This higher catalytic performance is assigned to the vital role of Cs₂CO₃ in deprotonating the alkynes and forming the product (please refer to Scheme 2).^{34,72} At the optimized conditions, the catalytic reaction performed with Ag@Pybpy-COF (10 mg) as a catalyst, phenylacetylene (1 mmol), and base (Cs₂CO₃), in DMF at 30 °C) showed a 52.5% yield of the corresponding product (3-phenylpropargylic acid) (Figure 6a). Increasing the reaction temperature to 50 °C led to the quantitative conversion of the alkyne, affording 98% yield of the product (3-phenylpropargylic acid) with 100% selectivity (Table 1). Further increase in the reaction temperature (70 °C) resulted in a reduction in the product yield, which could be ascribed to partial decarboxylation of propynoate intermediate at higher temperatures (Figure 6a).³⁵

Table 1: Optimization table for the carboxylation of terminal alkynes with CO₂ catalyzed by Ag@Pybpy-COF.^a

S. No.	Catalyst	Base	Temp. (°C)	Time (h)	Yield (%) ^b
1	-	-	50	12	-
2	Ag@Pybpy-COF	-	50	12	-
3	-	Cs ₂ CO ₃	50	12	08
4	AgNO ₃	Cs ₂ CO ₃	50	12	10.5
5	Pybpy-COF	Cs ₂ CO ₃	50	12	15
^c 6	Ag@Pybpy-COF	Cs ₂ CO ₃	50	12	51.4
7	Ag@Pybpy-COF	Cs ₂ CO ₃	50	12	98
8	Ag@Pybpy-COF	K ₂ CO ₃	50	12	-
9	Ag@Pybpy-COF	Na ₂ CO ₃	50	12	-
10	Ag@Pybpy-COF	Triethylamine	50	12	-
11	Ag@Pybpy-COF	КОН	50	12	-
^d 12	Ag@Pybpy-COF	Cs ₂ CO ₃	50	12	-
^e 13	Ag@Pybpy-COF	Cs ₂ CO ₃	50	12	16
^f 14	Ag@Pybpy-COF	Cs ₂ CO ₃	50	12	82
^h 15	Ag@Pybpy-COF	Cs ₂ CO ₃	50	12	38
ⁱ 16	Ag@Pybpy-COF	Cs ₂ CO ₃	50	12	-
17	Ag@Pybpy-COF	Cs ₂ CO ₃	25	12	40

^aReaction conditions: Ag@Pybpy-COF (10 mg), Phenylacetylene (1 mmol), base (1.5 mmol), CO₂ (1 bar), solvent (DMF 5 mL), 12 h. ^bIsolated yield. ^cCatalyst (5 mg), Solvent = ^dToluene, ^eTHF, ^fDMSO, ^hCatalyst (20 mg), and ⁱunder N₂ gas.

Further, the effect of catalyst (Ag@Pybpy-COF) loading on the yield of the product (3-phenylpropargylic acid) was also studied. The use of 5 mg of catalyst rendered 51.4% yield of the product (Table 1), and increasing the loading to 10 mg led to 98% yield of the product under the optimized conditions. Further increase in catalyst loading to 20 mg resulted in a reduction in product yield (Table 1) due to decarboxylation of the product.³⁵ Furthermore, the catalytic reaction performed in the

absence of carbon dioxide (under N_2) showed no product formation, which confirms the C_{sp} - C_{COOH} bond formation by the C-C coupling of alkyne moiety with CO_2 (Table 1). Additionally, the usefulness of a catalyst for CO_2 conversion from simulated flue gas/dilute gas (13% CO_2) was examined. The carboxylation of terminal alkynes was tested using dilute gas, which has a composition similar to that of dry flue gas (CO_2 : $N_2 = 13:87\%$) as a CO_2 source under the optimized conditions. Notably, about 62% yield (Table 2) of the product (3-phenylpropargylic acid) was obtained, highlighting the potential significance of the catalyst for the utilization of CO_2 from dilute gas under mild conditions.

Table 2. Carboxylation of various terminal alkynes with CO₂ catalyzed by Ag@Pybpy-COF.^a

R-	─ H + CO ₂ (1 bar)	Ag@Pybpy-COF Cs ₂ CO ₃ , DMF, 50 °C, 12 h	CI R	■ (0H
S.No.	Substrate	Product	Yield (%) ^b	TON^c
1	 н	$ \bigcirc \longrightarrow \bigcirc $	98.0	490
2^d	⟨¯⟩_=-н	$ \bigcirc \longrightarrow \bigcirc $	62.0	310
3	H ₃ C ————————————————————————————————————	$_{\rm H}$ $_{\rm H_3C}$ $\stackrel{\bigcirc}{=}$ $\stackrel{\bigcirc}{=}$ $\stackrel{\bigcirc}{<}$ $_{\rm OH}$	95.0	475
4	CI——H	$CI \longrightarrow OH$	97.0	485
5	Н₃СО-{	H_3CO \longrightarrow OH	93.0	465
6	F ₃ C — H	F_3C	99.0 H	495
7	Br—H	Br OH	96.0	480
8	∑ =-H		99.0 H	495

^aConditions: Catalyst [10 mg; (Ag 0.002 mmol)], alkynes (1 mmol), Cs_2CO_3 (1.5 mmol), CO_2 (1 bar), DMF (5 mL), 50 °C for 12 h. ^bIsolated yield, ^cTON = moles of the product formed/moles of the active metal sites in the catalyst, and ^dSimulated flue gas (13:87 % = $CO_2:N_2$).

Motivated by the high catalytic activity of Ag@Pybpy-COF for the carboxylation of phenylacetylene to propiolic acid at atmospheric pressure of CO₂, the scope of the reaction was further extended to various substituted phenylacetylenes under the optimized conditions (Table 2). Notably, Ag@Pybpy-COF could convert a variety of terminal alkynes into the corresponding value-added alkynyl carboxylic acids at mild conditions. Interestingly, phenylacetylenes containing the electronwithdrawing group undergo a higher conversion than those with the electron-donating functional group (Table 2).⁷³ Here, the electron-withdrawing group enhances the polarity of the terminal C-H bond of aromatic alkynes, thereby promoting facile deprotonation of alkynes in the presence of Cs₂CO₃. Further, heteroaromatic (thiophene) acetylene was converted to corresponding 3-(thiophene-3-yl)propiolic acid in high yield under the optimized conditions (Table 2). These results demonstrate the excellent catalytic activity of Ag@Pybpy-COF with diverse functional group tolerance for efficient carboxylation of various terminal alkynes at mild conditions. Moreover, a comparison of the catalytic performance of Ag@Pybpy-COF with literature-reported catalysts revealed its superior activity for the chemical fixation of CO₂ to propiolic acids (Table A5).

5.3.3. Carboxylative cyclization of propargylic amines with CO_2 catalyzed by Ag@Pybpy-COF

Motivated by the higher catalytic performance of Ag@Pybpy-COF for the carboxylation of terminal alkynes, the catalytic activity was tested for coupling of propargylic amines with CO₂ to produce bioactive 2-oxazolidinones. First, the catalytic performance was tested with N-benzylprop-2-yn-1-amine as a model substrate, and the reaction conditions were optimized (Table 3). At the optimized conditions, use of 10 mg of Ag@Pybpy-COF as catalyst, N-benzylprop-2-yn-1-amine (1 mmol), 0.1 mmol of 1,8-diazabicyclo[5.4.0]undec-7-ene (DBU), resulted in complete conversion of the amine into 2-oxazolidinone with 99% yield and 100% selectivity within 30 minutes at 50 °C and atmospheric pressure of CO₂ (Table 3).

Table 3: Optimization table for the carboxylic cyclization of CO₂ with propargylic amines catalyzed by Ag@Pybpy-COF.^a

S. No.	Catalyst	Base	Temperature	Time (h)	Yield
			(°C)		(%) ^b
1	Ag@Pybpy-	-	50	0.5	10
	COF				
2	Ag@Pybpy-	DBU	50	0.5	99
	COF				
3	-	DBU	50	0.5	-
4	Pybpy-COF	DBU	50	0.5	-
5	Ag@Pybpy-	DBU	25	0.5	30
	COF				
6 ^c	Ag@Pybpy-	DBU	50	0.5	-
	COF				

^aReaction conditions: Ag@Pybpy-COF (10 mg), *N*-benzylprop-2-yn-1-amine (1 mmol), base (0.1 equiv.), CO₂ (1 bar), and DMSO (2 mL), 0.5 h. ^bIsolated yield. ^cUnder N₂ gas.

Further, the control experiment in the absence of CO_2 (under N_2) under optimized conditions showed no product formation (Table 3), which confirms that 2-oxazolidinone is formed by chemical fixation of carbon dioxide with amine via C_{CO2} -N bond formation. Whereas the catalysis carried out with pristine COF (Pybpy-COF) as a catalyst did not show product formation, highlighting the importance of Ag(0) in catalyzing the formation of 2-oxazolidinones by coupling of CO_2 with propargylic amines (Table 3). The reaction carried out in the absence of DBU resulted in negligible product yield, suggesting its critical role in abstracting a proton of propargylic amine (Table 3). Further, the reaction scope was extended to various substituted propargylic amines. Interestingly, most of the propargylic amines were converted to respective oxazolidinones in excellent yield (> 95%) under the optimized conditions of atmospheric CO_2 within 30 minutes (Table 4). Moreover, a comparison of the catalytic performance with literature-reported heterogeneous catalysts revealed

the superior catalytic performance of Ag@Pybpy-COF for carboxylative cyclization of propargylic amines to value-added 2-oxazolidinones (Table A6).

Table 4. Carboxylative cyclization of propargylic amines with CO₂ catalyzed by Ag@Pybpy-COF.^a

н	R_1 + CO_2 (1 bar)	Ag@Pybpy-COF DMSO		N-R ₁
S. No.	Substrate	Product	Yield (%) ^b	TON^c
1	H N N	N-N-N-N-N-N-N-N-N-N-N-N-N-N-N-N-N-N-N-	99.0	495
2	H N F	N-N-F	97.0	485
3	H CH ₃	O N CH ₃	96.0	480
4	H CI	N—————————————————————————————————————	98.0	490
5	H OCH3	OCH ₃	95.0	475
6	H N S		98.0	490

^aConditions: Catalyst [10 mg; Ag (0.002 mmol)], propargylic amine (1 mmol), CO₂ (1

bar), DBU (0.1 equiv.), DMSO (2 mL), 50 °C for 0.5 h. ^bIsolated yield. ^cTON = moles of the product formed/moles of the active metal sites in the catalyst.

5.3.4. Mechanistic investigation for carboxylation of terminal alkynes with CO₂

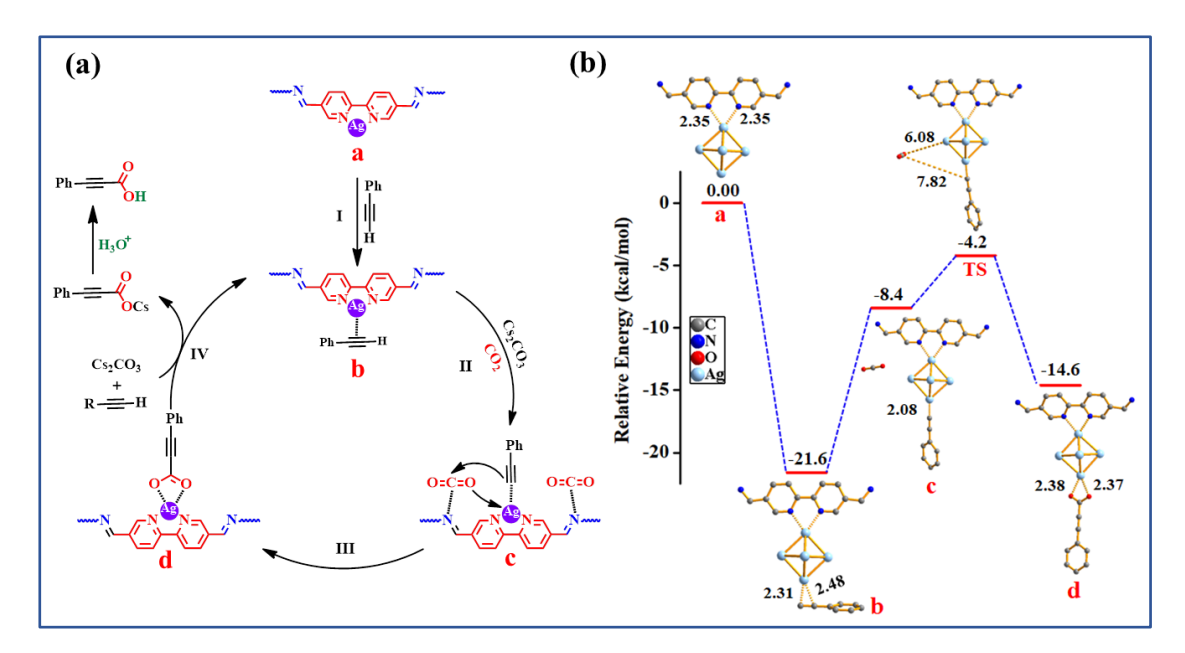
A plausible reaction mechanism for the carboxylation of phenylacetylene with CO_2 catalyzed by Ag@Pybpy-COF is shown in Scheme $2a.^{34,35}$ The catalytic reaction proceeds with the polarization of $C\equiv C$ bond of alkyne by its coordination with Ag~NP, resulting in silver acetylide intermediate formation in the presence of cesium carbonate. The formation of this intermediate was established by doing a control experiment in which Ag@Pybpy-COF was treated with phenylacetylene for 2 h and recovered. The FT-IR spectra of recovered COF showed stretching frequencies corresponding to $C\equiv C$, terminal C-H, and aromatic C-H bonds of phenylacetylene, supporting its coordination with Ag(0) in COF (Figure A43). Subsequent insertion of CO_2 led to the formation of silver carboxylate followed by transmetalation to generate cesium carboxylate, which was acidified to obtain the carboxylic acid product, and the catalyst was recycled for subsequent cycles.

To get further insight into mechanistic details, density functional theory (DFT) calculations were performed with phenylacetylene as model acetylene and its coupling with CO_2 to generate 3-phenylpropargylic acid (Scheme 2b). To start with, the binding interaction between the Ag_6 cluster and the bipy unit of COF was analyzed. For this, Ag_6 , bipyridine moiety of COF, and Ag_6 -COF cluster were fully relaxed, and binding energy (E_B) was calculated using the following equation:

$$E_B = E_{Ag_COF} - (E_{COF} + E_{Ag})$$

Here, E_{Ag_COF} , E_{COF} , and E_{Ag} represent the energy of the Ag_6 -COF cluster, pristine COF unit, and Ag_6 cluster, respectively. It was observed that Ag_6 binds strongly to the COF unit through the bipyridine N-sites at a distance of 2.35 Å, with a binding energy of -2.94 eV. The optimized structure of Ag_6 -COF complex **a** is shown in Scheme 2b. Next, the reactant phenylacetylene (R_1) was introduced to Ag_6 -COF, and the optimized structure of the resultant system shows the binding of phenylacetylene with Ag_6 -COF through bridging interactions to form complex **b** favored by adsorption energy of -21.6 kcal/mol and the distance between two acetylenic carbon atoms and Ag atom are 2.31 and 2.48 Å, respectively. Further, cesium carbonate deprotonates phenylacetylene, and the resultant phenyl acetyl moiety binds to the Ag cluster

through a Ph-C≡C sigma interaction with an Ag-C distance of 2.08 Å in the intermediate complex **c** with a reaction free energy of -8.4 kcal/mol. At the same time, the CO₂ molecule interacts with the imine (C=N) nitrogen of the COF unit (structure **c**). The activated Ag-C_{sp} bond is the insertion site for CO₂ and through the bond migration mechanism, the CO₂ molecule inserts to acetylenic carbon of the phenylacetylene to form the final carboxylate complex **d** with a reaction-free energy of -14.6 kcal/mol (Scheme 2b). The distance between the Ag cluster and two oxygen atoms is 2.38 and 2.37 Å, respectively. To study this step properly, we determined the transition state (TS) using the TS search LST/QST method. The energy barrier is -4.2 kcal/mol, validating the feasibility of this step. The relative energy profile for this mechanism is represented in Scheme 2b. The intermediate **c** and final complex **d** lie at -8.4 kcal/mol and -14.6 kcal/mol, respectively. The TS lies between the intermediate and final complex with a relative binding energy of -4.2 kcal/mol. Notably, the overall reaction-free energy is -14.6 kcal/mol, which supports the reaction feasibility.

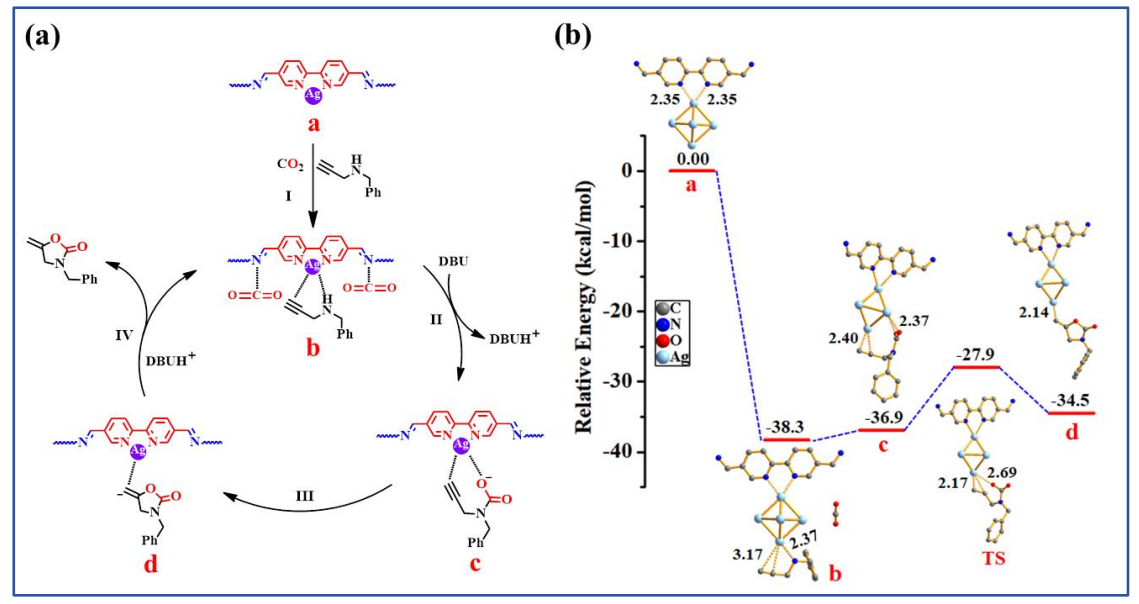


Scheme 2. (a) Plausible reaction mechanism for the carboxylation of terminal alkynes with CO₂ catalyzed by Ag@Pybpy-COF. (b) DFT energy profile for the carboxylation of terminal alkynes with CO₂ catalyzed by Ag@Pybpy-COF (bond distances are in Å). Color code: grey, C; blue, N; red, O; and pale blue, Ag. For clarity, only a fragment of COF is shown, and hydrogen atoms are omitted.

5.3.5. Mechanistic investigation for carboxylation of propargylic amines with CO₂

Based on the literature study, a plausible mechanism for carboxylative

cyclization of propargylic amine (N-benzylprop-2-yn-1-amine) with CO₂ catalyzed by Ag@Pybpy-COF is shown in Scheme 3a. 36,38 The coordination of propargylic amines with the framework underwent the same trial as that of terminal alkynes with Ag@COF. In support of this, the FTIR spectra of the COF treated with N-benzylprop-2-yn-1-amine showed characteristic peaks corresponding to propargylic amine, demonstrating its interaction with Ag@COF (Figure A45). Then, the presence of DBU facilitates abstraction of the proton of propargylic amine, and subsequent insertion of CO₂ leads to carbamate formation, which undergoes intramolecular cyclization to generate oxazolidinone and its elimination from the metal center regenerates the catalyst for subsequent cycles. The DFT calculations were performed to better understand the reaction mechanism and the plausible catalytic cycle (Scheme 3b). The reactants (N-benzylprop-2-yn-1-amine) and CO₂ were introduced to Ag₆-COF, and the optimized structure **a** is shown in Scheme 3b. At the initial complex **b**, the propargylic amine interacts with Ag6-COF via nitrogen atom at a distance of 2.37Å and acetylenic bond at a distance of 3.17Å with a relative energy of -38.3 kcal/mol as displayed in Scheme 3b. At the same time, the CO₂ molecule interacts with the imine (C=N) nitrogen of COF through a long-range interaction at 4.6 Å. Then, the intermediate complex c with a relative energy of -36.9 kcal/mol is formed, in which the CO₂ molecule attacks the amino group of propargylic amine to generate a carbamate intermediate (Scheme 3b). The distance between the O atom of CO₂ and the Ag cluster is 2.37Å. Subsequently, a ring closure reaction generates the final complex **d** with a free energy of -34.5 kcal/mol. As discussed in the previous section, we investigated this step by determining the TS using the TS search LST/QST method. The TS lies at -27.9 kcal/mol from the intermediate complex, validating the feasibility of this step. The relative energy profile for this mechanism is represented in Scheme 3b. The energy of the overall reaction is -34.5 kcal/mol, which substantiates the feasibility of this reaction. Thus, the catalytic pathway for carboxylative cyclization of propargylic amines with CO2 to generate 2-oxazolidinones catalyzed by Ag@Pybpy-COF is presented.



Scheme 3. (a) Plausible reaction mechanism for the carboxylative cyclization of propargylic amines with CO₂ catalyzed by Ag@Pybpy-COF. (b) DFT energy profile for the carboxylative cyclization of PAs with CO₂ catalyzed by Ag@Pybpy-COF (bond distances are in Å). Color code: grey, C; blue, N; red, O; and pale blue, Ag. For clarity, only a fragment of COF is shown, and hydrogen atoms are omitted.

5.3.6. Catalyst recycling and leaching test

The recyclability of Ag@Pybpy-COF for multiple cycles of reuse was tested by separating the catalyst by centrifugation after the catalytic reaction, washed with acetone, and utilized for subsequent catalytic cycles after activating at 100 °C for 12 h under vacuum. Notably, Ag@Pybpy-COF was recyclable for up to six cycles with negligible loss in the yield of phenylpropargylic acid, which supports the catalyst stability and recyclability (Figure 7a). Further, the recovered catalyst was characterized by various techniques to confirm its structural stability and Ag loading. The PXRD pattern and FT-IR spectra of the recycled sample match well with those of the parent COF, supporting its structural integrity (Figures A47 and A48). The XPS analysis and elemental mapping of recycled samples revealed the presence of constitute elements (Figure A49). Further, MP-AES analysis showed about 2.2 wt% of Ag close to that of the parent sample, supporting the stable anchoring of Ag NPs. In addition, the catalyst leaching test was performed by separating Ag@Pybpy-COF from the reaction mixture after 3h, led to no further increase in the yield of propiolic acid, supporting the absence of catalyst leaching (Figure 7b).

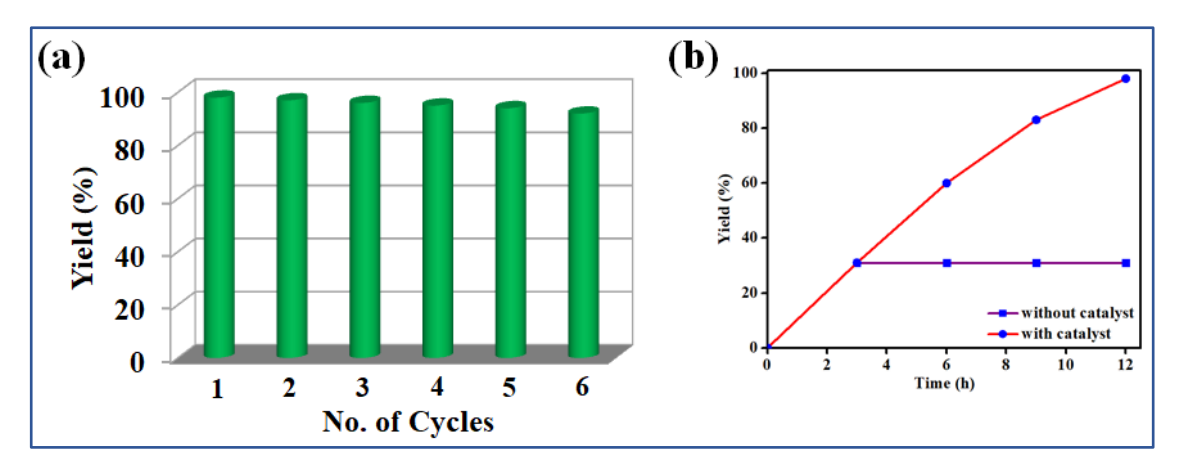


Figure 7. Recyclability (a) and leaching test (b) of Ag@Pybpy-COF.

5.4. Conclusion

This work demonstrates the application of highly porous Pybpy-COF for stable anchoring of catalytically active Ag(0) NPs and its application for the synthesis of two valuable commodity chemicals, alkynyl carboxylic acids, and 2-oxazolidinones by utilizing greenhouse gas, CO₂ at ambient conditions. The efficient carboxylation of various terminal alkynes with CO₂ via C-H bond functionalization was achieved to produce alkynyl carboxylic acids with diverse substrates scope in high yield and selectivity. Besides, carboxylative cyclization of diverse propargylic amines with CO₂ was accomplished to obtain high-value 2-oxazolidinones at a mild atmospheric pressure of CO₂. A detailed mechanistic path of the catalytic transformations has been elucidated from in-depth theoretical DFT studies. Moreover, the catalyst was highly recyclable for up to six cycles without significant loss in catalytic activity and structural rigidity. Overall, this work showcases effective CCU at a mild atmospheric pressure of CO₂.

5.5. References

- (1) Joos, F.; Plattner, G. -K.; Stocker, T. F.; Marchal, O.; Schmittner, A. Global Warming and Marine Carbon Cycle Feedbacks on Future Atmospheric CO₂. *Science* **1999**, 284, 464-467.
- (2) Jacobson, M. Z. Review of Solutions to Global Warming, Air Pollution, and Energy Security. *Energy Environ. Sci.* **2009**, *2*, 148-173.
- (3) Bakker, D.; Watson, A. Global change: A Piece in the CO₂ Jigsaw. *Nature* **2001**, 410, 765-766.

- (4) Ding, M.; Flaig, R. W.; Jiang, H. -L.; Yaghi, O. M. Carbon Capture and Conversion Using Metal-Organic Frameworks and MOF-based Materials. *Chem. Soc. Rev.* **2019**, *48*, 2783-2828.
- (5) Liang, J.; Huang, Y.-B.; Cao, R. Metal-Organic Frameworks and Porous Organic Polymers for Sustainable Fixation of Carbon Dioxide into Cyclic Carbonates. *Coord. Chem. Rev.* **2019**, *378*, 32-65.
- (6) Sakakura, T.; Choi, J. C.; Yasuda, H. Transformation of Carbon Dioxide. *Chem. Rev.* **2007**, *107*, 2365-2387.
- (7) Singh, S.; Verma, R.; Kaul, N.; Sa, J.; Punjal, A.; Prabhu, S.; Polshettiwar, V. Surface Plasmon-enhanced Photo-driven CO₂ Hydrogenation by Hydroxy-terminated Nickel Nitride Nanosheets. *Nat. Commun.* **2023**, *14*, 2551.
- (8) Tapiador, J.; Leo, P.; Gándara, F.; Calleja, G.; Orcajo, G. Robust Cu-URJC-8 with Mixed Ligands for Mild CO₂ Cycloaddition Reaction. *J. CO*₂ *Util.* **2022**, *64*, 102166.
- (9) Chandra Sau, S.; Bhattacharjee, R.; Hota, P. K.; Vardhanapu, P. K.; Vijaykumar, G.; Govindarajan, R.; Datta, A.; Mandal, S. K. Transforming Atmospheric CO₂ into Alternative Fuels: a Metal-Free Approach Under Ambient Conditions. *Chem. Sci.* **2019**, *10*, 1879-1884.
- (10) Das, R.; Muthukumar, D.; Pillai, R. S.; Nagaraja, C. M. Rational Design of a Zn^{II} MOF with Multiple Functional Sites for Highly Efficient Fixation of CO₂ under Mild Conditions: Combined Experimental and Theoretical Investigation. *Chem. Eur. J.* **2020**, *26*, 17445-17454.
- (11) Das, R.; Nagaraja, C. M. Highly Efficient Fixation of Carbon Dioxide at RT and Atmospheric Pressure Conditions: Influence of Polar Functionality on Selective Capture and Conversion of CO₂. *Inorg. Chem.* **2020**, *59*, 9765-9773.
- (12) Gogia, A.; Bhambri, H.; Mandal, S. K. Exploiting a Multi-Responsive Oxadiazole Moiety in One Three-Dimensional Metal-Organic Framework for Remedies to Three Environmental Issues. *ACS Appl. Mater. Interfaces* **2023**, *15*, 8241-8252.
- (13) Singh Dhankhar, S.; Ugale, B.; Nagaraja, C. M. Co-Catalyst Free Chemical Fixation of CO₂ into Cyclic Carbonates by using Metal-Organic Frameworks as Efficient Heterogeneous Catalysts. *Chem. Asian J.* **2020**, *15*, 2403-2427.
- (14) Biswas, S.; Dey, A.; Rahimi, F. A.; Barman, S.; Maji, T. K. Metal-Free Highly Stable and Crystalline Covalent Organic Nanosheet for Visible-Light-Driven Selective Solar Fuel Production in Aqueous Medium. *ACS Catal.* **2023**, *13*, 5926-5937.
- (15) Singh, G.; Nagaraja, C. M. Rational Design of Cu(I)-Anchored Porous Covalent

- Triazine Framework (CTF) for Simultaneous Capture and Conversion of CO₂ at Ambient Conditions. *J. CO₂ Util.* **2022**, *63*, 102132.
- (16) Ghosh, S.; Riyajuddin, S.; Sarkar, S.; Ghosh, K.; Islam, S. M. Pd NPs Decorated on POPs as Recyclable Catalysts for the Synthesis of 2-oxazolidinones from Propargylic Amines via Atmospheric Cyclizative CO₂ Incorporation. *ChemNanoMat* **2020**, *6*, 160-172.
- (17) Manjolinho, F.; Arndt, M.; Gooßen, K.; Gooßen, L. J. Catalytic C-H Carboxylation of Terminal Alkynes with Carbon Dioxide. *ACS Catal.* **2012**, *2*, 2014-2021.
- (18) Das, R.; Parihar, V.; Nagaraja, C. M. Strategic Design of a Bifunctional Ag(I)-Grafted NHC-MOF for Efficient Chemical Fixation of CO₂ from a Dilute Gas Under Ambient Conditions. *Inorg. Chem. Front.* **2022**, *9*, 2583-2593.
- (19) Singh, G.; Prakash, K.; Nagaraja, C. M. Fe(III)-Anchored Porphyrin-Based Nanoporous Covalent Organic Frameworks for Green Synthesis of Cyclic Carbonates from Olefins and CO₂ under Atmospheric Pressure Conditions. *Inorg. Chem.* **2023**, *62*, 13058-13068.
- (20) Das, R.; Nagaraja, C. M. Noble Metal-Free Cu(I)-Anchored NHC-based MOF for Highly Recyclable Fixation of CO₂ under RT and Atmospheric Pressure Conditions. *Green Chem.* **2021**, *23*, 5195-5204.
- (21) Biradha, K.; Das, S. K.; Bu, X. -H. Coordination Polymers as Heterogeneous Catalysts for Water Splitting and CO₂ Fixation. *Cryst. Growth Des.* **2022**, 22, 2043-2045.
- (22) Das, R.; Manna, S. S.; Pathak, B.; Nagaraja, C. M. Strategic Design of Mg-Centered Porphyrin Metal-Organic Framework for Efficient Visible Light-Promoted Fixation of CO₂ under Ambient Conditions: Combined Experimental and Theoretical Investigation. *ACS Appl. Mater. Interfaces* **2022**, *14*, 33285-33296.
- (23) Song, K. S.; Fritz, P. W.; Coskun, A. Porous Organic Polymers for CO₂ Capture, Separation and Conversion. *Chem. Soc. Rev.* **2022**, *51*, 9831-9852.
- (24) Das, R.; Ezhil, T.; Palakkal, A. S.; Muthukumar, D.; Pillai, R. S.; Nagaraja, C. M. Efficient Chemical Fixation of CO₂ from Direct Air under Environment-Friendly Co-Catalyst and Solvent-Free Ambient Conditions. *J. Mater. Chem. A* **2021**, *9*, 23127-23139.
- (25) Chen, C.; Wu, J.; Yan, G.; Huang, D. Recent Advances of Propiolic Acids in Organic Reactions. *Tetrahedron Lett.* **2020**, *61*, 151415.

- (26) Raja, G. C. E.; Ryu, J. Y.; Lee, J.; Lee, S. Ruthenium-Catalyzed C-H Activation of Salicylaldehyde and Decarboxylative Coupling of Alkynoic Acids for the Selective Synthesis of Homoisoflavonoids and Flavones. *Org. Lett.* **2017**, *19*, 6606-6609.
- (27) Trost, B. M.; Toste, F. D.; Greenman, K. Atom Economy. Palladium-Catalyzed Formation of Coumarins by Addition of Phenols and Alkynoates via a Net C-H Insertion. *J. Am. Chem. Soc.* **2003**, *125*, 4518-4526.
- (28) Shinabarger, D. L.; Marotti, K. R.; Murray, R. W.; Lin, A. H.; Melchior, E. P.; Swaney, S. M.; Dunyak, D. S.; Demyan, W. F.; Buysse, J. M. Mechanism of Action of Oxazolidinones: Effects of Linezolid and Eperezolid on Translation Reactions. *Antimicrob. Agents Chemother.* **1997**, *41*, 2132-2136.
- (29) Michalska, K.; Bednarek, E.; Gruba, E.; Lewandowska, K.; Mizera, M.; Cielecka-Piontek, J. Comprehensive Spectral Identification of Key Intermediates to the Final Product of the Chiral Pool Synthesis of Radezolid. *Chem. Cent. J.* **2017**, *11*, 82.
- (30) Moureau, F.; Wouters, J.; Vercauteren, D. P.; Collin, S.; Evrard, G.; Durant, F.; Ducrey, F.; Koenig, J. J.; Jarreau, F. X. A Reversible Monoamine Oxidase Inhibitor, Toloxatone: Structural and Electronic Properties. *Eur. J. Med. Chem.* **1992**, *27*, 939-948.
- (31) Sekine, K.; Yamada, T. Silver-Catalyzed Carboxylation. *Chem. Soc. Rev.* **2016**, 45, 4524-4532.
- (32) Zhang, X.; Zhang, W. -Z.; Ren, X.; Zhang, L. -L.; Lu, X. -B. Ligand-Free Ag(I)-Catalyzed Carboxylation of Terminal Alkynes with CO₂. *Org. Lett.* **2011**, *13*, 2402-2405.
- (33) Yoshida, M.; Mizuguchi, T.; Shishido, K. Synthesis of Oxazolidinones by Efficient Fixation of Atmospheric CO₂ with Propargylic Amines by using a Silver/1,8 Diazabicyclo[5.4.0]undec-7-ene (DBU) Dual-Catalyst System. *Chem. Eur. J.* **2012**, *18*, 15578-15581.
- (34) Lan, X.; Du, C.; Cao, L.; She, T.; Li, Y.; Bai, G. Ultrafine Ag Nanoparticles Encapsulated by Covalent Triazine Framework Nanosheets for CO₂ Conversion. *ACS Appl. Mater. Interfaces* **2018**, *10*, 38953-38962.
- (35) Dang, Q. -Q.; Liu, C. -Y.; Wang, X. -M.; Zhang, X. -M. Novel Covalent Triazine Framework for High-Performance CO₂ Capture and Alkyne Carboxylation Reaction. *ACS Appl. Mater. Interfaces* **2018**, *10*, 27972-27978.
- (36) Zhang, Y.; Lan, X.; Yan, F.; He, X.; Wang, J.; -Sandoval, L. R.; Chen, L.; Bai, G. Controllable Encapsulation of Silver Nanoparticles by Porous Pyridine-Based

- Covalent Organic Frameworks for Efficient CO₂ Conversion using Propargylic Amines. *Green Chem.* **2022**, *24*, 930-940.
- (37) Yang, H.; Zhang, X.; Zhang, G.; Fei, H. An alkaline-resistant Ag(I)-anchored Pyrazolate-Based Metal-Organic Framework for Chemical Fixation of CO₂. *Chem. Commun.* **2018**, *54*, 4469-4472.
- (38) Cao, C. -S.; Xia, S. -M.; Song, Z. -J.; Xu, H.; Shi, Y.; He, L. -N.; Cheng, P.; Zhao, B. Highly Efficient Conversion of Propargylic Amines and CO₂ Catalyzed by Noble-Metal-Free [Zn₁₁₆] Nanocages. *Angew. Chem. Int. Ed.* **2020**, *59*, 8586-8593.
- (39) Li, H.; Deng, G.; Wang, Z.; Cheng, K.; Li, Z.; Luo, X.; Yang, Y.; Sun, Y.; Li, P.-Z.; Wang, Z. Effective CO₂ Catalytic Conversion by Nitrogen-Rich Covalent Organic Framework-Immobilized Ag Nanoparticles. *ACS Appl. Nano Mater.* **2023**, *6*, 16424-16432.
- (40) Feng, X.; Ding, X.; Jiang, D. Covalent Organic Frameworks. *Chem. Soc. Rev.* **2012**, *41*, 6010-6022.
- (41) Côté, A. P.; Benin, A. I.; Ockwig, N. W.; O'Keeffe, M.; Matzger, A. J.; Yaghi, O. M. Porous, Crystalline, Covalent Organic Frameworks. *Science* **2005**, *310*, 1166-1170.
- (42) Gong, Y. -N.; Guan, X.; Jiang, H. -L. Covalent Organic Frameworks for Photocatalysis: Synthesis, Structural Features, Fundamentals, and Performance. *Coord. Chem. Rev.* **2023**, *475*, 214889.
- (43) Chen, Y.; Chen, Q.; Zhang, Z. Application of Covalent Organic Framework Materials as Heterogeneous Ligands in Organic Synthesis. *Chin. J. Org. Chem.* **2021**, *41*, 3826-3843.
- (44) Singh, G.; Nagaraja, C. M. Highly Efficient Metal/Solvent-Free Chemical Fixation of CO₂ at Atmospheric Pressure Conditions using Functionalized Porous Covalent Organic Frameworks. *J. CO₂ Util.* **2021**, *53*, 101716.
- (45) Chen, Y.-X.; Zhang, M.; Zhang, S.-Z.; Hao, Z.-Q.; Zhang, Z. Copper-decorated covalent organic framework as a heterogeneous photocatalyst for phosphorylation of terminal alkynes. *Green Chem.* **2022**, *24*, 4071-4081.
- (46) Ghosh, S.; Nakada, A.; Springer, M. A.; Kawaguchi, T.; Suzuki, K.; Kaji, H.; Baburin, I.; Kuc, A.; Heine, T.; Suzuki, H.; Abe, R.; Seki, S. Identification of Prime Factors to Maximize the Photocatalytic Hydrogen Evolution of Covalent Organic Frameworks. *J. Am. Chem. Soc.* **2020**, *142*, 9752-9762.
- (47) Chandra, S.; Kundu, T.; Dey, K.; Addicoat, M.; Heine, T.; Banerjee, R. Interplaying Intrinsic and Extrinsic Proton Conductivities in Covalent Organic

- Frameworks. Chem. Mater. 2016, 28, 1489-1494.
- (48) Han, Y.; Zhang, M.; Zhang, Y. -Q.; Zhang, Z. -H. Copper Immobilized at a Covalent Organic Framework: An Efficient and Recyclable Heterogeneous Catalyst for the Chan-Lam Coupling Reaction of Aryl Boronic Acids and Amines. *Green Chem.* **2018**, *20*, 4891-4900.
- (49) Zhao, J.; Ying, Y. P.; Wang, G. L.; Hu, K. D.; Yuan, Y. D.; Ye, H. L.; Liu, Z. L.; Lee, J. Y.; Zhao, D. Covalent Organic Framework Film Protected Zinc Anode for Highly Stable Rechargeable Aqueous Zinc-ion Batteries. *Energy Storage Mater.* **2022**, 48, 82-89.
- (50) Wu, C.; Li, X.; Shao, M.; Kan, J.; Wang, G.; Geng, Y.; Dong, Y.- B. Porphyrin Covalent Organic Framework for Photocatalytic Synthesis of Tetrahydroquinolines. *Chin. Chem. Lett.* **2022**, *33*, 4559-4562.
- (51) Bhambri, H.; Khullar, S. S.; Mandal, S. K.; Mandal, S. K. Nitrogen-Rich Covalent Organic Frameworks: A Promising Class of Sensory Materials. *Mater. Adv.* **2022**, *3*, 19-124.
- (52) Zhao, X.; Pachfule, P.; Thomas, A. Covalent Organic Frameworks (COFs) for Electrochemical Applications. *Chem. Soc. Rev.* **2021**, *50*, 6871-6913.
- (53) Huang, N.; Chen, X.; Krishna, R.; Jiang, D. Two-dimensional covalent Organic Frameworks for Carbon Dioxide Capture through Channel-Wall Functionalization. *Angew. Chem., Int. Ed.* **2015**, *54*, 2986-2990.
- (54) Dhankhar, S. S.; Nagaraja, C. M. Porous Nitrogen-Rich Covalent Organic Framework for Capture and Conversion of CO₂ at Atmospheric Pressure Conditions. *Micropor. Mesopor. Mat.* **2020**, *308*, 110314.
- (55) Liu, Z.; Huang, Y.; Chang, S.; Zhu, X.; Fu, Y.; Ma, R.; Lu, X.; Zhang, F.; Zhu, W.; Fan, M. Highly Dispersed Ru Nanoparticles on a Bipyridine-Linked Covalent Organic Framework for Efficient Photocatalytic CO₂ Reduction. *Sustainable Energy Fuels* **2021**, *5*, 2871-2876.
- (56) Sun, Q.; Wu, C.; Pan, Q.; Zhang, B.; Liu, Y.; Lu, X. S.; Sun, J.; Sun, L.; Zhao, Y. Three-Dimensional Covalent-Organic Frameworks Loaded with Highly Dispersed Ultrafine Palladium Nanoparticles as Efficient Heterogeneous Catalyst. *Chem Nano Mat* **2021**, *7*, 95-99.
- (57) Jin, S.; Sakurai, T.; Kowalczyk, T.; Dalapati, S.; Xu, F.; Wei, H.; Chen, X.; Gao, J.; Seki, S.; Irle, S.; Jiang, D. Two-Dimensional Tetrthiafulvalene Covalent Organic Frameworks: Towards Lattice Conductive Organic Salts. *Chem. Eur. J.* **2014**, *20*,

14608-14613.

- (58) Delley, B. From Molecules to Solids with the DMol³ Approach. *J. Chem. Phys.* **2000**, *113*, 7756-7764.
- (59) Liu, X.; Wang, M. -Y.; Wang, S. -Y.; Wang, Q.; He, L. -N. In Situ Generated Zinc(II) Catalyst for Incorporation of CO₂ into 2-Oxazolidinones with Propargylic Amines at Atmospheric Pressure. *Chem Sus Chem* **2017**, *10*, 1210-1216.
- (60) Bandomo, G. C. D.; Mondal, S. S.; Franco, F.; Bucci, A.; Martin-Diaconescu, V.; Ortuño, M. A.; van Langevelde, P. H.; Shafir, A.; López, N.; Lloret-Fillol, J. Mechanically Constrained Catalytic Mn(CO)₃Br Single Sites in a Two Dimensional Covalent Organic Framework for CO₂ Electroreduction in H₂O. *ACS Catal.* **2021**, *11*, 7210-7222.
- (61) Jia, J.; Bu, X.; Yang, X. A Cobalt Covalent Organic Framework: A Dual Functional Atomic-Level Catalyst for Visible-Light Driven C-H Annulation of Amides with Alkynes. *J. Mater. Chem. A* **2022**, *10*, 11514-11523.
- (62) Vardhan, H.; Pan, Y.; Yang, Z.; Verma, G.; Nafady, A.; Al-Enizi, A. M.; Alotaibi, T. M.; Almaghrabi, O. A.; Ma, S. Iridium Complex Immobilization on Covalent Organic Framework for Effective C-H Borylation. *APL Mater.* **2019**, *7*, 101111.
- (63) Chowdhury, A. H.; Chowdhury, I. H.; Biswas, S.; Islam, S. M. Application of Ag/TFPG-DMB COF in Carbamates Synthesis via CO₂ Fixation Reaction and one-pot Reductive N-Formylation of Nitroarenes Under Sunlight. *Mol. Catal.* **2020**, *493*, 111050.
- (64) Mi, Z.; Yang, P.; Wang, R.; Unruangsri, J.; Yang, W.; Wang, C.; Guo, J. Stable Radical Cation-Containing Covalent Organic Frameworks Exhibiting Remarkable Structure-Enhanced Photothermal Conversion. *J. Am. Chem. Soc.* **2019**, *141*, 14433-14442.
- (65) Chen, X.; Huang, N.; Gao, J.; Xu, H.; Xu, F.; Jiang, D. Towards Covalent Organic Frameworks with Predesignable and Aligned Open Docking Sites. *Chem. Commun.* **2014**, *50*, 6161-6163.
- (66) Ghosh, S.; Khan, T. S.; Ghosh, A.; Chowdhury, A. H.; Haider, M. A.; Khan, A.; Islam, S. M. Utility of Silver Nanoparticles Embedded Covalent Organic Frameworks as Recyclable Catalysts for the Sustainable Synthesis of Cyclic Carbamates and 2-Oxazolidinones via Atmospheric Cyclizative CO₂ Capture. *ACS Sustainable Chem. Eng.* **2020**, *8*, 5495-5513.

- (67) Modak, A.; Bhaumik, A. Surface-Exposed Pd Nanoparticles Supported Over Nanoporous Carbon Hollow Tubes as an Efficient Heterogeneous Catalyst for the C-C Bond Formation and Hydrogenation Reactions. *J. Mol. Catal. A: Chem.* **2016**, *425*, 147-156.
- (68) Zhang, L.; Bu, R.; Liu, X. -Y.; Mu, P. -F.; Gao, E. -Q. Schiff-Base Molecules and COFs as Metal-Free Catalysts or Silver Supports for Carboxylation of Alkynes with CO₂. *Green Chem.* **2021**, *23*, 7620-7629.
- (69) Salam, N.; Kundu, S. K.; Molla, R. A.; Mondal, P.; Bhaumik, A.; Islam, S. M. Ag-grafted Covalent Imine Network Material for One-pot Three-Component Coupling and Hydration of Nitriles to Amides in Aqueous Medium. *RSC Adv.* **2014**, *4*, 47593-47604.
- (70) Kumar, G.; Pillai, R. S.; Khan, N. H.; Neogi, S. Structural Engineering in Pre functionalized, Imine-Based Covalent Organic Framework *via* Anchoring Active Ru(II) Complex for Visible-Light Triggered and Aerobic Cross-Coupling of α -amino Esters with Indoles. *Appl. Catal.*, *B* **2021**, 292, 120149.
- (71) Guan, P.; Qiu, J.; Zhao, Y.; Wang, H.; Li, Z.; Shi, Y.; Wang, J. A Novel Crystalline Azine-Linked Three-Dimensional Covalent Organic Framework for CO₂ Capture and Conversion. *Chem. Commun.* **2019**, *55*, 12459-12462.
- (72) Liu, J.; Zhang, X.; Wen, B.; Li, Y.; Wu, J.; Wang, Z.; Wu, T.; Zhao, R.; Yang, S. Pre-Carbonized Nitrogen-Rich Polytriazines for the Controlled Growth of Silver Nanoparticles: Catalysts for Enhanced CO₂ Chemical Conversion at Atmospheric Pressure. *Catal. Sci. Technol.* **2021**, *11*, 3119-3127.
- (73) Bu, R.; Zhang, L.; Gao, L. -L.; Sun, W. -J.; Yang, S. -L.; Gao, E. -Q. Copper(I)-Modifed Covalent Organic Framework for CO₂ Insertion to Terminal Alkynes. *Mol. Catal.* **2021**, *499*, 111319.

Figures/Tables	Pages
Figure A1. FT-IR spectra of (a) 1,3,5-Triformylphloroglucinol	161
(black line) 2,5-diaminobenzenesulfonic acid (red line) and COF-	
SO ₃ H (blue line). (b) FT-IR spectra of 1,3,5-	
Triformylphloroglucinol (black line), 1,4-phenylenediamine (red	
line) and COF-H (blue line).	
Figure A2. TGA plot of (a) COF-SO ₃ H and (b) COF-H.	161
Analysis of gas adsorption isotherms	161
Figure A3 . Carbon dioxide adsorption isotherm for COF-SO ₃ H at	162
(a) 273 K and (b) 298 K. (the solid line shows the best fit to the data	
using the Langmuir-Freundlich equation).	
Figure A4. Carbon dioxide adsorption isotherm for COF-H at (a)	163
273 K and (b) 298 K. (the solid line shows the best fit to the data	
using the Langmuir-Freundlich equation).	
Figure A5. Enthalpy of carbon dioxide adsorption for (a) COF-	163
SO ₃ H and (b) COF-H calculated using Clausius-Clapeyron equation	
calculations.	
Figure A6. Linear fitting of CO ₂ , CH ₄ , and N ₂ isotherms of COF-	164
SO ₃ H used for calculation of Henry's selectivity constants.	
Figure A7. NH ₃ TPD plot of COF-SO ₃ H.	164
Table A1. Comparison of the catalytic activity of COF-SO ₃ H for	165
cycloaddition of CO ₂ with epichlorohydrin to produce cyclic	
carbonate.	
Figure A8. FT-IR spectra of COF-SO ₃ H recovered after five cycles	166
of catalysis.	
Figure A9. PXRD plot of COF-SO ₃ H recovered after five cycles of	166
catalysis.	
Figure A10. SEM images of COF-SO ₃ H before and after catalysis.	167
Figure A11. N ₂ adsorption isotherm of COF-SO ₃ H before and after	167
catalysis.	
Figure A12. FT-IR spectra of (a) COF-SO ₃ H (b) epichlorohydrin	168
and (c) COF-SO ₃ H treated with epichlorohydrin.	
Figure A13. PXRD pattern of bipy-CTF (i) and Cu(I)@bipy-CTF	168
	1

(a) 273 K and (b) 298 K (the solid line shows the best fit to the data using the Langmuir-Freundlich equation). (c) Enthalpy of carbon dioxide adsorption was determined using the Clausius-Clapeyron equation. Figure A17. Carbon dioxide adsorption isotherm for Cu(I)@bipy-CTF at (a) 273 K and (b) 298 K (the solid line shows the best fit to the data using the Langmuir-Freundlich equation). (c) Enthalpy of carbon dioxide adsorption was determined using the Clausius-Clapeyron equation. Figure A18. Linear fitting for (a) CO ₂ , (b) CH ₄ , and (c) N ₂ isotherms of Cu(I)@bipy-CTF was used for the calculation of Henry's selectivity constants. Table A2. Comparison of the catalytic activity of Cu(I)@bipyCTF for carboxylative cyclization of 2-methyl-3-butyne-2-ol with the reported POP-based catalysts. Figure A19. PXRD plot of Cu(I)@bipy-CTF as-prepared (red) and recovered after eight cycles of catalysis (blue). Figure A20. FT-IR spectra of Cu(I)@bipy-CTF (a) as-prepared and (b) recovered after eight cycles of catalysis. Figure A21. SEM images of Cu(I)@bipy-CTF (a), Cu(I)@bipy-CTF (b), 2-methyl-3-butyn-2-ol (c), Cu(I)@bipy-CTF treated with 2-methyl-3-butyn-2-ol (d), bipy-CTF (b), 2-methyl-3-butyn-2-ol	(ii).	
Figure A16. Carbon dioxide adsorption isotherm for bipy-CTF at (a) 273 K and (b) 298 K (the solid line shows the best fit to the data using the Langmuir-Freundlich equation). (c) Enthalpy of carbon dioxide adsorption was determined using the Clausius-Clapeyron equation. Figure A17. Carbon dioxide adsorption isotherm for Cu(I)@bipy- CTF at (a) 273 K and (b) 298 K (the solid line shows the best fit to the data using the Langmuir-Freundlich equation). (c) Enthalpy of carbon dioxide adsorption was determined using the Clausius- Clapeyron equation. Figure A18. Linear fitting for (a) CO ₂ , (b) CH ₄ , and (c) N ₂ isotherms of Cu(I)@bipy-CTF was used for the calculation of Henry's selectivity constants. Table A2. Comparison of the catalytic activity of Cu(I)@bipyCTF for carboxylative cyclization of 2-methyl-3-butyne-2-ol with the reported POP-based catalysts. Figure A19. PXRD plot of Cu(I)@bipy-CTF as-prepared (red) and recovered after eight cycles of catalysis (blue). Figure A20. FT-IR spectra of Cu(I)@bipy-CTF as-prepared (red) and recovered after eight cycles of catalysis (blue). Figure A21. SEM images of Cu(I)@bipy-CTF (a) as-prepared and (b) recovered after eight cycles of catalysis. Figure A22. FT-IR spectra of bipy-CTF (a), Cu(I)@bipy-CTF (b), 2-methyl-3-butyn-2-ol (c), Cu(I)@bipy-CTF treated with 2-methyl- 3-butyn-2-ol (d), bipy-CTF treated with 2-methyl- 3-butyn-2-ol (d), band c) Magnified FT-IR plots of P-COF (red) and Fe(III)@P-COF (blue). Figure A24. ¹³ C CP-MAS solid-state NMR spectrum of P-COF.	Figure A14. EDS plot of bipy-CTF (a) and Cu(I)@bipy-CTF (b).	169
(a) 273 K and (b) 298 K (the solid line shows the best fit to the data using the Langmuir-Freundlich equation). (c) Enthalpy of carbon dioxide adsorption was determined using the Clausius-Clapeyron equation. Figure A17. Carbon dioxide adsorption isotherm for Cu(I)@bipy-CTF at (a) 273 K and (b) 298 K (the solid line shows the best fit to the data using the Langmuir-Freundlich equation). (c) Enthalpy of carbon dioxide adsorption was determined using the Clausius-Clapeyron equation. Figure A18. Linear fitting for (a) CO ₂ , (b) CH ₄ , and (c) N ₂ isotherms of Cu(I)@bipy-CTF was used for the calculation of Henry's selectivity constants. Table A2. Comparison of the catalytic activity of Cu(I)@bipyCTF for carboxylative cyclization of 2-methyl-3-butyne-2-ol with the reported POP-based catalysts. Figure A19. PXRD plot of Cu(I)@bipy-CTF as-prepared (red) and recovered after eight cycles of catalysis (blue). Figure A20. FT-IR spectra of Cu(I)@bipy-CTF (a) as-prepared and (b) recovered after eight cycles of catalysis. Figure A21. SEM images of Cu(I)@bipy-CTF (a), Cu(I)@bipy-CTF (b), 2-methyl-3-butyn-2-ol (c), Cu(I)@bipy-CTF treated with 2-methyl-3-butyn-2-ol (d), bipy-CTF (b), 2-methyl-3-butyn-2-ol	Figure A15. MP-AES calibration curve for Cu(I)@bipy-CTF.	169
using the Langmuir-Freundlich equation). (c) Enthalpy of carbon dioxide adsorption was determined using the Clausius-Clapeyron equation. Figure A17. Carbon dioxide adsorption isotherm for Cu(I)@bipy-CTF at (a) 273 K and (b) 298 K (the solid line shows the best fit to the data using the Langmuir-Freundlich equation). (c) Enthalpy of carbon dioxide adsorption was determined using the Clausius-Clapeyron equation. Figure A18. Linear fitting for (a) CO ₂ , (b) CH ₄ , and (c) N ₂ isotherms of Cu(I)@bipy-CTF was used for the calculation of Henry's selectivity constants. Table A2. Comparison of the catalytic activity of Cu(I)@bipy-CTF for carboxylative cyclization of 2-methyl-3-butyne-2-ol with the reported POP-based catalysts. Figure A19. PXRD plot of Cu(I)@bipy-CTF as-prepared (red) and recovered after eight cycles of catalysis (blue). Figure A20. FT-IR spectra of Cu(I)@bipy-CTF (a) as-prepared and (b) recovered after eight cycles of catalysis. Figure A21. SEM images of Cu(I)@bipy-CTF (a) as-prepared and (b) recovered after eight cycles of catalysis. Figure A22. FT-IR spectra of bipy-CTF (a), Cu(I)@bipy-CTF (b), 2-methyl-3-butyn-2-ol (c), Cu(I)@bipy-CTF treated with 2-methyl-3-butyn-2-ol (d), bipy-CTF treated with 2-methyl-3-butyn-2-ol (d), bipy-CTF treated with 2-methyl-3-butyn-2-ol (d), bipy-CTF treated with 2-methyl-3-butyn-2-ol (b) pipy-CTF treated with 2-methyl-3-butyn-2-ol (d), bipy-CTF treated with 2-methyl-3-butyn-2-ol (d), bipy-C	Figure A16. Carbon dioxide adsorption isotherm for bipy-CTF at	170
dioxide adsorption was determined using the Clausius-Clapeyron equation. Figure A17. Carbon dioxide adsorption isotherm for Cu(I)@bipy-CTF at (a) 273 K and (b) 298 K (the solid line shows the best fit to the data using the Langmuir-Freundlich equation). (c) Enthalpy of carbon dioxide adsorption was determined using the Clausius-Clapeyron equation. Figure A18. Linear fitting for (a) CO ₂ , (b) CH ₄ , and (c) N ₂ isotherms of Cu(I)@bipy-CTF was used for the calculation of Henry's selectivity constants. Table A2. Comparison of the catalytic activity of Cu(I)@bipyCTF for carboxylative cyclization of 2-methyl-3-butyne-2-ol with the reported POP-based catalysts. Figure A19. PXRD plot of Cu(I)@bipy-CTF as-prepared (red) and recovered after eight cycles of catalysis (blue). Figure A20. FT-IR spectra of Cu(I)@bipy-CTF (a) as-prepared and (b) recovered after eight cycles of catalysis (blue). Figure A21. SEM images of Cu(I)@bipy-CTF (a) as-prepared and (b) recovered after eight cycles of catalysis (blue). Figure A22. FT-IR spectra of bipy-CTF (a), Cu(I)@bipy-CTF (b), 2-methyl-3-butyn-2-ol (c), Cu(I)@bipy-CTF treated with 2-methyl-3-butyn-2-ol (d), bipy-CTF (d), bipy-CTF (d), bipy-CTF (d), bipy-CTF	(a) 273 K and (b) 298 K (the solid line shows the best fit to the data	
equation. Figure A17. Carbon dioxide adsorption isotherm for Cu(I)@bipy- CTF at (a) 273 K and (b) 298 K (the solid line shows the best fit to the data using the Langmuir-Freundlich equation). (c) Enthalpy of carbon dioxide adsorption was determined using the Clausius- Clapeyron equation. Figure A18. Linear fitting for (a) CO ₂ , (b) CH ₄ , and (c) N ₂ isotherms of Cu(I)@bipy-CTF was used for the calculation of Henry's selectivity constants. Table A2. Comparison of the catalytic activity of Cu(I)@bipyCTF for carboxylative cyclization of 2-methyl-3-butyne-2-ol with the reported POP-based catalysts. Figure A19. PXRD plot of Cu(I)@bipy-CTF as-prepared (red) and recovered after eight cycles of catalysis (blue). Figure A20. FT-IR spectra of Cu(I)@bipy-CTF (a) as-prepared and (b) recovered after eight cycles of catalysis. Figure A21. SEM images of Cu(I)@bipy-CTF (a) as-prepared and (b) recovered after eight cycles of catalysis. Figure A22. FT-IR spectra of bipy-CTF (a), Cu(I)@bipy-CTF (b), 2-methyl-3-butyn-2-ol (c), Cu(I)@bipy-CTF treated with 2-methyl-3-butyn-2-ol (d), bipy-CTF treated with 2-methyl-3-butyn-2-ol. Figure A23. (a) FT-IR plot of P-COF (blue), BDA (purple), and TAPP (red). (b and c) Magnified FT-IR plots of P-COF (red) and Fe(III)@P-COF (blue). Figure A24. ¹³ C CP-MAS solid-state NMR spectrum of P-COF.	using the Langmuir-Freundlich equation). (c) Enthalpy of carbon	
Figure A17. Carbon dioxide adsorption isotherm for Cu(I)@bipy- CTF at (a) 273 K and (b) 298 K (the solid line shows the best fit to the data using the Langmuir-Freundlich equation). (c) Enthalpy of carbon dioxide adsorption was determined using the Clausius-Clapeyron equation. Figure A18. Linear fitting for (a) CO ₂ , (b) CH ₄ , and (c) N ₂ isotherms of Cu(I)@bipy-CTF was used for the calculation of Henry's selectivity constants. Table A2. Comparison of the catalytic activity of Cu(I)@bipy-CTF for carboxylative cyclization of 2-methyl-3-butyne-2-ol with the reported POP-based catalysts. Figure A19. PXRD plot of Cu(I)@bipy-CTF as-prepared (red) and recovered after eight cycles of catalysis (blue). Figure A20. FT-IR spectra of Cu(I)@bipy-CTF (a) as-prepared and (b) recovered after eight cycles of catalysis. Figure A21. SEM images of Cu(I)@bipy-CTF (a) as-prepared and (b) recovered after eight cycles of catalysis. Figure A22. FT-IR spectra of bipy-CTF (a), Cu(I)@bipy-CTF (b), 2-methyl-3-butyn-2-ol (c), Cu(I)@bipy-CTF treated with 2-methyl-3-butyn-2-ol (d), bipy-CTF treated with 2-methyl-3-butyn-2-ol. Figure A23. (a) FT-IR plot of P-COF (blue), BDA (purple), and TAPP (red). (b and c) Magnified FT-IR plots of P-COF (red) and Fe(III)@P-COF (blue). Figure A24. ¹³ C CP-MAS solid-state NMR spectrum of P-COF.	dioxide adsorption was determined using the Clausius-Clapeyron	
CTF at (a) 273 K and (b) 298 K (the solid line shows the best fit to the data using the Langmuir-Freundlich equation). (c) Enthalpy of carbon dioxide adsorption was determined using the Clausius-Clapeyron equation. Figure A18. Linear fitting for (a) CO ₂ , (b) CH ₄ , and (c) N ₂ isotherms of Cu(I)@bipy-CTF was used for the calculation of Henry's selectivity constants. Table A2. Comparison of the catalytic activity of Cu(I)@bipyCTF for carboxylative cyclization of 2-methyl-3-butyne-2-ol with the reported POP-based catalysts. Figure A19. PXRD plot of Cu(I)@bipy-CTF as-prepared (red) and recovered after eight cycles of catalysis (blue). Figure A20. FT-IR spectra of Cu(I)@bipy-CTF as-prepared (red) and recovered after eight cycles of catalysis (blue). Figure A21. SEM images of Cu(I)@bipy-CTF (a) as-prepared and (b) recovered after eight cycles of catalysis. Figure A22. FT-IR spectra of bipy-CTF (a), Cu(I)@bipy-CTF (b), 2-methyl-3-butyn-2-ol (c), Cu(I)@bipy-CTF treated with 2-methyl-3-butyn-2-ol. Figure A23. (a) FT-IR plot of P-COF (blue), BDA (purple), and TAPP (red). (b and c) Magnified FT-IR plots of P-COF (red) and Fe(III)@P-COF (blue). Figure A24. ¹³ C CP-MAS solid-state NMR spectrum of P-COF.	equation.	
the data using the Langmuir-Freundlich equation). (c) Enthalpy of carbon dioxide adsorption was determined using the Clausius-Clapeyron equation. Figure A18. Linear fitting for (a) CO ₂ , (b) CH ₄ , and (c) N ₂ isotherms of Cu(I)@bipy-CTF was used for the calculation of Henry's selectivity constants. Table A2. Comparison of the catalytic activity of Cu(I)@bipyCTF for carboxylative cyclization of 2-methyl-3-butyne-2-ol with the reported POP-based catalysts. Figure A19. PXRD plot of Cu(I)@bipy-CTF as-prepared (red) and recovered after eight cycles of catalysis (blue). Figure A20. FT-IR spectra of Cu(I)@bipy-CTF as-prepared (red) and recovered after eight cycles of catalysis (blue). Figure A21. SEM images of Cu(I)@bipy-CTF (a) as-prepared and (b) recovered after eight cycles of catalysis. Figure A22. FT-IR spectra of bipy-CTF (a), Cu(I)@bipy-CTF (b), 2-methyl-3-butyn-2-ol (c), Cu(I)@bipy-CTF treated with 2-methyl-3-butyn-2-ol (d), bipy-CTF treated with 2-methyl-3-butyn-2-ol. Figure A23. (a) FT-IR plot of P-COF (blue), BDA (purple), and TAPP (red). (b and c) Magnified FT-IR plots of P-COF (red) and Fe(III)@P-COF (blue). Figure A24. ¹³ C CP-MAS solid-state NMR spectrum of P-COF.	Figure A17. Carbon dioxide adsorption isotherm for Cu(I)@bipy-	171
carbon dioxide adsorption was determined using the Clausius-Clapeyron equation. Figure A18. Linear fitting for (a) CO ₂ , (b) CH ₄ , and (c) N ₂ isotherms of Cu(I)@bipy-CTF was used for the calculation of Henry's selectivity constants. Table A2. Comparison of the catalytic activity of Cu(I)@bipyCTF for carboxylative cyclization of 2-methyl-3-butyne-2-ol with the reported POP-based catalysts. Figure A19. PXRD plot of Cu(I)@bipy-CTF as-prepared (red) and recovered after eight cycles of catalysis (blue). Figure A20. FT-IR spectra of Cu(I)@bipy-CTF as-prepared (red) and recovered after eight cycles of catalysis (blue). Figure A21. SEM images of Cu(I)@bipy-CTF (a) as-prepared and (b) recovered after eight cycles of catalysis. Figure A22. FT-IR spectra of bipy-CTF (a), Cu(I)@bipy-CTF (b), 2-methyl-3-butyn-2-ol (c), Cu(I)@bipy-CTF treated with 2-methyl- 3-butyn-2-ol (d), bipy-CTF treated with 2-methyl-3-butyn-2-ol. Figure A23. (a) FT-IR plot of P-COF (blue), BDA (purple), and TAPP (red). (b and c) Magnified FT-IR plots of P-COF (red) and Fe(III)@P-COF (blue). Figure A24. ¹³ C CP-MAS solid-state NMR spectrum of P-COF.	CTF at (a) 273 K and (b) 298 K (the solid line shows the best fit to	
Clapeyron equation. Figure A18. Linear fitting for (a) CO ₂ , (b) CH ₄ , and (c) N ₂ isotherms of Cu(I)@bipy-CTF was used for the calculation of Henry's selectivity constants. Table A2. Comparison of the catalytic activity of Cu(I)@bipyCTF for carboxylative cyclization of 2-methyl-3-butyne-2-ol with the reported POP-based catalysts. Figure A19. PXRD plot of Cu(I)@bipy-CTF as-prepared (red) and recovered after eight cycles of catalysis (blue). Figure A20. FT-IR spectra of Cu(I)@bipy-CTF as-prepared (red) and recovered after eight cycles of catalysis (blue). Figure A21. SEM images of Cu(I)@bipy-CTF (a) as-prepared and (b) recovered after eight cycles of catalysis. Figure A22. FT-IR spectra of bipy-CTF (a), Cu(I)@bipy-CTF (b), 2-methyl-3-butyn-2-ol (c), Cu(I)@bipy-CTF treated with 2-methyl- 3-butyn-2-ol (d), bipy-CTF treated with 2-methyl-3-butyn-2-ol. Figure A23. (a) FT-IR plot of P-COF (blue), BDA (purple), and TAPP (red). (b and c) Magnified FT-IR plots of P-COF (red) and Fe(III)@P-COF (blue). Figure A24. ¹³ C CP-MAS solid-state NMR spectrum of P-COF.	the data using the Langmuir-Freundlich equation). (c) Enthalpy of	
Figure A18. Linear fitting for (a) CO ₂ , (b) CH ₄ , and (c) N ₂ isotherms of Cu(I)@bipy-CTF was used for the calculation of Henry's selectivity constants. Table A2. Comparison of the catalytic activity of Cu(I)@bipyCTF for carboxylative cyclization of 2-methyl-3-butyne-2-ol with the reported POP-based catalysts. Figure A19. PXRD plot of Cu(I)@bipy-CTF as-prepared (red) and recovered after eight cycles of catalysis (blue). Figure A20. FT-IR spectra of Cu(I)@bipy-CTF as-prepared (red) and recovered after eight cycles of catalysis (blue). Figure A21. SEM images of Cu(I)@bipy-CTF (a) as-prepared and (b) recovered after eight cycles of catalysis. Figure A22. FT-IR spectra of bipy-CTF (a), Cu(I)@bipy-CTF (b), 2-methyl-3-butyn-2-ol (c), Cu(I)@bipy-CTF treated with 2-methyl- 3-butyn-2-ol (d), bipy-CTF treated with 2-methyl-3-butyn-2-ol. Figure A23. (a) FT-IR plot of P-COF (blue), BDA (purple), and TAPP (red). (b and c) Magnified FT-IR plots of P-COF (red) and Fe(III)@P-COF (blue). Figure A24. ¹³ C CP-MAS solid-state NMR spectrum of P-COF.	carbon dioxide adsorption was determined using the Clausius-	
isotherms of Cu(I)@bipy-CTF was used for the calculation of Henry's selectivity constants. Table A2. Comparison of the catalytic activity of Cu(I)@bipyCTF for carboxylative cyclization of 2-methyl-3-butyne-2-ol with the reported POP-based catalysts. Figure A19. PXRD plot of Cu(I)@bipy-CTF as-prepared (red) and recovered after eight cycles of catalysis (blue). Figure A20. FT-IR spectra of Cu(I)@bipy-CTF as-prepared (red) and recovered after eight cycles of catalysis (blue). Figure A21. SEM images of Cu(I)@bipy-CTF (a) as-prepared and (b) recovered after eight cycles of catalysis. Figure A22. FT-IR spectra of bipy-CTF (a), Cu(I)@bipy-CTF (b), 2-methyl-3-butyn-2-ol (c), Cu(I)@bipy-CTF treated with 2-methyl- 3-butyn-2-ol (d), bipy-CTF treated with 2-methyl-3-butyn-2-ol. Figure A23. (a) FT-IR plot of P-COF (blue), BDA (purple), and TAPP (red). (b and c) Magnified FT-IR plots of P-COF (red) and Fe(III)@P-COF (blue). Figure A24. ¹³ C CP-MAS solid-state NMR spectrum of P-COF.	Clapeyron equation.	
Henry's selectivity constants. Table A2. Comparison of the catalytic activity of Cu(I)@bipyCTF 172 for carboxylative cyclization of 2-methyl-3-butyne-2-ol with the reported POP-based catalysts. Figure A19. PXRD plot of Cu(I)@bipy-CTF as-prepared (red) and recovered after eight cycles of catalysis (blue). Figure A20. FT-IR spectra of Cu(I)@bipy-CTF as-prepared (red) and recovered after eight cycles of catalysis (blue). Figure A21. SEM images of Cu(I)@bipy-CTF (a) as-prepared and (b) recovered after eight cycles of catalysis. Figure A22. FT-IR spectra of bipy-CTF (a), Cu(I)@bipy-CTF (b), 2-methyl-3-butyn-2-ol (c), Cu(I)@bipy-CTF treated with 2-methyl-3-butyn-2-ol (d), bipy-CTF treated with 2-methyl-3-butyn-2-ol. Figure A23. (a) FT-IR plot of P-COF (blue), BDA (purple), and TAPP (red). (b and c) Magnified FT-IR plots of P-COF (red) and Fe(III)@P-COF (blue). Figure A24. ¹³ C CP-MAS solid-state NMR spectrum of P-COF.	Figure A18. Linear fitting for (a) CO ₂ , (b) CH ₄ , and (c) N ₂	172
Table A2. Comparison of the catalytic activity of Cu(I)@bipyCTF for carboxylative cyclization of 2-methyl-3-butyne-2-ol with the reported POP-based catalysts. Figure A19. PXRD plot of Cu(I)@bipy-CTF as-prepared (red) and recovered after eight cycles of catalysis (blue). Figure A20. FT-IR spectra of Cu(I)@bipy-CTF as-prepared (red) and recovered after eight cycles of catalysis (blue). Figure A21. SEM images of Cu(I)@bipy-CTF (a) as-prepared and (b) recovered after eight cycles of catalysis. Figure A22. FT-IR spectra of bipy-CTF (a), Cu(I)@bipy-CTF (b), 2-methyl-3-butyn-2-ol (c), Cu(I)@bipy-CTF treated with 2-methyl-3-butyn-2-ol. Figure A23. (a) FT-IR plot of P-COF (blue), BDA (purple), and TAPP (red). (b and c) Magnified FT-IR plots of P-COF (red) and Fe(III)@P-COF (blue). Figure A24. ¹³ C CP-MAS solid-state NMR spectrum of P-COF.	isotherms of Cu(I)@bipy-CTF was used for the calculation of	
for carboxylative cyclization of 2-methyl-3-butyne-2-ol with the reported POP-based catalysts. Figure A19. PXRD plot of Cu(I)@bipy-CTF as-prepared (red) and recovered after eight cycles of catalysis (blue). Figure A20. FT-IR spectra of Cu(I)@bipy-CTF as-prepared (red) and recovered after eight cycles of catalysis (blue). Figure A21. SEM images of Cu(I)@bipy-CTF (a) as-prepared and (b) recovered after eight cycles of catalysis. Figure A22. FT-IR spectra of bipy-CTF (a), Cu(I)@bipy-CTF (b), 2-methyl-3-butyn-2-ol (c), Cu(I)@bipy-CTF treated with 2-methyl-3-butyn-2-ol (d), bipy-CTF treated with 2-methyl-3-butyn-2-ol. Figure A23. (a) FT-IR plot of P-COF (blue), BDA (purple), and TAPP (red). (b and c) Magnified FT-IR plots of P-COF (red) and Fe(III)@P-COF (blue). Figure A24. ¹³ C CP-MAS solid-state NMR spectrum of P-COF.	Henry's selectivity constants.	
reported POP-based catalysts. Figure A19. PXRD plot of Cu(I)@bipy-CTF as-prepared (red) and recovered after eight cycles of catalysis (blue). Figure A20. FT-IR spectra of Cu(I)@bipy-CTF as-prepared (red) 173 and recovered after eight cycles of catalysis (blue). Figure A21. SEM images of Cu(I)@bipy-CTF (a) as-prepared and (b) recovered after eight cycles of catalysis. Figure A22. FT-IR spectra of bipy-CTF (a), Cu(I)@bipy-CTF (b), 2-methyl-3-butyn-2-ol (c), Cu(I)@bipy-CTF treated with 2-methyl-3-butyn-2-ol. Figure A23. (a) FT-IR plot of P-COF (blue), BDA (purple), and 175 TAPP (red). (b and c) Magnified FT-IR plots of P-COF (red) and Fe(III)@P-COF (blue). Figure A24. ¹³ C CP-MAS solid-state NMR spectrum of P-COF. 175	Table A2. Comparison of the catalytic activity of Cu(I)@bipyCTF	172
Figure A19. PXRD plot of Cu(I)@bipy-CTF as-prepared (red) and recovered after eight cycles of catalysis (blue). Figure A20. FT-IR spectra of Cu(I)@bipy-CTF as-prepared (red) and recovered after eight cycles of catalysis (blue). Figure A21. SEM images of Cu(I)@bipy-CTF (a) as-prepared and (b) recovered after eight cycles of catalysis. Figure A22. FT-IR spectra of bipy-CTF (a), Cu(I)@bipy-CTF (b), 2-methyl-3-butyn-2-ol (c), Cu(I)@bipy-CTF treated with 2-methyl-3-butyn-2-ol (d), bipy-CTF treated with 2-methyl-3-butyn-2-ol. Figure A23. (a) FT-IR plot of P-COF (blue), BDA (purple), and TAPP (red). (b and c) Magnified FT-IR plots of P-COF (red) and Fe(III)@P-COF (blue). Figure A24. ¹³ C CP-MAS solid-state NMR spectrum of P-COF.	for carboxylative cyclization of 2-methyl-3-butyne-2-ol with the	
recovered after eight cycles of catalysis (blue). Figure A20. FT-IR spectra of Cu(I)@bipy-CTF as-prepared (red) and recovered after eight cycles of catalysis (blue). Figure A21. SEM images of Cu(I)@bipy-CTF (a) as-prepared and (b) recovered after eight cycles of catalysis. Figure A22. FT-IR spectra of bipy-CTF (a), Cu(I)@bipy-CTF (b), 2-methyl-3-butyn-2-ol (c), Cu(I)@bipy-CTF treated with 2-methyl-3-butyn-2-ol (d), bipy-CTF treated with 2-methyl-3-butyn-2-ol. Figure A23. (a) FT-IR plot of P-COF (blue), BDA (purple), and TAPP (red). (b and c) Magnified FT-IR plots of P-COF (red) and Fe(III)@P-COF (blue). Figure A24. ¹³ C CP-MAS solid-state NMR spectrum of P-COF.	reported POP-based catalysts.	
Figure A20. FT-IR spectra of Cu(I)@bipy-CTF as-prepared (red) and recovered after eight cycles of catalysis (blue). Figure A21. SEM images of Cu(I)@bipy-CTF (a) as-prepared and (b) recovered after eight cycles of catalysis. Figure A22. FT-IR spectra of bipy-CTF (a), Cu(I)@bipy-CTF (b), 2-methyl-3-butyn-2-ol (c), Cu(I)@bipy-CTF treated with 2-methyl-3-butyn-2-ol (d), bipy-CTF treated with 2-methyl-3-butyn-2-ol. Figure A23. (a) FT-IR plot of P-COF (blue), BDA (purple), and TAPP (red). (b and c) Magnified FT-IR plots of P-COF (red) and Fe(III)@P-COF (blue). Figure A24. ¹³ C CP-MAS solid-state NMR spectrum of P-COF.	Figure A19. PXRD plot of Cu(I)@bipy-CTF as-prepared (red) and	173
and recovered after eight cycles of catalysis (blue). Figure A21. SEM images of Cu(I)@bipy-CTF (a) as-prepared and (b) recovered after eight cycles of catalysis. Figure A22. FT-IR spectra of bipy-CTF (a), Cu(I)@bipy-CTF (b), 2-methyl-3-butyn-2-ol (c), Cu(I)@bipy-CTF treated with 2-methyl-3-butyn-2-ol (d), bipy-CTF treated with 2-methyl-3-butyn-2-ol. Figure A23. (a) FT-IR plot of P-COF (blue), BDA (purple), and TAPP (red). (b and c) Magnified FT-IR plots of P-COF (red) and Fe(III)@P-COF (blue). Figure A24. ¹³ C CP-MAS solid-state NMR spectrum of P-COF.	recovered after eight cycles of catalysis (blue).	
Figure A21. SEM images of Cu(I)@bipy-CTF (a) as-prepared and (b) recovered after eight cycles of catalysis. Figure A22. FT-IR spectra of bipy-CTF (a), Cu(I)@bipy-CTF (b), 2-methyl-3-butyn-2-ol (c), Cu(I)@bipy-CTF treated with 2-methyl-3-butyn-2-ol (d), bipy-CTF treated with 2-methyl-3-butyn-2-ol. Figure A23. (a) FT-IR plot of P-COF (blue), BDA (purple), and TAPP (red). (b and c) Magnified FT-IR plots of P-COF (red) and Fe(III)@P-COF (blue). Figure A24. ¹³ C CP-MAS solid-state NMR spectrum of P-COF.	Figure A20. FT-IR spectra of Cu(I)@bipy-CTF as-prepared (red)	173
(b) recovered after eight cycles of catalysis. Figure A22. FT-IR spectra of bipy-CTF (a), Cu(I)@bipy-CTF (b), 2-methyl-3-butyn-2-ol (c), Cu(I)@bipy-CTF treated with 2-methyl- 3-butyn-2-ol (d), bipy-CTF treated with 2-methyl-3-butyn-2-ol. Figure A23. (a) FT-IR plot of P-COF (blue), BDA (purple), and TAPP (red). (b and c) Magnified FT-IR plots of P-COF (red) and Fe(III)@P-COF (blue). Figure A24. ¹³ C CP-MAS solid-state NMR spectrum of P-COF.	and recovered after eight cycles of catalysis (blue).	
Figure A22. FT-IR spectra of bipy-CTF (a), Cu(I)@bipy-CTF (b), 2-methyl-3-butyn-2-ol (c), Cu(I)@bipy-CTF treated with 2-methyl- 3-butyn-2-ol (d), bipy-CTF treated with 2-methyl-3-butyn-2-ol. Figure A23. (a) FT-IR plot of P-COF (blue), BDA (purple), and TAPP (red). (b and c) Magnified FT-IR plots of P-COF (red) and Fe(III)@P-COF (blue). Figure A24. ¹³ C CP-MAS solid-state NMR spectrum of P-COF.	Figure A21. SEM images of Cu(I)@bipy-CTF (a) as-prepared and	174
2-methyl-3-butyn-2-ol (c), Cu(I)@bipy-CTF treated with 2-methyl-3-butyn-2-ol. Figure A23. (a) FT-IR plot of P-COF (blue), BDA (purple), and TAPP (red). (b and c) Magnified FT-IR plots of P-COF (red) and Fe(III)@P-COF (blue). Figure A24. ¹³ C CP-MAS solid-state NMR spectrum of P-COF.	(b) recovered after eight cycles of catalysis.	
3-butyn-2-ol (d), bipy-CTF treated with 2-methyl-3-butyn-2-ol. Figure A23. (a) FT-IR plot of P-COF (blue), BDA (purple), and TAPP (red). (b and c) Magnified FT-IR plots of P-COF (red) and Fe(III)@P-COF (blue). Figure A24. ¹³ C CP-MAS solid-state NMR spectrum of P-COF.	Figure A22. FT-IR spectra of bipy-CTF (a), Cu(I)@bipy-CTF (b),	174
Figure A23. (a) FT-IR plot of P-COF (blue), BDA (purple), and TAPP (red). (b and c) Magnified FT-IR plots of P-COF (red) and Fe(III)@P-COF (blue). Figure A24. ¹³ C CP-MAS solid-state NMR spectrum of P-COF. 175	2-methyl-3-butyn-2-ol (c), Cu(I)@bipy-CTF treated with 2-methyl-	
TAPP (red). (b and c) Magnified FT-IR plots of P-COF (red) and Fe(III)@P-COF (blue). Figure A24. ¹³ C CP-MAS solid-state NMR spectrum of P-COF. 175	3-butyn-2-ol (d), bipy-CTF treated with 2-methyl-3-butyn-2-ol.	
Fe(III)@P-COF (blue). Figure A24. ¹³ C CP-MAS solid-state NMR spectrum of P-COF. 175	Figure A23. (a) FT-IR plot of P-COF (blue), BDA (purple), and	175
Figure A24. ¹³ C CP-MAS solid-state NMR spectrum of P-COF. 175	TAPP (red). (b and c) Magnified FT-IR plots of P-COF (red) and	
-	Fe(III)@P-COF (blue).	
Figure A25 EDS plot of D COE	Figure A24. ¹³ C CP-MAS solid-state NMR spectrum of P-COF.	175
rigure A23. ED3 plot of r-COr.	Figure A25. EDS plot of P-COF.	176

	77
content in M@D COE (M	
content in M@P-COF ($M = Fe(III)$ (a), $Fe(II)$ (b), and $Zn(II)$ (c).	
Figure A28. XPS plot of P-COF, (a) survey spectrum (b) N1s.	77
Figure A29. FT-IR (a) and PXRD (b) plots of P-COF (I),	78
Zn(II)@P-COF (II), and Fe(II)@P-COF (III).	
Figure A30. Carbon dioxide adsorption isotherm for P-COF at (a)	78
273 K and (b) 298 K and Fe(III)@P-COF at (c) 273 K and (d) 298	
K. (The solid line shows the best fit to the data using the Langmuir-	
Freundlich equation).	
Figure A31. Enthalpy of carbon dioxide adsorption for Fe(III)@P-	79
COF was calculated by using the Clausius-Clapeyron equation.	
Table A3: Comparison of catalytic activity of Fe(III)@P-COF with 18	80
the reported examples of heterogeneous catalysts known for	
epoxidation of styrene.	
Table A4: Comparison of catalytic activity of Fe(III)@P-COF with 18	81
the reported examples of heterogeneous catalysts known for the	
one-pot oxidative carboxylation of styrene.	
Figure A32. FT-IR spectra of P-COF (a), Fe(III)@P-COF (b),	82
styrene oxide (c), Fe(III)@P-COF treated with styrene oxide (d) P-	
COF treated with styrene oxide (e).	
Figure A33. FT-IR plot of Fe(III)@P-COF before (red) and after	82
catalysis (blue).	
Figure A34. SEM images of as-synthesized (a) and recycled (b)	83
Fe(III)@P-COF.	
Figure A35. ¹ H NMR (400 MHz, CDCl ₃ , 20 °C) stack plot for 18	83
direct oxidative carboxylation of styrene catalyzed by the	
Fe(III)@P-COF at different time intervals (* peak due to TBAB).	
Figure A36. (a) FT-IR stack plot for PyNH ₂ (pink), bpyCHO (red), 18	84
and Pybpy-COF (blue). (b) FT-IR stack plot of Pybpy-COF (I) and	
Ag@Pybpy-COF (II).	
Figure A37. EDS plot of Pybpy-COF (a) and Ag@Pybpy-COF (b).	85
Figure A38. Elemental mapping of Pybpy-COF and Ag@Pybpy- 18	85

COF (a and b), C (red), N (green), and Ag (light blue), respectively.	
Figure A39. MP-AES calibration curve for Ag@Pybpy-COF.	186
Figure A40. Carbon dioxide adsorption isotherms of Pybpy-COF	186
carried out at 273 K, and 298 K (a and b) (the solid line shows the	
best fit to the data using the Langmuir-Freundlich equation). (c) The	
enthalpy of carbon dioxide adsorption determined using the	
Clausius-Clapeyron equation.	
Figure A41. Carbon dioxide adsorption isotherms for Ag@Pybpy-	187
COF performed at 273 K and 298 K (a and b) (the solid line shows	
the best fit to the data using the Langmuir-Freundlich equation). (c)	
The enthalpy of carbon dioxide adsorption determined using the	
Clausius-Clapeyron equation.	
Figure A42. Linear fitting of CO ₂ , N ₂ , and CH ₄ isotherms of	188
Ag@Pybpy-COF used for calculation of Henry's selectivity	
constants.	
Table A5: Comparison of catalytic activity of Ag@Pybpy-COF	188
with previously reported heterogeneous catalysts for the	
carboxylation of terminal alkynes.	
Figure A43. (a) FT-IR stack plot of Pybpy-COF (I), Ag@Pybpy-	189
COF (II), ethynylbenzene (III), Ag@Pybpy-COF treated with	
ethynylbenzene (IV). (b) Magnified view of the selected region of	
FT-IR stack plot.	
Figure A44. Optimized structures of the intermediates and	189
transition state (TS) in the catalytic carboxylation of terminal alkyls	
with CO ₂ catalyzed by Ag@Pybpy-COF (bond distances are in Å).	
Table A6: Comparison of catalytic activity of Ag@Pybpy-COF	190
with previously reported heterogeneous catalysts for the	
carboxylative cyclization of propargylic amines.	
Figure A45. FT-IR stack plot of Pybpy-COF (I), Ag@Pybpy-COF	191
(II), N-benzylprop-2-yn-1-amine (III), Ag@Pybpy-COF treated	
with N-benzylprop-2-yn-1-amine (IV).	
Figure A46. Optimized structures of intermediates and transition	191
state in the catalytic carboxylative cyclization of propargylic amines	

with CO ₂ catalyzed by Ag@Pybpy-COF (bond distances are in Å).		
Figure A47. PXRD spectra of Ag@Pybpy-COF (I) and recycled	192	
catalyst (II) after catalysis.		
Figure A48. FT-IR spectra of Ag@Pybpy-COF (I) and recycled	192	
catalyst (II) after catalysis.		
Figure A49. Elemental mapping for Ag@Pybpy-COF recycled after	193	
five cycles of catalysis, C (red), N (green), and Ag (light blue).		

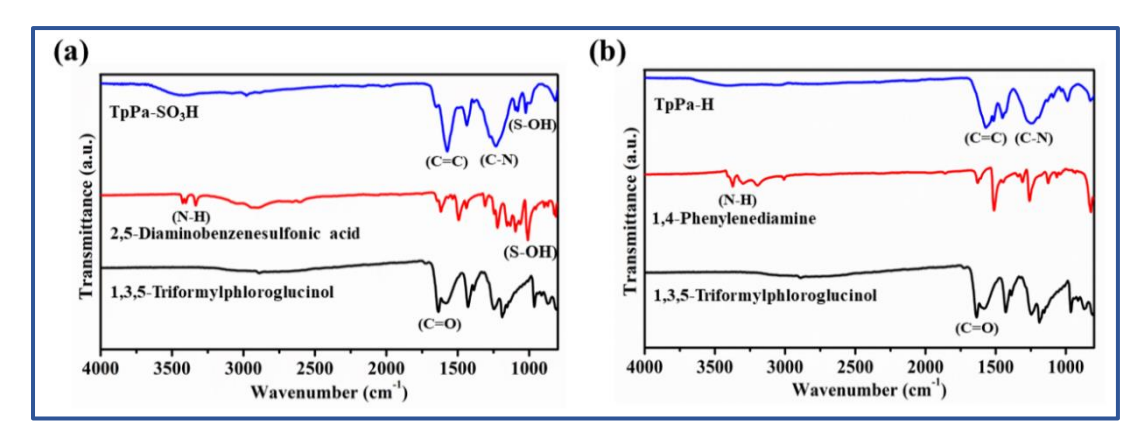


Figure A1. FT-IR spectra of (a) 1,3,5-Triformylphloroglucinol (black line) 2,5-diaminobenzenesulfonic acid (red line) and COF-SO₃H (blue line). (b) FT-IR spectra of 1,3,5-Triformylphloroglucinol (black line), 1,4-phenylenediamine (red line) and COF-H (blue line).

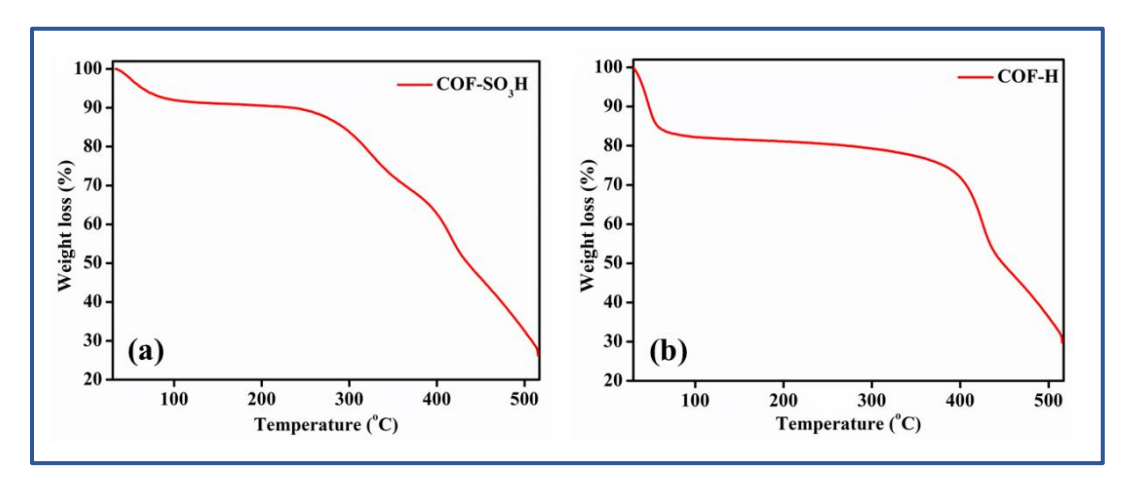


Figure A2. TGA plot of (a) COF-SO₃H and (b) COF-H.

Analysis of gas adsorption isotherms

Clausius-Clapeyron equation¹ was used to calculate the enthalpies of carbon dioxide adsorption and by using the Langmuir Freundlich equation² an accurate fit was retrieved to get a precise prediction of CO₂ adsorbed at saturation. A modification of the Clausius-Clapeyron equation was used for the calculations.

$$ln(P1/P2) = \Delta H_{ads}(T2 - T1/R.T1.T2).....(i)$$

where P_1 and P_2 = Pressures for isotherm at 273 K and 298 K, respectively.

 T_1 and T_2 = Temperatures for isotherm at 273 K and 298 K, respectively.

 ΔH_{ads} = Enthalpy of adsorption.

R = Universal gas constant = 8.314 J/K/mol).

The pressure is a function of the amount of gas adsorbed which was determined by

using Langmuir-Freundlich fit.

$$Q/Q_m = B.P^{(1/t)}/1 + (B.P^{(1/t)}).....$$
 (ii)

where Q = moles of gas adsorbed.

 Q_m = moles of gas adsorbed at saturation.

B and t = constants.

P = Pressure.

By rearranging equation (ii) we get equation (iii)

$$P = [(Q/Q_m)/\{B - (B.(Q/Q_m)\}]^t.....(iii)$$

Substituting equation (iii) into equation (i) we get

$$\Delta H_{ads} = \{\text{R.T1.T2/(T2-T1)}\}. \ln \frac{[(\text{Q/Q}_{\text{m1}})/\{\text{B-(B.Q/Q}_{\text{m1}})\}]^{\text{t1}}}{[(\text{Q/Q}_{\text{m2}})/\{\text{B-(B.Q/Q}_{\text{m2}})\}]^{\text{t2}}}......(iv)$$

In equation (iv), subscripts 1 and 2 represent data corresponding to 273 K and 298 K, respectively.

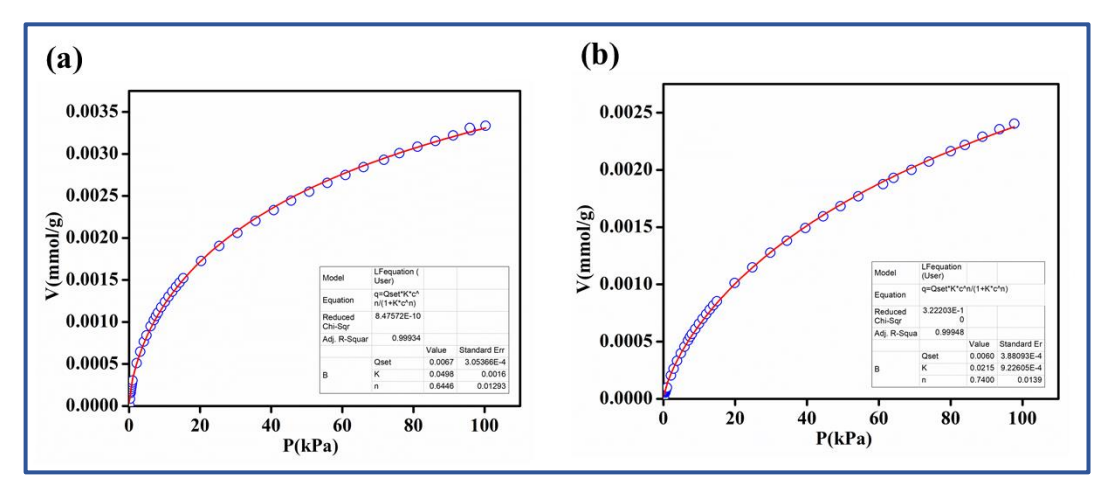


Figure A3. Carbon dioxide adsorption isotherm for COF-SO₃H at (a) 273 K and (b) 298 K. (the solid line shows the best fit to the data using the Langmuir-Freundlich equation).

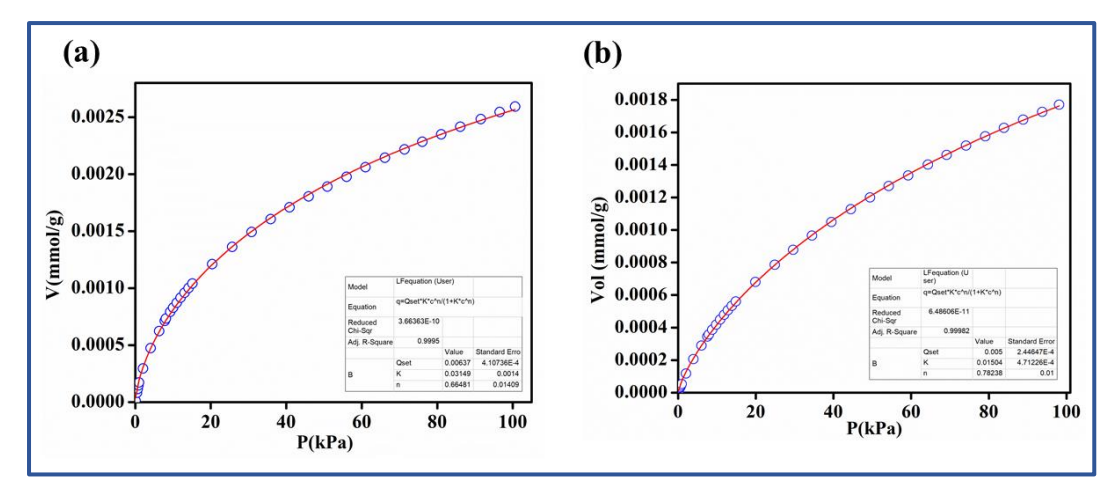


Figure A4. Carbon dioxide adsorption isotherm for COF-H at (a) 273 K and (b) 298 K. (the solid line shows the best fit to the data using the Langmuir-Freundlich equation).

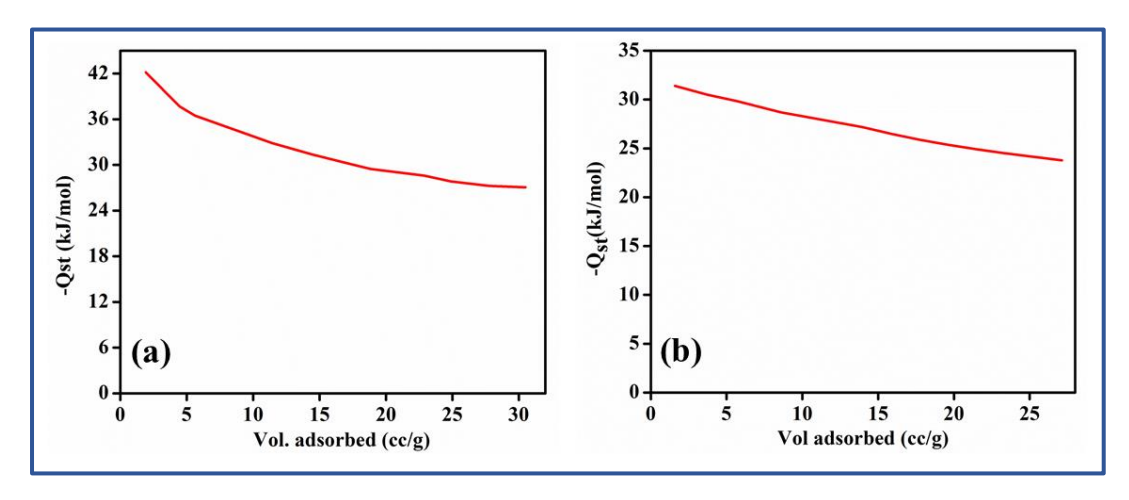


Figure A5. Enthalpy of carbon dioxide adsorption for (a) COF-SO₃H and (b) COF-H calculated using Clausius-Clapeyron equation calculations.

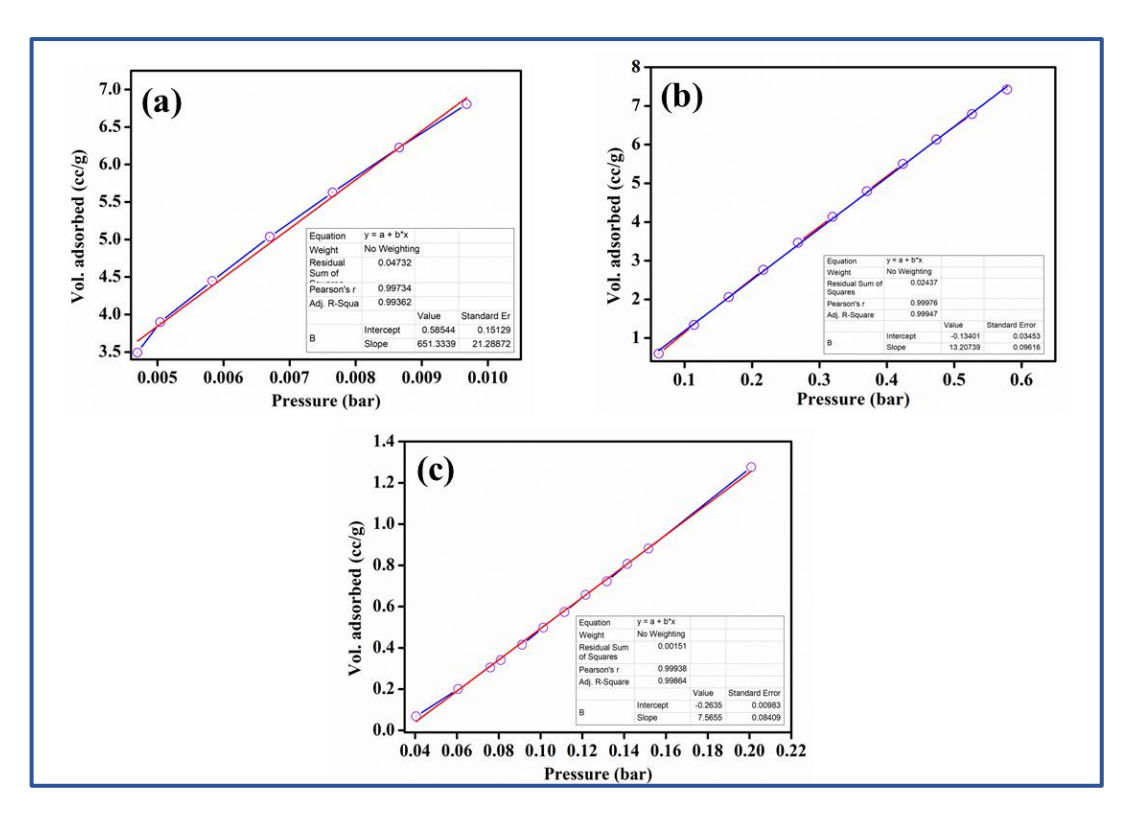


Figure A6. Linear fitting of CO₂, CH₄, and N₂ isotherms of COF-SO₃H used for calculation of Henry's selectivity constants.

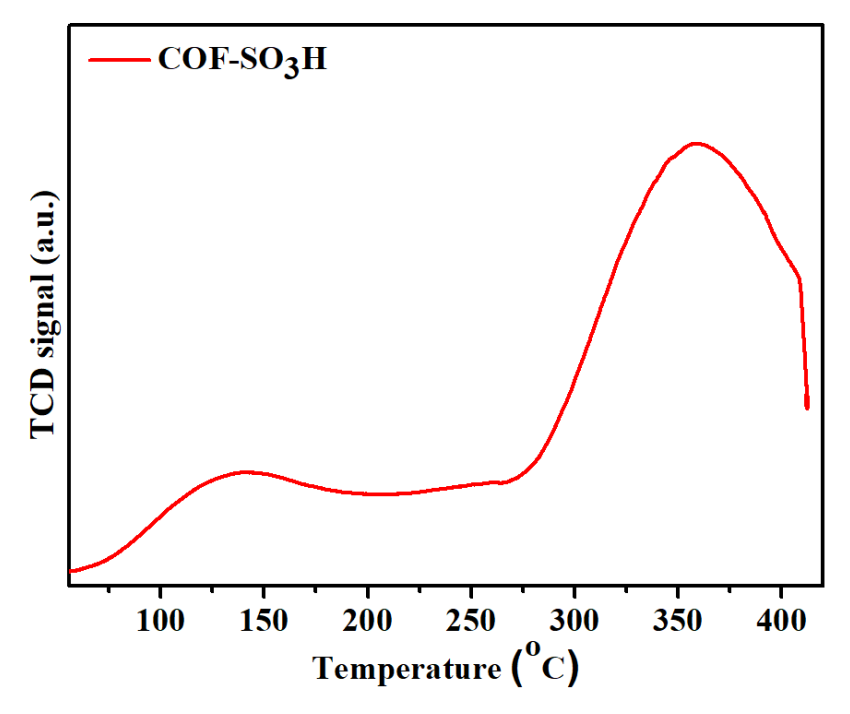


Figure A7. NH₃ TPD plot of COF-SO₃H.

Table A1. Comparison of the catalytic activity of COF-SO₃H for cycloaddition of CO₂ with epichlorohydrin to produce cyclic carbonate.

S. No.	Catalyst	Active sites	Pressure (bar)	Conversion (%)	References
1.	COF-JLU7	-ОН	01	92	3
2.	COF-salen-Co	Co(II)	20	91	4
3.	COF1/ZnBr ₂	Zn(II)	01	>99	5
4.	COF-366-Zn	Zn(II)	15	71.2	6
5.	2,3-DhaTph COF	-OH	01	77	7
6.	Co/TPA- TCIF(BD)	Co(II)	5	95.1	8
7.	Cu/POP-Bpy	Cu(II)	01	59.2	9
8.	Zn/POP-Bpy	Zn(II)	01	58.1	9
9.	Co/POP-Bpy	Co(II)	01	50.3	9
10.	PAF	Zn(II)	10	73	10
11.	1-Co	Co (III)	20	88	11
12.	1-Cr	Cr (III)	20	95	11
13.	COF-SO ₃ H	-SO ₃ H	01	>99	This work

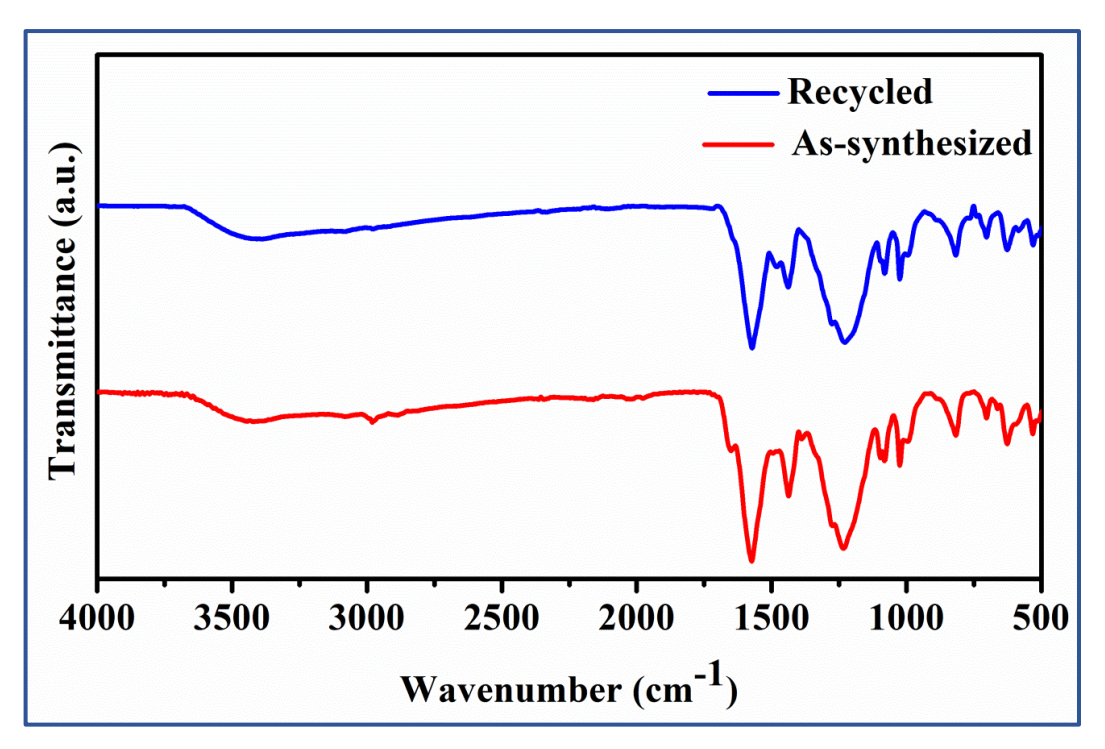


Figure A8. FT-IR spectra of COF-SO₃H recovered after five cycles of catalysis.

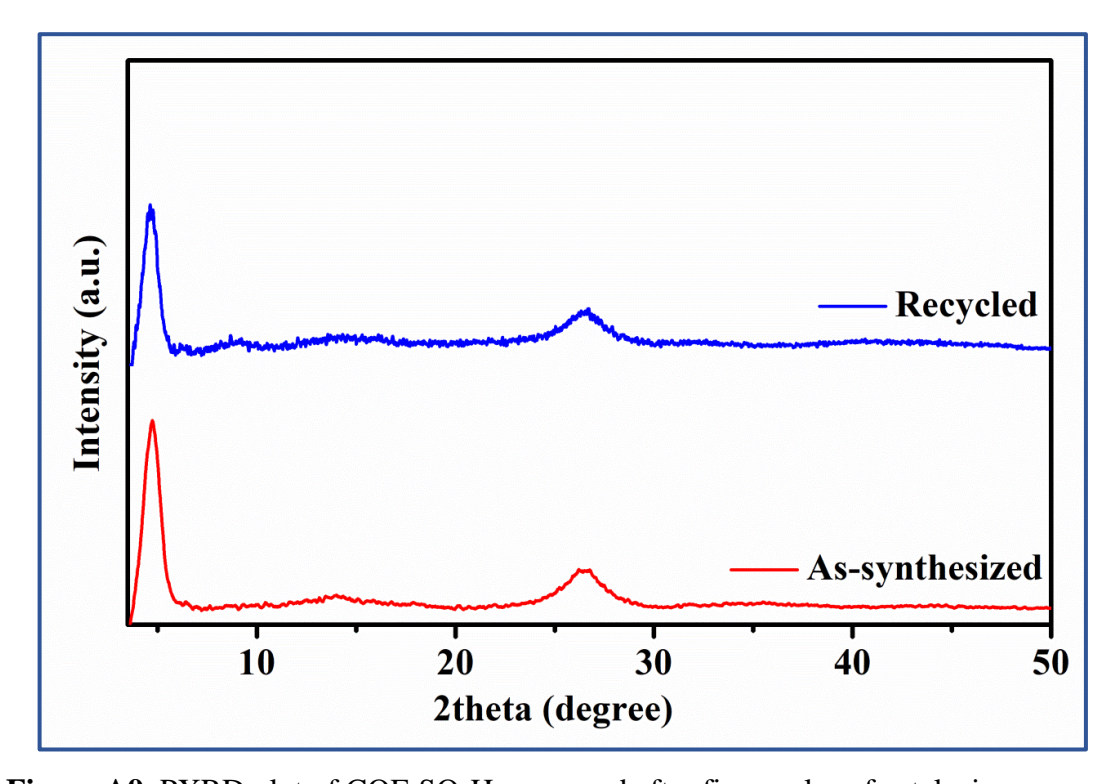


Figure A9. PXRD plot of COF-SO₃H recovered after five cycles of catalysis.

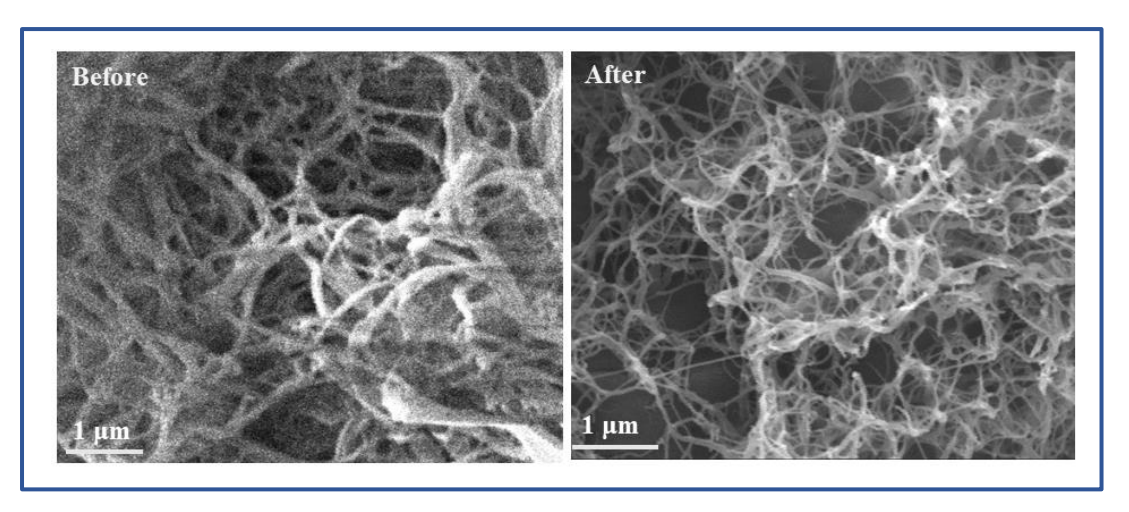


Figure A10. SEM images of COF-SO₃H before and after catalysis.

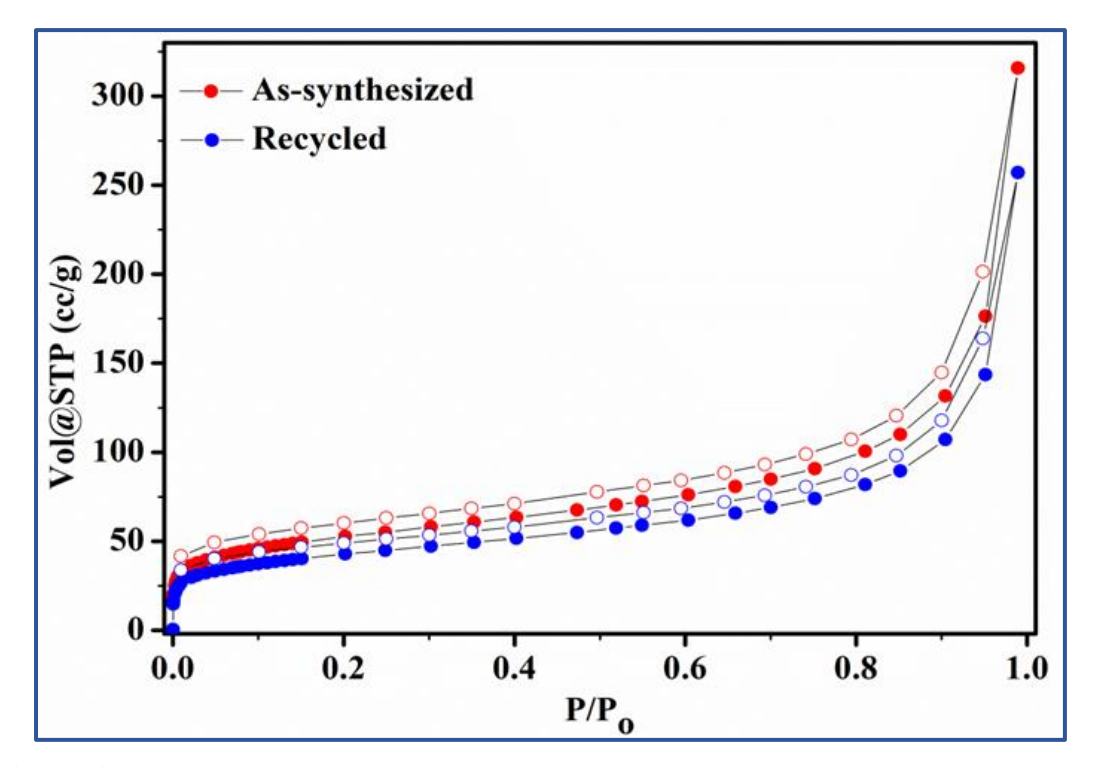


Figure A11. N₂ adsorption isotherm of COF-SO₃H before and after catalysis.

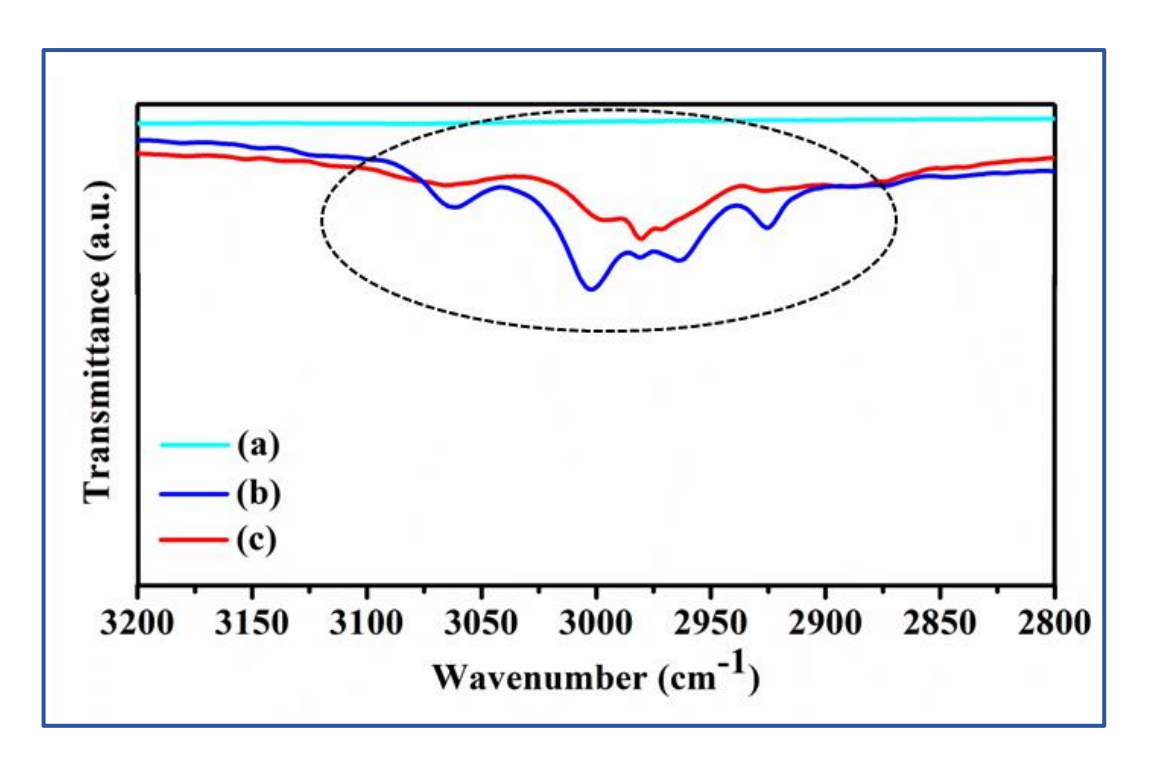


Figure A12. FT-IR spectra of (a) COF-SO₃H (b) epichlorohydrin and (c) COF-SO₃H treated with epichlorohydrin.

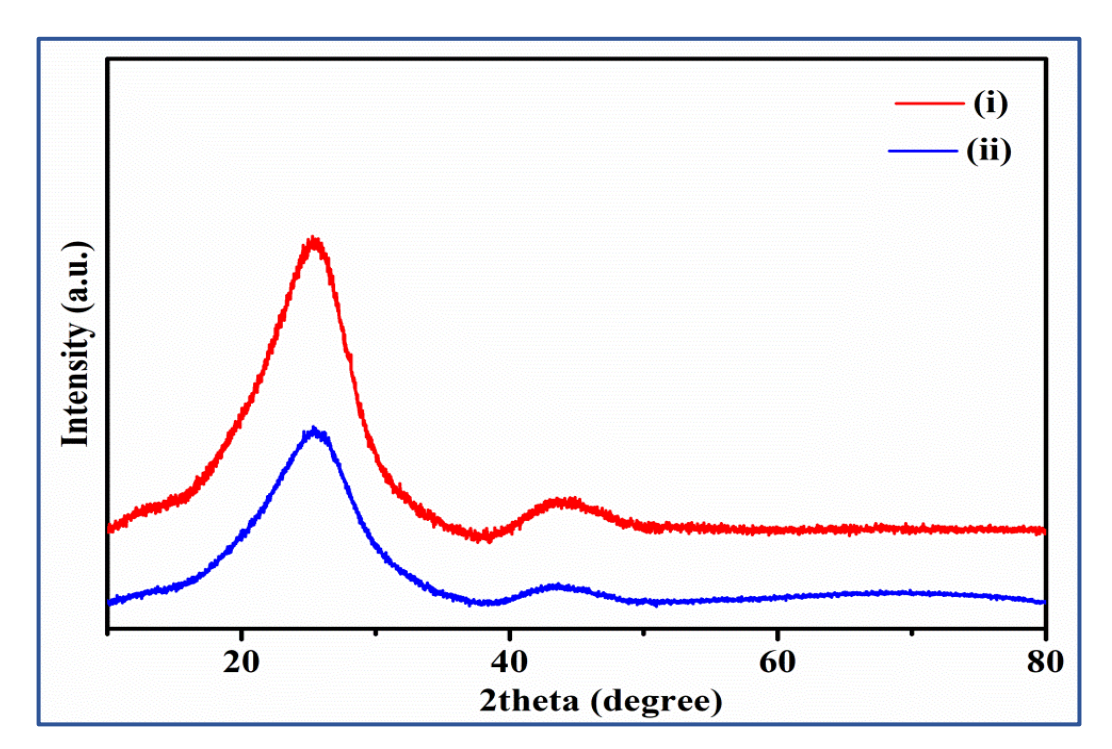


Figure A13. PXRD pattern of bipy-CTF (i) and Cu(I)@bipy-CTF (ii).

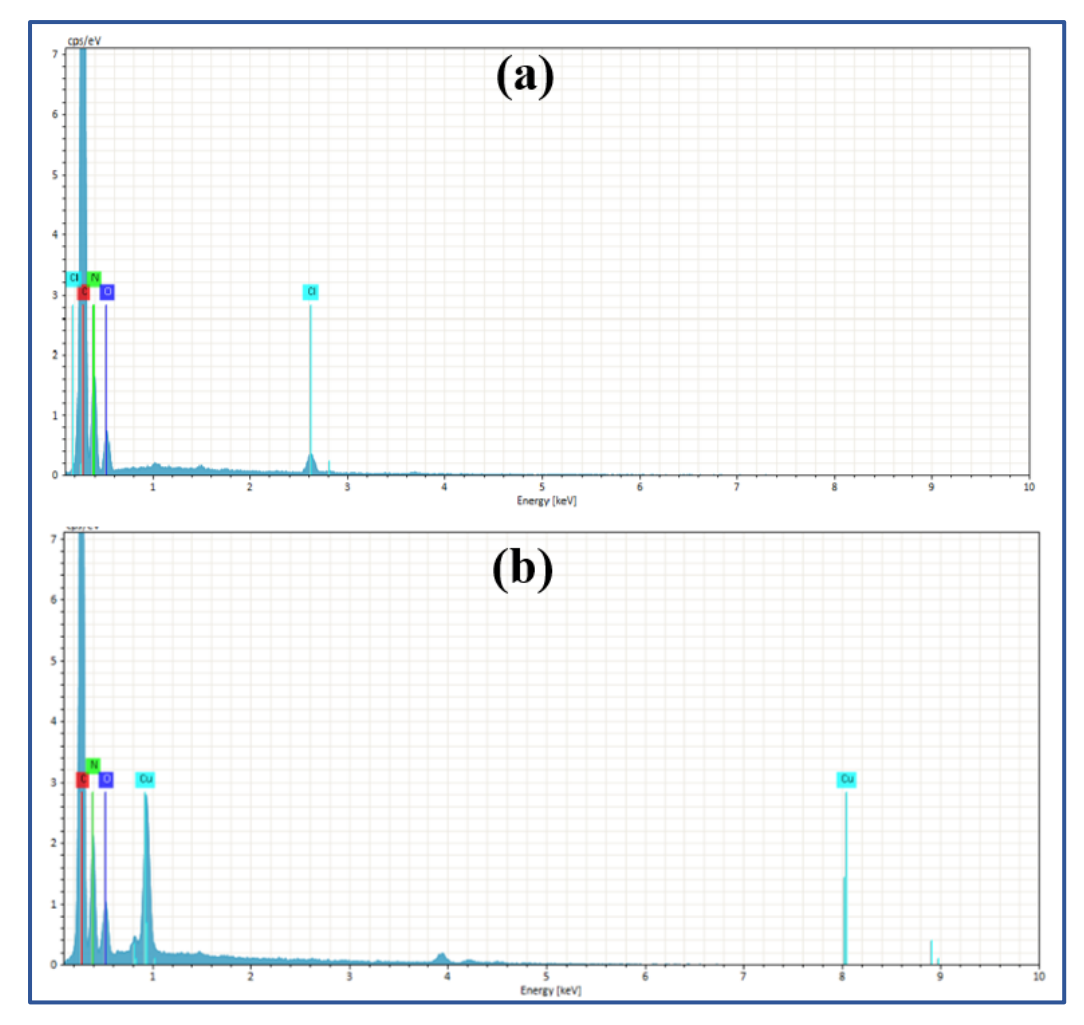


Figure A14. EDS plot of bipy-CTF (a) and Cu(I)@bipy-CTF (b).

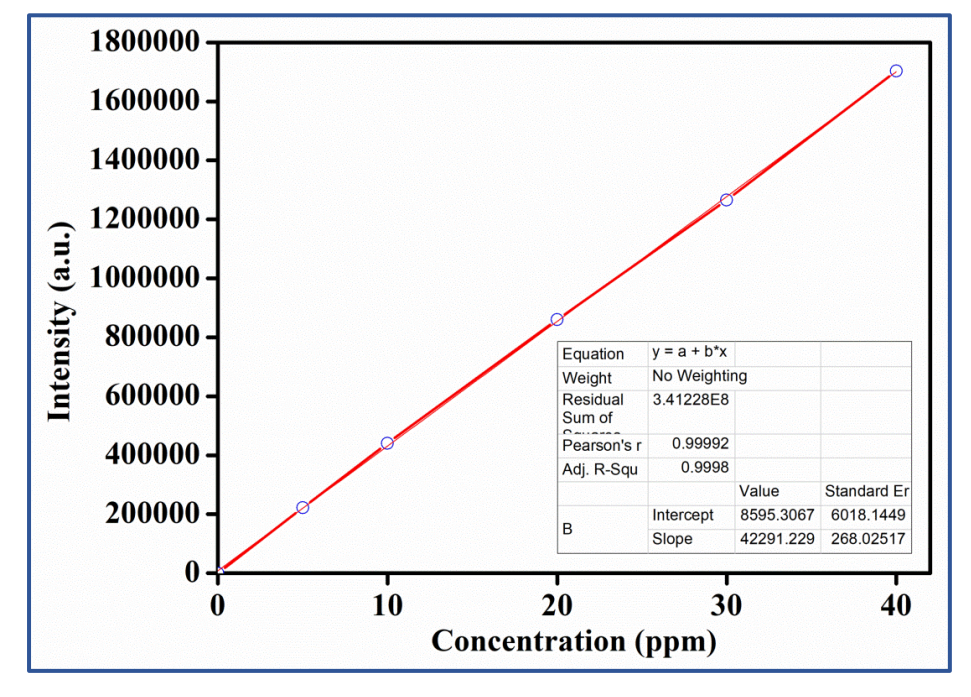


Figure A15. MP-AES calibration curve for Cu(I)@bipy-CTF.

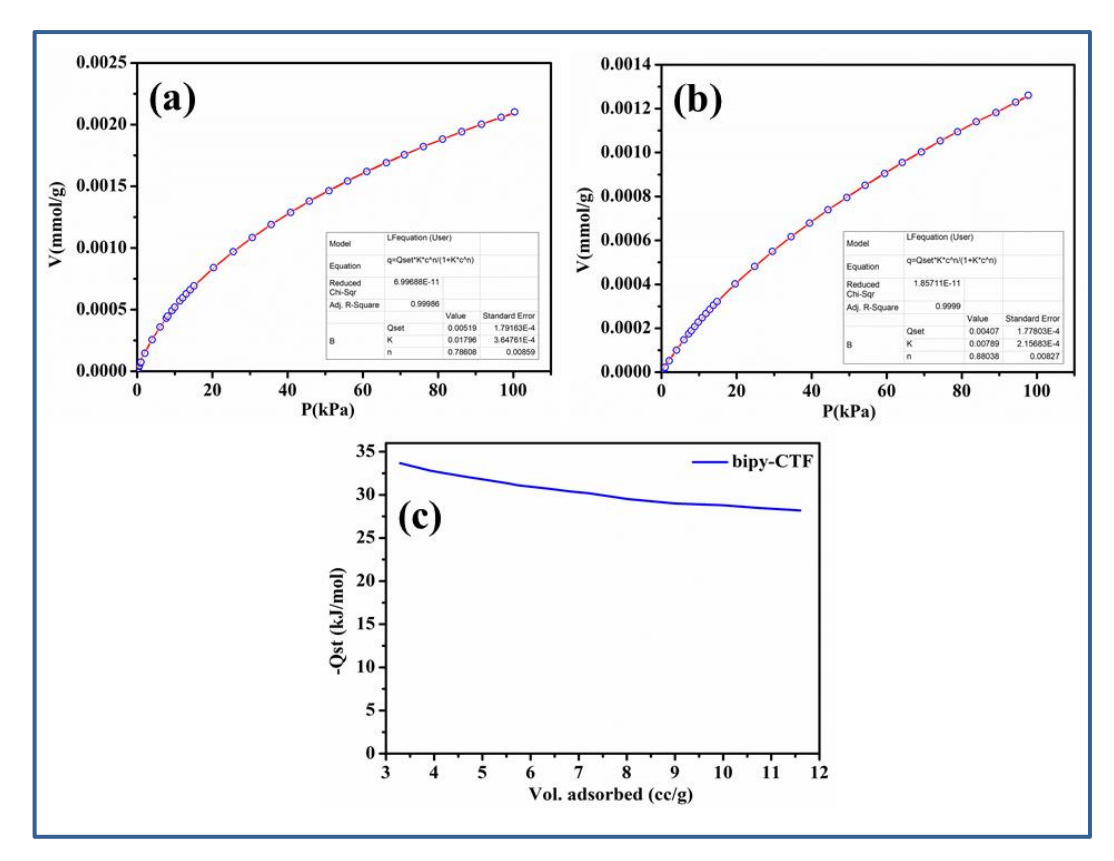


Figure A16. Carbon dioxide adsorption isotherm for bipy-CTF at (a) 273 K and (b) 298 K (the solid line shows the best fit to the data using the Langmuir-Freundlich equation). (c) Enthalpy of carbon dioxide adsorption was determined using the Clausius-Clapeyron equation.

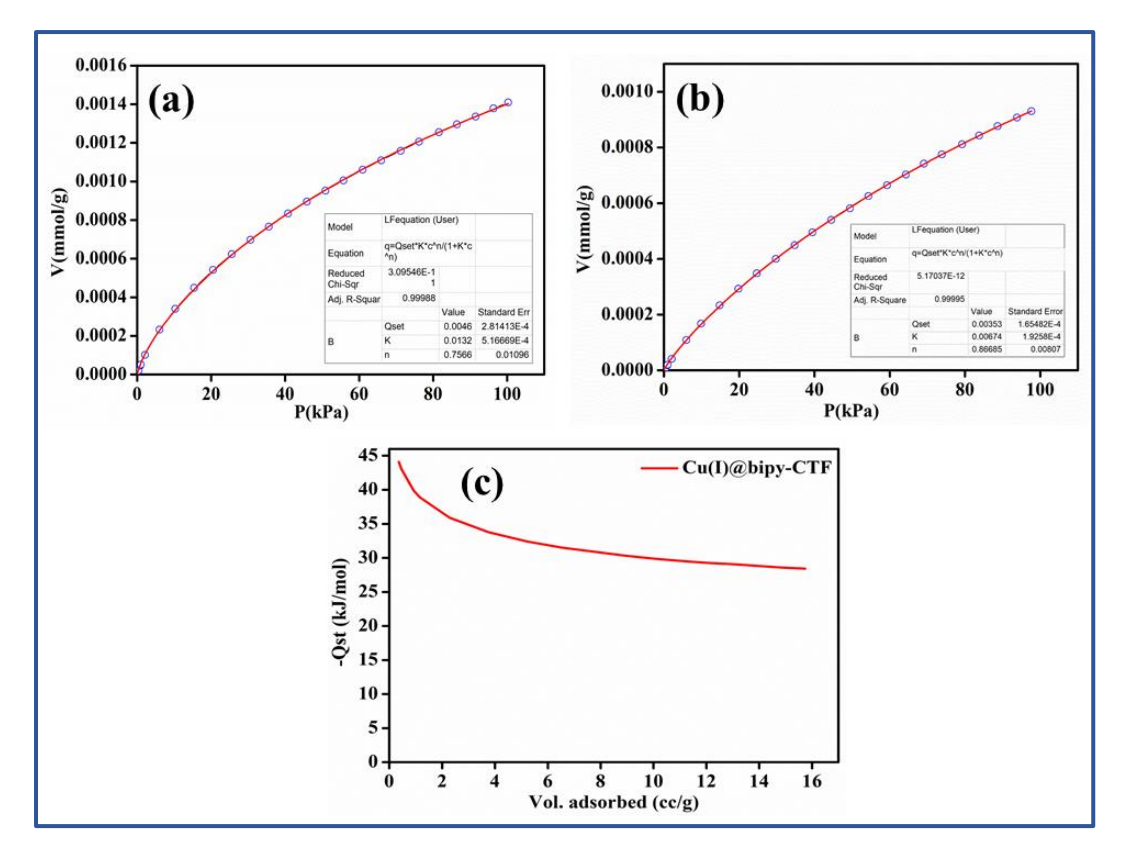


Figure A17. Carbon dioxide adsorption isotherm for Cu(I)@bipy-CTF at (a) 273 K and (b) 298 K (the solid line shows the best fit to the data using the Langmuir-Freundlich equation). (c) Enthalpy of carbon dioxide adsorption was determined using the Clausius-Clapeyron equation.

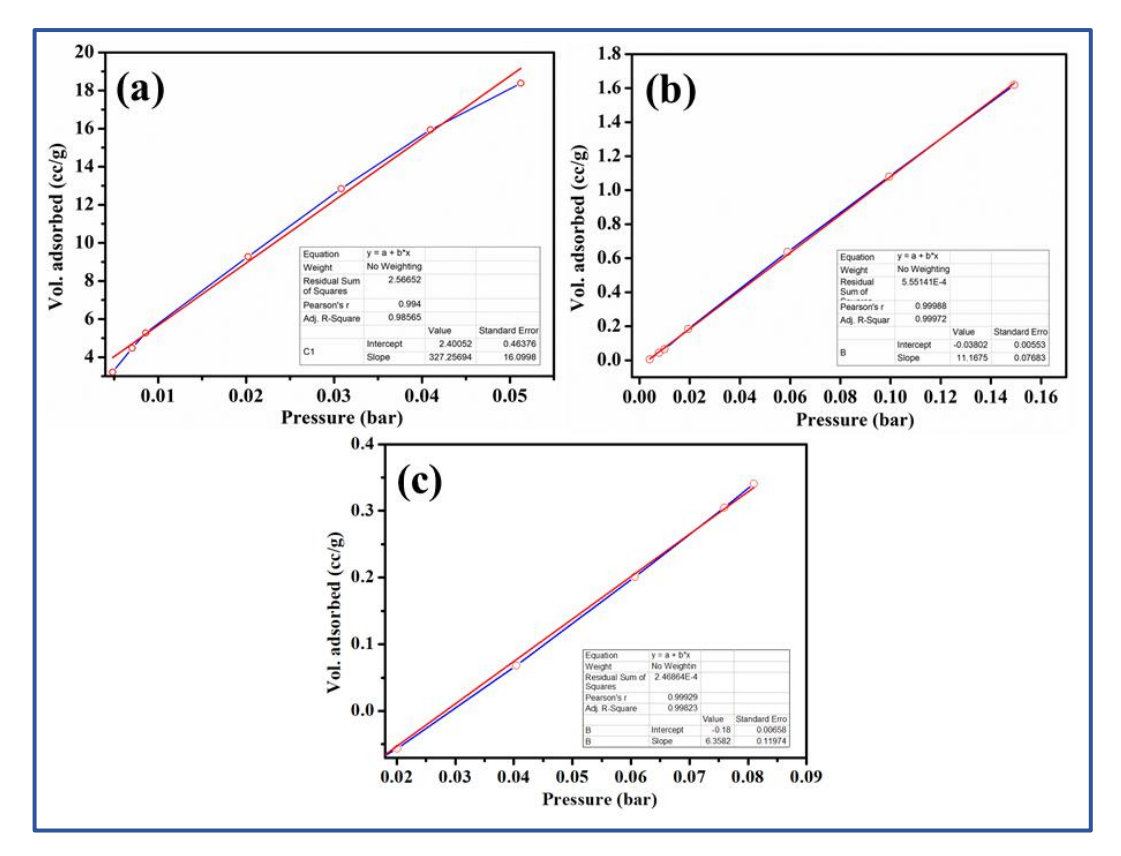


Figure A18. Linear fitting for (a) CO₂, (b) CH₄, and (c) N₂ isotherms of Cu(I)@bipy-CTF was used for the calculation of Henry's selectivity constants.

Table A2. Comparison of the catalytic activity of Cu(I)@bipyCTF for carboxylative cyclization of 2-methyl-3-butyne-2-ol with the reported POP-based catalysts.

S. No.	Catalyst	Active	Pressure Conversion		References
		sites	(bar)	(%)	
1.	Ag@COF	Ag(0)	1	91.2	12
2.	Ag@3D-HNU5	Ag(0)	1	99	13
3.	PAzo-POP-Ag	Ag(0)	10	95	14
4.	F-MOP-3-Ag	Ag(I)	10	99	15
5.	AgN@COF	Ag(0)	1	95	16
6.	Cu(I)@bipy-CTF	Cu(I)	1 (balloon)	96	This work

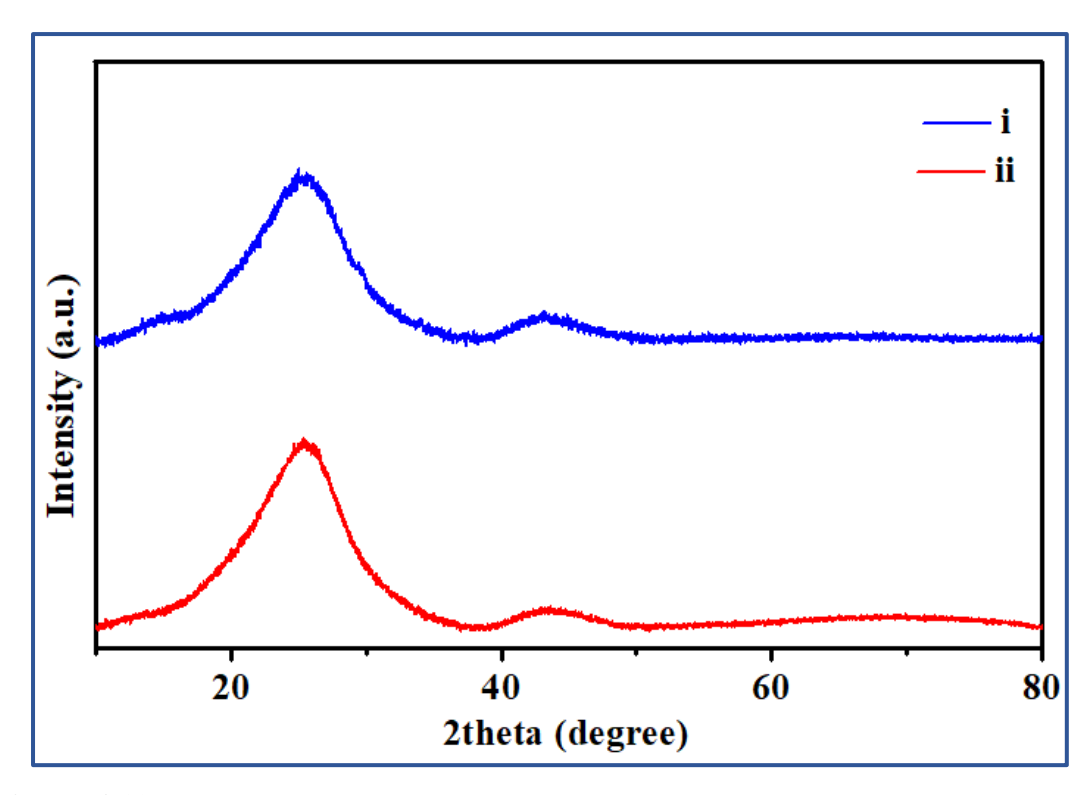


Figure A19. PXRD plot of Cu(I)@bipy-CTF as-prepared (red) and recovered after eight cycles of catalysis (blue).

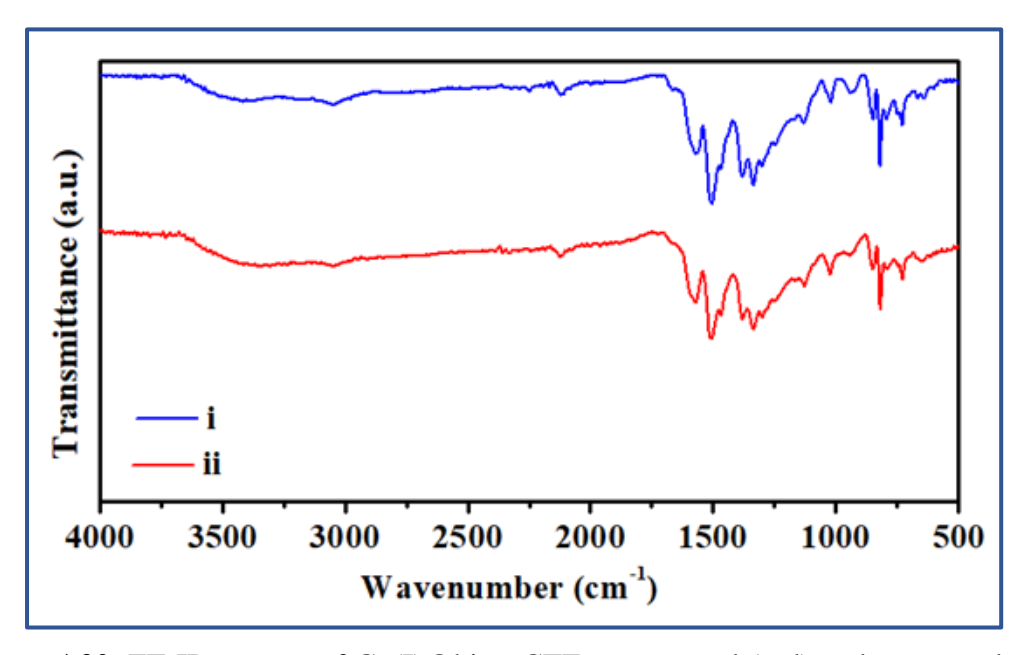


Figure A20. FT-IR spectra of Cu(I)@bipy-CTF as-prepared (red) and recovered after eight cycles of catalysis (blue).

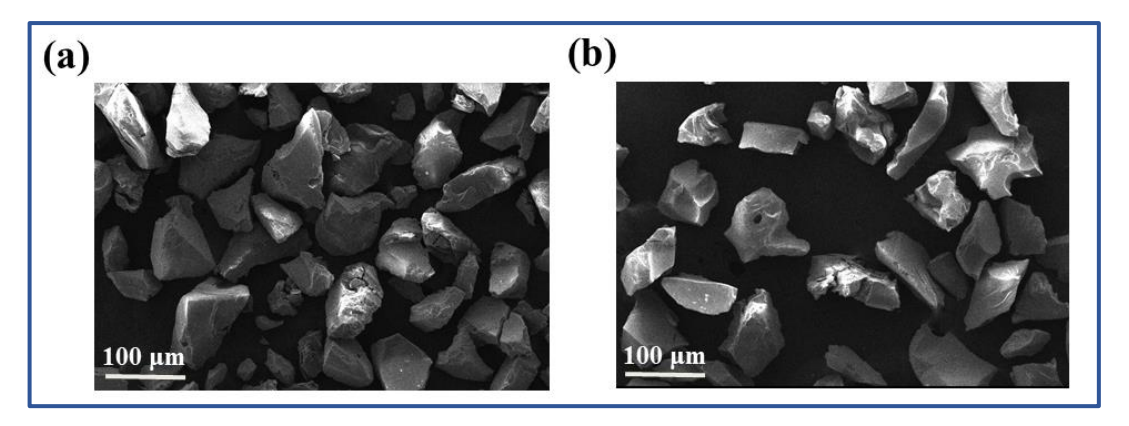


Figure A21. SEM images of Cu(I)@bipy-CTF (a) as-prepared and (b) recovered after eight cycles of catalysis.

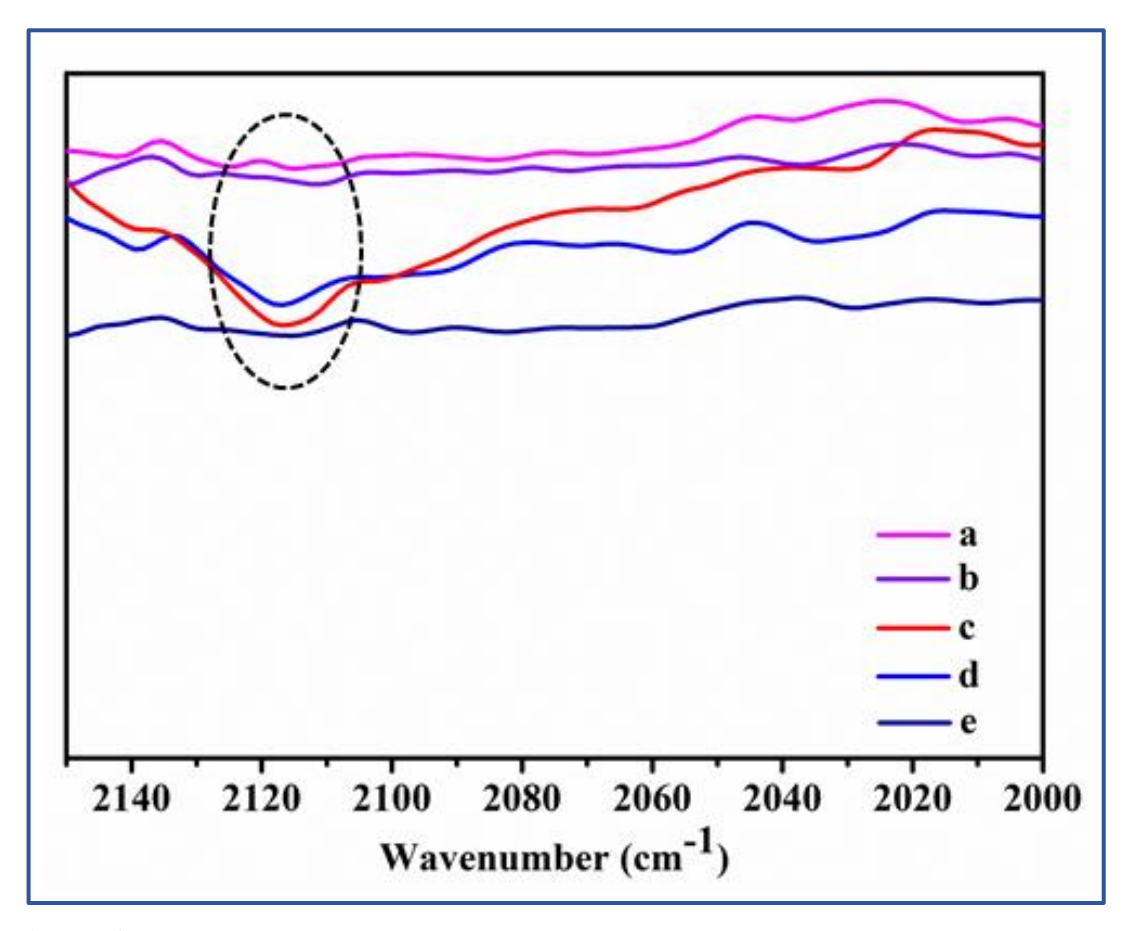


Figure A22. FT-IR spectra of bipy-CTF (a), Cu(I)@bipy-CTF (b), 2-methyl-3-butyn-2-ol (c), Cu(I)@bipy-CTF treated with 2-methyl-3-butyn-2-ol (d), bipy-CTF treated with 2-methyl-3-butyn-2-ol.

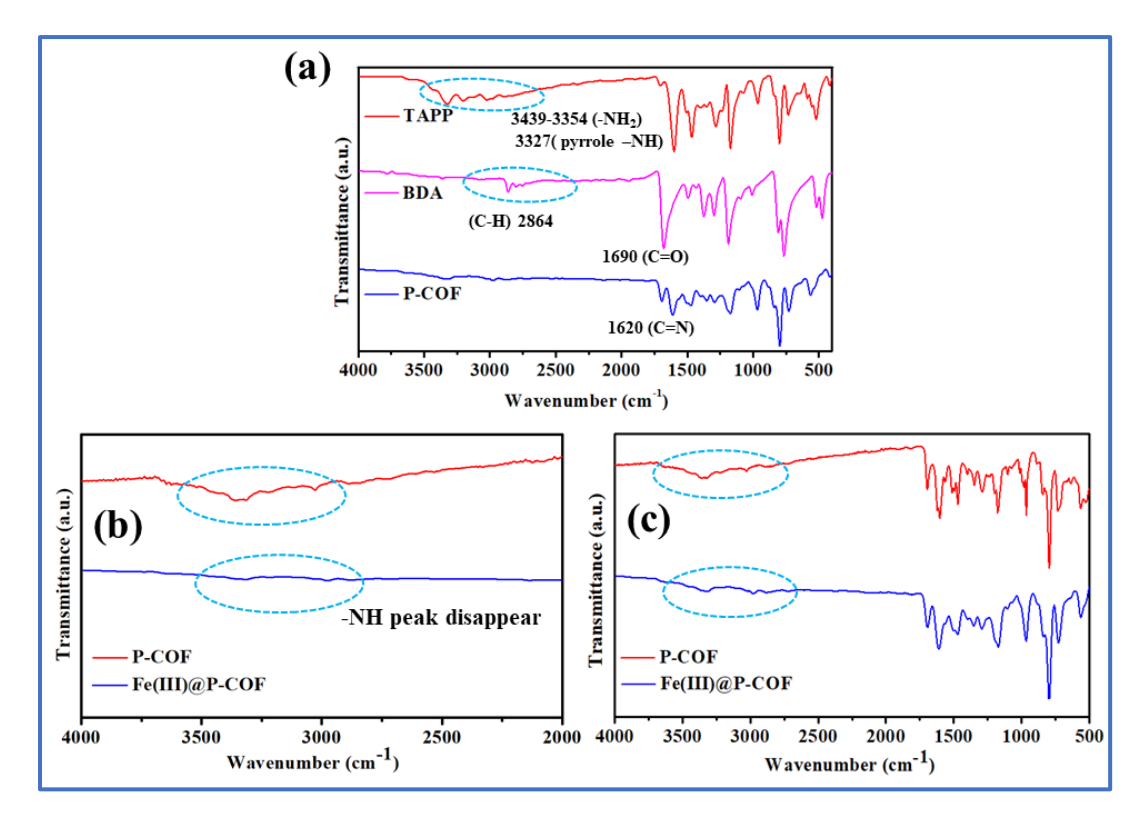


Figure A23. (a) FT-IR plot of P-COF (blue), BDA (purple), and TAPP (red). (b and c) Magnified FT-IR plots of P-COF (red) and Fe(III)@P-COF (blue).

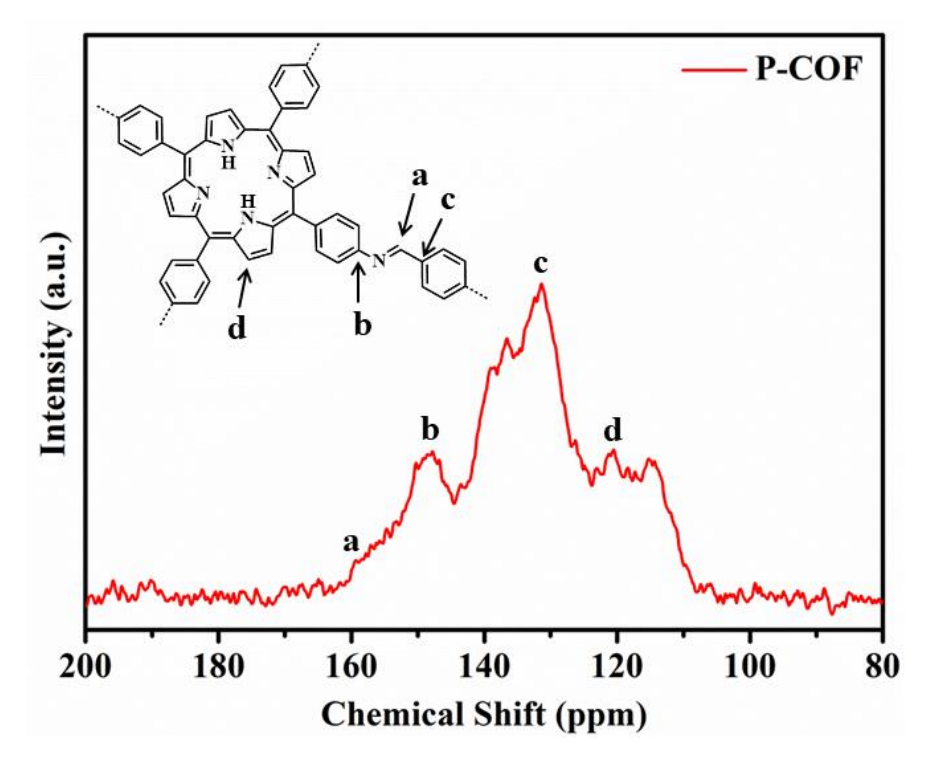


Figure A24. ¹³C CP-MAS solid-state NMR spectrum of P-COF.

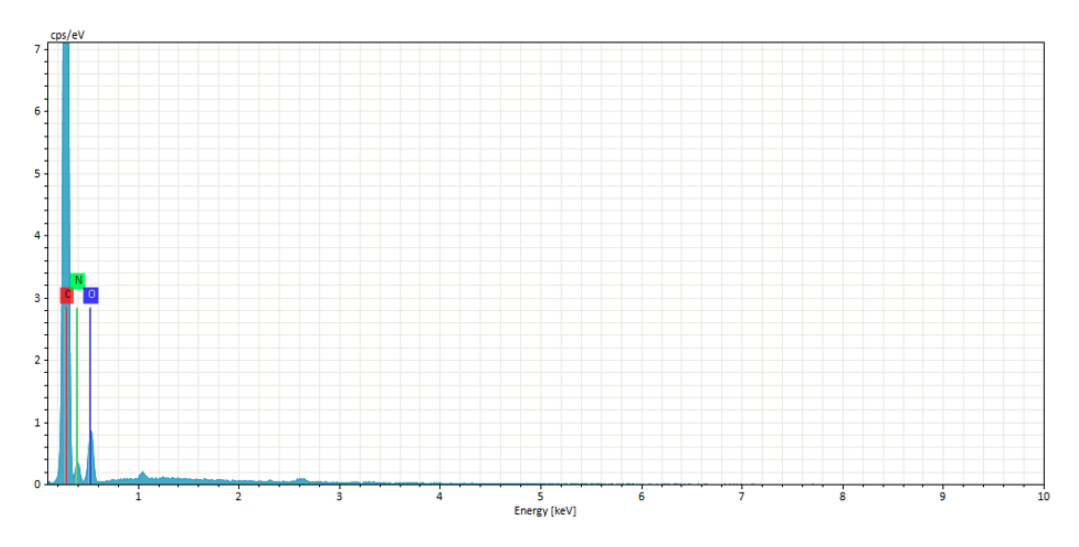


Figure A25. EDS plot of P-COF.

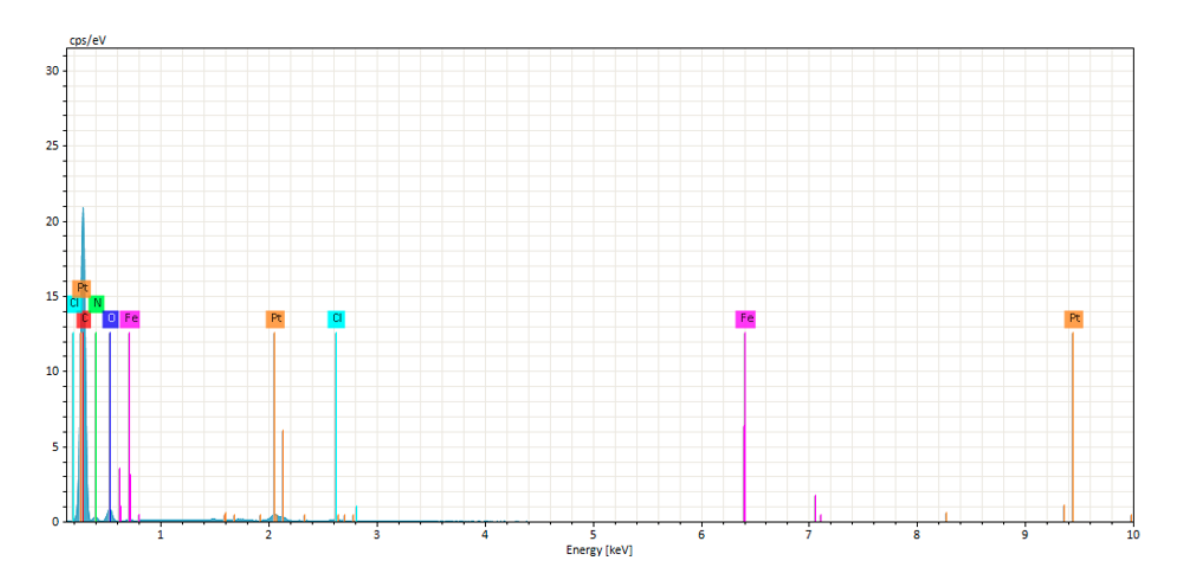


Figure A26. EDS plot of Fe(III)@P-COF.

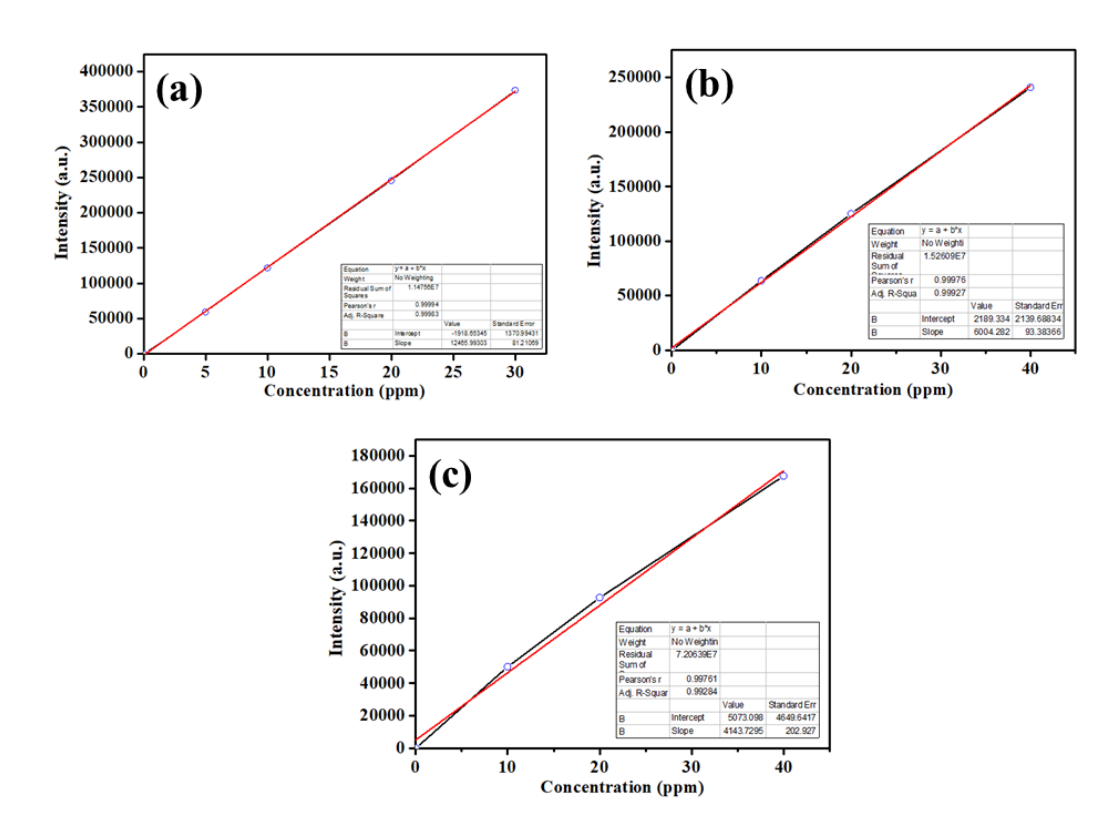


Figure A27. MP-AES calibration curve for estimation of metal content in M@P-COF (M = Fe(III) (a), Fe(II) (b), and Zn(II) (c).

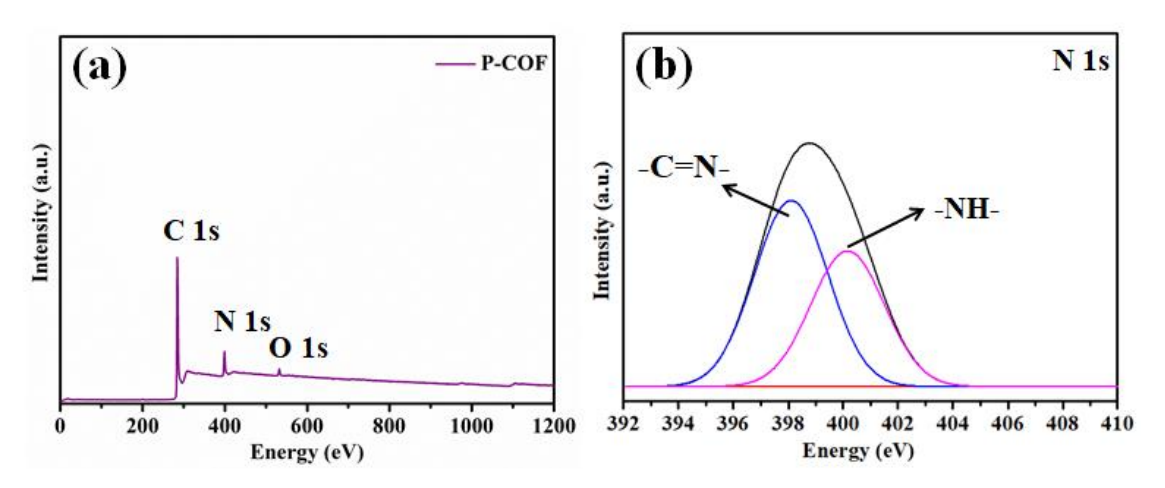


Figure A28. XPS plot of P-COF, (a) survey spectrum (b) N1s.

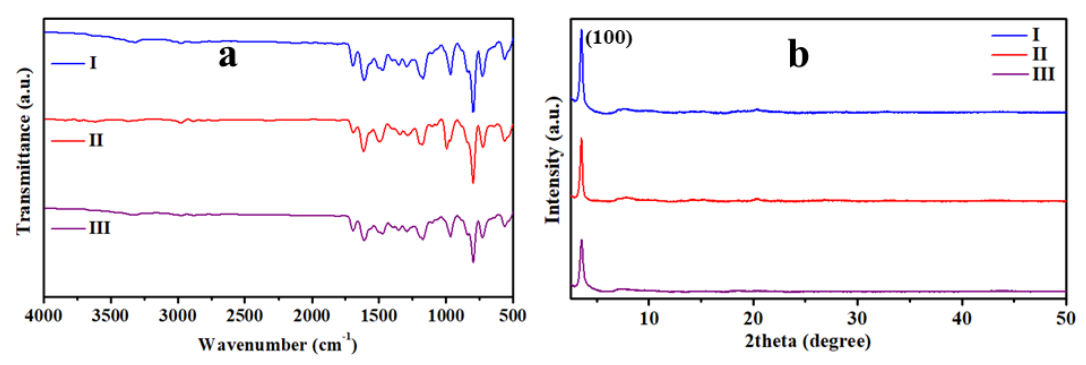


Figure A29. FT-IR (a) and PXRD (b) plots of P-COF (I), Zn(II)@P-COF (II), and Fe(II)@P-COF (III).

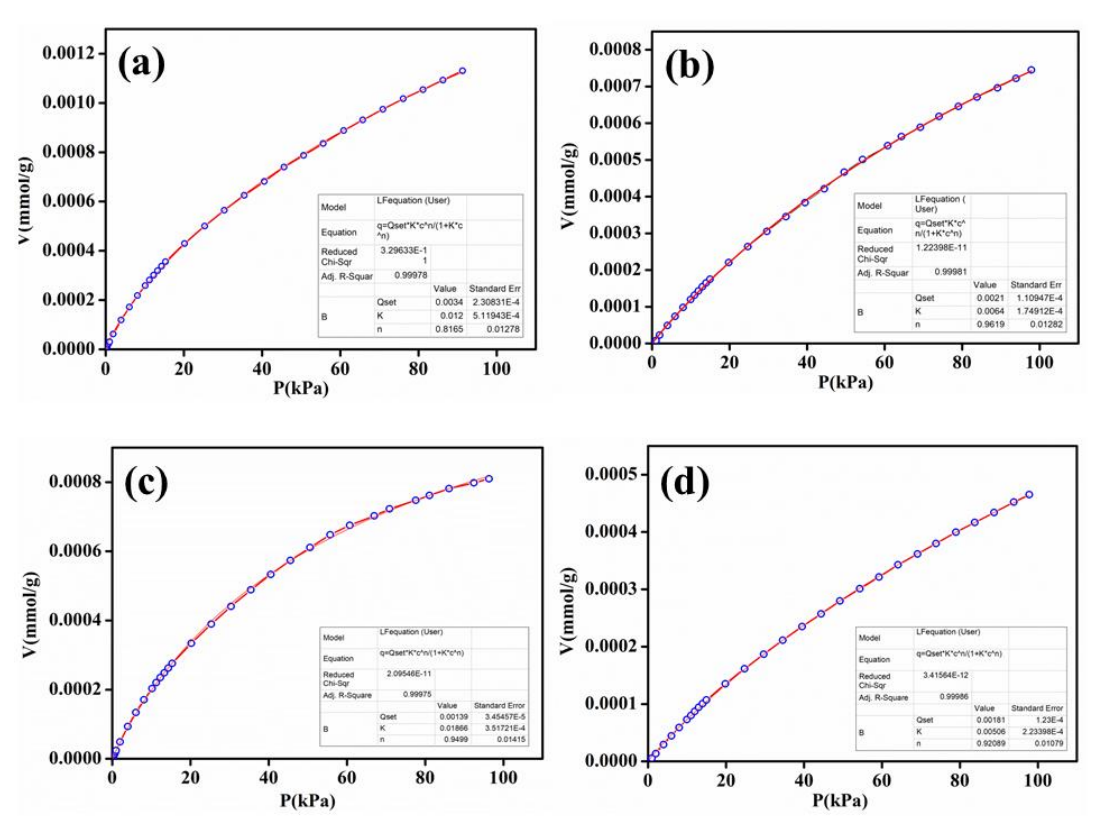


Figure A30. Carbon dioxide adsorption isotherm for P-COF at (a) 273 K and (b) 298 K and Fe(III)@P-COF at (c) 273 K and (d) 298 K. (The solid line shows the best fit to the data using the Langmuir-Freundlich equation).

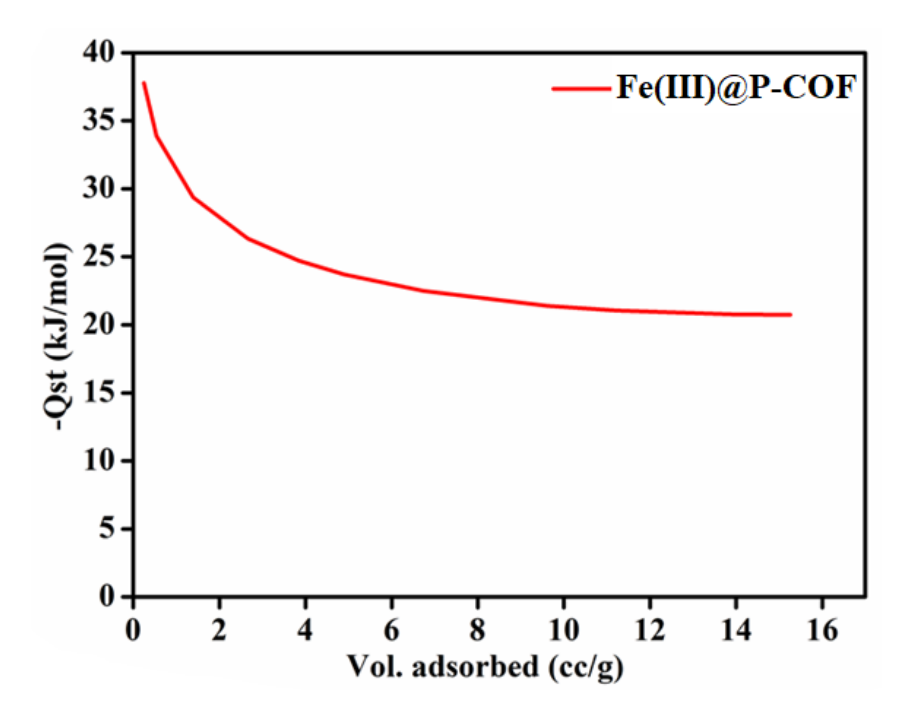


Figure A31. Enthalpy of carbon dioxide adsorption for Fe(III)@P-COF was calculated by using the Clausius-Clapeyron equation.

Table A3: Comparison of catalytic activity of Fe(III)@P-COF with the reported examples of heterogeneous catalysts known for epoxidation of styrene.

S.	Catalyst	Oxidant	Time	Conversion	References
No.			(h)		
1	(Compound 1) Perylene bis-imide linked iron(III) porphyrin chloride framework	ТВНР	08	99	17
2	(Compound 2) Perylene bis-imide linked manganese (III) porphyrin chloride framework	ТВНР	08	99	17
3	(Mn-CPF-1) covalent- porhyrinic framework	ТВНР	24	99	18
4	[Mn(salen)Cl] (1)	PhIO	03	91	19
5	[Mn(3,5-dtButsalhd)Cl] (5)	PhIO	03	61.3	19
6	Mn-CPF-2	ТВНР	24	93	18
7	Fe@MOF1	PhIO	18	90.9	20
8	Compound 1 [Co(Hoba) ₂ (H ₂ O) ₂](H ₂ oba = 4,4'-oxydibenzoic acid)	ТВНР	06	96	21
9	Fe(III)@P-COF	PhIO	18	>99	This work

Table A4: Comparison of catalytic activity of Fe(III)@P-COF with the reported examples of heterogeneous catalysts known for the one-pot oxidative carboxylation of styrene.

S.	Catalyst	CO ₂	Co-	Temp.	Time	Conversion	References
No		(bar)	catalyst	(° C)	(h)	(%)	
•			(TBAB)				
			(mmol)				
1	MNP@SiO ₂ -	10	PPNCl	80	24	99	22
	8Mn		(0.02)				
2	Fe@MOF1	08	0.2	50	24	98.6	20
	T 1000	0.0	0.00	70	40		22
3	Ti-MMM-E	08	0.02	50	48	71	23
4	MOF-590	01	0.3	80	10	93	24
5	Co(II)@CSU	01	0.4	75	12	98	25
)	, , ,	U1	0.4	13	12	90	23
	ST-2						
6	Cr-MIL-101	08	0.02	25	24	39	26
7	CSMCRI-10	08	0.09	80	08	92.6	27
8	Fe(III)@P-	01	0.3	80	24	>99	This Work
	COF						

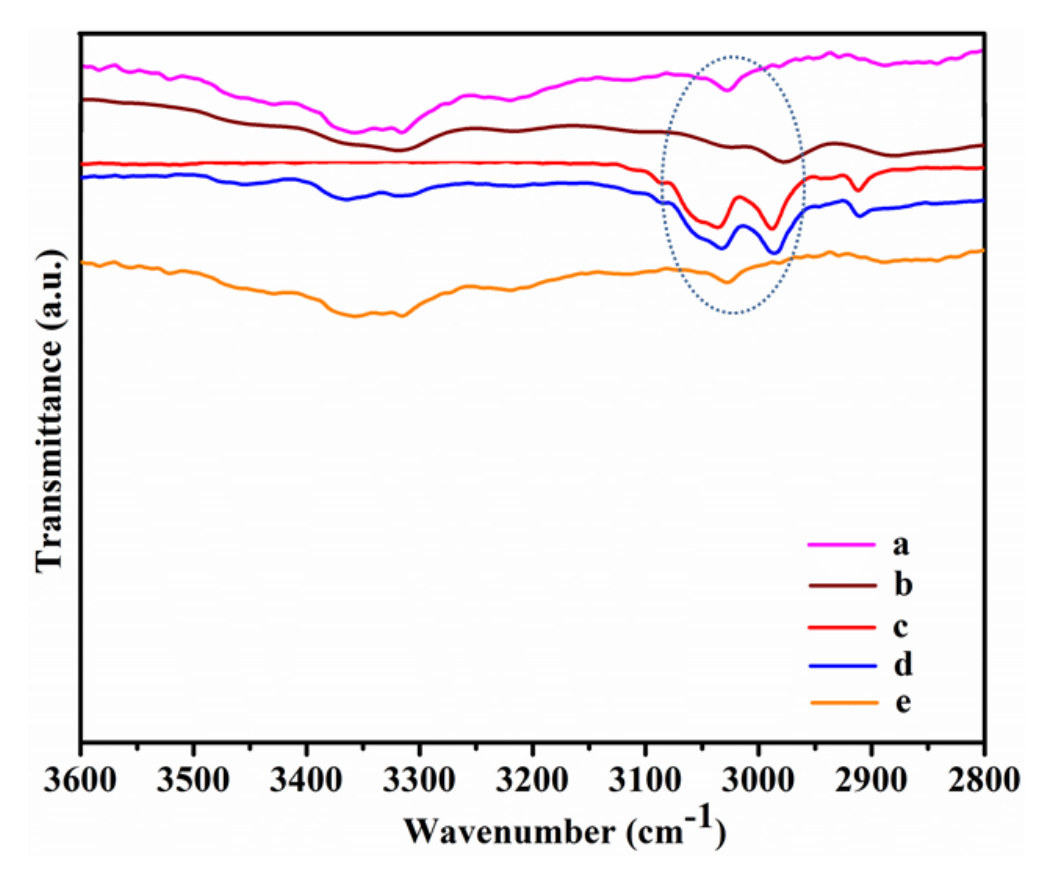


Figure A32. FT-IR spectra of P-COF (a), Fe(III)@P-COF (b), styrene oxide (c), Fe(III)@P-COF treated with styrene oxide (d) P-COF treated with styrene oxide (e).

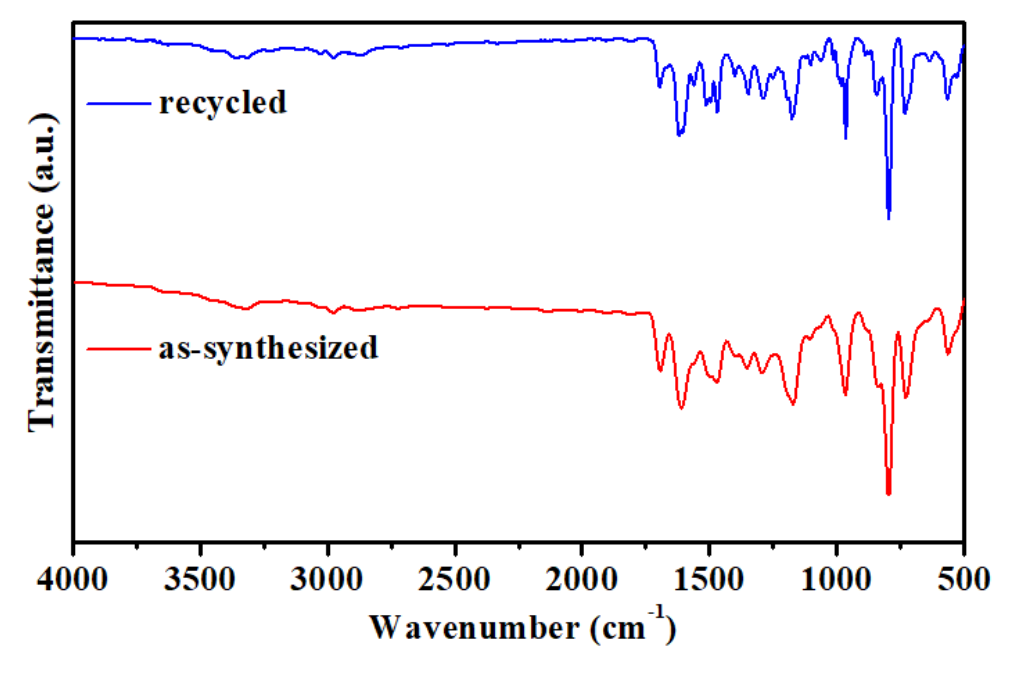


Figure A33. FT-IR plot of Fe(III)@P-COF before (red) and after catalysis (blue).

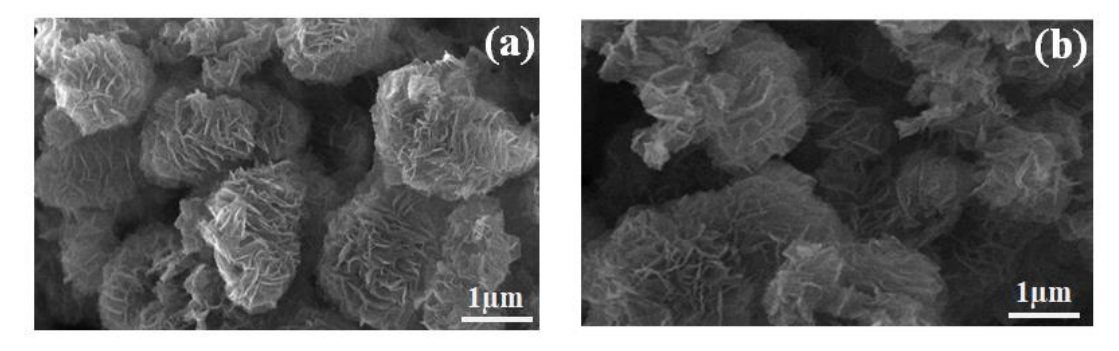


Figure A34. SEM images of as-synthesized (a) and recycled (b) Fe(III)@P-COF.

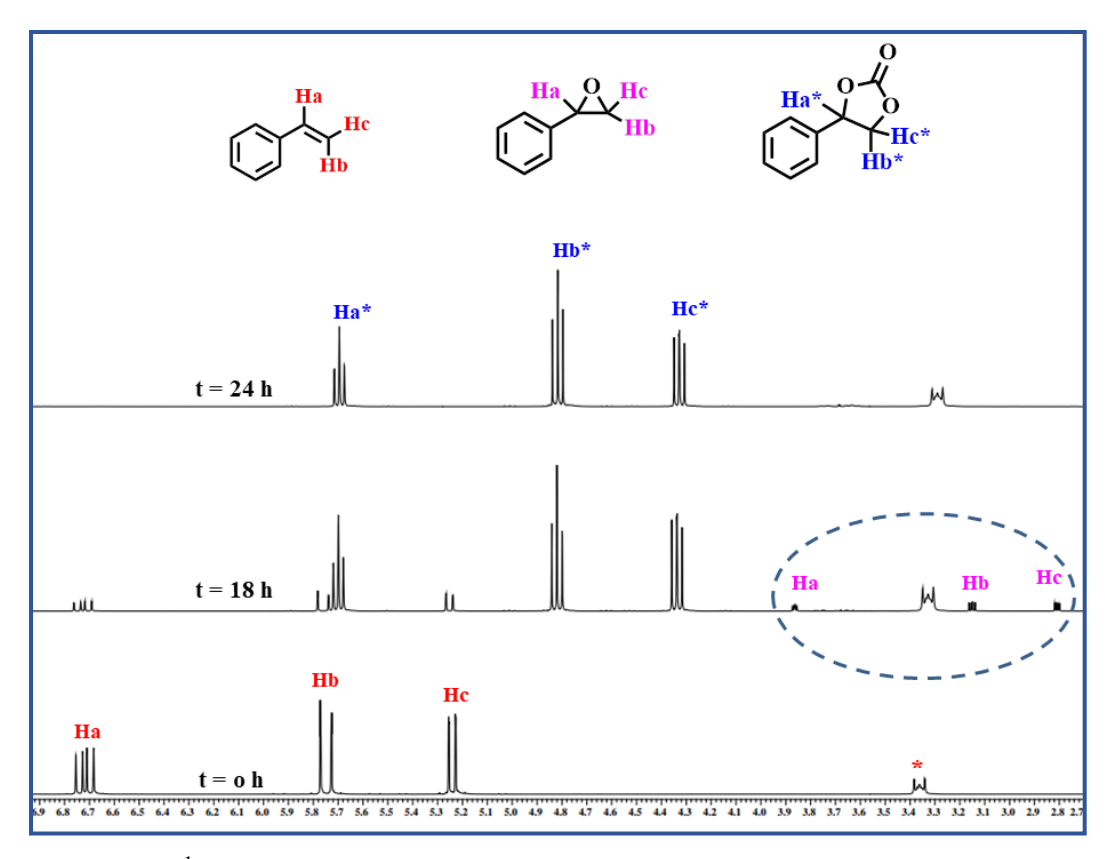


Figure A35. ¹H NMR (400 MHz, CDCl₃, 20 °C) stack plot for direct oxidative carboxylation of styrene catalyzed by the Fe(III)@P-COF at different time intervals (* peak due to TBAB).

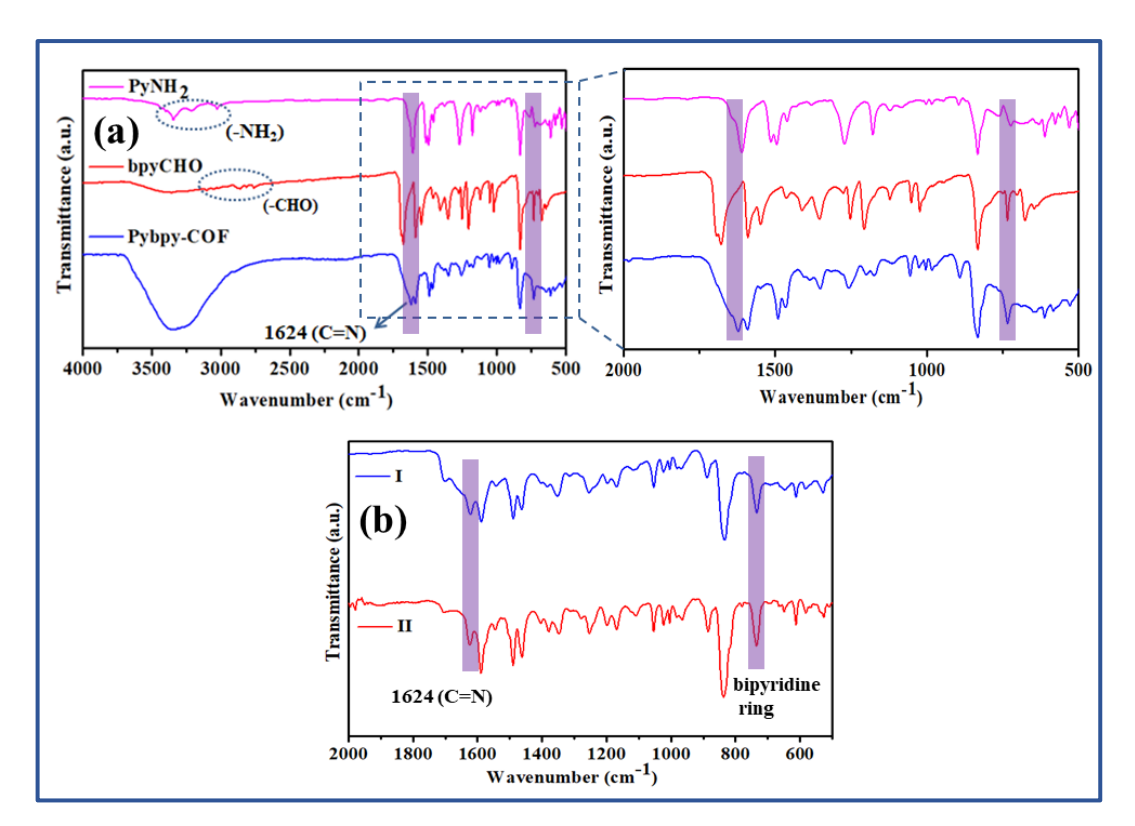


Figure A36. (a) FT-IR stack plot for PyNH₂ (pink), bpyCHO (red), and Pybpy-COF (blue). (b) FT-IR stack plot of Pybpy-COF (I) and Ag@Pybpy-COF (II).

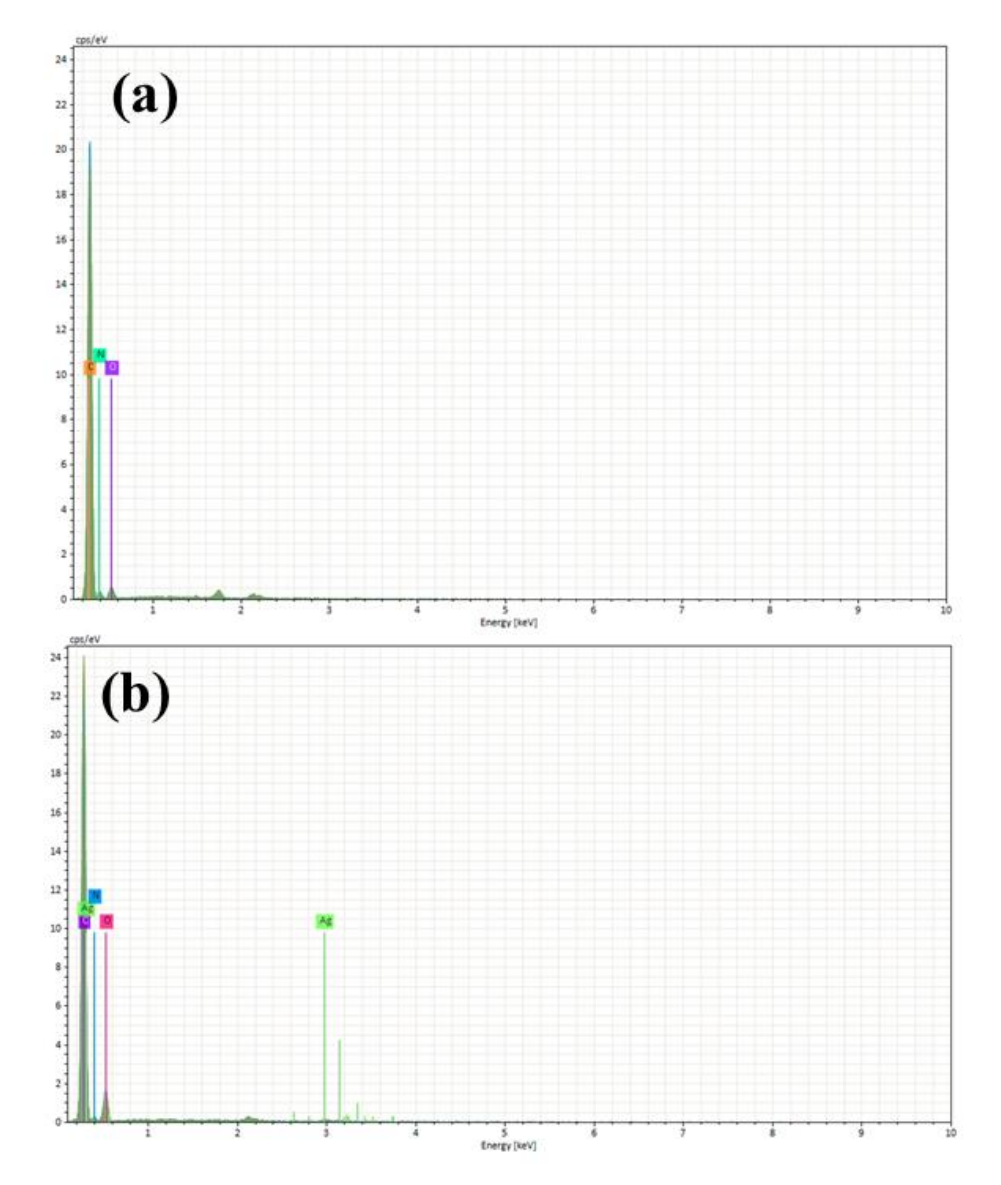


Figure A37. EDS plot of Pybpy-COF (a) and Ag@Pybpy-COF (b).

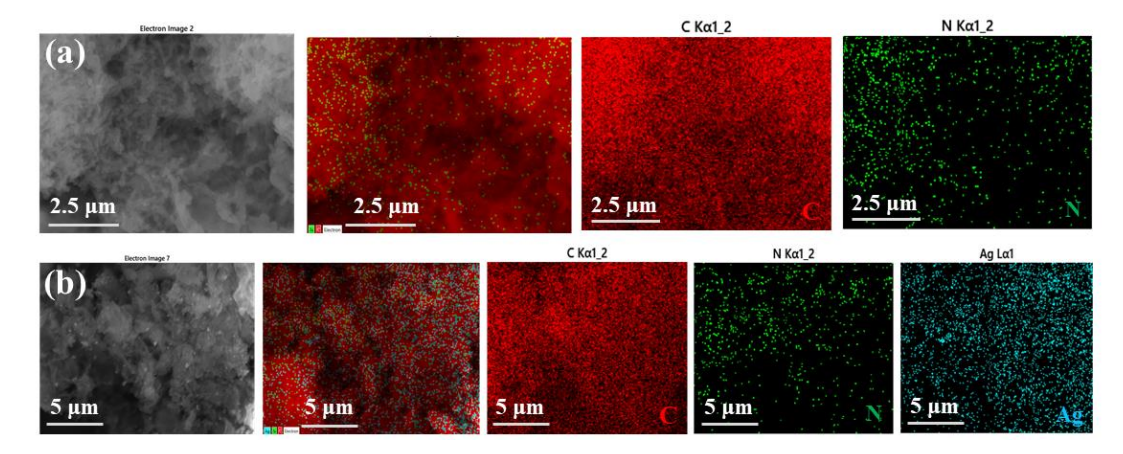


Figure A38. Elemental mapping of Pybpy-COF and Ag@Pybpy-COF (a and b), C (red), N (green), and Ag (light blue), respectively.

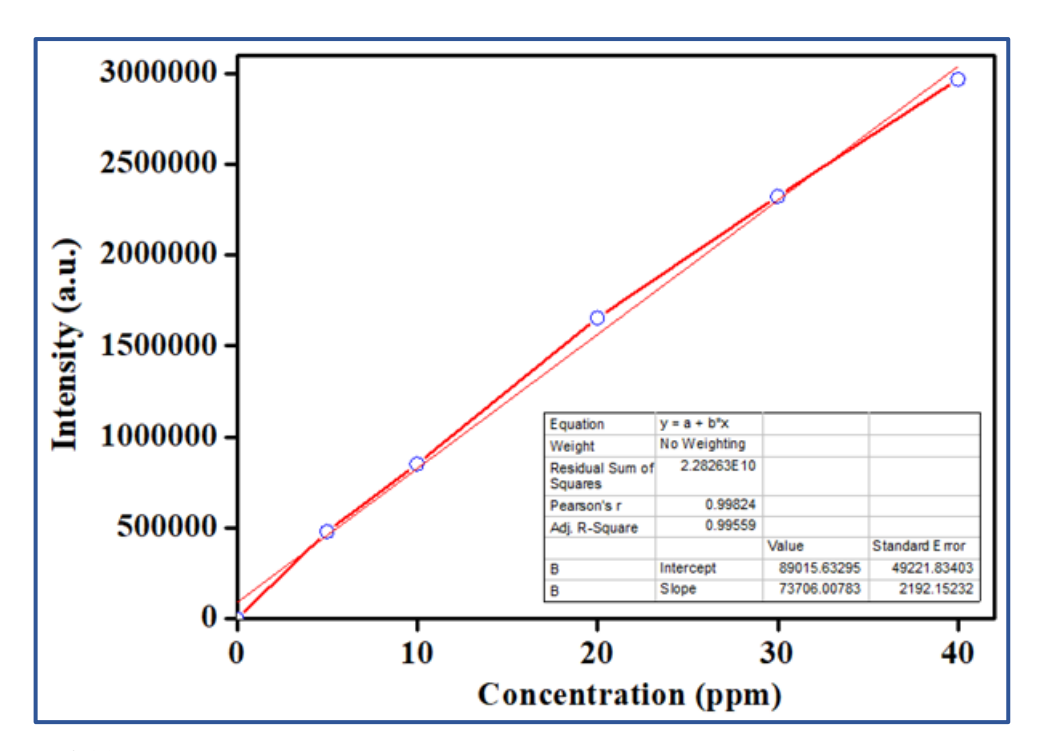


Figure A39. MP-AES calibration curve for Ag@Pybpy-COF.

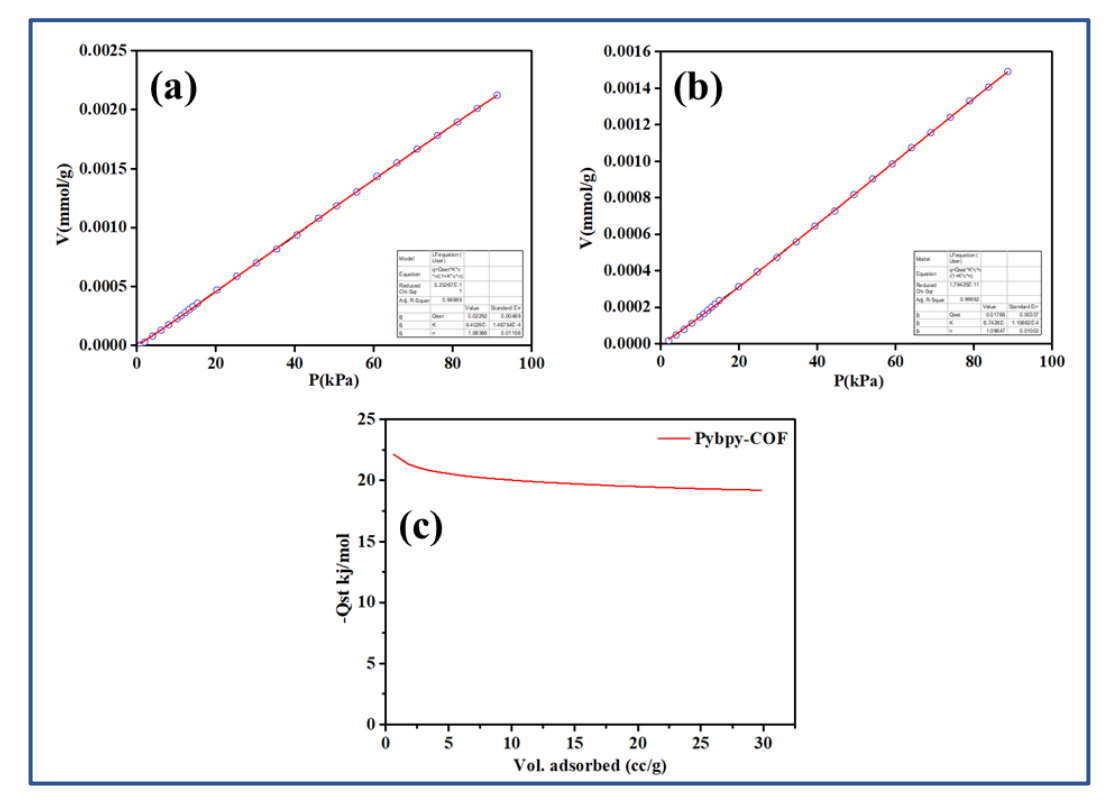


Figure A40. Carbon dioxide adsorption isotherms of Pybpy-COF carried out at 273 K, and 298 K (a and b) (the solid line shows the best fit to the data using the Langmuir-Freundlich equation). (c) The enthalpy of carbon dioxide adsorption determined using the Clausius-Clapeyron equation.

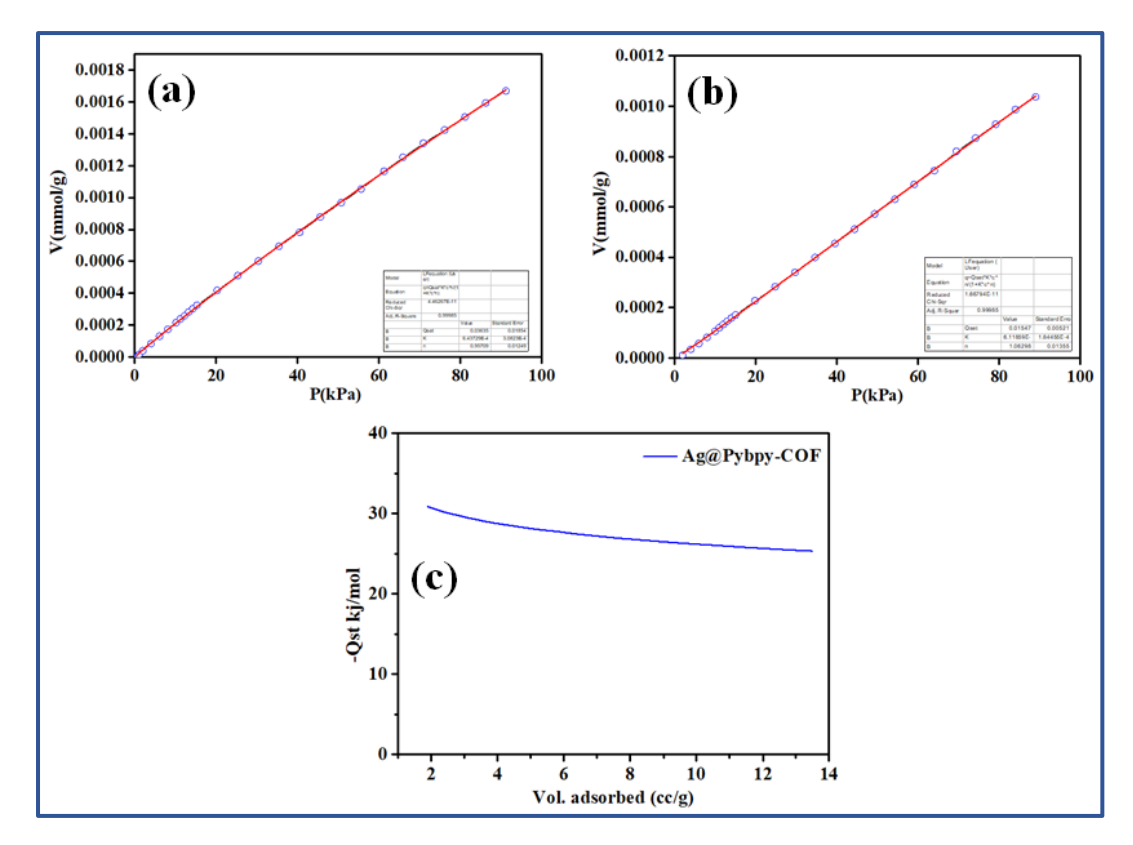


Figure A41. Carbon dioxide adsorption isotherms for Ag@Pybpy-COF performed at 273 K and 298 K (a and b) (the solid line shows the best fit to the data using the Langmuir-Freundlich equation). (c) The enthalpy of carbon dioxide adsorption determined using the Clausius-Clapeyron equation.

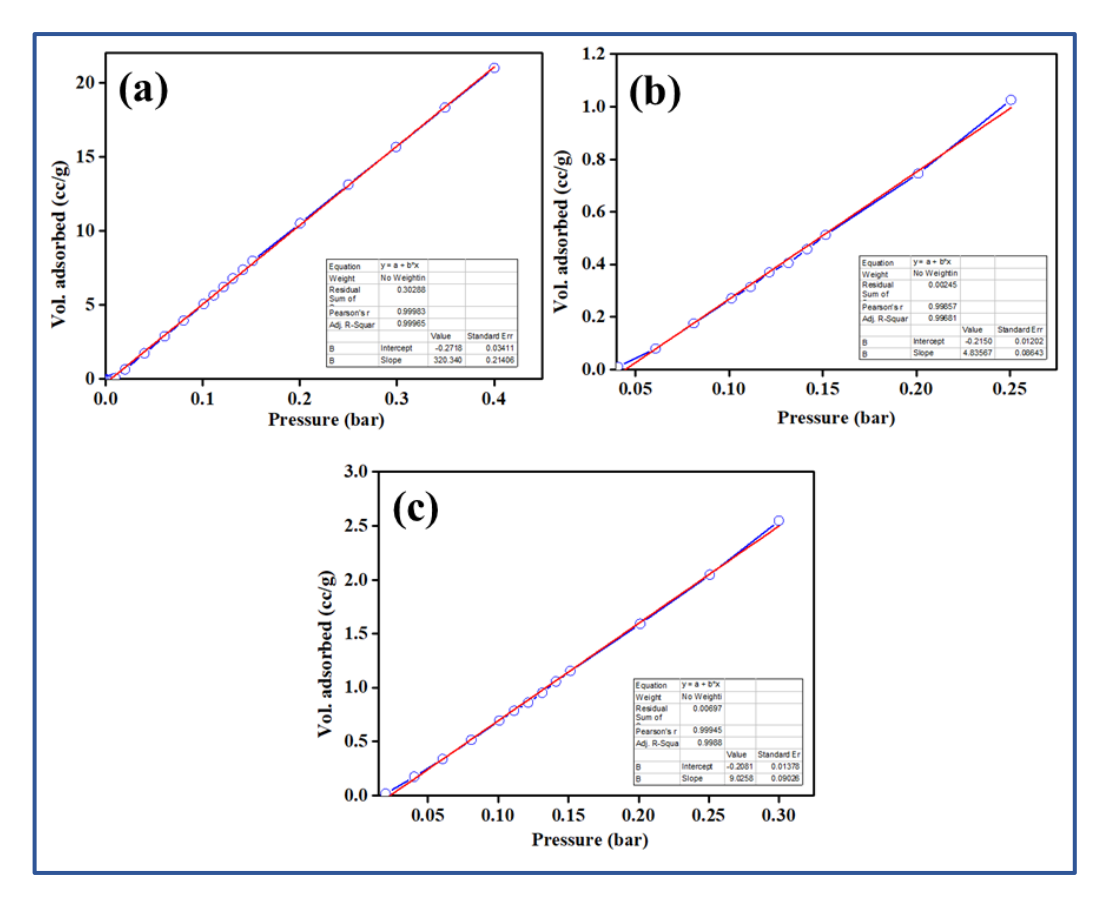


Figure A42. Linear fitting of CO₂, N₂, and CH₄ isotherms of Ag@Pybpy-COF used for calculation of Henry's selectivity constants.

Table A5: Comparison of catalytic activity of Ag@Pybpy-COF with previously reported heterogeneous catalysts for the carboxylation of terminal alkynes.

S.	Catalyst	Temp.	CO ₂	Time	Yield	References
No.		(° C)	(bar)	(h)	(%)	
1	MOP-Pz-Ag	50	1	24	92	28
2	Ag@p-CTF-250	50	1	16	96	29
3	Ag ⁰ @CTFN-2	60	1	24	97	30
4	Ag ⁰ @CTFN-3	60	1	24	97	30
5	CTF-DCE-Ag	50	1	20	90.2	31
6	AgNPs@m-PS-PC	70	1	12	91	32
7	Ag@Pybpy-COF	50	1	12	98	This work

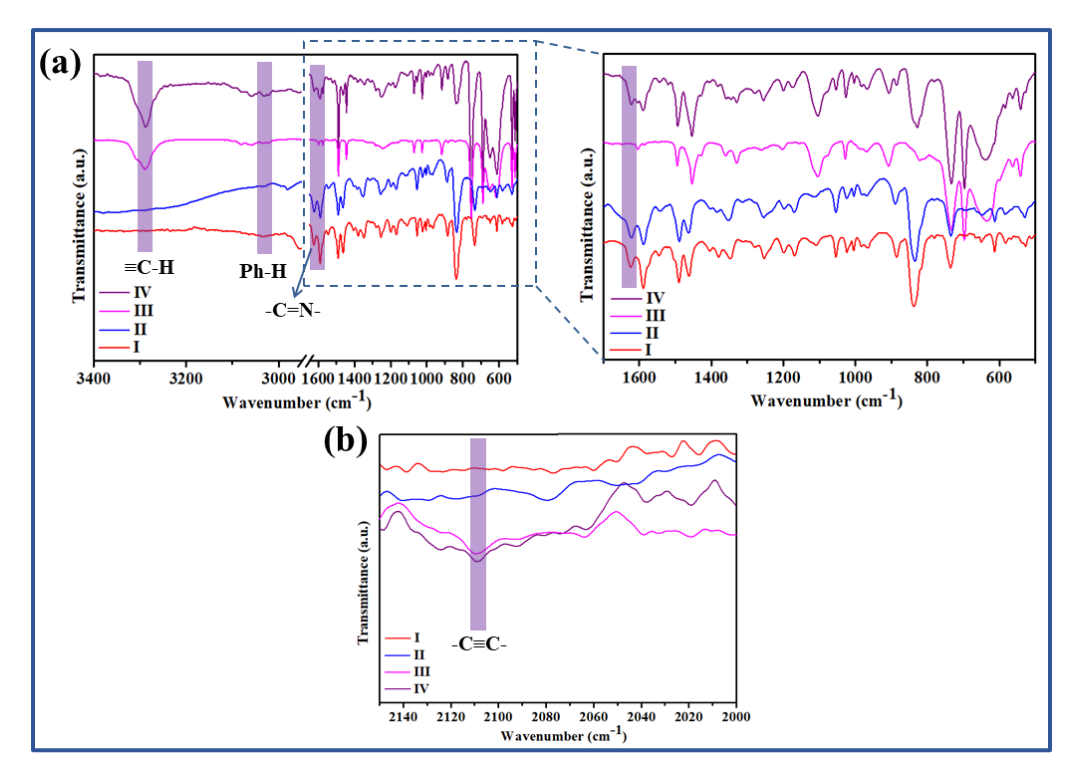


Figure A43. (a) FT-IR stack plot of Pybpy-COF (I), Ag@Pybpy-COF (II), ethynylbenzene (III), Ag@Pybpy-COF treated with ethynylbenzene (IV). (b) Magnified view of the selected region of FT-IR stack plot.

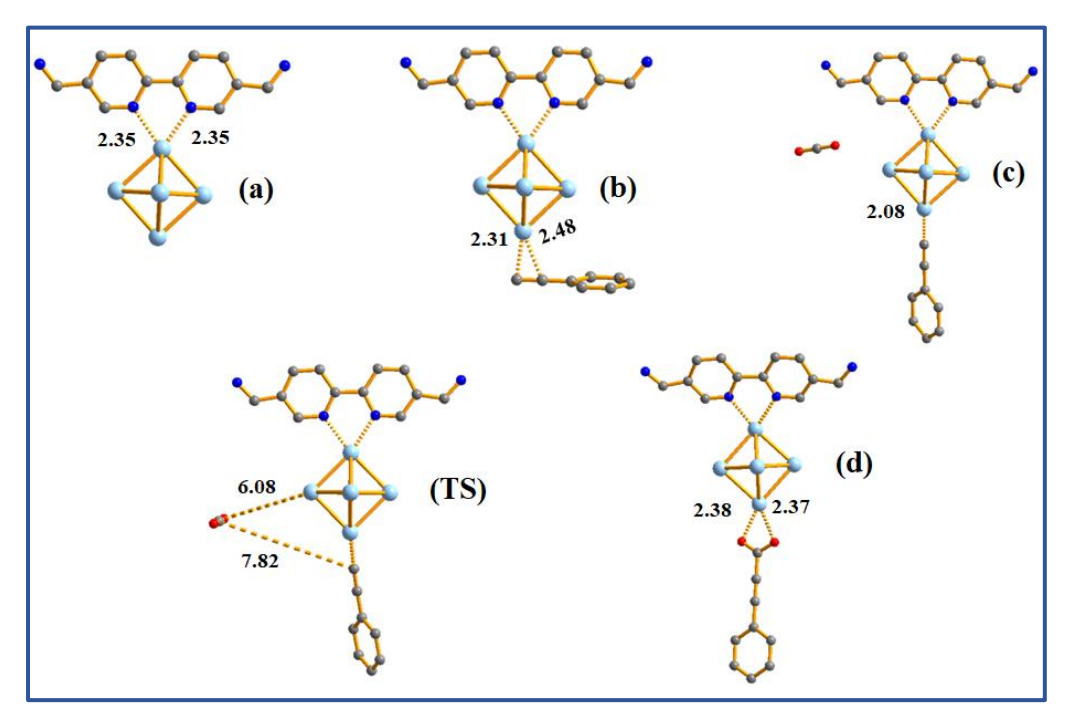


Figure A44. Optimized structures of the intermediates and transition state (TS) in the catalytic carboxylation of terminal alkyls with CO_2 catalyzed by Ag@Pybpy-COF (bond distances are in Å).

Table A6: Comparison of catalytic activity of Ag@Pybpy-COF with previously reported heterogeneous catalysts for carboxylative cyclization of propargylic amines.

S.	Catalyst	Temperature	Base	CO ₂	Time	Yield	References
No.	Suury st	(°C)	(mmol) (DBU)	(bar)	(h)	(%)	
1	Ag@2,6-	50	0.25	1	2	99	33
	FPP-TAPT						
2	Ag@3,5-	50	0.25	1	2	91	33
	FPP-TAPT						
3	Ag@NPOP-	50	0.1	1	2	97	34
	1						
4	Ag@NPOP-	50	0.1	1	2	93	34
	2						
5	Ag@BT-	60	0.25	1	14	99.3	35
	COP						
6	Ag@BT-	60	0.25	1	14	84.9	35
	COP						
7	Ag@BT-	60	0.25	1	14	40.4	35
	COP						
8	Ag@Pybpy-	50	0.1	1	0.5	99	This work
	COF						

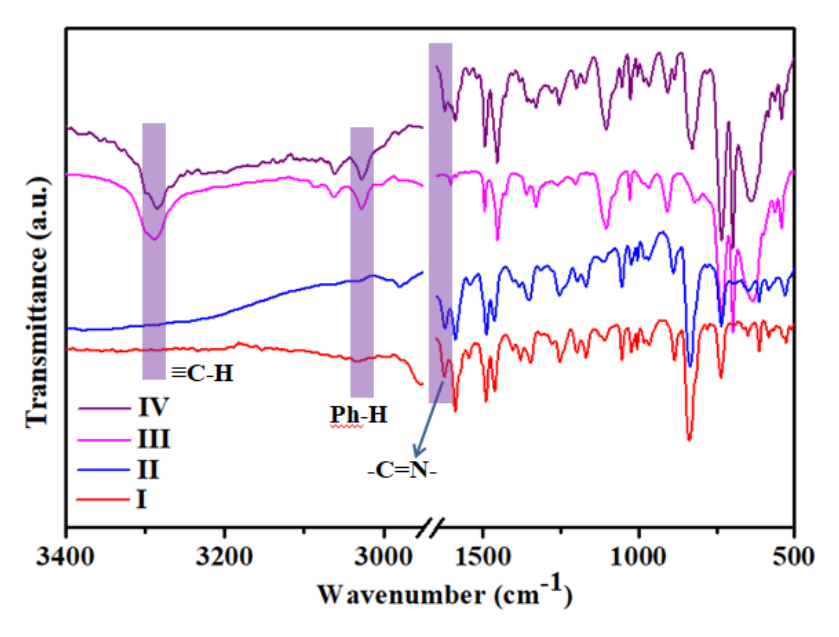


Figure A45. FT-IR stack plot of Pybpy-COF (I), Ag@Pybpy-COF (II), N-benzylprop-2-yn-1-amine (III), Ag@Pybpy-COF treated with N-benzylprop-2-yn-1-amine (IV).

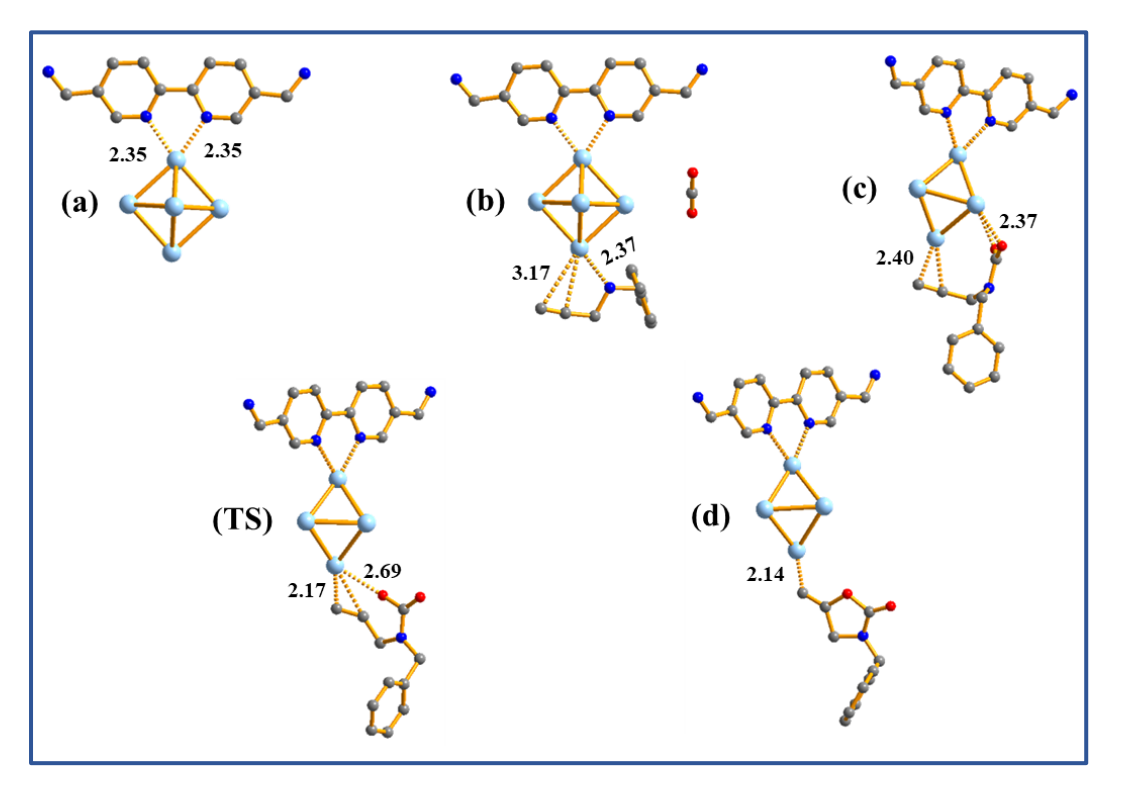


Figure A46. Optimized structures of intermediates and transition state in the catalytic carboxylative cyclization of propargylic amines with CO_2 catalyzed by Ag@Pybpy-COF (bond distances are in Å).

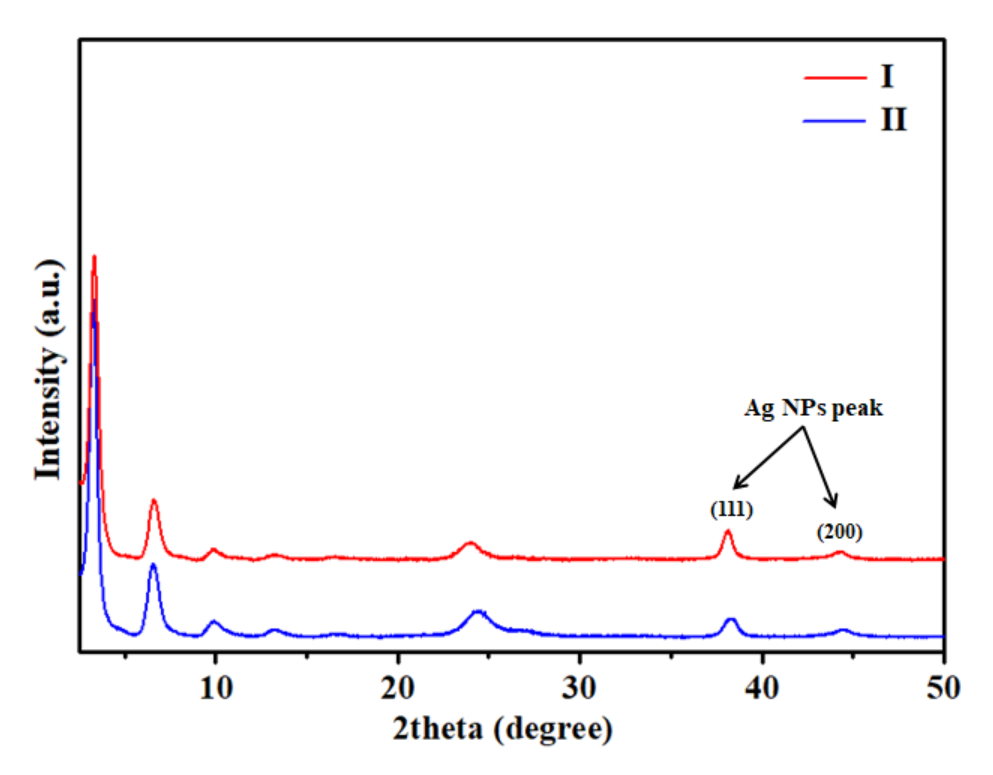


Figure A47. PXRD spectra of Ag@Pybpy-COF (I) and recycled catalyst (II) after catalysis.

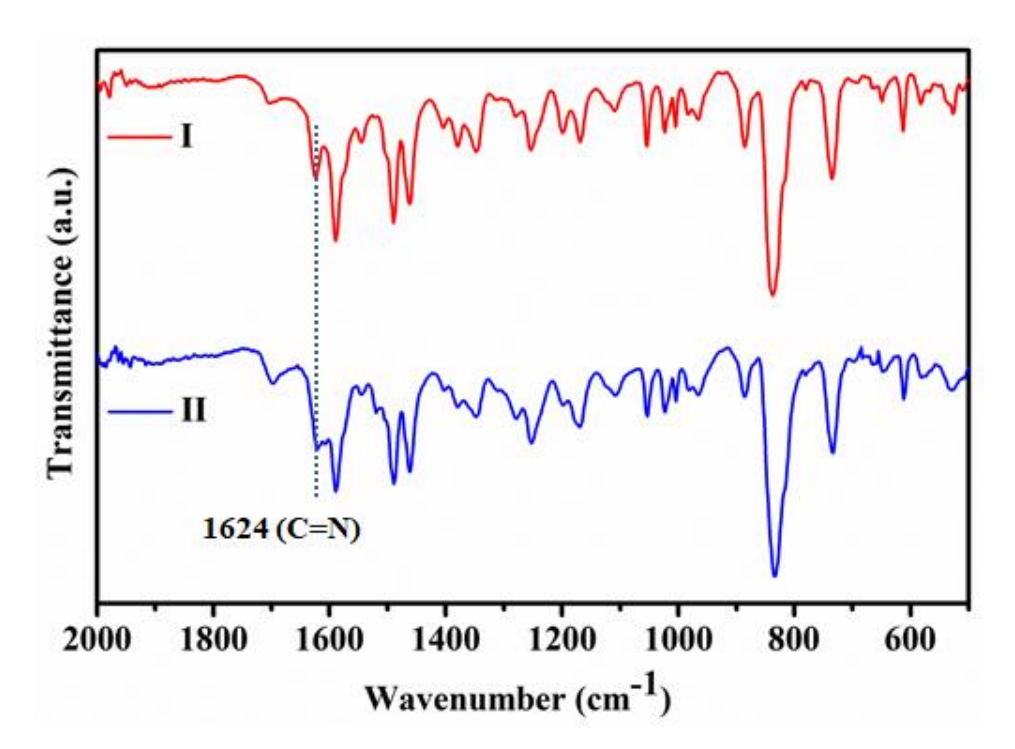


Figure A48. FT-IR spectra of Ag@Pybpy-COF (I) and recycled catalyst (II) after catalysis.

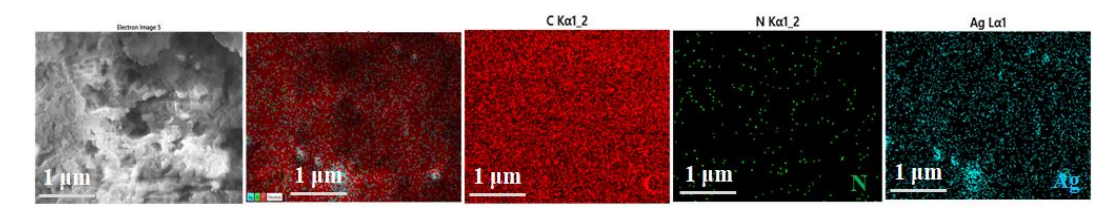


Figure A49. Elemental mapping for Ag@Pybpy-COF recycled after five cycles of catalysis, C (red), N (green), and Ag (light blue).

References

- (1) Pan, H.; Ritter, J. A.; Balbuena, P. B. Examination of the approximations used in determining the isosteric heat of adsorption from the Clausius-Clapeyron equation. *Langmuir* **1998**, *14*, 6323-6327.
- (2) Yang, R. T. Gas Separation by Adsorption Processes, Butterworth, Boston, 1997.
- (3) Zhi, Y.; Shao, P.; Feng, X.; Xia, H.; Zhang, Y.; Shi, Z.; Mu, Y.; Liu, X. Covalent organic frameworks: efficient, metal-free, heterogeneous organocatalysts for chemical fixation of CO₂ under mild conditions. *J. Mater. Chem. A* **2018**, *6*, 374-382.
- (4) Li, H.; Feng, X.; Shao, P.; Chen, J.; Li, C.; Jayakumar, S.; Yang, Q. Synthesis of covalent organic frameworks via in situ salen skeleton formation for catalytic applications. *J. Mater. Chem. A* **2019**, *7*, 5482-5492.
- (5) Dhankhar, S. S.; Nagaraja, C. M. Porous nitrogen-rich covalent organic framework for capture and conversion of CO₂ at atmospheric pressure conditions. *Micropor. Mesopor. Mat.* **2020**, *308*, 110314.
- (6) Xu, K.; Dai, Y.; Ye, B.; Wang, H. Two dimensional covalent organic framework materials for chemical fixation of carbon dioxide: excellent repeatability and high selectivity. *Dalton Trans.* **2017**, *46*, 10780-10785.
- (7) Saptal, V.; Shinde, D. B.; Banerjee, R.; Bhanage, B. M. State-of-the-art catechol porphyrin COF catalyst for chemical fixation of carbon dioxide via cyclic carbonates and oxazolidinones. *Catal. Sci. Technol.* **2016**, *6*, 6152-6158.
- (8) Puthiaraj, P.; Kim, H. S.; Yu, K.; Ahn, W. S. Triphenylamine-based covalent imine framework for CO₂ capture and catalytic conversion into cyclic carbonates. *Micropor. Mesopor. Mat.* **2020**, 297, 110011.
- (9) Dai, Z.; Sun, Q.; Liu, X.; Guo, L.; Li, J.; Pan, S.; Bian, C.; Wang, L.; Hu, X.; Meng, X.; Zhao, L.; Deng, F.; Xiao, F. -S. A Hierarchical Bipyridine-Constructed

- Framework for Highly Efficient Carbon Dioxide Capture and Catalytic Conversion. *ChemSusChem* **2017**, *10*, 1186-1192.
- (10) Wang, J.; Zhang, Y. Facile synthesis of N-rich porous azo-linked frameworks for selective CO₂ capture and conversion. *Green Chem.* **2016**, *18*, 5248-5253.
- (11) Alkordi, M. H.; Weselinski, Ł. J.; D'Elia, V.; Barman, S.; Cadiau, A.; Hedhili, M. N.; Cairns, A. J.; AbdulHalim, R. G.; Basset, J. -M.; Eddaoudi, M.; CO₂ conversion: the potential of porous-organic polymers (POPs) for catalytic CO₂-epoxide insertion. *J. Mater. Chem. A* **2016**, *4*, 7453-7460.
- (12) Chakraborty, D.; Shekhar, P.; Singh, H. D.; Kushwaha, R.; Vinod, C. P.; Vaidhyanathan, R. Ag nanoparticles supported on a resorcinol-phenylenediamine based covalent organic framework for chemical fixation of CO₂. *Chem. Asian J.* **2019**, *14*, 4767-4773.
- (13) Guan, P.; Qiu, J.; Zhao, Y.; Wang, H.; Li, Z.; Shi, Y.; Wang, J. A novel crystalline azine linked three-dimensional covalent organic framework for CO₂ capture and conversion. *Chem. Commun.* **2019**, *55*, 12459-12462.
- (14) Yang, Z.; Yu, B.; Zhang, H.; Zhao, Y.; Chen, Y.; Ma, Z.; Ji, G.; Gao, X.; Han, B.; Liu, Z. Metalated mesoporous poly(triphenylphosphine) with azo functionality: efficient catalysts for CO₂ conversion. *ACS Catal.* **2016**, *6*, 1268-1273.
- (15) Yang, Z. -Z.; Zhao, Y.; Zhang, H.; Yu, B.; Ma, Z.; Ji, G.; Liu, Z. Fluorinated microporous organic polymers: design and applications in CO₂ adsorption and conversion. *Chem. Commun.* **2014**, *50*, 13910-13913.
- (16) Islam, S. S.; Biswas, S.; Molla, R. A.; Yasmin, N.; Islam, S. M. Green synthesized AgNPs embedded in COF: an efficient catalyst for the synthesis of 2-oxazolidinones and α -alkylidene cyclic carbonates via CO₂ fixation. *ChemNanoMat* **2020**, *6*, 1386-1397.
- (17) Singh, M. K.; Bandhyopadhyay, D. Design and synthesis of nanoporous perylene bis imide linked metalloporphyrin frameworks and their catalytic activity. *J. Chem. Sci.* **2016**, *128*, 1-8.
- (18) Zhang, W.; Jiang, P.; Wang, Y.; Zhang, J.; Zhang, P. Bottom-up approach to engineer two covalent porphyrinic frameworks as effective catalysts for selective oxidation. *Catal. Sci. Technol.* **2015**, *5*, 101-104.
- (19) Silva, A. R.; Freire, C.; Castro, B. D. Modulation of the catalytic activity of manganese(III) salen complexes in the epoxidation of styrene: influence of the oxygen source. *New J. Chem.* **2004**, 28, 253-260.

- (20) Sharma, N.; Dhankhar, S. S.; Kumar, S.; Kumar, T. J. D.; Nagaraja, C. M. Rational Design of a 3D Mn^{II}-Metal-Organic Framework Based on a Nonmetallated Porphyrin Linker for Selective Capture of CO₂ and One-Pot Synthesis of Styrene Carbonates. *Chem. Eur. J.* **2018**, *24*, 16662-16669.
- (21) Zhang, J.; Biradar, A. V.; Pramanik, S.; Emge, T. J.; Asefa, T.; Li, J. new layered metalorganic framework as a promising heterogeneous catalyst for olefin epoxidation reactions. *Chem. Commun.* **2012**, *48*, 6541-6543.
- (22) Dias, L. D.; Carrilho, R. M. B., Henriques, C. A.; Calvete, M. J. F.; Masdeu-Bultj, A. M.; Claver, C.; Rossi, L. M.; Pereira, M. M. Hybrid Metalloporphyrin Magnetic Nanoparticles as Catalysts for Sequential Transformation of Alkenes and CO₂ into Cyclic Carbonates. *ChemCatChem* **2018**, *10*, 2792-2803
- (23) Maksimchuk, N. V.; Ivanchikova, I. D.; Ayupov, A. B.; Kholdeeva, O. A. Onestep solvent-free synthesis of cyclic carbonates by oxidative carboxylation of styrenes over a recyclable Ti-containing catalyst. *Appl. Catal. B* **2016**, *181*, 363-370.
- (24) Nguyen, H. T. D.; Tran, Y. B. N.; Nguyen, H. N.; Nguyen, T. C.; Gandara, F.; Nguyen, P. T. K. A Series of Metal-Organic Frameworks for Selective CO₂ Capture and Catalytic Oxidative Carboxylation of Olefins. *Inorg. Chem.* **2018**, *57*, 13772-13782.
- (25) Jin, H. -G.; Chen, F.; Zhang, H.; Xu, W.; Wang, Y.; Fanand, J.; Chao, Z. S. Postmetalation of a new porphyrin ligand-based metal-organic framework for catalytic oxidative carboxylation of olefins. *J. Mater. Sci.* **2020**, *55*, 16184-16196.
- (26) Zalomaevaa, O. V.; Maksimchuka, N. V.; Chibiryaevb, A. M.; Kovalenkoc, K. A.; Fedin, V. P.; Balzhinimaev, B. S. Synthesis of cyclic carbonates from epoxides or olefins and CO₂ catalyzed by metal-organic frameworks and quaternary ammonium salts. *J. Energy Chem.* **2013**, *22*, 130-135
- (27) Seal, N.; Karthick, K.; Singh, M.; Kundu, S.; Neogi, S. Mixed-ligand-devised anionic MOF with divergent open Co(II)-nodes as chemo-resistant, bi-functional material for electrochemical water oxidation and mild-condition tandem CO₂ fixation. *Chem. Eng. J.* **2022**, *429*, 132301.
- (28) Cui, Y.; Xu, Z.; Li, H. -Y.; Young, D. J.; Ren, Z. -G.; Li, H. -X. Synthesis of a Pyrazole-based Microporous Organic Polymer for High-Performance CO₂ Capture and Alkyne Carboxylation. *ACS Appl. Polym. Mater.* **2020**, *2*, 4512-4520.
- (29) Liu, J.; Zhang, X.; Wen, B.; Li, Y.; Wu, J.; Wang, Z.; Wu, T.; Zhao, R.; Yang, S. Pre-Carbonized Nitrogen-Rich Polytriazines for the Controlled Growth of Silver

- Nanoparticles: Catalysts for Enhanced CO₂ Chemical Conversion at Atmospheric Pressure. *Catal. Sci. Technol.* **2021**, *11*, 3119-3127.
- (30) Lan, X.; Du, C.; Cao, L.; She, T.; Li, Y.; Bai, G. Ultrafine Ag Nanoparticles Encapsulated by Covalent Triazine Framework Nanosheets for CO₂ Conversion. *ACS Appl. Mater. Interfaces* **2018**, *10*, 38953-38962.
- (31) Dang, Q. -Q.; Liu, C. -Y.; Wang, X. -M.; Zhang, X. -M. Novel Covalent Triazine Framework for High-Performance CO₂ Capture and Alkyne Carboxylation Reaction. *ACS Appl. Mater. Interfaces* **2018**, *10*, 27972-27978.
- (32) Salam, N.; Priyanka, P.; Ghosh, S.; Mandi, U.; Khan, A.; Alam, S. M.; Das, D.; Islam, S. M. Ag NPs Encapsulated by an Amine-Functionalized Polymer Nanocatalyst for CO₂ Fixation as a Carboxylic Acid and the Oxidation of Cyclohexane Under Ambient Conditions. *New J. Chem.* **2020**, *44*, 5448-5456.
- (33) Zhang, Y.; Lan, X.; Yan, F.; He, X.; Wang, J.; -Sandoval, L. R.; Chen, L.; Bai, G. Controllable Encapsulation of Silver Nanoparticles by Porous Pyridine-Based Covalent Organic Frameworks for Efficient CO₂ Conversion using Propargylic Amines. *Green Chem.* **2022**, *24*, 930-940.
- (34) Wu, J.; Ma, S.; Cui, J.; Yang, Z.; Zhang, J. Nitrogen-Rich Porous Organic Polymers with Supported Ag Nanoparticles for Efficient CO₂ Conversion. *Nanomater*. **2022**, *12*, 3088.
- (35) Bai, X.; Zhang, Y.; Yan, F.; Lan, X.; Thiadiazol-Based Conjugated Organic Polymer Anchoring Ag Nanoparticles for Efficient Conversion of CO₂ into Oxazolidinones from Propargylic Amines. *Appl. Surf. Sci.* 2022, 604,15456.

BIO-DATA

1. Name: Gulshan Singh

Ph.D. Scholar

Contact no. 9569042646

Email: 2019cyz0017@iitrpr.ac.in and gulshanjaggi83@gmail.com

Department of Chemistry

Indian Institute of Technology,

Ropar, Punjab-140001

2. Permanent Address:

Name- Gulshan Singh, S/o Sh. Balbir Singh,

Village-Bhawani, PO-Jangal, Pathankot

Punjab-143531.

3. Educational Qualification:

S.	Qualification	School/College/Department	University/Institute	Passing	Class
No.				Year	
1	Matric (10 th)	S. N. Public High School,	PSEB, Punjab,	2009	First
		Ludhiana	India		
2	SSEC (12 th)	Govt. Senior Sec. School	PSEB, Punjab,	2011	First
		(Boys), Ludhiana	India		
3	B. Sc	S. C. D. Govt. College for	Panjab University,	2014	First
		Boys, Ludhiana	India		
4	M. Sc.	GHG Khalsa College,	Panjab University,	2016	First
	(Chemistry)	Gurusar, Sadhar	India		
5	Ph. D. in	Department of	Indian Institute of	2024	NA
	Chemistry	Chemistry	Technology Ropar,		
			Punjab, India		

Publication based on all research works

- (1) **Singh, G.;** Nagaraja, C. M. Highly efficient metal/solvent-free chemical fixation of CO₂ at atmospheric pressure conditions using functionalized porous covalent organic frameworks. *J. CO₂ Util.* **2021**, *53*, 101716.
- (2) **Singh, G.**; Nagaraja, C. M. Rational design of Cu(I)-anchored porous covalent triazine framework (CTF) for simultaneous capture and conversion of CO₂ at ambient conditions. *J. CO₂ Util.* **2022**, *63*, 102132.
- (3) **Singh, G.;** Prakash, K.; Nagaraja, C. M. Fe(III)-Anchored Porphyrin-Based Nanoporous Covalent Organic Frameworks for Green Synthesis of Cyclic Carbonates from Olefins and CO₂ under Atmospheric Pressure Conditions. *Inorg. Chem.* **2023**, *62*, 13058-13068.
- (4) **Singh, G.;** Duhan, N.; Kumar, T. J. D.; Nagaraja, C. M. Pyrene-Based Nanoporous Covalent Organic Framework for Carxylation of C-H Bonds with CO₂ and Value-Added 2-Oxazolidinones Synthesis under Ambient Conditions. *ACS Appl. Mater. Interfaces* **2024**, *16*, 5857-5868.
- (5) Kishan, R.; Rani, P.; **Singh, G.;** Nagaraja, C. M. Functionalized Covalent Triazine Framework (CTF) for Catalytic CO₂ Fixation and Synthesis of Value-Added Chemicals. *Cryst. Growth Des.* **2024**, *24*, 7878-7887.
- (6) Parihar, V.; Singh, G.; Duhan, N.; Kumar, S.; Kumar, T. J. D.; Nagaraja, C. M. Non-Noble Metal Anchored 2D Covalent Organic Framework for Ambient CO₂ Fixation to High-Value Compounds. *ChemSusChem*, 2024, e202401497.

Oral/Poster presentations at conferences

- 1. Presented oral at Chem Fest-2024, Department of Chemistry, IIT Ropar.
- 2. Presented poster at "32nd CRSI national symposium in chemistry (CRSI-NSC-32)" organized by the Department of Chemistry BITS Pilani, Pilani Campus, February-2024. (Won best poster award)
- 3. Presented poster at 20th International Conference on "Modern Trends in Inorganic Chemistry" organized by the Indian Institute of Sciences, Bengaluru, December-2023. (Won best poster award)
- 4. Presented poster at "Catalysis for energy, environment and sustainability (CEES-2023) and CO₂ India network 2nd annual meet" organized by the Indian Institute of Technology, Mandi, September-2023.
- 5. Presented poster at "8th International Conference on Metal-Organic Frameworks and Open Framework" held at Internation Congress Center Dresden, Germany, September-2022.
- 6. Presented poster at "29th CRSI national symposium in chemistry (CRSI-NSC-29)" organized by the Indian Institute of Science Education and Research (IISER) Mohali, July-2022.